University of Strathclyde Glasgow

SEX-DEPENDENT MITOCHONDRIAL FUNCTION IN THE RIGHT VENTRICLE IN PULMONARY ARTERIAL HYPERTENSION

By

Chelbi Coyle (BSc Hons, MRes)

A thesis submitted in fulfilment of the requirements for the degree of Doctor of Philosophy

Strathclyde Institute of Pharmacy and Biomedical Sciences

University of Strathclyde

Glasgow G4 0RE

Declaration of Authenticity and Authors Rights

This thesis is the result of the author's original research. It has been composed by the author and has not been previously submitted for examination which has led to the award of degree. Part of the research has been published previously into a peer-reviewed journal.

Signed: C Coyle

Date: 02/08/2024

Abstract

Background: Pulmonary arterial hypertension (PAH) has a female predominance with a ~4:1 female-to-male ratio. However, female PAH patients exhibit better right ventricular (RV) compensation in the face of increased pulmonary arterial pressures and thus better survival than the males. The sex differences and the associated mechanism in RV in PAH are not well characterised. Additionally, the mitochondria become dysfunctional in PAH, which involves a glycolytic shift in the mitochondrial metabolism. The mitochondria also undergo excessive fission in PAH, losing their filamentous structure and becoming fragmented. These key mitochondrial dysfunctional features have been shown to contribute to RV dysfunction, and within PAH, the status of the RV serves as the main determinant of survival. Hence, we aim to explore whether there are any sex differences in mitochondrial function and RV remodelling in a Sugen-hypoxia (SuHx) induced PAH rat model. The work in this thesis also describes the impact of a mitochondria-targeted antioxidant, Mitoquinone (MitoQ), *in vivo* and whether MitoQ is able to exhibit protective activity with regard to RV status in PAH.

Methods: Male and female Sprague-Dawley rats were injected with Sugen (25 mg/kg) and exposed to hypoxia for 3 weeks followed by up to 5 weeks in normoxia. Control rats received vehicle (CMC) and were kept in normoxia for up to 8 weeks. RV haemodynamics were measured via pressure-volume (PV) loop measurement using the open chest method. Confocal imaging was performed on fresh RV tissue stained with mitochondrial dyes to examine mitochondrial properties. RV fibrosis, myocyte size, and right coronary artery (RCA) remodelling were assessed by staining the RV tissue with picrosirius red. Mitochondria-linked biogenesis, dynamics and oxidative stress genes were examined in both the RV and lung tissue by quantitative polymerase chain reaction (qPCR). The effect of MitoQ (300 nM) and estradiol (E2; 10 nM) on mitochondrial superoxide levels, cell proliferation and protein expression were examined *in vitro* in male and female human cardiac fibroblasts (HCF) and primary RV fibroblasts isolated from male monocrotaline (MCT) rats. MitoQ (5 mg/kg) was given by intraperitoneal injection (IP) injection to male and female SuHx rats twice a week from week 5 post Sugen injection. The rats were assessed *in vivo* using the PV loop method to obtain the

hemodynamic parameters. RV from these rats were then examined histologically for collagen deposition and myocyte size.

Results: SuHx caused significant increases in RV systolic pressure (RVSP), RV hypertrophy, RV fibroblast proliferation, and RV myocyte size in both sexes. Although SuHx did not cause differences in the RVSP and effective arterial elastance (Ea) between the sexes, it caused a slightly greater increase in RV end-systolic elastance (Ees) in females vs. males, leading to a preserved RV-pulmonary artery coupling (Ees/Ea) in females and a significant decrease in Ees/Ea in males. SuHx caused a significant increase in RV end diastolic pressure (RVEDP) only in males, which was associated with a significantly higher amount of RV interstitial fibrosis and increased expression of fibrotic gene expression in males vs. females. The male SuHx rats had more severe RCA remodelling in their smaller vessels (diameter of 15-50 μm) which was not detected in the females. SuHx caused a significant decrease in mitochondrial membrane potential and fusion in RV from male SuHx rats only. Within the lung, SuHx reduced mitochondrial biogenesis and mitochondrial fusion gene expression in only the male SuHx rats. E2 (10 nM) and MitoQ (300 nM) were able to mediate protective effects by reducing mitochondrial superoxide levels, fibroblast proliferation in male and female HCF cells and male MCT RV fibroblasts. Both MitoQ and E2 were able to reduce markers of fibrosis protein expression and increase mitochondrial biogenesis protein expression. *In vivo*, MitoQ (5 mg/kg) was not able to reduce RVSP, RVEDP, RV hypertrophy, and Ea or increase Ees in the SuHx rats of both sexes. However, MitoQ reduced RV interstitial fibrosis and increased RV-pulmonary artery coupling (Ees/Ea) in male SuHx rats.

Conclusion: Overall, this project shows that the male SuHx rats have worse RV hemodynamic parameters, which correlate with worse interstitial collagen production. Mitochondrial function in the RV and lung displayed sexual dimorphisms, with the male RV associated with more impaired mitochondrial properties compared to the females. We show that both E2 and MitoQ are protective *in vitro* by reducing MitoSOX, cell proliferation, and collagen expression. Meanwhile, MitoQ treatment *in vivo* was not able to reverse the RV hypertrophy in either sex. However, it did improve the RV-pulmonary artery coupling and lower RV collagen deposition in the male SuHx rats. Taken together, this provides preliminary evidence that

male SuHx rats are associated with worse PAH characteristics and that MitoQ could potentially offer therapeutic value for RV, but only in the male sex in PAH.

Acknowledgements

Firstly, I would like to express my sincerest gratitude and appreciation to my supervisors, Dr. Lian Tian and Prof. Margaret R MacLean. Thank you for giving me the opportunity to carry out my PhD study in your lab. I have been so fortunate to have two supervisors who offer a great deal of enthusiasm towards their research, and it has been a pleasure to learn from you both. Your guidance, support, expertise and endless patience have been instrumental throughout my PhD journey. You have both given me a strong scientific grounding that I will take with me for the rest of my scientific career. I will be forever grateful for both of your mentorships.

I would also like to thank all the MacLean group members – Rosie Gaw, Josh Dignam, Gregor Aitchison, Smriti Sharma, Ayman Gebril, Hicham Labazi and Sofia LaForest. I have been so lucky to be part of a great lab group who have always supported me and taught me so much. Your excellent demonstrations, encouragement during the hard days and answers to my questions have helped shape me into the scientist that I am today. My PhD experience would have not been the same without you all. Thank you to Margaret Nilsen from the University of Glasgow for always being there to help me in histology. I would also like to thank Dr Susan Currie for your advice and support and for always making sure that I knew your door was always open whenever needed, I really appreciated this. I would also like to extend my thanks to Linda Horan, Lee Wheeler and Peter Conte for all your assistance and patience during my time in the animal unit.

Finally, and most importantly, thank you to all my family and friends who have been by my side all the way. I would like to express my deepest gratitude and say a special thank you to my Mum and Dad. You have always been there and supported me in achieving my goals. I am beyond grateful for your continuous encouragement, motivation and overwhelming love throughout my entire time at university. I really couldn't have done it without you. My final thanks goes to my partner, Callum. You have been extremely patient, caring and understanding throughout my PhD journey. Thank you so much for putting up with my constant PhD chat and for being a great listener. Your encouragement, reassurance and constant faith has given me the strength to keep going and give it my all until the end, and

even more so during times where I doubted myself. You are truly the best and I can't wait for all our adventures that are still to come.

My PhD has been such a challenging but rewarding process and I will always be forever grateful for the opportunity and experience I have had, which was made possible by Dr. Lian Tian and Prof. Margaret R MacLean. Thank you.

Table of Contents

List of presented work, publications and awards

Poster presentation

- **British cardiovascular research day (BSCR),** September 2022, Belfast, UK. Awarded: British Society of Cardiovascular (BSCR) Travel Award. Published abstract Medical Science Forum: https://www.mdpi.com/2673-9992/27/1/2

- **Early career cardiovascular research day (ECCR),** November 2022, Manchester, UK. Awarded: British Heart Foundation (BHF) Travel Award.

- **Strathclyde postgraduate research day,** February 2023, University of Strathclyde, Glasgow, UK. Awarded: best poster presentation prize.

- **Scottish cardiovascular forum (SCF),** February 2024, St. Andrews, UK. Awarded: best poster prize presentation. Published abstract BMJ Heart: https://heart.bmj.com/content/heartjnl/110/Suppl_2/A6.1.full.pdf

Oral presentation

- **Life science early career research day (ECR),** February 2023, Glasgow, UK. Awarded: best oral communication prize.

Peer-reviewed paper

- **Chelbi Coyle, Margaret R MacLean and Lian Tian: Influence of estrogen on right ventricular mitochondrial function in pulmonary hypertension.** Global Translational Medicine https://accscience.com/journal/GTM/articles/online_first/1729

List of Abbreviations

5-HT	5-hydroxytryptamine
6MWD	6-minute walk distance
ActRIIA	Activin receptor type IIA
ADP	Adenosine diphosphate
AIF	Apoptosis inducing factor
ALK-1	Activin receptor-like kinase 1
Ang II	Angiotensin II
AP1	Activator protein 1
APAH	Associated pulmonary arterial hypertension
ARE	Antioxidant response elements
ATP	Adenosine triphosphate
BMPR2	Bone morphogenetic protein receptor 2
BPU	Biological procedures unit
BRD4	Bromodomain 4
BSA	Bovine serum albumin
cAMP	Cyclic adenosine monophosphate
CAV1	Caveolin 1
CH	Chronic hypoxia
CMC	Carboxymethyl cellulose
CO	Cardiac output
Col 1a1	Collagen type 1 alpha 1 chain
Col 3a1	Collagen type 3 alpha 1 chain
CoQ	Coenzyme Q
COX	Cyclooxygenase
Ct	Cycle threshold
CTGF	Connective tissue growth factor
CYP	Cytochrome P450
DCAD	Dichloroacetate
DHEA	Dehydroepiandrosterone
DMSO	Dimethylsulfoxide
DNM1L / Drp1	Dynamin 1-like protein
DNM2	Dynamin 2
DNMT	DNA methyltransferases
dNTP	Deoxynucleotides triphosphates
E1	Estrone
E2	Estradiol
E3	Estriol
Ea	Effective arterial elastance
ECM	Extracellular matrix
Ees	End systolic elastance
Ees/Ea	RV-pulmonary arterial coupling

ENG	Endoglin
ER	Estrogen receptor
ERE	Estrogen response element
ERK	Extracellular signal-regulated kinase
ET-1	Endothelin 1
ETC	Electron transport chain
ETRA	Endothelin-1 receptor antagonists
FADH	Flavin adenine dinucleotide
FAO	Fatty acid oxidative
GAPDH	Glyceraldehyrde-3-phosphate dehydrogenase
GPCR	G-protein coupled receptor
GPER	G-protein estrogen receptor
GTPase	Guanosine diphosphatases
H&E	Haematoxylin and Eosin
H_2O_2	Hydrogen peroxide
HBSS	Hanks balanced salt solution
HCF	Human cardiac fibroblasts
HIF-1α	Hypoxia inducible factor 1 alpha
HIV	Human immunodeficiency virus
HK	Hexokinase
HO-1	Hemeoxygenase 1
HPAH	Heritable pulmonary arterial hypertension
hPASMC	Human pulmonary artery smooth muscle cells
HPV	Hypoxic pulmonary vasoconstriction
HR	Heart rate
HRE	Hypoxia response element
HSP90AA1	Heat shock protein 90 alpha family class A member 1
IHC	Immunohistochemistry
IMM	Inner mitochondrial membrane
IMS	Intermembrane space
IP	Intraperitoneal
IPAH	Idiopathic pulmonary arterial hypertension
KCNK3	Potassium channel subfamily k member 3
LAS X	Leica application suite X
LO	Lipooxygenase
LTBP-2	Latent transforming growth factor β binding protein 2
LV	Left ventricle
LVEDP	Left ventricular end diastolic pressure

LVSP	Left ventricular systolic pressure
MAO-A	Monoamine oxidase A
MAPK	Mitogen activated protein kinases
MCT	Monocrotaline
MFN1/2	Mitofusin 1/2
MiD49 / MiD51	Mitochondrial dynamics proteins
MitoQ	Mitoquinone
MitoSox	Mitochondrial superoxide
MMP	Mitochondrial membrane potential
MnSOD	Manganese superoxide dismutase
mPAP	Mean pulmonary arterial pressure
MRC	Mitochondrial respiratory complex
mtDNA	Mitochondrial DNA
MTP	Mitochondrial transition pore
mtRNA	Mitochondrial RNA
mtROS	Mitochondrial reactive oxygen species
MVEC	Microvascular endothelial cells
MVEC	Microvascular endothelial cells
MXI-1	Max interacting protein 1
NADH	Nicotinamide adenine dinucleotide
NADPH	Nicotinamide adenine dinucleotide phosphate
Ndufs2	NADH dehydrogenase ubiquinone iron-sulfur protein 2
NFAT	Nuclear factor of activated T cells
NFE2L2	Nuclear factor erythroid 2-related factor 2
NIH	National institute of Health
NO	Nitric oxide
NOS	Nitric oxidase synthase
NOX	NADPH oxidase
NQO1	NAD(P)H dehydrogenase (quinone 1)
NRF 1/2	Nuclear respiratory factor 1/2
NRF1	Nuclear respiratory factor 1
NRF2	Nuclear respiratory factor 2
OCR	Oxygen consumption rate
OMM	Outer mitochondrial membrane
OPA1	Optic atrophy 1
PA	Pulmonary artery
PAB	Pulmonary arterial banding
PAH	Pulmonary arterial hypertension
PAP	Pulmonary artery pressure
PASMC	Pulmonary artery smooth muscle cells
PBS	Phosphate buffered saline

PCG1α	Peroxisome proliferator activated receptor gamma coactivator 1-alpha
PCNA	Proliferating cell nuclear antigen
PDE	Phosphodiesterase
PDH	Pyruvate dehydrogenase
PDK	Pyruvate dehydrogenase kinase
PFA	Paraformaldehyde
PGC1α	Peroxisome proliferator activated receptor gamma co activator 1 alpha
PH	Pulmonary hypertension
PI3K	Phosphatidylinositol 3-kinase
PPARγ	Peroxisome proliferator activated receptor gamma
PSR	Picrosirius red
PV	Pressure volume
PVDF	Polyvinylidene fluoride
PVR	Pulmonary vascular resistance
PVS	Pulmonary vascular system
qPCR	Quantitative polymerase chain reaction
RA	Right arterial
RCA	Right coronary artery
REVEAL	Registry to evaluate early and long-term PAH disease management
RHC	Right heart catherization
RNS	Reactive nitrogen species
ROI	Region of interest
ROS	Reactive oxygen species
RV	Right ventricle
RV-PA	Right ventricular-pulmonary artery
RVEDP	Right ventricular end diastolic pressure
RVEF	Right ventricle ejection fractions
RVFAC	Right ventricular fractional area change
RVSP	Right ventricular systolic pressure
S.E.M	Standard error mean
SD	Sprague dawley
sGC	Soluble guanylate cyclase
siRNA	Small interfering RNA
SMAD 9	SMAD family member 9
SOD2	Superoxide dismutase 2
Sp1	Specificity protein 1
SuHx	Sugen hypoxia
SV	Stroke volume
TAC	Transverse aortic constriction
TCA	Tricarboxylic acid
TFAM	Mitochondrial transcription factor A

TGF-β	Transforming growth factor beta
TGFβ1	Transforming growth factor β 1
TRPV4	Transient receptor potential cation channel subfamily V member 4
TSC22D1	Transforming growth factor β 1 stimulated clone 22
VEGF	Vascular endothelin growth factor 1/2 antagonist
VWF	Von Willebrand factor
WHO	World Health organization
XO	Xanthine oxidase

List of Tables

List of Figures

CHAPTER 1

1. Introduction

1.1 Thesis overview

This thesis is focused on pulmonary arterial hypertension (PAH), which is a specific group of pulmonary hypertension (PH). The introduction chapter will briefly cover the fundamental properties involved in the initiation and progression of this disease and the current therapies available. This thesis will also focus on the mitochondria, a principal target within the right ventricle (RV) as well as the sex differences which exist within this disease. Finally, it will cover the involvement and impact of oxidative stress in PAH.

1.1.1 Pulmonary hypertension classifications

Pulmonary hypertension (PH) is a term used to describe a resting mean pulmonary artery pressure (mPAP) ≥ 20 mmHg, measured by right heart catherization (RHC) (Galiè et al., 2019, Simonneau et al., 2019). It can occur from a broad variety of conditions, which the World Health Organisation (WHO) has now established into five different groups; 1) PAH, 2) PH due to left heart disease, 3) PH due lung diseases and/or hypoxia, 4) PH due to pulmonary artery obstruction and 5) PH with unclear multifactorial mechanisms (Table 1.1) (Simonneau et al., 2019).These groups all share similar pathological mechanisms, however, their underlying causes all vary which influence the diagnosis, prognosis and treatment.

This project will focus on PAH which belongs to group 1 and can be further subcategorised into seven different categories: idiopathic (IPAH), heritable (HPAH), drug and toxin induced, associated (APAH), PAH due to pulmonary veno-occlusive disease and/or pulmonary capillary hemangiomatosis and persistent PH of the newborn syndrome (Table 1.1) (Prins and Thenappan, 2016, Simonneau et al., 2019). IPAH is illustrated when there is no genetic history of the disease, and the cause remains unknown. In HPAH, 80% of the time this is due to a mutation in a gene member belonging to the transforming growth factor beta (TGF-β) superfamily, known as bone morphogenetic protein receptor 2 (BMPR2) (Simonneau et al., 2013, Sahay, 2019). Although, this mutation can also be seen 11-40% of the time in IPAH patients (Montani et al., 2013a). There are also other gene mutations reported to be involved in HPAH, however, these only account for 5% of the HPAH cases, thereby confirming the involvement of environmental factors (Simonneau et al., 2019, Montani et al., 2013a). Drug

and toxin induced PAH is when there has been exposure to certain drugs and toxins which play a direct role in the development of PAH. There is a list of drugs in which the European Respiratory Society have organised into four subgroups based on their risk factor, ranging from definite, likely, possible and unlikely (Table 1.2) (Montani et al., 2013a). APAH occurs from a number of systemic diseases including connective tissue disease, human immunodeficiency virus (HIV) infection, portal hypertension, congenital heart disease and schistosomiasis (Simonneau et al., 2013). PAH can also occur from pulmonary veno-occlusive disease and/or pulmonary capillary hemangiomatosis and persistent PH of the newborn.

Table 1.1. WHO pulmonary hypertension (PH) group classifications and subtypes

WHO CLASSIFICATIONS	SUBTYPES
GROUP 1: PULMONARY ARTERIAL HYPERTENSION	1.1 Idiopathic 1.2 Heritable 1.2.1 BMPR2 1.2.2 ALK-1, ENG, SMAD9, CAV1, KCNK3 1.2.3 Unknown 1.3 Drug and toxin-induced 1.4 Associated with: 1.4.1 Connective tissue disease 1.4.2 HIV infection 1.4.3 Portal hypertension 1.4.4 Congenital heart disease 1.4.5 Schistosomiasis 1.5 Pulmonary veno-occlusive disease and/or pulmonary capillary Hemangiomatosis 1.6 Persistent pulmonary hypertension of the newborn
GROUP 2: PULMONARY HYPERTENSION DUE TO LEFT HEART DISEASE	1. Left ventricular systolic dysfunction 2. Left ventricular diastolic dysfunction 3. Valvular disease 4. Congenital/acquired left heart inflow/outflow tract obstruction and congenital cardiomyopathies
GROUP 3: PULMONARY HYPERTENSION DUE TO LUNG DISEASES AND/OR HYPOXIA	1. Obstructive lung disease 2. Restrictive lung disease 3. Other lung diseases with mixed restrictive/obstructive pattern 4. Hypoxia without lung disease 5. Developmental lung disorders
GROUP 4: PULMONARY HYPERTENSION DUE TO PULMONARY ARTERY OBSTRUCTION	1.Chronic thromboembolic PH 2.Other pulmonary artery obstructions

GROUP 5: PULMONARY HYPERTENSION WITH UNCLEAR MULTIFACTORIAL MECHANISMS	1. Hematologic disorders: chronic haemolytic anaemia, myeloproliferative disorders, splenectomy 2. Systemic disorders: sarcoidosis, pulmonary histiocytosis, Lymphangioleiomyomatosis and Metabolic disorders: glycogen storage disease, Gaucher disease, thyroid disorders 3. Others: tumoral obstruction, fibrosing mediastinitis, chronic renal failure, segmental PH 4. Complex congenital heart disease

Bone morphogenetic protein receptor 2 (BMPR2), activin receptor-like kinase 1 (ALK1), endoglin (ENG), SMAD family member 9 (SMAD 9), caveolin 1 (CAV1), potassium channel subfamily k member 3 (KCNK3), human immunodeficiency virus (HIV). Adapted from (Simonneau et al., 2019).

Table 1.2. European Respiratory Society list of drugs with their probability of inducing pulmonary arterial hypertension (PAH). Adapted from (Montani et al., 2013b)

Definite	**Likely**	**Possible**	**Unlikely**
Aminorex	L-Tryptophan	Cocaine	Cigarette smoking
Fenfluramine	Amphetamines	St John's Wort	Oral contraceptives
Dexfenfluramine		Selective serotonin reuptake inhibitor	Estrogen
Toxic rapeseed oil		Chemotherapeutic agents	
Benfluorex		Phenylpropanolamine	
Dasatinib		Pergolide	
Methamphetamines			

1.1.2 Epidemiology of PAH

PAH is a chronic and rapidly progressive disease. Due to this, many registries across the globe have contributed knowledge regarding PAH epidemiology, including the USA, UK, France, Spain and China. The first registry was the National Institute of Health (NIH) in the USA, which estimated that PAH has a 1 year median survival rate of ~68%, 3 year survival rate at ~48% and 5 year survival rate at ~34% (McLaughlin et al., 2004). However, these survival rates have shifted over time, according to the UK and Ireland registry which reported that within 1, 3 and 5 year the mean survival rates have increased to 92.7%, 73.3% and 61.1%, respectively (Ling et al., 2012). Recent study on US registry has also reported mortality rates, at 1, 2 and 3 years: 1%, 4-6% and 7-11% for low risk PAH patients, 7-8%, 11-16% and 18-20% for intermediate patients and 12-19%, 22-38% and 28-55% for high risk PAH patients, respectively (Chang et al., 2022). The improvement that has been detected over the years, is most likely a result of better understanding of PAH and management, aiding for earlier detection and hence, clinical intervention.

PAH is a rare disease with an estimated prevalence of around 10 to 52 cases per million in which it predominately affects females (4:1 ratio vs. males) (Badesch et al., 2010, Hoeper and Simon, 2014). In most of the cases, the mean age of presentation has been reported to be over the age of 50 years (Ling et al., 2012, Memon and Park, 2017). However, in 1987 the NIH registry illustrated the mean age to be 36 years ± 15 years (Frost et al., 2011, Memon and Park, 2017). Despite this being lower, the NIH did report that the younger cohort appear to have a greater survival rate compared to the older patients, who are also more likely to be diagnosed at a later stage of the disease and with other comorbidities (Hoeper and Simon, 2014, Memon and Park, 2017). It has also been confirmed that one third of PAH patients are obese (Min et al., 2020). However, the obese patients are suggested to have lower mortality rates compared to their non-obese counterparts (Frank et al., 2020). Whilst, other studies suggest that obesity contributes to PAH progression, otherwise known as the “obesity paradox” (Poms et al., 2013, Min et al., 2020).

The NIH registry also studied the racial predisposition of PAH, in which they found that 85.4% of the patients were Caucasian, 12.3% African American and 2.3% Hispanic (Prins and Thenappan, 2016). The Registry to Evaluate Early and Long-term PAH Disease Management

(REVEAL) found a similar pattern of racial distribution (Frost et al., 2011). However, when this was adjusted for age and gender, blacks were reported to be overrepresented meanwhile Asians were slightly underrepresented (Frost et al., 2011). It must also be noted that within the USA, the baseline obesity rates are higher than the PAH cohort, whilst other countries (France and Scotland) face a lower obesity rate but higher PAH rate (Agarwal et al., 2017, Weatherald et al., 2018, McLean et al., 2019).

1.1.3 Diagnosis of PAH

Diagnosis of PAH is difficult given that early symptoms are non-specific such as shortness of breath, fatigue, an increase in heart rate, and fainting (Figure 1.1) (Kondo et al., 2019). Due to this, many patients already have an advanced form of the disease by the time they're finally diagnosed. As well as this, the only way to definitively diagnose PAH is by right heart catherization (RHC) and given the invasiveness of this procedure, clinicians are reluctant to perform this unless there is strong evidence that the patient is suffering from PAH. It does not help that symptoms may not present for months or even years later, with the mean time of symptom onset to diagnosis estimated around 2 years (Kiely et al., 2019). Although, RHC is the only way to get a definitive diagnosis, there is the involvement of several other diagnostic procedures before a diagnosis is confirmed, which includes: blood tests for biomarkers such as brain natriuretic peptide, electrocardiograms, echocardiograms, chest X-rays and cardiopulmonary exercise testing (Figure 1.1) (Kiely et al., 2019).

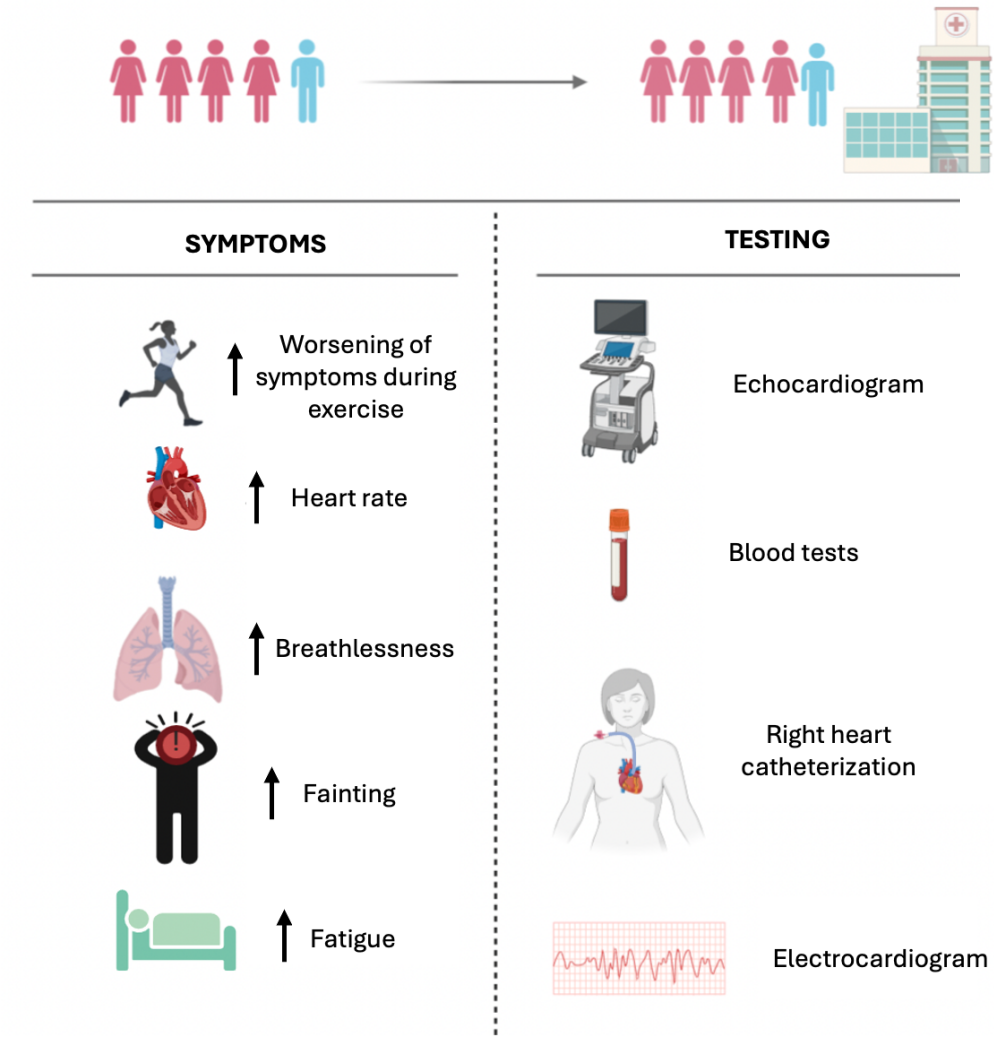

Figure 1.1. Brief overview of the early non-specific symptom's patients may present with prior to testing

Patients will initially experience worsening of symptoms during exercise, an increase in breathlessness, fatigue, heart rate and fainting. The initial screening can be seen in the form of echocardiograms, electrocardiograms, blood tests and the gold standard right heart catherization. Figure created with BioRender.com.

1.2 Pathophysiology of PAH

The normal pulmonary vasculature becomes disrupted in a number of ways, including through uncontrolled proliferation, migration and apoptosis of the cells which regulate vascular function. This can lead to complete obstruction of the pulmonary arteries, thrombosis and inflammation (Humbert et al., 2022a, Fukumoto, 2024). All of these exist to varying degrees within PAH and are key hallmarks (Prins and Thenappan, 2016, Humbert et al., 2019). The main pathological features can be defined by the increase in pulmonary vascular resistance (PVR), pulmonary artery pressure (PAP), vascular cellular proliferation and vasoconstriction of the pulmonary arteries leading to pulmonary vascular remodelling (Simonneau et al., 2019). As the disease progresses, this is usually accompanied by right ventricular (RV) hypertrophy and eventually RV failure, leading to death (Thenappan et al., 2018). It is noted that though the PAH development starts within the pulmonary vasculature, the prognosis of PAH and survival is mainly determined by the response of the RV to the RV afterload (Ghio et al., 2010, Voelkel et al., 2015). However, the mechanisms driving the RV remodelling are understudied and currently no effective therapy directly targets the RV in PAH.

1.2.1 Vasoconstriction of pulmonary vasculature

One of the main pathogenic factors contributing to PAH is chronic and inappropriate vasoconstriction (tightening and narrowing of the vessel lumen) within the pulmonary vasculature (Humbert et al., 2004). Vasoconstriction will be activated under hypoxic conditions and within seconds, and is usually referred to as hypoxic pulmonary vasoconstriction (HPV) (Tarry and Powell, 2017). As a result, this creates a rise in PAP, and the blood flow is subsequently re-diverted to portions in the lung which are more sufficiently oxygenated and do not have elevated PAP (Dunham-Snary et al., 2017). The HPV mechanism has been shown to mainly occur within group 3 of PH rather than group 1. Instead, group 1 vasoconstriction is predominately mediated by numerous potent endogenous vasoconstrictors derived from the vascular endothelium which are released into the pulmonary circulation and activate vasoconstriction. These include endothelin-1 (ET-1), serotonin (5-hydroxytryptamine, 5-HT), angiotensin II (Ang II), prostaglandins, thromboxane and histamine (Humbert et al., 2004, Maclean and Dempsie, 2010, Chester and Yacoub, 2014,

Tanriverdi, 2023). In PAH, these tend to be upregulated meanwhile the vasodilators, including prostacyclin and nitric oxide (NO) are downregulated (Humbert et al., 2004). Whilst it is true, that this imbalance itself evokes vasoconstriction, the increased synthesis of the vasoconstrictors extends further beyond vasoactivity. The release of ET-1 and 5-HT also serve as key stimulators of pulmonary artery smooth muscle cells (PASMC) contraction and proliferation, meanwhile, thromboxane activates platelet aggregation (Farber and Loscalzo, 2004, Prins and Thenappan, 2016, MacLean, 2018). Currently, the majority of the therapeutic interventions for PAH are those which target vasoconstriction in the pulmonary vasculature.

1.2.2 Pulmonary vascular remodelling: proliferation and cell migration

Hyperproliferation and migration of the pulmonary endothelial, fibroblasts and PASMCs and their resistance to apoptosis has been widely recognised as key drivers in a PAH setting. This eventually leads to cellular hypertrophy, accumulation of extracellular matrix deposits, distal muscularisation, formation of occlusive plexiform lesions and inflammation (Xu and Erzurum, 2011). These features all produce tightening and narrowing of the blood vessel lumen and can at times lead to complete obliteration (Chopra et al., 2012).

All pulmonary artery (PA) blood vessels share the same vessel wall composition, which is separated into three different layers (Figure 1.2). The innermost layer, tunica intima consists primarily of the endothelial cells (Mazurek et al., 2017). The middle layer is the thickest layer and is the tunica media layer composed mainly of smooth muscle cells and the outermost layer, the tunica adventitia is composed of the fibroblasts and collagen fibres (Nogueira-Ferreira et al., 2014, Mazurek et al., 2017). Within PAH, medial and adventitial thickening are the most prominent with intimal thickening less so (Stenmark and McMurtry, 2005). The PA vessels differ from the systemic vessels as it is coupled to a lower-pulmonary circulation pressure versus the systemic circulation which faces much higher pressure conditions. Due to this, the PA vessel wall is thinner, with larger diameters and a lack of basal tone. Meanwhile, the systemic arteries are more muscular (Suresh and Shimoda, 2016).

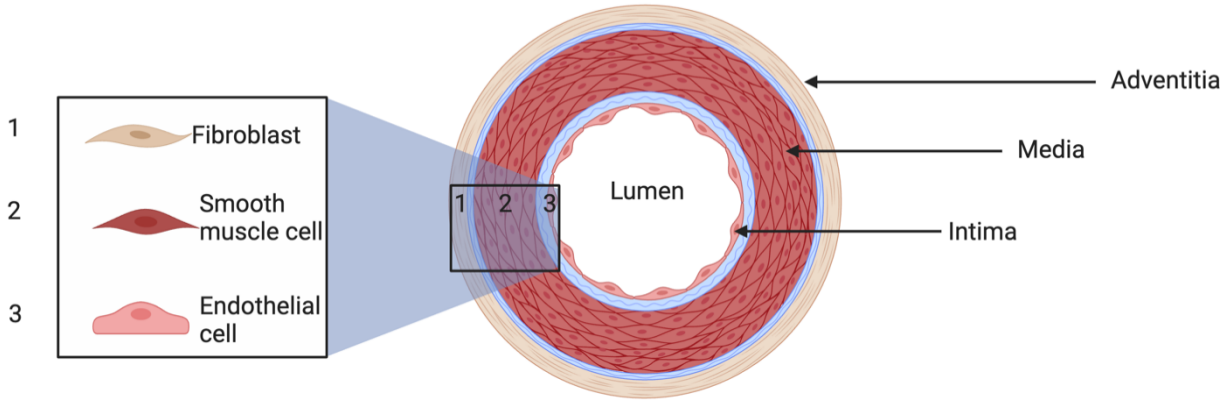

Figure 1.2. The three distinct layers of the pulmonary artery blood vessels

1. The fibroblasts form the outermost layer, the tunica adventitia. 2. The middle layer, the tunica media consists of the smooth muscle cells. 3. The innermost layer, the tunica intima is lined by the endothelial cells. Figure created with BioRender.com.

1.2.3 RV remodelling and failure

The RV consists of a thin wall, approximately 3-5mm in thickness, which is about one-third of that compared to the left ventricle (Figure 1.3) (Ho and Nihoyannopoulos, 2006, Del Rio et al., 2019). Under normal circumstances, the RV is coupled to a low-pressure pulmonary circulation system, unlike the LV which faces a higher afterload and hence, higher resistance (Rana et al., 2019, He et al., 2023). During times when oxygen demand needs to be increased, such as periods of exercise in healthy individuals, the RV can accommodate up to 3-4 times increase in stroke volume by the heart increasing its contractility, such that SV is increased (Matthews and McLaughlin, 2008).

However, in PAH, the remodelling of the distal pulmonary arteries subsequently produces a persistent increase in the mPAP and PVR which as a result, increases the RV afterload pressure (the wall tension experienced during ejection of blood) (Pinsky, 2016). Ultimately, this increase in afterload pressure triggers RV hypertrophy (an increase in muscle mass), RV dilatation, right atrial (RA) enlargement and tricuspid regurgitation, all which contributes towards RV failure (Figure 1.4) (Ryan et al., 2015b).

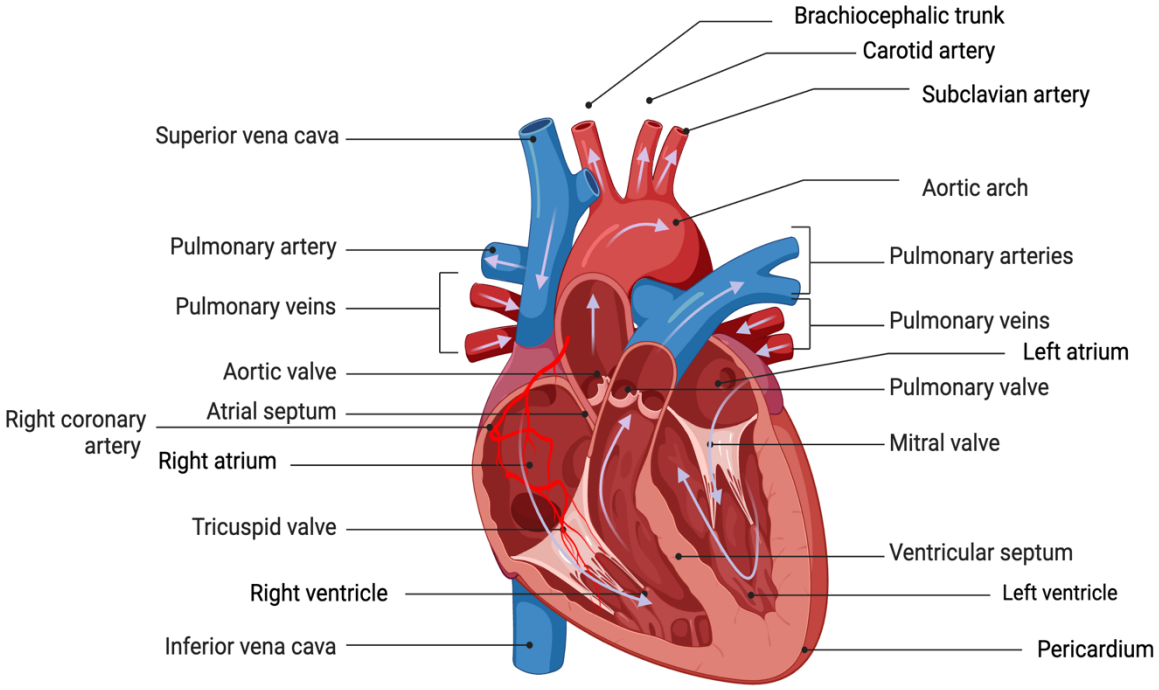

Figure 1.3. The structure of a healthy heart and its major blood vessels

The blood flow through the heart is represented by the arrows. Image is adapted from Jean-Francis Berry (2020). The physiology of the heart. Figure created with BioRender.com.

In the early phase, RV hypertrophy will occur in a compensatory manner to the increased PVR, this will be adaptive, in which the RV function is concentric and retained (Ryan and Archer, 2014). Similar to the pulmonary remodelling, as time proceeds, the chronic and progressive increase in afterload will result in the RV compensatory mechanisms failing and this will transition into maladaptive RV hypertrophy (Ryan and Archer, 2014). At this point, the RV contractility will be fully impaired meaning that the RV is no longer able to maintain the cardiac output (CO) required for the metabolic demands of the body (Frump et al., 2018). On a cellular and molecular level, this adaptive remodelling is associated with decreased mitochondrial function, calcium handling, sarcomere organisation and increased reactive oxygen species (ROS) (Vonk Noordegraaf and Galiè, 2011, Ryan and Archer, 2014). Maladaptive remodelling is accompanied by an increase in oxidative stress, myocyte apoptosis, fibrosis, inflammation and metabolic dysfunction (Frump et al., 2018).

In the face of this increased pressure, the RV will start to undergo dilatation which further negatively impacts RV perfusion by increasing myocardial oxygen demand and thus, simultaneously increasing heart rate (HR) (Ryan and Archer, 2014). As the HR increases to try limit the reduction in stroke volume (SV), and given that there is already contractile dysfunction and afterload mismatch, this results in RV-PA uncoupling (Vonk Noordegraaf and Galiè, 2011, Naeije, 2015). The RV dilatation can also lead to functional tricuspid regurgitation which further reduces the SV as the blood flows backwards into the RA (Casa et al., 2013, Rana et al., 2019). At this stage, a decrease in left ventricular (LV) filling will occur alongside flattening of the interventricular septum (Cativo Calderon et al., 2017). This series of events occurs in a vicious cycle until eventually RV failure is underway. This can be characterised when the cardiac index is <2.5L/min/m^2 and RA pressure >8 mmHg (Ryan and Archer, 2014).

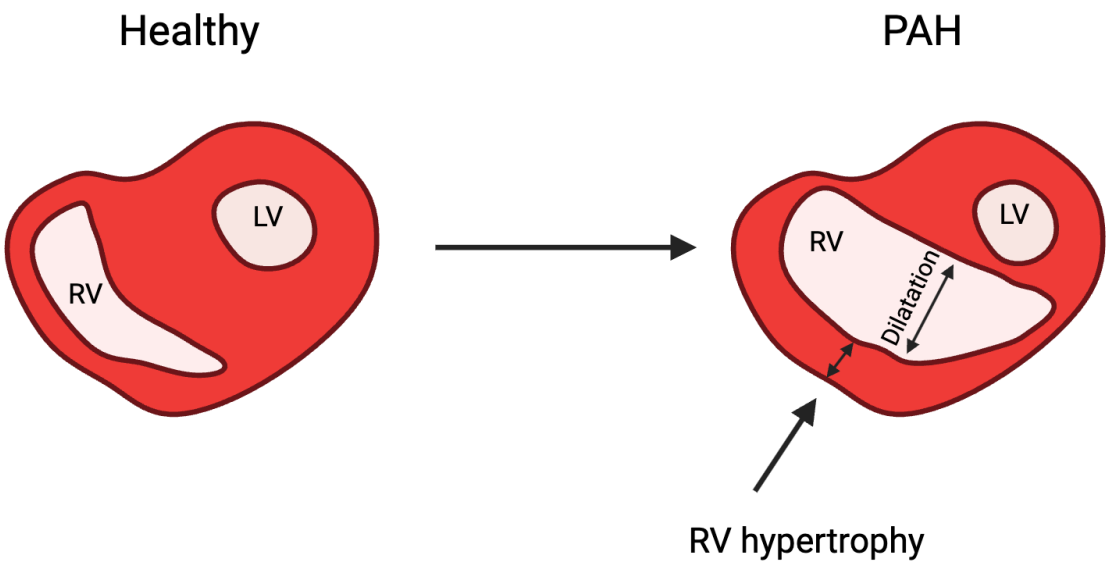

Figure 1.4. Cross sectional view of a healthy heart versus PAH heart

Enlargement of the right ventricle (RV) during pulmonary arterial hypertension (PAH). The RV adapts to the increased pulmonary pressures by increasing contractility where it subsequently undergoes RV dilatation and increases the wall thickness leading to enlargement, otherwise known as RV hypertrophy. At advanced stages this will lead to atrophy of the left ventricle (LV). Figure created with BioRender.com.

1.2.4 RV fibrosis

Fibrosis is a process in which the fibroblasts (collagen producing cells) undergo excessive proliferation leading to an accumulation in collagen formation (Wynn, 2008). There are two main types of collagen; type I and type III (Safdar et al., 2014). Type I contributes to the collagen stiffness, meanwhile type III contributes to the collagen elasticity (Singh et al., 2023). Within the RV in PAH animal models, it has been found that there is a greater accumulation of thick type I collagen fibres versus thin type III fibres (Schimmel et al., 2022, Cheng et al., 2020). As well as this, there also appears to be reduced collagen degradation in PAH models versus wildtype models as a potential explanation for the increased collagen accumulation (Cheng et al., 2020). The collagen accumulation within the RV is similar to the RV hypertrophy process in which it will transition from adaptive to maladaptive (Andersen et al., 2019). Usually, the adaptive collagen accumulation will initially be beneficial in which it attempts to help the myocardium withstand the high pressures (Andersen et al., 2019). Eventually as this transitions to maladaptive, the collagen network turnover becomes dysregulated, there is loss of the myocardium supportive extracellular matrix (ECM) network and noncompliance, ultimately accelerating PAH progression (Andersen et al., 2019).

1.2.5 RV ischemia

Under normoxic conditions the RV receives a constant supply of blood during both systole and diastole with the oxygen supply and demand maintained by autoregulation. This ensures that the blood flow is maintained at a constant despite changes in coronary pressure (Ren et al., 2019, Agrawal et al., 2020). However, in the face of increased PAP leading to RV hypertrophy and enhanced workload, this initiates a supply demand discrepancy between the RV and right coronary artery (RCA) as the pressure gradient begins to decrease (Agrawal et al., 2020, Sree Raman et al., 2021). Immediately, vasodilation will be stimulated and there will be an increase in right coronary blood flow in the RV (Ren et al., 2019). Although, as RV failure transitions into maladaptive, the coronary perfusion pressure begins to decrease alongside blood flow to the RV leading to ischemia (Agrawal et al., 2020). Within PAH, it is believed that in the early beginning stages there will be an increase in RCA flow. However overtime, this can lead to RCA vessel remodelling which will then reduce RCA flow and contribute to RV

ischemia, and eventually RV dysfunction which occurs at the later stage of PAH (Ryan and Archer, 2015).

1.2.6 Right coronary artery in PAH

The RCA serves as the main supply of blood to the right side of the heart (Figure 1.3). It is composed of the same three layers seen in the PA, the tunica intima, tunica media and tunica adventitia (Figure 1.2). It was originally thought that in instances of increased blood flow to the RV via the RCA, that the RCA vessel wall would undergo structural remodelling due to changes in the RCA's elastin and collagen composition (Garcia and Kassab, 2009). Ultimately, this vessel adaptation in response to increased blood flow would lead to wall stress and finally, vessel stiffness (Garcia and Kassab, 2009). Using a right ventricle pressure overload pig model, known as pulmonary arterial banding (PAB), Garcia and Kassab were the first study to examine the RCA vessels in a RV hypertrophic model and test this theory. The PAB model involves placing a silk suture or clip around the main PA, therefore causing the RV workload to be enhanced as it has to work harder to ensure it can eject blood through the restricted PA. This creates a significant increase in RV pressure overload, RV contractility and overtime leads to RV dysfunction (Sharifi Kia et al., 2021). Indeed, they found increases in elastin in the axial and circumferential directions of the vessel (Garcia and Kassab, 2009). As well as this, they also found increases in the elastin and collagen area in the adventitial layer of the RCA, overall suggesting vessel stiffness (Garcia and Kassab, 2009).

Within PAH, as the demand of the RV increases, the rate of the RV perfusion supplied by the RCA will also have to increase (Gomez-Arroyo et al., 2012). Eventually, the RV ability to compensate becomes limited by reduced RV perfusion which is RCA dependent (Hamud et al., 2021). Direct correlations with impaired RCA flow have been made in IPAH patients, with RCA flow initially maintaining high during diastole and then reducing during systole (van Wolferen et al., 2008). The reduction seen during systole is linked to the increased RV mass, increased muscle contractility, muscle thickening and RV pressure (van Wolferen et al., 2008), and in cases of severe RV hypertrophy the overall RCA flow is reduced (van Wolferen et al., 2008). RCAs taken directly from patients with PAH and from male monocrotaline PH rats, exhibit thickened walls when compared with their controls (Meloche et al., 2017). Both PAH patients and rat RCAs had increased proinflammatory IL-6 gene expression and DNA damage

detected by measuring p53-binding protein 1 protein levels (Meloche et al., 2017). They also detected an increase in bromodomain 4 (BRD4) protein in both patient and RCAs (Meloche et al., 2017). BRD4 is known to be overexpressed in the lungs of patients with PAH and is known to play a role in the remodelling process by acting as a trigger for proliferation and driver towards an anti-apoptotic phenotype (Meloche et al., 2017).

Overall, further research is required to understand the consequences of the reduced RCA flow in PAH patients and animal models, and whether this impaired RCA flow leads to RV ischemia that contributes to RV dysfunction.

1.3 Mitochondrial dysfunction in PAH

The mitochondria are membrane bound organelles, present in most eukaryotic cells. They are often referred to as the powerhouses of the cell as they provide cells with majority of their energy in the form of adenosine triphosphate (ATP) (Riou et al., 2023). However, they are involved in many other integral processes which are required for normal cellular function, including apoptosis, calcium signalling, cell growth and control of the cell cycle (Osellame et al., 2012). Hence, any dysfunctions in mitochondrial activity are frequently associated with diseases (Osellame et al., 2012).

The mitochondria itself are formed from an inner mitochondrial (IMM) and outer mitochondrial membrane (OMM) (Figure 1.5) (Friedman and Nunnari, 2014). The OMM is highly porous allowing for small uncharged molecules and ions, including ROS to pass through from the cytoplasm into the mitochondria via voltage dependent anion channel mechanisms or by translocator TOM40 and TOB/SAM complexes (Endo and Yamano, 2010). In between the OMM and IMM is what is known as the intermembrane space (IMS) which is the home of a key protein, cytochrome C (Endo and Yamano, 2010). The IMM contains a tight diffusion barrier which only allows ions and molecules through via TIM23 and TIM22 complexes (Endo and Yamano, 2010, Dabir et al., 2013). The folds in the IMM form the cristae, creating a greater surface area for the IMM reactions to take place (Leveille et al., 2017). Enclosed within the IMM is the mitochondrial matrix, which constitutes many of the mitochondria's enzymes, DNA and ribosomes (Figure 1.5). The mitochondrial DNA (mtDNA) encodes 37 genes, of which

11 are mRNA, 22 tRNA and 2 rRNA inherited exclusively from the mother (Taanman, 1999, Luo et al., 2018).

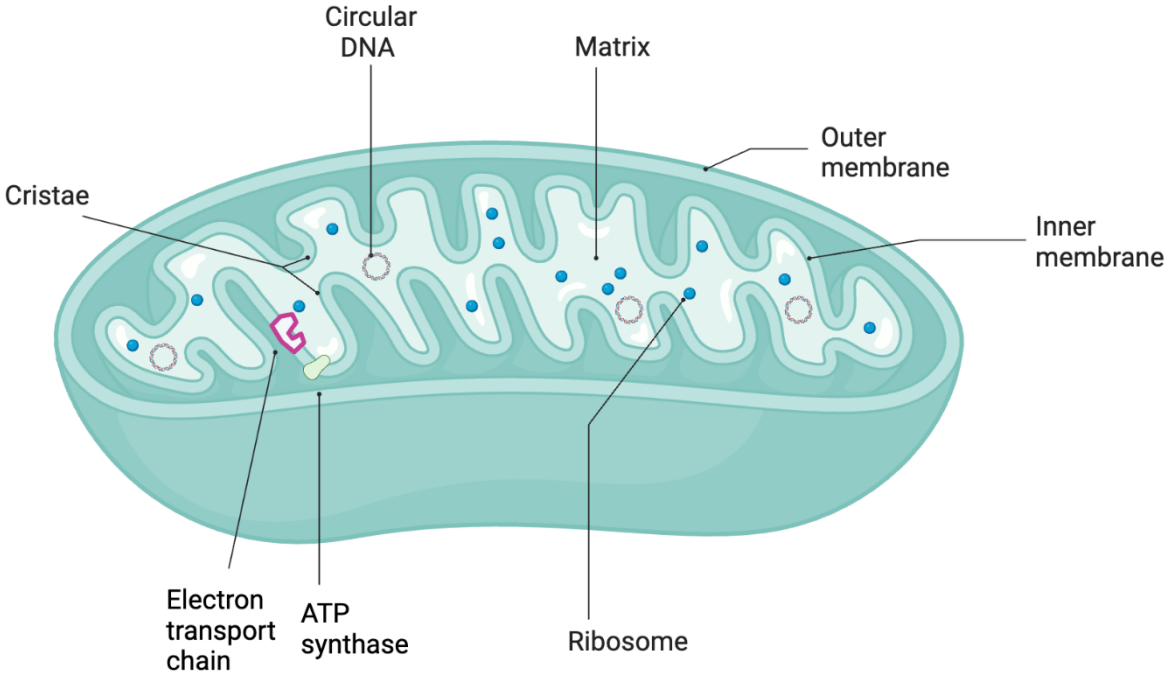

Figure 1.5. The structure of the mitochondria

Highlighting the location of the cristae, inner mitochondrial membrane (IMM), outer mitochondrial membrane (OMM), matrix, ribosomes, ATP synthase, electron transport chain and circular DNA. Figure created with BioRender.com.

1.3.1 Mitochondrial dynamics in PAH

The mitochondria are usually organised into a filamentous network, which is tightly controlled via fusion and fission events (Meyer et al., 2017). Fusion of the mitochondria helps to maintain normal functions despite the presence of mitochondrial defects. Meanwhile, mitochondrial fission helps identify the dysfunctional mitochondria, and facilitates its removal by segregating it from the network (Youle and van der Bliek, 2012). These events are mediated predominately by dynamin related guanosine diphosphatases (GTPases) that also ensures there is a balance between the two competing processes (Youle and van der Bliek, 2012). However, in PAH, this balance becomes disrupted usually by excessive fission, which then leads to a reduction in ATP production, mitochondria motility and an increase in oxidative stress (Dasgupta et al., 2020) (Figure 1.6). Subsequently, the filamentous morphology is lost and the mitochondria become fragmented (Dasgupta et al., 2020). One of the most important proteins in mediating fission is dynamin 1-like protein (DNM1L; or dynamin-related protein 1, Drp1) which is recruited to the OMM where it accumulates into concentrated foci via the help of the four mitochondrial dynamic proteins 49 (MiD49) and 51 (MiD51), mitochondrial fission 1 protein (Fis1) and mitochondrial fission factor (MFF) (Figure 1.6) (Samangouei et al., 2018). The MiD49 and MiD51 are critical in mediating mitochondrial fission as knockout of these proteins will significantly reduce DNM1L recruitment and promote mitochondrial elongation (Samangouei et al., 2018). In PAH, there is overexpression of MiD49 and MiD51 proteins which upregulates DNM1L recruitment and hence, enhances mitochondria fission (Chen et al., 2018a, Samangouei et al., 2018). Meanwhile, the expression of the fusion proteins, Mitofusin 1 (MFN1) and Mitofusin 2 (MFN2) are significantly downregulated in pulmonary artery tissue from PAH rats (Luo et al., 2023, Santos et al., 2024). Various other stressors such as ROS and high cytosolic Ca^{2+} levels can also alter the mitochondrial dynamics leading to fragmentation (Shah et al., 2019).

A

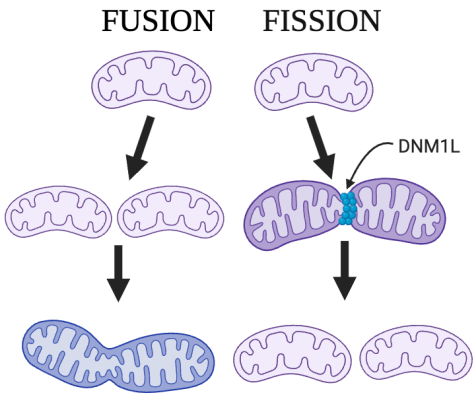

B

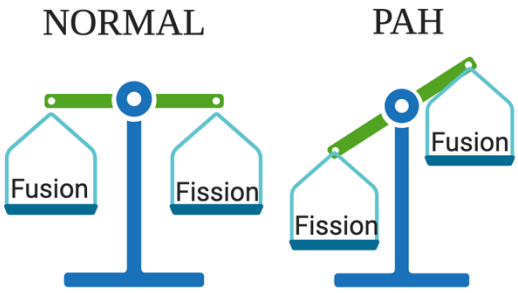

Figure 1.6. Schematic illustration of mitochondrial fusion and fission

Mitochondrial fusion is represented by the joining of the mitochondria. Meanwhile, fission can be seen by the splitting of them (Figure A) which can be mediated by the dynamin 1-like protein (DML1) which is shown as concentrated foci located at the outer mitochondria membrane (Figure A). Under normal conditions, these will be equally balanced however in PAH this is disrupted by excessive fission. Figure created with BioRender.com.

1.3.2 Mitochondrial metabolism in PAH

The mitochondria generates cellular energy through a three step process involving; glycolysis, TCA cycle and oxidative phosphorylation which involves both the electron transport chain and chemiosmosis (Zhao et al., 2019a) (Figure 1.7). This will be initiated by the intake of glucose into the cytoplasm which undergoes glycolysis to form pyruvate. Pyruvate dehydrogenase (PDH) then catalyses pyruvate into acetyl coenzyme A (acetyl coA) which is transported into the mitochondrial matrix (Li et al., 2015). This will then undergo a series of oxidation reactions via the tricarboxylic acid (TCA) cycle (Breault et al., 2023).

Nicotinamide adenine dinucleotide (NADH) and flavin adenine dinucleotide ($FADH_2$) serve as two main products from the TCA cycle which facilitate the electron transport chain (ETC). The ETC consists of four mega complexes (complex I, II, III and IV) which are located in the IMM (Figure 1.7) (Zhao et al., 2019a). NADH donates its electrons to complex I, which energize the complex in a manner that allows it to form a proton gradient, whereby it pumps hydrogen ions from the mitochondrial matrix uphill to the IMS (Guo et al., 2018). The electrons from complex I are then passed onto coenzyme Q (CoQ), whilst $FADH_2$ similarly donates its electrons directly to complex II (Guo et al., 2018). However, no proton pump is generated here, thus, the electrons are transported to CoQ which delivers them to complex III (Guo et al., 2018). Similar to complex I, this will generate a proton gradient allowing for the hydrogen ions to be pumped from the matrix into the IMS. At this stage, the electrons will be transported to cytochrome C which will accept them and shuttle them to complex IV, in which the proton gradient continues to form and pumps more of the hydrogen ions to the IMS (Guo et al., 2018). Finally, oxygen serves as the terminal electron acceptor which is reduced and formed into water. At this point, ATP synthases which consists of F_0F_1 subunits, uses its F_0 to allow for the proton gradient generated over the ETC to flow back into the mitochondrial matrix (Guo et al., 2018). Meanwhile, the F_1 subunit undergoes conformational changes which allow it to catalyse adenosine diphosphate (ADP) into ATP (Guo et al., 2018, Zhao et al., 2019b).

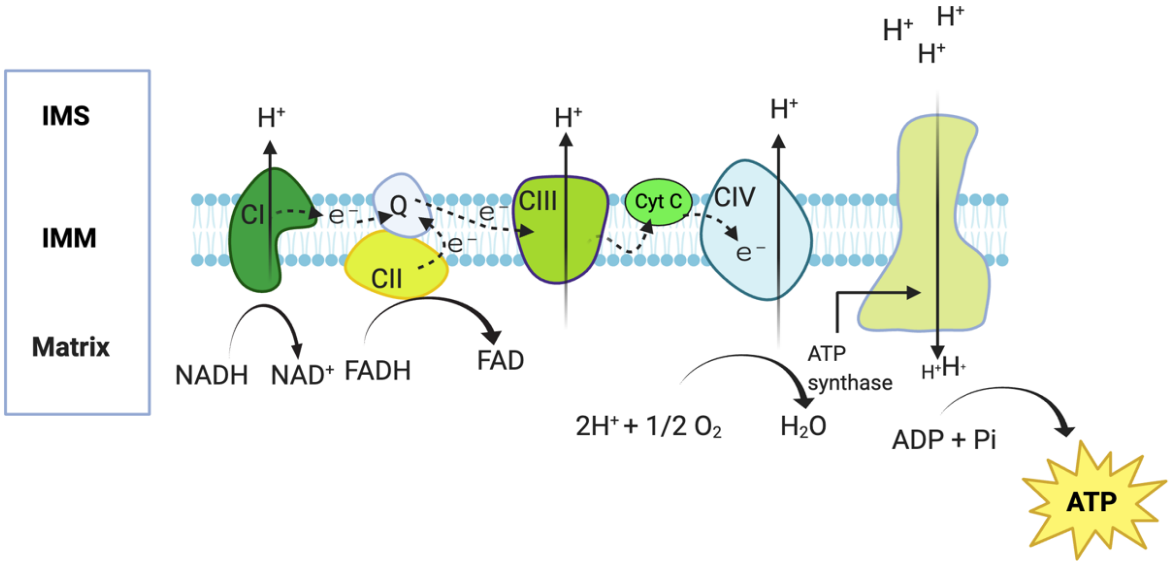

Figure 1.7. Electron transport chain

The electron transport chain (ETC) series of reactions take place within the inner mitochondria membrane (IMM) where the electrons are passed along the complexes. During this, a proton gradient is formed in complex I, III and IV. This is then utilized at the final stage complex which synthesises adenosine diphosphate (ADP) + inorganic phosphate (Pi) to form adenosine triphosphate (ATP). Figure created with BioRender.com.

In many cases of PAH, metabolism dysregulations occur which ultimately produces a chronic shift in energy production. This shift is a result from the cells opting for ATP production via glycolysis as opposed to mitochondrial oxidative phosphorylation and is also referred to as the Warburg phenomenon (Wallace, 2005). This was initially discovered to occur in a number of cancerous cells and can be defined as when the mitochondria chooses to behave in an anaerobic manner despite being in an oxygen rich environment (Wallace, 2005). This then effects other mechanisms such as silencing of transcription of superoxide dismutase 2 (SOD2) and a reduction in hydrogen peroxide (H_2O_2) which all lead to activation of hypoxia inducible factor 1 α (HIF-1α) (Figure 1.8) (Dasgupta et al., 2020). HIF-1α then upregulates pyruvate dehydrogenase kinase (PDK) activity thereby inhibiting PDH (Soni and Padwad, 2017). This inhibition of PDH prevents the conversion of pyruvate into acetyl CoA and stimulates the mitochondria to alter its ROS production causing it to be upregulated in response to the hypoxia (Handy and Loscalzo, 2012, Chen et al., 2018b). At the same time, it must be noted that reduced ROS levels have been detected from the PASMC from human PAH patients and are said to be primary changes that occurred in the absence of hypoxia (Wigfield et al., 2008, Dromparis et al., 2010). This is known as the "Redox hypothesis of HPV" model which is where some studies suggest that the mitochondria sense hypoxia and decrease mtROS production (Bonnet and Boucherat, 2018). However, this model has been challenged by the "ROS hypothesis" which is the opposing theory that hypoxia increases mtROS (Bonnet and Boucherat, 2018). Since, studies have investigated into whether ROS is reduced or increased during acute and chronic hypoxia within the pulmonary vasculature. Pak et al, found that mtROS was increased within the PASMC following acute hypoxic exposure but not chronic hypoxia exposure (Pak et al., 2018). Whilst other studies have reported a decrease of mtROS during the acute phase and an increase in ROS following chronic exposure (Wu et al., 2007). These conflicting results have prompted many questions such as which types of ROS are responsible for the changes, whether the Warburg metabolism is responsible and which hypothesis best represents what is seen in PAH. Nonetheless, future experiments are needed to resolve these contradicting findings.

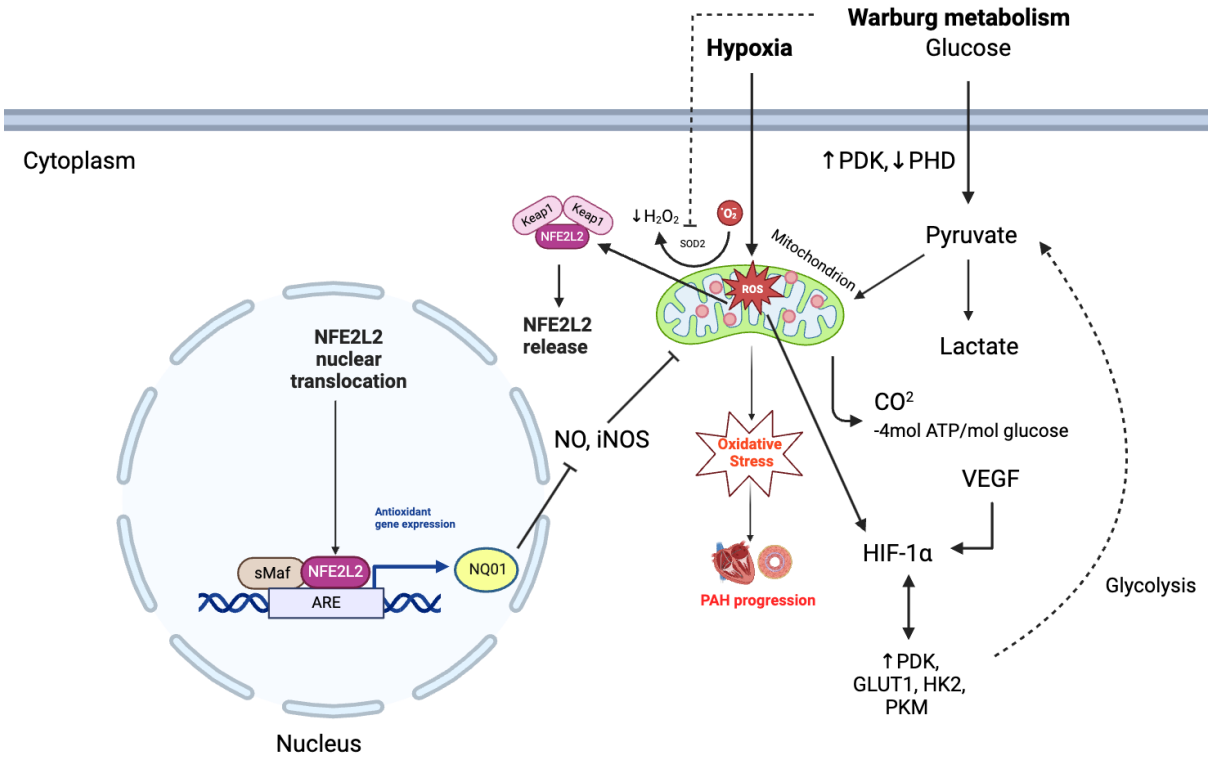

Figure 1.8. Representative image of the pathways involved in ROS

Once the Warburg metabolism is triggered, this upregulates the expression of PDK which contributes to the suppression of oxidative phosphorylation. Glucose is broken down into pyruvate which is then formed into lactate. The pyruvate can be imported into the mitochondrion and then is broken down into carbon dioxide (CO_2). Hypoxia will increase the production of reactive oxygen species (ROS). ROS will stabilize hypoxia inducible factor 1 alpha (HIF1α), a master regulator of the Warburg metabolism. HIF1α will then upregulate the expression of pyruvate dehydrogenase (PDK), glucose transporter 1 (GLUT1), hexokinase 2 (HK2) and pyruvate kinase (PKM) stimulating glycolysis to keep the HIF1α pathway regulated. The Warburg metabolism can also prevent the conversion of superoxide to hydrogen peroxide by inhibiting superoxide dismutase 2 (SOD2). Under normal conditions, Kelch-like ECH-associated protein 1 (Keap1) is ubiquitinated to Nuclear factor erythroid 2-related factor 2 (NFE2L2) however after exposure to ROS, Keap1 becomes inactivated which leads to the

phosphorylation and release of NFE2L2 which is then translocated into the nucleus where it binds to antioxidant response element (ARE) sites. This then activates the expression of antioxidant genes including NAD(P)H dehydrogenase (quinone 1) (NQO1). NQO1 will then inhibit the expression of nitric oxide (NO) and inducible nitric oxide (iNOS) and when activated via antioxidant gene expression this will then counteract ROS. High ROS levels will lead to increases in oxidative stress which contributes to PAH progression. Figure created with BioRender.com.

1.3.3 Mitochondrial biogenesis in PAH

Mitochondrial biogenesis refers to the process in which new mitochondria are formed. It is controlled predominately by peroxisome proliferator activated receptor γ (PPARγ) coactivator 1α (PGC-1α) (Gureev et al., 2019). PGC-1α is a versatile transcription coactivator which is predominantly expressed in tissues in which the mitochondria are most abundant, such as the RV (Liang and Ward, 2006, Cheng et al., 2018). Here, it interacts with a variety of transcription factors that play a role in many responses including those involved in mitochondrial biogenesis (Jung and Kim, 2014). The exact mechanism by which PGC-1α achieves this is still being studied, however it has been shown to involve nuclear respiratory factor 1 and 2 (NRF1/2) and signalling via the estrogen related receptor α (ERRα) (Dominy and Puigserver, 2013, Jung and Kim, 2014). The relationship between PGC-1α and the NRF system is considered to be major as PGC-1α directly and dramatically modulates NRF1/2 gene expression and its downstream gene, TFAM, the key gene involved in mtDNA replication and repair (Picca and Lezza, 2015). Meanwhile, mutated NRF1 can equally inhibit PGC-1α-stimulated mitochondrial biogenesis. During hypoxia, there are also reductions in PPARγ which leads to depletion in PGC-1α and this result has been long established to decreased mitochondrial biogenesis, detrimental structural changes and dysfunction (Agrawal et al., 2020). Additionally, there are other factors which can contribute to reduced PGC-1α levels including a loss of BMPR2 (Diebold et al., 2015). Particularly, within the RV, PGC-1α has been found to be significantly reduced in male monocrotaline (MCT), Sugen-hypoxia (SuHx) rats and ovariectomized female SuHx rats and also displays a trend toward decrease in the RV from limited PAH patients (Enache et al., 2013, Gomez-Arroyo et al., 2013, Liu et al., 2017). Reduced PGC-1α level is associated with impaired mitochondrial and RV function in male SuHx rats and also ovariectomized female SuHx rats (Enache et al., 2013, Gomez-Arroyo et al., 2013, Liu et al., 2017) and treatment with E2 before the induction of PAH preserved PGC-1α level and mitochondrial and RV function in the female SuHx rats (Liu et al., 2017). Therefore, upregulation of PGC-1α could be identified as a potential target to limit mitochondrial dysfunction.

1.3.4 Oxidative stress in PAH

Oxidative stress refers to when there is an imbalance between oxidant and antioxidant production, due to an excessive production of the oxidants thereby preventing the cells ability to produce an effective antioxidant response (Ray et al., 2012). Under normal conditions, this balance is highly controlled however under PAH conditions there is enhanced levels of oxidative stress as a result of an increased production of ROS and reactive nitrogen species (RNS) (Demarco et al., 2010). This increase in ROS is triggered by numerous mediators including those involved in the pulmonary vascular remodelling, RV fibrosis and hypertrophy. As well as this, ROS can also be increased when the mitochondria undergoes a metabolic shift from oxidative stress to the Warburg metabolism (Pokharel et al., 2023). The increase in ROS will also exacerbate PAH pathogenesis via promoting cell proliferation, apoptotic resistant cells, inflammatory signalling and hypertrophy of the smooth muscle layer within the pulmonary arteries, further disrupting the pulmonary vasculature and RV (Demarco et al., 2010). As well as this, when the mitochondria is exposed to high levels of oxidative stress this increases its susceptibility to mitochondrial DNA damage and thereby, mitochondrial dysfunction (Pokharel et al., 2023). Importantly, this increase in ROS levels has been detected in patients with PAH (Wong et al., 2013, Jernigan et al., 2017). As well as this, in human PAH patients that have increased ROS also have reduced antioxidant SOD2, suggesting decreased antioxidant capacity (Bonnet et al., 2006, Archer et al., 2010).

Cellular ROS include the free radicals such as superoxide and non-radicals such as hydrogen peroxide listed in Table 1.3. ROS can be generated either endogenously by the cytoplasm, cell membrane, endoplasmic reticulum, peroxisome or more predominately during the electron transport chain located in the IMM (Figure 1.7) (Tirichen et al., 2021). As well as this, ROS can also be produced in a response to exogenous sources such as bacterial invasion (Ray et al., 2012, Zorov et al., 2014). Above all, the mitochondria serve as one of the most important sources of ROS as they are responsible for generating approximately 90% and also contain many of the required enzymes for ROS production (Balaban et al., 2005, Tirichen et al., 2021). The major site for ROS production within the mitochondria ETC is at complex I and complex III, with complex II producing ROS to a lesser extent (Tirichen et al., 2021). There are also other

enzymatic and metabolic sources such as nicotinamide adenine dinucleotide phosphate (NADPH) oxidases (NOX), cyclooxygenases (COX), lipoxygenases (LO), uncouple NOS and xanthine oxidases (XO) known to generate superoxide (Demarco et al., 2010). Under normal circumstances, the free radicals tend to be short lived as they are scavenged by the antioxidants. There are around 4000 antioxidants, which include the SODs, glutathione peroxidase and catalases (Hatwalne, 2012). One of the most important antioxidant transcription factors is said to be nuclear factor erythroid 2-related factor 2 (NFE2L2) because of its interaction with antioxidant response element (ARE). ARE is responsible for amplifying the gene expression of potent antioxidants such as the SODs and glutathione peroxidases (Alves et al., 2021). One of the main target genes associated with NFE2L2 activation is NAD(P)H dehydrogenase (quinone 1) (NQO1) (Qin et al., 2022). Activation of NFE2L2/NQO1 can then upregulate the expression of anti-inflammatory enzymes such as the hemeoxygenases (HO-1) thereby contributing towards protective cellular activity (Lopes et al., 2015, Qin et al., 2022). Mice hearts which have knockout of NFE2L2 have demonstrated an increase mitochondrial DNA damage, worse cardiac hypertrophy and cardiac dysfunction when compared with their littermates following chronic cardiac pressure overload (Lopes et al., 2015). Human PASMC from PAH patients stimulated with serotonin was found to increase ROS through NADPH oxidase (Nox) mechanisms (Hood et al., 2017). This was correlated with reduced NFE2L2, antioxidant catalase activity, promotion of cell proliferation and ECM remodelling (Hood et al., 2017). Mitochondrial ROS has been shown to stimulate Nox2 activity whilst, Nox2 has also been shown to stimulate mitochondrial ROS, suggesting that the cross talk between mitochondria and Nox may be due to a feed-forward mechanism (Fukai and Ushio-Fukai, 2020). Additionally, Nox1 upregulation by Ang-II has also been linked to mitochondrial dysfunction and vascular senescence (Schulz et al., 2014). The mechanism by which Nox can stimulate mitochondrial ROS production remains unknown.

Another study demonstrated that when they employed a potent NFE2L2 and NQO1 activator, Sulforaphane, it produced significant cardiac protection by preventing SuHx-induced RV dysfunction, remodelling, inflammation, and RV fibrosis and also reduced pulmonary dysfunction, inflammation and pulmonary fibrosis in male mice (Kang et al., 2020). Given the

importance of NFE2L2, it has received a large amount of attention, all which point towards it being protective.

Overall, in an attempt to reduce or prevent oxidative stress, a strong antioxidant response must be generated, with the key gene transcription factors such as NFE2L2 and its downstream target genes, NQO1 playing crucial roles. Thus, suppression of these genes will likely play a role in contributing to ROS generation and oxidative stress within PAH (Qin et al., 2022).

Table 1.3. Examples of reactive oxygen species (ROS) and reactive nitrogen species (RNS) generated free radicals

ROS and RNS
Superoxide (the most abundant)
Hydrogen peroxide
Hydroxyl radical (the most potent)
Singlet oxygen
Nitric oxide
Peroxynitrite
Lipid hydroperoxides
Alkoxyl radical
Peroxyl radical
Sulfate radical
Nitrogen-centered radical (Sp)

1.4 Sex differences in PAH

Within the PAH population there is a 4:1 ratio of females versus males, thus, implying that females have an increased susceptibility (Batton et al., 2018). Although PAH occurs more commonly in women, it has been found that they have a greater survival outcome compared to the males (DesJardin et al., 2024). The reason for this has been correlated to women having better RV function where it can adapt more efficiently to the increased PVR (Swift et al., 2015). Meanwhile, males have been associated with worse RV adaptation resulting in poorer RV ejection and hence, lower SV values (Swift et al., 2015, Keen et al., 2020). Although, it must be noted that the status of RV ejection and SV volume also greatly depends on other factors including both age and race (Swift et al., 2015). This conflict between susceptibility versus survival led to research focusing upon sex hormone signalling, particularly the role of estrogen (E2) (Umar et al., 2012). Circulating E2 has been found to be elevated in pre-menopausal PAH, post-menopausal PAH and male PAH patients (Denver et al., 2020, Baird et al., 2021, Dignam et al., 2023). As a result, this led to the debate of whether elevated E2 proposed a greater risk of developing PAH. However, as it stands a great deal of controversy remains between E2's function in PAH with further investigation required. We briefly review some of the literature available regarding E2's role below.

In healthy post-menopausal women using HRT, the higher E2 levels are correlated with improved RV function and lower incidence of PAH (Rodriguez-Arias and García-Álvarez, 2021). As well as this, estrogen treatment following Sugen-hypoxia (SuHx) exposure in male and female rat models has shown to also mediate protective effects within both the RV and pulmonary vasculature (Liu et al., 2014, Frump et al., 2015). E2 treatment has also been shown to mediate beneficial effects in the MCT model by reducing PASMC proliferation, reducing vasoconstrictor ET-1 and upregulating vasodilator NO (Farhat et al., 1993, Yuan et al., 2013). The female rats also manifest a milder PH phenotype with better survival rates versus the male rats (Sun et al., 2021b). Additionally, ovariectomised female rats exhibit a poorer PH status which is then alleviated by the treatment of E2 (Earley and Resta, 2002, Umar et al., 2011). Whilst, in contrast inhibiting estrogen synthesis with aromatase inhibitors such as anastrozole and metformin have shown to abolish the PH phenotype in female SuHx rats and female chronic hypoxic mice, implying that E2 exerts a pathogenic role (Mair et al.,

2014b, Dean et al., 2016). Anastrozole was also found to reduce the PH phenotype by lowering ROS within the pulmonary vasculature in obese mice that developed mild PH (Mair et al., 2019). Estrogen inhibition has also been shown to prevent (fulvestrant and anastrozole) and treat (tamoxifen) PAH in BMPR2 mutant mice (Chen et al., 2017b).

Another example of sex differences in PAH can be seen in the mutations for the BMPR2 gene. Females are found to have a higher penetrance of the BMPR2 mutation (40%) versus the males (14%) (Austin et al., 2009, Morris et al., 2021). E2 signalling has also been correlated with reduced BMPR2 function in normal PASMCs without BMPR2 mutation and drives a pro-proliferative phenotype in the PASMCs (Mair et al., 2015), suggesting that E2 may predispose women to PAH and promote the development of PAH. As a whole, this can be referred to as the sex paradox in PAH.

1.4.1 Estrogen

Estrogen serves as one of the major sex hormones in the female body. There are three different types: estrone (E1), estradiol (E2) which also exists in two different isoforms, 17αE2 and 17βE2 and estriol (E3) (Cui et al., 2013). During a lifetime, the levels of each estrogen will fluctuate significantly. Within healthy males aged between 26-77 years, the normal circulating E2 level is 43-113 pmol/L (Vesper et al., 2014). In pre-menopausal women, E2 is the most predominate estrogen, with its concentrations varying depending on the oestrous cycle, in which normal ranges usually sit between 275-1650 pmol/L and in post-menopausal women this falls to <40 pmol/L. Given that the E2 levels are significantly reduced within post-menopausal women, they instead experience higher levels of E1 (Mendelsohn and Karas, 1999). Meanwhile, E3 is the dominating circulating estrogen in pregnant women, although their E2 levels can increase to as much as 26 nmol/L (Cui et al., 2013, Baird et al., 2021).

1.4.2 Estrogen synthesis

The estrogens are synthesised from cholesterol, which takes place predominately in the ovaries, placenta and to a lesser extent in the skin, liver, adipose tissue and brain (Cui et al., 2013). Cholesterol will undergo a series of reactions mediated largely by members of the

cytochrome P450 family (Tofovic, 2010) (Figure 1.9). Firstly, it will be converted into pregnenolone via CYP11A1. This will then be followed by CYP17A1 to dehydroepiandrosterone (DHEA) or 3β-hydroxysteroid dehydrogenase (3βHSD) to progesterone which is then converted into androstenedione (Lahm et al., 2014). This serves as an intermediate which can be converted via CYP2C11 into 16α-hydroxyandrostenedione or by 17β-hydroxysteriod dehydrogenase type 3 (17βHSD3) into testosterone. E1 can then be formed by CYP19A1, otherwise known as aromatase, catalysing androstenedione (Lahm et al., 2014). As a result of E1, this can be transformed into 17β-oestradiol by 17βHSD1 or into 16α-hydroxyestrone by CYP1B1 which can then go onto form E3. At the same time, E3 can be formed by aromatase catalysing 16α-hydroxyandrostenedione. Finally, 17β-oestradiol can be formed by the activity of aromatase catalysing testosterone (Lahm et al., 2014).

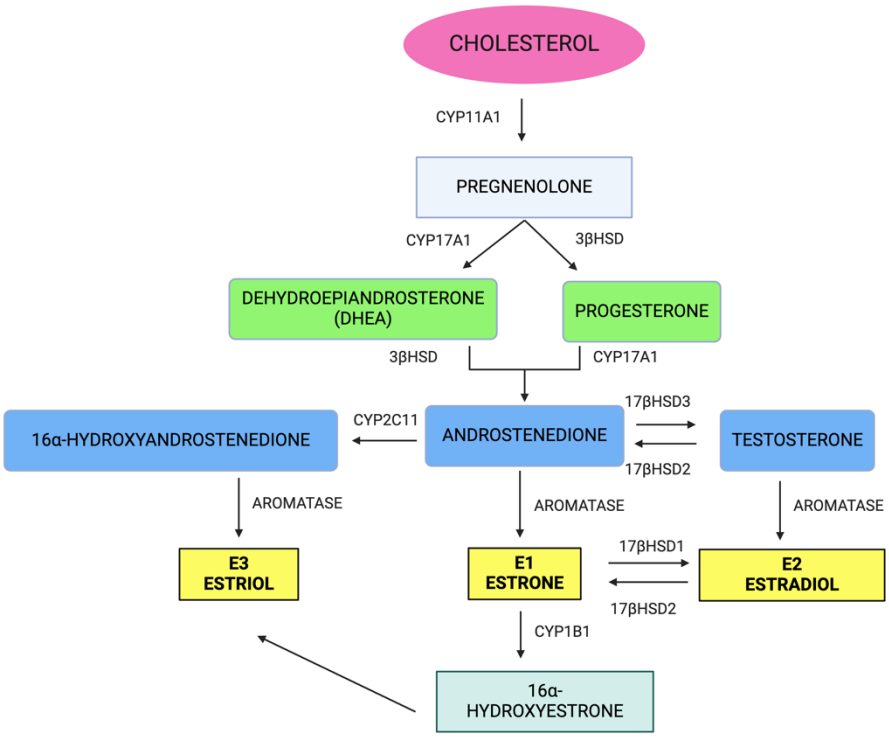

Figure 1.9. The synthesis of E1, E2 and E3

Cholesterol serves as the precursor molecule which is converted into pregnenolone via the cytochrome P450 (CYP) enzyme, CYP1A1. The remainder of the reactions are also catalysed predominately by the CYP enzymes. Pregnenolone is biotransformed into either dehydroepiandrosterone (DHEA) or progesterone and then into androstenedione. This serves as an intermediate which can be directly converted into: estrone (E1) via aromatase, estradiol (E2) via conversion into testosterone or estriol (E3) via conversion into 16α-hydroxyandrostenedione. Figure created with BioRender.com.

1.4.3 Estrogen receptors

Once synthesised, estrogen will mediate its signalling through coupling to one of its three receptors: ERα, ERβ (which belong to the type 1 nuclear receptor family) and the g-protein-coupled estrogen receptor (GPER). ER have been found to reside in the nucleus, mitochondria, cytoplasm and plasma membrane as an extra-nuclear receptor (Revankar et al., 2005, Levin and Hammes, 2016). Meanwhile GPER is expressed in the plasma membrane as well as in the endoplasmic reticulum (Thomas et al., 2005) (Figure 1.10). The estrogen receptors have been found to be present within cardiac cells including the cardiomyocytes, fibroblasts and endothelial cells (Luo and Kim, 2016). Estrogen will diffuse into the cell where it will then locate the ER and this will lead to detachment of the HSP protein and trigger receptor dimerization. Here, they interact with chromatin at specific DNA sequences known as estrogen response element (ERE) or transcription factors (AP-1, STATs, Elk-1, CREB, NF-κB, Sp-1 and ATF-2) which can lead to transactivation or transrepression of gene expression (Zimmerman et al., 2016, Fuentes and Silveyra, 2019). These effects will usually take hours or several days to occur, which can be defined as genomic activity (Liu et al., 2018). Meanwhile, the extra-nuclear ER can mediate both genomic and non-genomic activity (Fuentes and Silveyra, 2019). A great deal remains unknown regarding how these receptors travel to the plasma membrane, although it does appear to require palmitoylation. Once at the membrane, these receptors work in a G-protein coupled receptor (GPCR) manner by signalling through associated GPCRs such as GPER1 and mGluRs (Klinge, 2008, Krentzel et al., 2021). The non-genomic actions involve activation of four signalling pathways: 1) cAMP/protein kinase A, 2) the phospholipase C (PLC)/protein kinase C, 3) the Ras/Ras/MAPK pathway and 4) the phosphatidylinositol 3-kinase (PI3K)/Akt signalling pathway (Fuentes and Silveyra, 2019). Once at the plasma membrane, ERα and ERβ can also indirectly signal through the genomic pathway. This occurs when the protein kinases can phosphorylate transcription factor particularly, Elk-1, CREB and NF-κB allowing the ERα and ERβ to indirectly regulate gene transcription (Fuentes and Silveyra, 2019). Hence, the extra-nuclear ER can also allow estrogen to influence gene expression without binding to the cytosolic ER through the classical nuclear translocation pathway. GPER was first identified following when studies inhibited ERα and ERβ and found that it did not abolish the effects of estrogen, indicating that

there was another receptor present (Li et al., 2000, Ullrich et al., 2008). Unlike ERα and ERβ, GPER is not able to bind to transcription factors and cannot directly regulate gene expression. However, it may be able to influence the genes indirectly via activating particular proteins that can then influence transcriptional activity (Romano and Gorelick, 2018).

In PAH, ERα has been reported to be highly expressed, especially in the PASMC in females, meanwhile ERβ is markedly increased in the PASMC of PAH male patients (Wright et al., 2015). The increased levels of ERα activates the extracellular signal-regulated kinase (ERK)/mitogen activated protein kinase (MAPK) and phosphatidylinositol 3-kinase (PI3K)/Akt signalling pathway which drives pro-proliferation within the PASMC and hence, pulmonary remodelling (Wright et al., 2015). Meanwhile, the role of ERβ has generated a protective status due to its anti-proliferative activity (Warner and Gustafsson, 2010). ERβ knockout mice have also exhibited increased mortality, and abnormal vascular function (Zhu et al., 2002). Due to this, previous studies have employed ERβ agonists in male MCT rats and found that it mediates protective activity by restoring lung and RV function and structure (Umar et al., 2011). E2 therapy was not able to achieve these same results in the presence of a ERβ antagonist, suggesting that E2 rescue action is likely mediated through ERβ (Umar et al., 2011).Alternatively, the GPER receptor is responsible for the rapid (occurring over seconds to minutes) non genomic effects as a result of binding to estrogen (Liu et al., 2018). This activation has shown to facilitate vasodilation as it stimulates the release of endothelial NO, inhibits calcium channels whilst increasing the opening state of the potassium channels (Liu et al., 2018). At the same time, it can counteract vasoconstriction by inhibiting the potent Ang II levels (Lindsey et al., 2014). Indeed, mice with GPER deficiency have increased production of endothelial prostanoid thereby enhancing vasoconstricting activity (Meyer et al., 2012). These findings do predict that GPER could serve as a protective factor in PAH. In support of this, GPER mutations have also been correlated to obesity, cardiovascular dysfunctions, insulin resistance and glucose intolerance (Prossnitz and Hathaway, 2015).

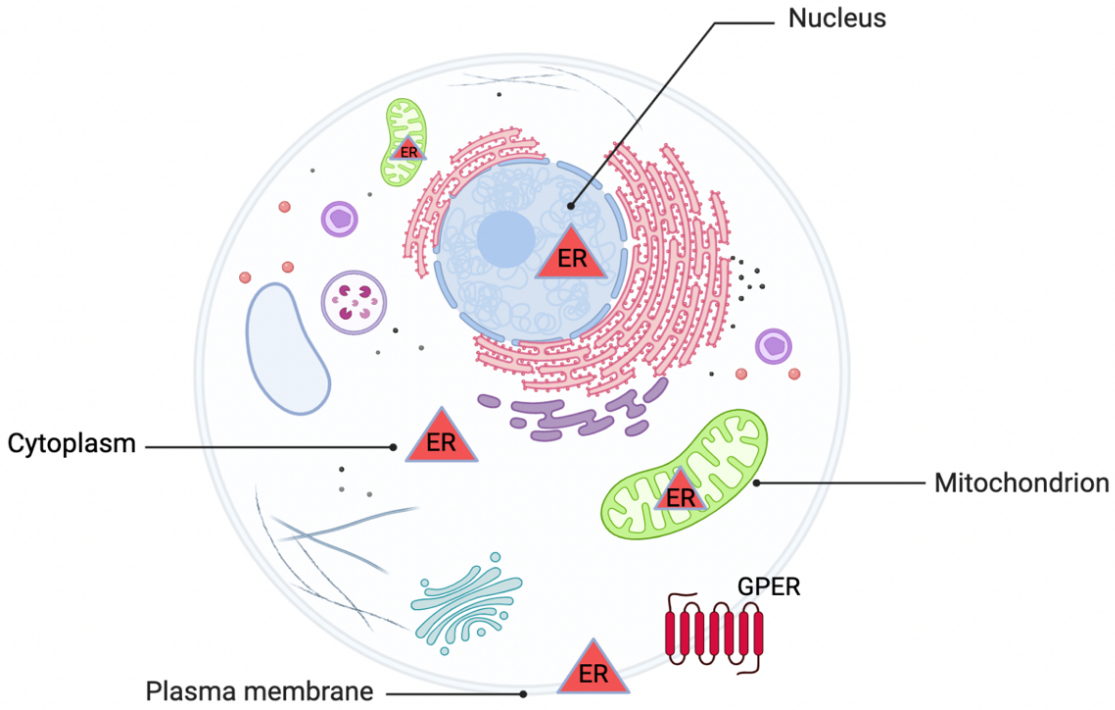

Figure 1.10. Location of the estrogen receptors

Estrogen receptor ERα and ERβ have been found to reside in the nucleus, cytoplasm, mitochondria and plasma membrane which belong to the type 1 nuclear receptor family. Meanwhile, extra nuclear receptor G protein coupled estrogen receptor (GPER) is expressed in the plasma membrane. Figure created with BioRender.com.

1.4.4 Estrogen in the pulmonary vasculature

Within human PAH patients, several lines of research point towards E2 contributing to the progression of PAH given its higher prevalence in the females (Hester et al., 2019, Hye et al., 2021). Studies have also shown in males that have higher circulating E2 levels, there is a greater risk of developing PAH (Ventetuolo et al., 2016, Kawut et al., 2024). To solve this, patients were treated with an aromatase inhibitor, known as anastrozole to block the conversion of E2, and thereby reduce the circulating E2 levels (Kawut et al., 2024). Aromatase expression has been detected within the smooth muscle layer of the pulmonary arteries from both male and female control and PAH patients (Mair et al., 2014b). Anastrozole was found to increase the 6-minute walk distance (6MWD) in a phase II randomized clinical trial (ClincialTrials.gov identifier: NCT03229499 and NCT01545336) at the six months' time point, meanwhile the placebo group had a reduced 6MWD (Kawut et al., 2024). As well as this, estrogen receptor modulator (SERM), tamoxifen has also been recruited in a clinical trial of PAH patients to antagonise estrogen production (ClinicalTrials.gov identifier: NCT03528902) with results yet to be posted. When E2 is given exogenously in animal models of PH, it can exhibit both protective effect as well as pathogenic effects within the pulmonary vasculature (Yuan et al., 2013, Lahm et al., 2014). One of the first animal studies to establish E2 protection was on ovariectomized hypoxic PH female rats, which produced a 10-20% worsening of hemodynamic parameters, remodelling and erythropoiesis which was subsequently alleviated by replacement of E2 (Resta et al., 2001, Earley and Resta, 2002, Xu et al., 2010). Since, studies have found that treatment of E2 decreased vascular endothelial growth factor secretion and cell proliferation within the lungs of hypoxia induced PH male rats (Lahm et al., 2012). Similarly, another study demonstrated application of E2 suppressed PASMC proliferation in chronic hypoxia male rats (Xu et al., 2010). In a study using male MCT rats, E2 was found to repair lung structure and function by restoring the loss of blood vessels (Umar et al., 2011). The increased protection mediated by E2 in the animal models of PH could represent that in human PAH there is altered E2 signalling. However, studies inhibiting endogenous estrogen synthesis using anastrozole and metformin has also shown to attenuate pulmonary hypertension as mentioned in section 1.4. The controversies in E2 signalling, expression, and metabolism between both human PAH and PH animal models require further investigation.

1.4.5 Estrogen in the RV

Whilst it is unknown whether E2 exerts protective or pathogenic effects in the pulmonary vascular system (PVS), it is believed to be beneficial in the context of the RV. This stemmed from increased estrogen levels correlating to higher right ventricle ejection fractions (RVEF) which is linked to improved survival in females (Ventetuolo et al., 2011). This in turn, improves RV contractility without increasing afterload pressure thereby enhancing ventricular-vascular coupling efficacy (Liu et al., 2017). In addition, repletion of E2 in rat models of PAH reduced RV apoptotic signalling, oxidative stress, dysfunctional mitochondrial and expression of pro-inflammatory cytokines. This attenuated RV hypertrophy and improved RV function under both rest and exercising states (Frump et al., 2015).

Another study demonstrated that ERα is protective in female PAB rats, meanwhile female KO ERα exhibit poorer RV function. Whilst the WT female rats RV function is preserved and protected from RV-vascular uncoupling, diastolic dysfunction and fibrosis from the PAB RV pressure overload (Cheng et al., 2020). Additionally, a previous study found that female rats which were depleted in estrogen had reduced PGC-1α expression which as a result reduced mitochondrial volume density (Scarpulla, 2011). Estrogen repletion was then able to preserve RV PGC-1α expression and hence, mitochondrial content (Liu et al., 2017). As a result of normal mitochondrial function, this enabled for better RV contractility (Hsieh et al., 2005, Liu et al., 2017). Currently, there is only one ongoing clinical study which is the first to examine the effect of E2 precursor DHEA on RV function in a group of PAH patients (ClincialTrials.gov identifier: NCT03648385).

1.4.6 The effects of estrogen on mitochondrial function

Estrogen can affect the mitochondria both indirectly via targeting the nucleus or directly by regulating the expression of mitochondrial genes (Figure 1.11). Indirect modulation occurs via ER binding to the ERE, activator protein 1 (Ap1) and specificity protein 1 (Sp1) of genes in the nucleus (Iorga et al., 2017). Here, they have been found to upregulate PGC-1α which induces NRF1 expression and this stimulates an increase in mitochondrial respiratory complex (MRC) genes, mitochondrial transcription factor A (TFAM), mitochondrial transcription factor B (TFB1M and TFB2M) which are then imported to the mitochondria (Klinge, 2008). This

upregulates ETC oxidative phosphorylation and mtDNA transcription, thereby enhancing mitochondria biogenesis (Klinge, 2008). However, the increase in mitochondrial number and size has found to be cell specific (Irwin et al., 2008, Klinge, 2008, Rosario et al., 2009). For instance, there was no increase in mitochondrial biogenesis following E2 treatment found in ovariectomized rats brain cells (Irwin et al., 2008).

This binding of ER to E2 responsive genes in the nucleus is the long-established mechanism regarding estrogens actions. However, both ERα and ERβ have been detected within the mitochondria, with ERβ accounting as the main receptor (Yang et al., 2009). Interestingly, these receptors appear to be derived from the same genes which code for nuclear ERα and ERβ. This finding comes from an ERα/β knockout study which showed complete absence of mitochondrial ER in the knockout mice (Pedram et al., 2006). Within MCF7 cells, the receptors were identified in the mitochondrial matrix, however it is likely that the localisation of the ER will vary depending on the cell type (Chen et al., 2004). Activation of these receptors via binding to ER can directly influence mtDNA gene transcription and function. It has been proposed that these effects are mediated via the plasma membrane ER receptors due to conformational changes, rapid increases in cytosolic calcium and cAMP levels elicited upon activation, although this does require further investigation (Improta-Brears et al., 1999, Velarde, 2014). Exogenous estrogen treatment has shown to increase the levels of ETC cytochrome c and complex IV subunits and reduce ROS expression (Razmara et al., 2007). This repression in ROS was due to estrogen binding to ER and activating MAPK and NF-κB thereby enhancing manganese superoxide dismutase (MnSOD) activity (Razmara et al., 2007). As MnSOD is a major mtROS scavenger, this illustrated estrogens protective activity upon mtDNA, however whether this plays a significant role remains undetermined.

Within the human mitochondrial genome, there has been a variety of partial ERE sites detected in genes: cytochrome oxidase (CO) II, 7S rRNA, 12S rRNA, D-loop region, tRNA-met, unidentified reading frame 1 and 5 (Felty and Roy, 2005). Similarly, in the rat genome they have been found in genes: CO I, CO II, tRNA-gln, CO b, URF 4, URF5, 12S rRNA, 16S rRNA and D-loop region (Felty and Roy, 2005). Estrogen treatment has shown to enhance mitochondrial gene transcription, demonstrated by a 3- to 16-fold increase in CO II following E2 treatment (Van Itallie and Dannies, 1988). The mechanism by which E2 achieves this remains unclear,

however it is possible that the partial ERE may be responsible. As well as regulation of transcription, estrogen has also been found to modulate the mitochondrial proteins. This was revealed by E2 regulating FoF_1 ATP synthase activity via binding to oligomycin sensitive-conferring protein (Moreno et al., 2013).

Alongside ATP production, the mitochondria also serves as the site for estrogen biosynthesis as it contains many of the required enzymes (Velarde, 2014). Even when estrogen is administered exogenously it is preferentially translocated to the mitochondria. The high fluidity of the mitochondria membranes and lipophilic nature of E2 allows for it to diffuse easily into the mitochondria. Thus, the mitochondria essentially act as an "estrogen sink" (Moreno et al., 2013). Once in the mitochondria, E2 has shown to selectively bind to ERE in the D-loop region in both human and mouse mtDNA (Felty and Roy, 2005, Klinge, 2008). On the other hand, estrogen helps to maintain low levels of ROS thereby preventing mitochondrial damage. If the mitochondrial does become damaged this will inhibit estrogen biosynthesis leading to a decline in estrogen levels and an increase in ROS production which would further accelerates mitochondrial dysfunction (Velarde, 2014).

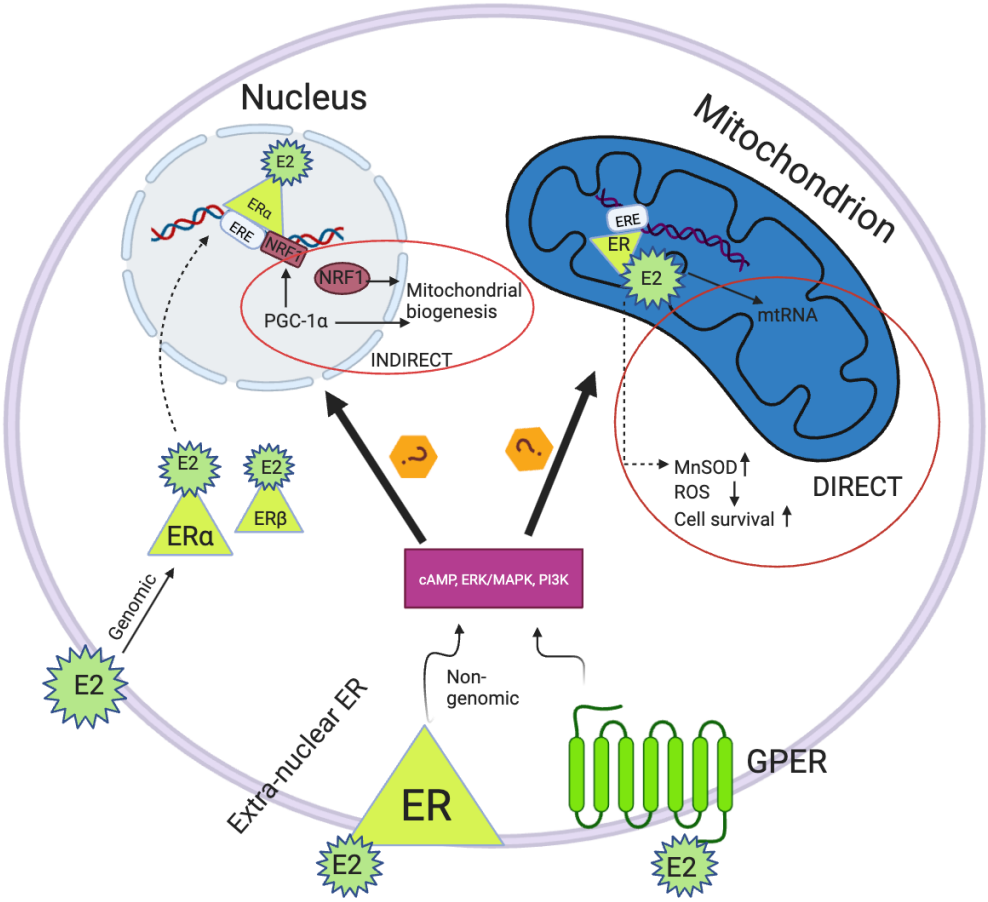

Figure 1.11. Effects of estradiol on mitochondrial function

Genomic activity: estradiol (E2) diffuses into the cell and locates the estrogen receptor (ER) in the cytoplasm, where it undergoes dimerization. In the genomic activity, the ERs are then translocated to the nucleus where they bind to the estrogen responsive element (ERE) and regulate expression of transcription factors including nuclear respiratory factor 1 (NRF1). Concomitantly, peroxisome proliferator-activated receptor-gamma coactivator 1-alpha (PGC-1α) expression is enhanced and together this stimulates mitochondrial biogenesis which is responsible for the indirect effects upon mitochondrial function. Direct effects of E2: E2 binds to ER within the mitochondria and induces an increase in mitochondrial RNA (mtRNA) activity and manganese superoxide dismutase (MnSOD) and reduces reactive oxygen species (ROS) generation. Non-genomic activity: E2 binds to extra-nuclear ER and G-protein coupled estrogen receptor (GPER) activating cyclic adenosine monophosphate (cAMP), extracellular signal regulated kinase / mitogen activated protein kinase (ERK/MAPK) and phosphoinositide 3-kinase (PI3K). Figure created with BioRender.com.

1.4.7 Sex differences in mitochondrial function

Mitochondrial function differs between the sexes. It has been reported that women exert greater mitochondrial respiration compared to men with similar VO_{2max} (Farhat et al., 2017, Cardinale et al., 2018). Above all, when the mitochondria reach dysfunctional it contributes significantly to PAH development. One study which investigated the impact on mtDNA mutations in both female and male mice with hypertension, found that the mutations have a greater impact on the males (Golob et al., 2015). The male mice demonstrated significant increases in arterial diameter, aortic pressure, ventricular pressure, E_a and left circumflex coronary arteries velocity (Golob et al., 2015). Meanwhile, in female mice there was no significant increases in pressures and arterial stiffening detected. The protective mechanism in the female mice is proposed to be partially estrogen mediated (Golob et al., 2015).

A housekeeping gene, 16S rRNA which reduces overtime with age was found to be increased four-fold in female versus male rats of the same age (Borrás et al., 2003). As this is an indicator of cellular aging, this implies that female mitochondria behave as though they are younger than the male mitochondria (Borrás et al., 2003). The same study also found that mtDNA oxidative damage is four times higher in male rats compared to female (Borrás et al., 2003). This was explained by the higher expression and activity of mitochondrial antioxidant enzymes glutathione peroxidase and MnSOD in the females. These were confirmed to be more than double when compared to the males of the same age (Borrás et al., 2003).

1.4.8 Sex differences within the RV mitochondrial function in PAH

Within PAH, clinical studies have shown that the mitochondria become dysfunctional, however the underlying sex differences have not been examined likely due to the limited number of PAH patients. Although, as described above, sex does indeed play a role in mitochondrial function, and it is proposed that females will exert better mitochondrial function within the RV in PAH. One study showed that female SuHx rats which underwent an ovariectomy reduced mitochondrial density and PGC1α protein expression levels which was associated with impaired mitochondrial and RV function (Liu et al., 2014). Treatment with exogenous E2 prior to PH induction preserved the PGC1α level and restored mitochondria and RV function (Liu et al., 2014). The differences between the exogenous and endogenous

E2 on mitochondria function remains unclear. As well as this, it also remains unclear if the better mitochondria and RV function is largely due to E2 activity.

1.5. Animal models of pulmonary hypertension

It has been discovered that the sex differences that occur in humans, are similar to that of animals. Female rats present with a less severe PH phenotype due to better RV adaptation and lower PAP than the males following chronic hypoxia induced PH (Rabinovitch et al., 1981). However, the female preserved PH status is abolished following ovariectomy suggesting that estrogen may be protective against PH (Earley and Resta, 2002). As with the chronic hypoxia model, female sex also appears to be protective in the monocrotaline model (Umar et al., 2011). However, the female sex is not always favored in the animal models of PH. Female mice presenting with an overexpression of the serotonin transporter SERT+, developed severe PAH which was attenuated by ovariectomy whilst the males SERT+ mice remained unaffected (White et al., 2010). Hence, as with humans, the effects of estrogen can also be dimorphic in the animal models of PH. We chose to utilize animal work into this project as it serves as an invaluable tool for discovering the mechanisms of PH and its dimorphisms between the two sexes. Within PH, there has been the development of various animal models (Table 1.4). Despite this progression, there still remains to be a model developed which fully mimics the PH characteristics that is seen in humans. Table 1.4 highlights some of the major PH models which have been commonly used over the years, although it must be noted that not all of the models are listed.

1.5.1 Monocrotaline model

The monocrotaline (MCT) model, derived from the plant *Crotalaria spectabilis* seeds was first found to induce PH in rats in 1967 (Maarman et al., 2013). Nowadays, the alkaloid agent from the plant will be injected into rats at a single subcutaneous dosage of (60-80 mg/kg) (Maarman et al., 2013). This induces PASMC proliferation together with RV hypertrophy (Wu et al., 2022). Alongside this, MCT will also induce hepatoxicity, myocarditis, renal insufficiency and lung injury therefore its effects are not completely in line with PH as seen in humans (Wu et al., 2022). The MCT model produces the most profound myocarditis and as a result the MCT model has been critiqued for its toxicity, which has sparked concerns regarding animal

welfare. As well as this, the MCT has yet to be confirmed to be able to recapitulate some of the PH features (RV hypertrophy and PA remodeling) in the female rats, perhaps due to the protective effects of estrogen or the differences in the metabolism (Long et al., 2022). Therefore, making this an unfavorable model for studying the sex differences. In the male rats, there is also the absence of the angio-proliferative lesions in the lungs similar to the plexiform lesions in humans (Dignam et al., 2022)

1.5.2 Sugen-hypoxia model

The Sugen-5416 hypoxia (SuHx) model involves either a single or weekly subcutaneous injection (20-25mg/kg) of a vascular endothelial growth factor receptor (VEGF) 1/2 antagonist (Sugen) followed by 3 weeks in hypoxia (Vitali et al., 2014). Once returned to normoxia (for a minimum duration of 3 weeks), the SuHx model will continue to worsen. The SuHx model is best recapitulated within the rat species rather than the mice. The first study to test SuHx in mice, illustrated that it did indeed provide some PAH hallmarks but did not mimic the severity of PH (Ciuclan et al., 2011). It was found that the mouse model did not present with obliterative angiopathy and the PA remodeling and RV hypertrophy reverted to normal after exposure to normoxia preventing it from progressing to RV failure (Vitali, 2019). Thus, the rat model is thought to best represent the pathological changes that occur within the pulmonary vasculature. This is seen via the VEGF receptor antagonist inducing endothelial cell apoptosis that eventually leads to progressive proliferative endotheliopathy, causing angio-obliterative lesions to develop (Vitali et al., 2014). These lesions develop during the normoxia period and are similar to the plexiform lesions that are seen in human PH patients, which do not form in the MCT model. Therefore, SuHx model can be deemed as a sustained and progressive model, which cannot be confirmed for the other models.

1.5.3 Pulmonary artery banding model

The pulmonary arterial banding (PAB) model focuses entirely on the RV failure response, rather than the pulmonary aspect of the disease. It is appealing as it minimizes toxicity and the need for hypoxia (Akazawa et al., 2020). This model has a real advantage given that RV therapies are the most in demand when it comes to PH therapy/treatment (Akazawa et al., 2020). Additionally, it can be performed on both mice and rats. This is where the pulmonary

artery is banded via a clip or a silk suture, with the level of constriction altered accordingly (Mamazhakypov et al., 2021). Once the clip/suture is put in place and tied the constriction will then remain fixed. Typically, animals will be maintained for ~5 weeks which should be sufficient time to produce an increase in RV pressure load (Akazawa et al., 2020). The greater the constriction the more severe the outcome, with severe constriction groups resulting in high mortality rates (Borgdorff et al., 2015).

1.5.4 Chronic hypoxia model

Lastly, the chronic hypoxia (CH) model involves exposure to 10% O_2 for 3-4 weeks in the hypobaric chamber (Wu et al., 2022). This has shown to induce muscularization of the small pulmonary arteries and veins as well as apoptosis of endothelial cells (Wu et al., 2022). Alterations in the RV are limited with the CH model, with only signs of RV hypertrophy occurring and minimum evidence of RV failure (Stenmark et al., 2009). As well as this, analysis of the CH is limited as upon return to normoxia the CH model will slowly start to undergo reversal of the pathological changes (Wu et al., 2022). Both rats and mice can be used for this model, although the key features that lead to pulmonary remodeling are less pronounced in the mouse model (Maarman et al., 2013). Thus, the CH model is a suitable model for less severe PH.

Although, most studies will typically use one model, it is recommended to utilize them all prior to proceeding to human studies (Akazawa et al., 2020). Nonetheless, each animal model has aided our understanding in PAH significant amounts.

Table 1.4. List of pulmonary hypertension (PH) animal models

Model	**Species**
Monocrotaline	Rats
Sugen-hypoxia	Rats
Pulmonary artery banding	Rats/Mice
Chronic hypoxia	Rats/Mice

1.6 Treatments of PAH

As it stands, there is no cure for PAH. Although, over the years there has been a significant improvement in PAH research leading to the implementation of a variety of medications. However, prior to use in PAH, these medications were initially developed for systemic vascular disease and therefore do not address PAH specific mechanisms (Dromparis et al., 2010). These are categorised into four different classes: endothelin-1 receptor antagonists (ETRA), prostanoids, soluble guanylate cyclase (sGC) and phosphodiesterase (PDE) 5 inhibitors (Humbert and Ghofrani, 2016) (Table 1.5). Additionally, patients will also be recommended to take calcium channel blockers, however these are believed to only benefit up to 5% of PAH patient long termly (Medarov and Judson, 2015). All these drugs overlap in that their main mechanism is to achieve vasodilation in the pulmonary arteries.

Following clinical severity assessments, if a patient can be classified as low risk, it is recommended that they will be treated using monotherapy (Galiè et al., 2016). If there is an inadequate response, or if the patient is at a more advanced stage of the disease, combinational therapy can be used as this has shown to produce a greater clinical outcome (Galiè et al., 2016). This will typically involve duo-therapy, for instance, prostanoid epoprostenol combined with ETRA bosentan (Kemp et al., 2012). A clinical trial which took place in 2020 directly compared triple oral therapy (selexipag, macitentan and tadalafil) with double oral therapy (macitentan, tadalafil and placebo) in patients with newly diagnosed PAH (TRITON study; NCT02558231). They demonstrated marked improvements in hemodynamic parameters, however no differences between the two groups. Although they did suggest that treatment with triple therapy (targeting three pathways) could slow down disease progression versus double therapy (Chin et al., 2021). As well as this, in order to prevent thrombosis and oedema from occurring, majority of patients will also be prescribed anti-coagulation medication and diuretics (Galiè et al., 2016). If all treatment options have been exhausted and prove to be ineffective, lung transplantation can be offered if the patient is deemed as a viable candidate (Long et al., 2011). Recently, a new line of treatment became available which is a first-in-class fusion protein, named Sotatercept (Humbert et al., 2021). Sotatercept was designed to trap members of the TGF-β signal transduction superfamily, including anti-proliferative BMPRII and pro-proliferative activin receptor type IIA (ActRIIA)

(Doggrell, 2023, Humbert et al., 2023). Inhibition of the TGF-β superfamily members has been found to promote inhibition of the excessive proliferation of the vasculature cells and enhance apoptotic signalling, thereby reducing the pulmonary vascular remodelling and inflammation (Yung et al., 2020, Andre et al., 2021, Joshi et al., 2022). Recently, Sotatercept passed the STELLAR phase III trial and was approved by the FDA for the treatment of PAH (March, 2024) in adults, sold under the brand name Winreviar (Kingwell, 2024). The results from the STELLAR trial following 24-weeks of treatment with Sotatercept on RV function demonstrated an improvement in haemodynamic parameters by reducing mPAP, RV work and power and overall improving cardiac function following RHC (Souza et al., 2023). Following echocardiography analysis, Sotatercept revealed an improvement in right ventricular-pulmonary artery coupling (RV-PA), a reduction in tricuspid regurgitation, an increase in RV fractional area change (RVFAC) and reduction in RV volume. Overall, Sotatercept does illustrate a substantial improvement on RV function (Souza et al., 2023). Extension studies are ongoing with Sotatcerpt regarding its safety and tolerability with the likelihood of being completed in 2027 (Kingwell, 2024). Nonetheless, this marks a huge milestone and breakthrough for the treatment of PAH.

In PAH, diagnosis usually takes place once the disease is well established. Therefore, treatment intervention works to target the structural and functional changes which have already taken place to prevent this from progressing, whilst also alleviating the patients' symptoms. The current pharmacological treatments have shown to increase survival rates; however, they cannot reverse the pathological pulmonary remodelling. Additionally, all these therapies target the vasoconstriction component, with no therapies targeting the RV directly. This is important as RV function is one of the main determinants of mortality. Thus, there is a great need for novel therapeutics which are able to reverse the pulmonary vascular remodelling as well as target the RV dysfunction.

Table 1.5. Current medications involved in the treatment of pulmonary hypertension (PAH)

(Humbert and Ghofrani, 2016, Humbert et al., 2022b, Souza et al., 2023)

Drug Class	Approved drugs	Route of administration
ET-1 receptor antagonists	Bosentan	Oral
	Macitentan	Oral
	Ambrisentan	Oral
Prostanoids	Epoprostenol	Intravenous
	Treprostinil Beraprost	Intravenous, oral, inhaled, subcutaneous
	Iloprost	Inhaled
PDE 5 inhibitors	Sildenafil	Oral or Intravenous
	Tadalafil	Oral
Calcium channel blockers	Amlodipine	Intravenous, oral
Guanylate cyclase stimulators	Riociguat	Oral
Activin signalling inhibitor	Sotatercept	Subcutaneous injection

1.6.1 Targeting the mitochondria in PAH

It is understood that targeting mitochondrial function may be essential in regressing PAH development. Particularly cells such as the cardiomyocytes rely on the mitochondria for almost 90% of ATP production (Piquereau et al., 2013). To date, studies have been carried out using a PDK inhibitor known as dichloroacetate (DCA) which has been able to improve the PH phenotype in the PAH animal models and improve symptoms in some PAH patients (Culley and Chan, 2018). Small interfering RNA (siRNA) has also been employed to reduce PDK expression which was able to normalize mitochondrial metabolism by restoring mitochondrial activity and improving normal cell phenotype (Yuan et al., 2016). The inhibition of PDK via siRNA approach and DCA promotes upregulation of PDH activity and restoration of oxygen consumption rate (OCR) (Tian et al., 2020a). This reduces mitochondrial fission, collagen production, stabilises rates of proliferation and apoptosis as well as reduces fibrosis (Tian et al., 2020a). Indeed, this lowers RV pressures, improves contractility and overall, RV function (Tian et al., 2020a).

A novel mitochondria tetrapeptide, elamipretide has been found to diffuse across the OMM and bind to cardiolipin in the IMM (Sabbah et al., 2016). Cardiolipin is almost exclusively found in the IMM, where it interacts with a myriad of proteins, enzymes and metabolite carriers involved in oxidative phosphorylation (Paradies et al., 2019). When elamipretide binds to cardiolipin it has shown to inhibit the cardiolipin-cytochrome c formation, reduce ROS generation and caspase-3 activation, consequently suppressing apoptotic pathways (Sabbah et al., 2016). At the same time, it enhances ATP synthesis, improving mitochondrial function and has been able to attenuate PAH induced by transverse aortic constriction (TAC) in mice (Lu et al., 2016a). Another drug which limits ROS production is an xanthine oxidase inhibitor, allopurinol. This is an FDA urate-lowering medication used in a variety of conditions and has been largely studied in cancer, with recent investigations underway in PAH. It has revealed to enhance myocardial efficiency and ameliorate hypoxia in rat PAH models (Badlam and Bull, 2017).

Additionally, there has been inhibitors developed which target members of the apoptosis inhibitor family, including YM155 which inhibits survivin expression. Survivin localizes itself to the mitochondria and is highly expressed in PAH animal models (Dohi et al., 2004). Conversely, it is usually undetectable in non-PAH tissue and therefore also serves as a valuable PAH marker. YM155 treatment in a PAH animal model has demonstrated to reverse the proliferation stimulated by hypoxia and upregulate apoptosis (Zhang et al., 2016). Similarly, another study revealed that YM155 treatment reduced right ventricular systolic pressure (RVSP) and RV hypertrophy (Blanco et al., 2019).

The fatty acid oxidative (FAO) pathway has also been targeted to promote activation of PDH via the randle cycle. Trimetazidine, an FAO inhibitor leads to improved glucose oxidation and has been studied in a PAH context. Here, they found an increase in glucose oxidation which lead to improved RVEF and capacity (Sakti Muliawan et al., 2020). Another FAO inhibitor, ranolazine has demonstrated therapeutic benefits in PAH animal models in which it attenuated monocrotaline induced PAH and RV dysfunction (Liles et al., 2012). Ranolazine studied amongst symptomatic PAH patients was found to be safe, well tolerated and able to reduce RV size and improve systolic function (Khan et al., 2015, Gomberg-Maitland et al., 2015). Both trimetazidine and ranolazine are already approved for use in the treatment of angina and have undergone clinical trials for use in PAH. However, neither yielded success as they did not reach within the therapeutic range due to potential under-dosing, heterogeneity of patients, differences in PAH severity and the multitude of background therapies (Gomberg-Maitland et al., 2015, Sitbon et al., 2019).

Inhibition of NFAT by VIVT or cyclosporine has shown to depolarise the mitochondrial membrane potential which leads to efflux of cytochrome c, increase in ROS production and apoptosis (Dromparis et al., 2010). In the monocrotaline rat model, this reversed both pulmonary remodelling and RV hypertrophy (Bonnet et al., 2007, Chen et al., 2017a). Therefore, NFAT inhibition could be a useful therapeutic strategy in human PAH. Initially, targeting mitochondria metabolism was studied for cancer therapy, with it only recently emerging as a PAH target. Although, it is doubtful that targeting a single

mitochondrial pathway will be able to attenuate PAH, instead, approaches which target downstream/upstream multifactorial signalling pathways will be necessary.

1.6.2 Mitochondria targeted MitoQ as a potential therapeutic in PAH

Mitoquinone (MitoQ) composed of coenzyme Q 10 and lipophilic triphenylphosiumcation (TPP^+) works as a mitochondrial targeted antioxidant drug (Figure 1.12) (Gottwald et al., 2018, Punetha et al., 2023). The lipophilic TPP^+ cation makes it possible for MitoQ to enter into the mitochondrial IMM by passing easily through the phospholipid bilayers where it can accumulate within the mitochondria (Pak et al., 2018). Once accumulated within the mitochondria, it is absorbed into the matrix surface of the IMM (Smith and Murphy, 2010). The active ubiquinol can be oxidised by ROS to the inactive ubiquone. Ubiquone will then be recycled to the active quinol form by complex II (Smith and Murphy, 2010). MitoQ has been confirmed to be protective against lipid peroxidation (Kelso et al., 2001, Asin-Cayuela et al., 2004). Additionally, it has shown promising results in isolated mitochondria, tissue, cells, and animal studies and has been utilised in many clinical trials to help in the treatment and symptoms of multiple sclerosis (ClincialTrials.gov identifier: NCT03166800), breast cancer (ClincialTrials.gov identifier: NCT05146843), severe viral illness (ClincialTrials.gov identifier: NCT05381454), asthma (ClincialTrials.gov identifier: NCT04026711), Parkinson's disease (ClincialTrials.gov identifier: NCT00329056), hepatitis C (ClincialTrials.gov identifier: NCT00433108), chronic kidney disease (ClincialTrials.gov identifier: NCT02364648), COPD (ClincialTrials.gov identifier: NCT05605548), ulcerative colitis (ClincialTrials.gov identifier: NCT05539625) and sickle cell anaemia (ClincialTrials.gov identifier: NCT04109820).

MitoQ has been tested in mice which underwent PAB or chronic hypoxic exposure for 4 weeks to induce PH. It was confirmed that MitoQ was protective against acute hypoxia induced increases in superoxide but not chronic hypoxia induced PH (Pak et al., 2018). MitoQ treatment did however reduce RV hypertrophy and dilatation in the chronic hypoxic mice (Pak et al., 2018). Similarly, MitoQ treatment reduced superoxide concentration within the RV and also attenuated RV dilatation and hypertrophy and as a result, prevented RV dysfunction following PAB (Pak et al., 2018). Male rats which were exposed to chronic hypoxia

for 4 weeks were treated with MitoQ prior to their placement in the hypoxia chambers. MitoQ had no effect on their body weight, attenuated RV hypertrophy and reduced RVSP (Yan et al., 2023). Rats which were placed into a hypoxia chamber for 15 days but exposed to intermittent short duration reoxygenation (three times for one hour per day) were treated with MitoQ during their reoxygenation period (Li et al., 2024b). They found that MitoQ reduced RVSP, the thickness of RV free wall and hence, RV hypertrophy index values, the thickness of the larger distal arteries and proliferation of the PASMCs (Li et al., 2024b). To date, there has been no studies directly testing MitoQ on SuHx animal models in both sexes, however there is one study which tests on primary microvascular endothelial cells (MVECs) extracted from male 4-month-old Wistar SuHx rats, which were placed into hypoxia for 3 weeks followed by 2 weeks in normoxia. MitoQ was found to attenuate migration and proliferation, Ca^{2+} entry induced by TRPV4 and mitochondrial fragmentation in SuHx MVECs (Suresh et al., 2019).

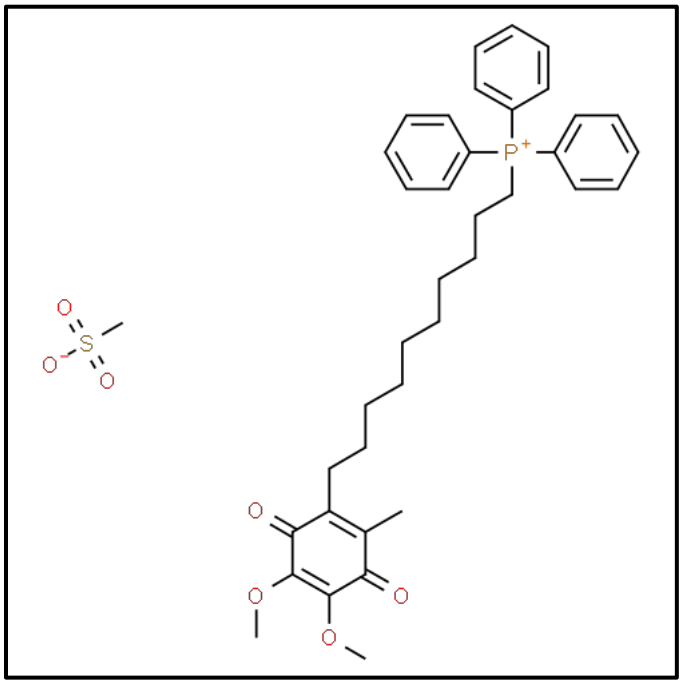

Figure 1.12. Chemical structure of Mitoquinone (MitoQ)

1.7 Hypothesis and aims

Mitochondria have been envisaged as a promising target given their crucial role in RV function and its clear suppression in PAH. Given that mitochondrial function is impaired in PAH, and that fibrosis and oxidative stress are exacerbated in the failing RV, we hypothesize that there is a sex difference in mitochondrial properties (dynamics, membrane potential and superoxide levels) in the RV in PAH and restoring mitochondrial function could restore normal cellular phenotype and improve RV function in PAH. To help us achieve this, we propose that reducing oxidative stress via a mitochondria-targeted antioxidant, MitoQ, will reduce RV fibrosis and hypertrophy and improve RV function in PAH via NFE2L2-ROS pathway. In addition, given that males demonstrate a worse PH status than the females, we propose that the effects we will see from MitoQ treatment will be more pronounced in males.

The individual aims are:

1. **Characterize sex differences in the SuHx PH rat model.** To characterize the SuHx rat model and examine the sex differences in hemodynamic parameters, RV hypertrophy and fibrosis (i.e., interstitial collagen deposition), and cell proliferation.
2. **Assess the sex differences in RV and lung mitochondrial function.** To examine the RV mitochondrial dynamics (fusion vs. fission), membrane potential, and superoxide production from male and female SuHx RV tissue. Additionally, we examine the mitochondrial genes linked to mitochondrial dynamics, membrane potential, and superoxide production from the rat RV and lung. We also examine whether SuHx influences RCA remodeling by examining the perivascular collagen deposition and intima-media thickness and the associated sex differences.
3. **Investigate the role of a mitochondria-targeted antioxidant drug, MitoQ, on human cardiac fibroblasts and male MCT RV fibroblasts *in vitro* and SuHx rats *in vivo***. To investigate the mitochondrial superoxide production using human cardiac fibroblasts exposed to hypoxia and treated with MitoQ and estradiol (E2). Similarly, we test MitoQ and E2 on male MCT RV fibroblasts and examine their collagen and NFE2L2 protein expression following treatment. We then follow up by directly treating SuHx rats *in vivo* with MitoQ and examining the benefits of MitoQ on RV function.

CHAPTER 2

2. Materials and Methods

2.1 Materials and chemicals

Table 2.1. List of materials and chemicals that were used in the experiments

Materials and Chemicals	Supplier	Catalogue number or RefSeqNumber
RNase-free DNase kit	Qiagen	79254
miRNeasy	Qiagen	217004
Stainless steel beads	Qiagen	69989
QIAzol lysis reagent	Qiagen	79306
SYBR green master mix	Thermo Scientific	10658255
Reverse transcription kit	Thermo Scientific	10117254
PCR 96 well plates	Thermo Scientific	10670986
96 well PCR seals	Thermo Scientific	11570274
PCR 384 well plates	Thermo Scientific	10005724
384 well PCR seals	Thermo Scientific	10567414
PBS tablets	Thermo Scientific	18912014
Hanks' Balanced Salt Solution (HBSS, without $Ca^{2+,}$ Mg^{2+})	Thermo Scientific	WD3187641
L-glutamine	Merck	G7513
Penicillin/streptomycin	Thermo Scientific	15140122
Fetal bovine serum	Lab tech	FB1001500
Tryspin	Thermo Scientific	R001100
UltraPure™ Distilled water DNAase/RNAase free	Invitrogen	2692477
RNAase Zap™	Thermo Scientific	01074932
ReliaPrep™ RNA cell mini prep system	Promega	0000574367

LUNA universal master mix	New England biolabs	10204127
HK2 primer	IDT	NM012735
PPARGC1A primer	IDT	NM031347
TFAM primer	IDT	NM031326
NRF1 primer	IDT	NM001100708
NRF2 primer	IDT	NM001108841
MFN1 primer	IDT	NM138976
ESR1 primer	IDT	NM012754
TSC22D1 primer	IDT	MN001109912
ESR2 primer	IDT	NM012754
HSP90aa1	IDT	NM175761
MFN2 primer	IDT	NM014874
DNM2 primer	IDT	NM013199
OPA1 primer	IDT	NM133585
NFE2L2 primer	IDT	NM031789
NQO1 primer	IDT	NM017000
SOD2 primer	IDT	NM017051
MAO-A primer	IDT	NM033653
LTBP2 primer	IDT	NM021586
TGFβ1 primer	IDT	NM021578
CTGF primer	IDT	NM022266
COL 1A1 primer	IDT	NM053304
COL 3A1 primer	IDT	NM032085
GAPDH primer	IDT	NM017008
20X TBS Tween™ 20 buffer	Thermo scientific	YD366733
NuPage SeeBlu™ plus 2 prestained standard marker	Invitrogen	2818371
Pierce™ BCA protein assay kit	Thermo scientific	WG327907

LDS NuPage sample buffer	Invitrogen	2394081
Transfer buffer (20X)	Novex by life technologies	2461350
NuPage™ SDS running buffer (20X)	Invitrogen	2683236
Antioxidant	Thermo Scientific	NP0005
SuperBlock™ T20 (TBS) blocking buffer	Thermo scientific	YB365093
PVDF membrane	Thermo scientific	SC2304912A
Bovine serum albium	Sigma Aldrich	9048468
Skim milk powder	Millipore	70166
Methanol	VWR	20847307
NuPAGE™ 4-12% Bis-Tris mini precast polyacrylamide gels 1.0mm x 10 well	Invitrogen	22020411
NFE2L2 antibody	Invitrogen	YJ3965233
GAPDH antibody	Abcam	AB8245
Anti-rabbit	Sigma	A0545
Pierce ECL western blotting substrate	Thermo Scientific	YF367056
Pierce RIPA buffer	Thermo Scientific	YC365115
Restore™ PLUS western blot stripping buffer	Thermo scientific	XJ357026
SU 5416	Tocris	204005469
Carboxymethylcelluose sodium	Sigma	9004324
HEPES	Sigma	SLBL2149V
Sodium chloride	Sigma	SZBE2100V
Polysorbate 80	Sigma	11211P12
Benzyl alcohol	Sigma	SHBK5943

Isoflurane	Covetrus	2800025
Formalin	Merck	HT50112
Millar pressure volume catheter	AD instruments	SPR869NR
MitoQ	Selleckchem	S8978
NucBlu	Thermo Scientific	R37605
MitoSox™ mitochondrial superoxide indicator	Thermo Scientific	2647630
MitoTracker™ green FM	Invitrogen	2301075
TMRM	Thermo Scientific	T668
13mm coverslips	VWR	6311578
Mr Frosty™ Freezing container	Thermo Scientific	51000001
Cryovials	Star lab	21121
Ki-67	Cell signalling	12075S
1.5ml centrifuge tubes	Star lab	K195636H
50ml falcon tube	Corning	30622006
15ml falcon tube	Corning	30022001
2ml centrifuge tubes	Eppendorf	0030120094
Penicillin-Streptomycin	Merck	P4458
17β-Estradiol	Merck	3301
T75 flask	Corning	14423038
T25 flask	TPP	20210196
BioLite™ 35mm cell culture treated surface petri dish	Thermo Scientific	130180
BioLite™ 60mm cell culture treated surface petri dish	Thermo Scientific	130181

Hypoxia incubator chamber	Stem cell technologies	27310
BioLite™ 100mm cell culture treated surface petri dish	Thermo Scientific	130182
Mitoquinone	Cambridge bioscience	CAY29317
Female human cardiac fibroblasts	Promocell	494Z0436
Male human cardiac fibroblasts	Promocell	479Z0181
Fibroblast growth medium 3	Promocell	C-23025
Growth medium 3 supplement mix	Promocell	C-39345
Phosphate buffered saline (PBS)	Gibco	2662260
TrypLE™ Express	Gibco	12604013
DMSO	Merck	D2650
Monocrotaline rat (male) RV fibroblasts	Kindly donated from Dr. Lian Tian post-doctoral study.	N/A
Dulbeccos Modified Eagle Medium (DMEM)	Gibco	2662099
Ethanol	Supelco	I1307083
Xylene substitute	Thermo Scientific	10524305
Picrosirius red	Abcam	Ab246832
H&E staining kit (Haematoxylin and Eosin)	Abcam	Ab245880
DPX	Merck	0652
Elastin stain (miller)	TCS	HS780

Van Gieson	TCS	HS780
Goat serum	Thermo Scientific	10098792
Square 22x22mm glass cover slip	Fisher Scientific	12363138
Histoclear	National Diagnostics	HS200
Biopsy cassettes	Thermo Scientific	11651210
Methanol	VWR	221234017
Eosin Y solution	TCS Biosciences	210103
Bovine serum albumin	Sigma-Aldrich	A9647
2-Mercaptoethanol	Sigma-Alright	M3148
Cell lysis buffer (10X)	Cell signalling	9803S
Triton X-100	Merck	T9284
Prolong gold antifade	Invitrogen	11569306
BLOXall blocking solution	Vector Laboratories	ZK0501
PCNA antibody	Abcam	Ab18197
Impact AEC substrate kit	Vector Laboratories	ZK0417
2.5% normal horse serum	Vector Laboratories	ZK0314
Aquatex	Sigma Aldrich	10856200
Square 40mm glass cover slip	Fisher Scientific	12363128
Square 50mm glass cover slip	Fisher Scientific	12373128
Superfrost™ plus adhesion microscope slides (25x75x1mm)	Epredia	101123-9
ImmPRESS HRP horse anti-rabbit IgG polymer kit	Vector laboratories	ZK0830
ImmPRESS HRP Horse anti-mouse IgG polymer kit	Vector laboratories	ZL0112
Citric acid	Fisher Scientific	BP339500

Sodium citrate	Fisher Scientific	1884595
Tween 20	Sigma Aldrich	9005645
Col1a1	Cell signalling	CST 91144S
E2	Merck	E2758
TFAM	Invitrogen	PA529571
NFE2L2	Invitrogen	PA588084
Ki-67	Cell signalling	CST12075S
488 goat anti-rabbit IgG	Invitrogen	A11034

2.2 Animal studies

2.2.1 Ethical approval

All animal studies were performed in the Strathclyde biological procedures unit (BPU) under the personal license numbers (I95560681) and (I97819091) and project license number (PP4061704) held by Dr. Lian Tian (University of Strathclyde, Glasgow). All experiments were approved by the Home Office UK in compliance with the Animals Procedures Act 1986.

2.2.2 Animal model of PAH

2.2.3 Animals

Male and female Sprague-Dawley (SD) rats were obtained from Envigo (Bicester, UK). Upon arrival to the BPU they were quarantined for at least 7 days to allow for acclimatisation prior to use in experimental procedures. All animals arrived at Strathclyde BPU at 6 weeks old, with experiments beginning at week 7 or 8. Rats were randomly assigned to treatment groups.

2.2.4 SuHx rat model of PAH

Both male and female SD rats received a single subcutaneous injection of SU5416 (25mg/kg) in line with the following literature (de Raaf et al., 2014, Labazi et al., 2023). Prior to injections rats were weighed, with females weighing between 150-170g and males between 180-240g. Sugen (25mg/kg) was dissolved in 0.5% carboxymethyl cellulose (CMC) (0.9% sodium chloride, 0.4% polysorbate 80 and 0.9% benzyl alcohol in dH_20). Male and female SD control rats received a single dose of vehicle (0.5% CMC) and remained in normoxia for up to 8 weeks.

Following Sugen injection, male and female SD rats were placed into the hypobaric chambers in their cages which had *ad libitum* access to food and water. The atmospheric pressure within the chambers was slowly dropped on the first day from 1000mbar to 750mbar at a rate of 50mbar every 30 minutes to allow the rats to acclimatise to the hypoxia. On the second day the pressure was further dropped from 750mbar to 550mbar. The pressure remained here (10% oxygen and 90% nitrogen) until the cages needed to be changed (once or twice weekly)

and then otherwise until the end of their time in hypoxia (approx. 3 weeks). The atmospheric pressure was increased in a similar rate of 100mbar at 30-minute intervals from 550mbar to 1000mbar when required. After the 3 weeks in hypoxia, rats were then placed in normoxia for up to 5 weeks (Figure 2.1).

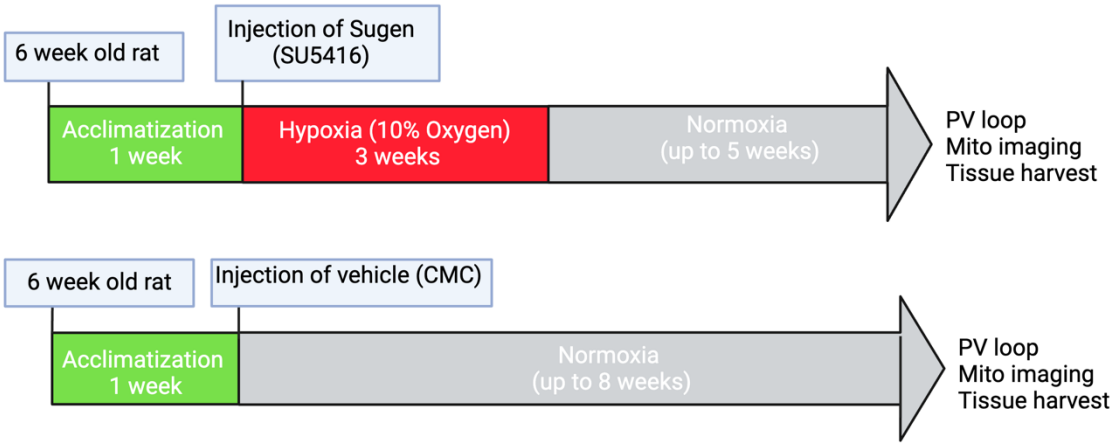

Figure 2.1. Schematic illustration of protocol timeline

Upon arrival to the SIPBS biological procedures unit (BPU) at 6 weeks old, male and female Sprague-dawley rats were given a subcutaneous injection of Sugen (SU5416) or vehicle and then exposed to hypoxia for 3 weeks followed by 5 weeks in normoxia or up to 8 weeks in normoxia. Rats were then hemodynamically assessed by obtaining pressure-volume (P-V) loop data and after the rats were sacrificed their tissues were collected for future downstream experiments.

2.2.5 SuHx rats treated with MitoQ

In a separate animal study, we followed the exact same protocol to achieve the SuHx induced PH rat model, with the rats placed into normoxia for up to 4-weeks, instead of the 5 weeks. During their 4 weeks in normoxia, rats were treated with a mitochondrial targeted antioxidant drug Mitoquinone (MitoQ; 5 mg/kg) twice weekly (commencing approximately one week after rats were placed into normoxia) via intraperitoneal (IP) injections. Control rats also received an IP injection of 5% dimethylsulfoxide (DMSO) in PBS, twice weekly. At the end of the 4 -weeks, rats underwent pressure-volume (PV) loop measurement and were sacrificed via anaesthetic overload with the heart and lung tissue harvested.

2.2.6 MitoQ preparation

Mitoquinone (MitoQ) (Sellekchem, MW = 678.8) was prepared by dissolving in PBS with 5% dimethylsulfoxide (DMSO) to obtain a working solution of 2.5mg/mL (5mg/kg) as based on the current literature (Chandran et al., 2009, Xiao et al., 2017, Li et al., 2024a).

2.2.7 *In vivo* pressure-volume measurement

The rats were placed into an induction chamber where they were anaesthetized by inhalation of 4% of isoflurane supplemented with O_2. Following successful induction of anaesthetic, the rats were weighed and the anaesthetic (3% isoflurane) was maintained via a face mask. The rats were placed in the supine position and the depth of anaesthetic was measured by pinching the toe prior to all experiments. Rats were then intubated via insertion of endotracheal tube to supply anaesthetic (3% isoflurane) in oxygen during the surgical procedure. The animals were also placed on a heat mat with a rectal probe to ensure their body temperature was within range (37.5°C to 37.8°C) during anaesthesia. Endotracheal intubations were carried out by either Dr. Lian Tian or myself.

The rats were anaesthetised and the fur was removed to allow for the skin to be exposed. A cut was made over the xiphoid cartilage. The cartilage was then used to guide the cut through

the chest wall in a lateral manner at both sides until the diaphragm was seen. The diaphragm was then cut through carefully until the heart became clearly visible. Forceps were used to remove any pericardium tissue attached to the heart. A 26-gauge needle was inserted directly in the RV to create an incision which was then removed. The Millar ultra-PV catheter tip (SPR-869NR; AD Instruments, Oxfordshire, UK) was inserted into the incision. Adjustment of the catheter was made until the PV loop remained stable. Once stabilised, the PV loop was then recorded for 10 minutes with the PowerLab 35 series data acquisition system with Labchart Pro. The same procedure was then applied to the LV. All PV loop measurements were performed by Dr Lian Tian.

2.2.8 Tissue harvest

After PV loop measurements were taken, rats were sacrificed via anaesthetic overdose (5% isoflurane), followed by the heart and lungs removed entirely. To ensure the measurements were only of the ventricles, the atria and connective tissue were removed. For some rats prior to tissue sectioning and storage, two very small fresh pieces of RV (less than 1% of the whole RV weight) were taken for confocal imaging immediately after tissue harvest. Then the RV and LV plus septum weights were recorded and Fulton index was calculated as the ratio of RV weight to LV+Septum weight. Three or four pieces of the RV and LV were then sectioned and snap-frozen in liquid nitrogen for quantitative polymerase chain reaction (qPCR) and western blot at a later date. Another piece of RV and LV+septum was fixed in 10% formalin in which it remained in for more than 2 days. Finally, four pieces of lung tissues from the right lung were sectioned and snap-frozen for use at a later date, whilst the left lung was perfused until the lung appeared fully inflated and fixed in 10% formalin for more than 2 days. All samples which were snap-frozen were then stored in the -80 freezer until future use.

2.2.9 Pressure-volume data analysis

Left ventricle systolic pressure (LVSP) and left ventricle end diastolic pressure (LVEDP) were obtained from the LV PV loop recordings. RV systolic pressure (RVSP), RV end diastolic pressure (RVEDP) and HR were obtained from the RV PV loop recordings. The pulmonary effective arterial elastance (Ea) was calculated as the RV end-systolic pressure divided by the

SV, which is an estimate of the pulmonary vascular load and hence, RV afterload. The RV end-systolic elastance (Ees) is a measurement of ventricular contractility and was estimated by the single-beat method (Takeuchi et al., 1991, Shishido et al., 2000, Brimioulle et al., 2003, Bellofiore et al., 2018, Tian et al., 2020b). RV-pulmonary vascular coupling was defined as the Ees/Ea ratio which determines the efficiency of RV's response to RV afterload.

2.3 Imaging on mitochondria in fresh RV tissues and analysis

2.3.1 Mitochondrial superoxide, membrane potential and morphology measurements

Two small fresh pieces of the RV free wall were taken immediately after the heart was harvested and placed into a 12-well plate with chilled Hanks' balanced salt solution (HBSS). 30nM of TMRM (indicator of mitochondrial membrane potential; Table 2.2) and 300nm of MitoTracker green (staining mitochondria) were added to a dish followed by two drops of NucBlue® Live ReadyProbes® Reagent to stain the nucleus. Similarly, 5μM of MitoSOX (Mitochondrial Superoxide indicator) was then added to a separate dish with two drops of NucBlue® Live ReadyProbes® Reagent. The tissue was then incubated for 15 minutes for MitoSox and 30 minutes for TMRM and MitoTracker green at 37°C, 17-21% O_2 and 5% CO_2. The tissue was then quickly washed in HBSS and transferred onto 35mm glass bottom dish with HBSS with a coverslip on top of the tissue to ensure good contact of the tissue with the glass bottom. Images were captured using the Leica TCS SP8 confocal microscope on the Leica Application Suite X (LAS X) software (Leica SP8; Leica Microsystems, Wetzlar, Germany).

TMRM is used an indicator of the mitochondrial membrane potential. MitoTracker green stains mitochondria and is used to measure mitochondrial morphology. MitoSOX is used to determine mitochondrial superoxide and NucBlue is used to stain the nucleus.

Table 2.2. List of mitochondrial dyes

Dye used	Concentration	Staining
TMRM	30nm	Mitochondrial membrane potential
MitoTracker green	300nm	Mitochondrial morphology
MitoSOX	5μM	Mitochondrial superoxide
NucBlue	Two drops/ml	Nucleus

2.3.2 Image analysis

MitoSox and TMRM intensity were quantified using the ImageJ software (National Institutes of Health, Bethesda, MD, USA). This was achieved by placing a rectangle box on top of the region of interest (ROI) to obtain the mean fluorescent intensity value. The same measurements for the rectangle box were used consistently throughout. Around 3 to 6 ROI were taken for each individual image, these were then averaged. Each animal had around 7-15 images and the final average was then plotted as the data for this animal. For mitochondrial morphology, one of the grades (0, 1, 2, and 3) was given for each image depending on the morphology of the mitochondria. The higher the grade is, the more filamentous or less fragmented the mitochondria are. The grades of images from the same animal were then averaged as the data for that animal.

2.4 Quantitative PCR on RV

Table 2.3. List of primers and their sequences

Primers	Primer sequences	Company
PCGα	5'-ACCCACAGAGAACAGAAACAG-3' Forward 5'-GGTCAGAGGAAGAGATAAAGTTGT-3' Reverse	IDT
ESR1	5'-CAATGCACCATCGATAAGAACC-3' Forward 5'-GCTTCAACATTCTCCCTCCTC-3' Reverse	
ESR2	5'-GGTGATTGCGAAGAGTGGTAT-3' Forward 5'-CAGATGTTCCATGCCCTTGT-3' Reverse	
NRF1	5'-GATGCTTCAGAACTGCCAAC-3' Forward 5'-GTCATTTCACCGCCCTGTA-3' Reverse	
NRF2	5'-CTCAGAGCAAGTGACGAGAT-3' Forward 5'-ACTCCTTCATTACCCAAACCAC-3' Reverse	
TSC22D1	5'-CTGCTTCTCTCTTCCCGTTG-3' Forward 5'-TTGCACCAGATCCATAGCTTGC-3' Reverse	
SOD2	5'-CGACCTACGTGAACAATCTGA-3' Forward 5'-ATTGAACTTCAGTGCAGGCT-3' Reverse	
TFAM	5'-AGCTAAACACCCAGATGCAA-3' Forward 5'-GTACACCTTCCACTCAGCTTT-3' Reverse	
HSP90aa1	5'-GGTGCGGTTAGTCACGTTT-3' Forward 5'-CGACCTCCTCTTCCTCCATT-3' Reverse	
MAO-A	5'GAGAAGAACTGGTGTGAGGAG-3' Forward 5'-ACTGTGTTGCTGTCTCTGTG-3' Reverse	
GAPDH	5'-AACCCATCACCATCTTCCAG-3' Forward 5'-CCAGTAGACTCCACGACATAC-3' Reverse	
HK2	5'-GCTCTCAAAATGTTGCCTACC-3' Forward 5'-CATTGTCCGTCACCCTTACTC-3' Reverse	
MFN 1	5'-GATTGATAAGTTCTGCCTTGATGC-3' Forward	

	5’-CCGCTCATTCACCTTATGGAA-3’ Reverse	
MFN 2	5’-GTGACGTAGTGAGTGTGATGG-3’ Forward 5’-GTTGAGGTTGGCTATTGATTGAC-3’ Reverse	
OPA1	5’-CTGAGCCAGGTTACTCCAAAG-3’ Forward 5’-TGTTCCTGAGTTCATGGTCTG-3’ Reverse	
DNM2	5’-ATCACCAAGCTAGACCTGATG-3’ Forward 5’-TTTCTGCCCTCGATGTCTTTC-3’ Reverse	
NFE2L2	5’-CAGTGGATCTGTCAGCTACTC-3’ Forward 5’-CAAGCGACTCATGGTCATCTA-3’ Reverse	
NQ01	5’-ACGTATGCCACCATGTATGAC-3’ Forward 5’-GCCAGAGAATGACGTTCATGT-3’ Reverse	
SOD2	5’-CGACCTACGTGAACAATCTGA-3’ Forward 5’ATTGAACTTCAGTGCAGGCT-3’ Reverse	
CTGF	5’-CCTGTGAAGCTGACCTAGAG-3’ Forward 5-GCCAGAAAGCTCAAACTTGAC-3’ Reverse	
COL 1A1	5’-CGCAAAGAGTCTACATGTCTAGG-3’ Forward 5’-CATTGTGTATGCAGCTGACTTC-3’ Reverse	
COL 3A1	5’-TTCTTCTCACCCTGCTTCAC-3’ Forward 5’-TCTCTAGACTCATAGGACTGACC-3’ Reverse	
TGFβ1	5’-ACTACGCCAAAGAAGTCACC-3’ Forward 5’-CCGAATGTCTGACGTATTGAAGA-3’ Reverse	
LTBP2	5’-GGCTACGTCATGGTCAGAAG—3’ Forward 5’-AGTTGACGCATCTCCCATC-3’ Reverse	

2.4.1 RNA extraction

The RNA extraction was performed on the RV tissue using the miRNeasy mini kit according to the manufacturer's instructions. All samples were kept on ice at all time points throughout the experiment. Before RNA extraction took place, each tissue sample was exposed to 700µL of QIAzol. The tissue was then homogenised using the Tissue Lyser II machine set at 25Hz with 3x30 second intervals. This was then followed by a 5-minute incubation at room temperature to promote dissociation. Briefly, 140µL of chloroform was added to each sample and shaken vigorously for 15 seconds. These were incubated at room temperature for 3 minutes and centrifuged at 12,000 x g for 15 minutes at 4°C. Following centrifugation, the samples separate into three distinct layers with the upper aqueous layer containing the RNA. 300µL of RNA is transferred into a tube containing 525µL of 100% ethanol and thoroughly mixed via pipetting. The mixed RNA and ethanol were transferred into collection tubes and centrifuged at 8,000 x g for 15 seconds at room temperature. This process was repeated until all the sample was used with the flow-through discarded each time. To wash the RNA, 350µL of RWT buffer was added to each tube and centrifuged at ≥ 8,000 x g for 15 seconds with the flow through discarded. 80µL of DNase master mix was added to ensure there were no small DNA traces left and this was incubated for 15 minutes at room temperature. 350µL of RWT was added to each column and centrifuged for 15 seconds with the flow-through discarded. This was followed with two wash steps with 500µL of RPE, firstly the columns were centrifuged at 8,000 x g for 15 seconds and then 8,000 x g for 2 minutes with the flow-through discarded both times. The columns were then transferred into new tubes and centrifuged at 16,000 x g for 2 minutes. Similarly, the columns were transferred into new tubes with 36µL of RNA free water and left to incubate at room temperature for 2 minutes. This was followed by centrifugation at 7,800 x g for 1 minute which was repeated twice. The RNA concentration was then quantified using a Nanodrop 1000 Spectrophotometer machine (Thermo Scientific, UK).

2.4.2 cDNA conversion

For the cDNA conversion, 500-1000ng of RNA was utilized from the mRNA extraction. For one reaction 24.6µL of master mix was made up, consisting of 4µL of 10x RT buffer, 8.8µL of magnesium chloride, 8µL of deoxynucleotide triphosphates (dNTP), 2µL of random hexamers, 0.8µL of RNA inhibitor and 1µL of multiscribe. The master mix was then added to the tubes followed by 15.4µL of RNA free water and 500-1000ng of RNA to give a total final reaction volume of 40µL. The tubes were centrifuged at 3000 x g for 1 minute. Each tube was then run on the Veriti® Thermal Cycler (Applied Biosystems, UK) for the steps in Table 2.4.

Table 2.4. cDNA cycling conditions.

Step	Temperature (°C)	Time (minutes)
1	25	10
2	48	30
3	95	5
4	4	Infinite time

2.4.3 qPCR

Real time qPCR was performed using the SYBR green master mix and Integrated DNA technologies probes. All samples were done in triplicates on a 384 well plate. Firstly, the master mix was made by combining 5µL of SYBR green with 3µL of RNA free water and 0.5µL of primer and vortexed. Finally, 1.5µL of cDNA was added to the plate to give a final reaction volume of 10µL. The plate was then centrifuged at 3,000 x g for 2 minutes. The fluorescence was then measured using the ViiA7 Real Time PCR System machine (Thermo Scientific, UK). The cycling conditions were as follows: initial copy 50°C for 2 minutes followed by 95°C for 10 minutes. The start of the 40 cycles: 95°C for 15 seconds and 60°C for 18 seconds. Finally, the last stage (the melt curve) 95°C for 15 seconds and 60°C for 1 minute (Table 2.5). Gene expression was analysed using the comparative cycle threshold (Ct) method and compared

to either glyceraldehyde-3-phosphate dehydrogenase (GAPDH) housekeeper for RV tissue or β-actin for lung tissue.

Table 2.5. Quantitative polymerase chain reaction (qPCR) cycling conditions.

Step	Temperature (°C)	Time
Initial copy	50	2 minutes
Initial copy	95	10 minutes
Step 1	95	15 seconds
Step 2	60	18 seconds
Melt curve	95	15 seconds
Melt curve	60	1 minute

2.4.4 qPCR analysis

Gene expression is represented as a ratio to the housekeeper (HK). This ratio was obtained from calculating the difference between the mean CT value of the gene of interest and the mean value of GAPDH or β-actin, otherwise known as the ΔΔCT value. The CT values for GAPDH RV tissues from one plate were 23.38 ± 0.16, 23.23 ± 0.58, 22.21 ± 0.56 and 21.76 ± 0.24 for male control, male SuHx, female control and female SuHx, respectively. No significance was detected across the different the groups for several qPCR plates. Therefore, we deemed GAPDH to be a stable HK for our RV tissue. Additionally, the CT values for β-actin from one plate were 18.53 ± 0.64, 16.14 ± 0.73, 18.06 ± 0.72 and 17.71 ± 0.61 for male control, male SuHx, female control and female SuHx, respectively. Similar to the RV, no significant differences were detected across the different groups and also across different qPCR plates.

2.5 Western blot on RV

2.5.1 Protein extraction from tissue

Following *in vivo* work, RV tissue was stored in the -80 until it was required. The tissue was then placed on ice and transferred into a 2ml centrifuge tube, with two 5mm stainless steel beads (Qiagen, UK). 500μL of cell lysis buffer (protease inhibitor cocktail, EDTA, purified water) was added to each tube. Each tissue sample was homogenised using the Tissue Lyser II (Qiagen, UK) for 4 x 30 seconds set at 25Hz. If required, the tissue was processed at an additional 4 x 30 secs at 25Hz to ensure it had fully broken down. The tissue was then left on ice for 30 mins and occasionally vortexed. The samples were then centrifuged at 4°C for 15 minutes at 10,000rpm. The supernatant was then transferred into fresh 1.5ml centrifuge tubes ensuring it did not disturb the pellet.

2.5.2 Protein quantification by BCA assay

Bovine serum albumin (BSA) standards were prepared by diluting them with dH_2O as protein concentration references. These were made at final concentrations of 0mg/ml, 0.5mg/ml, 0.75mg/ml, 1.0mg/ml, 1.25mg/ml, 1.5mg/ml, 1.75mg/ml and 2mg/ml. RV samples were then diluted at 1:10 with dH_2O. All samples were then vortexed and centrifuged prior to being added in 10μL to the 96-well plate. The BSA standards and samples were all added in duplicate. The working reagent (reagent A and reagent B) which was prepared at a 50:1 ratio was then added in a volume of 200μL. The 96-well plate was then incubated at room temperature in the dark for 20 minutes. Following incubation, the plate was placed into the GloMax® Explorer Multimode microplate reader (Promega, UK). The BSA protein assay (Abs 560) setting was selected, and the protein calculation was assessed (mg/ml). As the samples were done in duplicates, the mean concentration was then calculated. The protein samples were then stored in the -80°C freezer until required.

2.5.3 RV sample preparation

The samples were then prepared, and their protein concentration adjusted for the western blot to ensure all samples were loaded at the same concentration (40μg). This was achieved by adding NuPAGE™ LDS sample loading buffer (4x), 2ME (10x), dH_2O and the appropriate protein volume to 1.5ml centrifuge tube. All agents and protein samples were placed on ice at all time points until the samples were ready, which were then heated to 90°C for 10 minutes to denature the proteins. The samples were then quickly centrifuged for 2 minutes and stored in the -80°C freezer until needed.

2.5.4 Gel electrophoresis

NuPAGE™ 4-12% Bis-Tris mini precast polyacrylamide gels (Invitrogen, UK) were assembled into the western blot tank. The tank was then filled with 700ml of 5% (v/v) NuPAGE™ MOPS SDS running buffer (20x) in dH_2O. The SeeBlu Plus2 molecular weight ladder was then loaded into the wells, followed by the protein samples (40 μg). The gels were then left to run at 150V for 1.5 hours at 280mA using the Life Technologies PowerEase™ power supply.

2.5.5 Protein transfer

After the proteins had successfully separated across the gel, the proteins were then transferred onto a polyvinylidene fluoride (PVDF) membrane. The transfer buffer consisted of 5% (v/v) NuPage™ transfer buffer, 20% (v/v) methanol and 75% (v/v) dH_2O. Prior to the transfer, sponges and filter paper were soaked in transfer buffer, these where then stacked into a cassette, with a roller used each time to ensure there were no air bubbles. The gel was then carefully removed from the tank and placed on top of the PVDF membrane. The cassette containing the sponges, filter paper, membrane and gel was then placed into the transfer tank with around 500ml of transfer buffer. The Life Technologies PowerEase™ power supply was set at 40V and 280mA for 2 hours, with the tank placed on top of an ice tray to ensure that it did not overheat. Ponceau red was occasionally applied to the PVDF membranes following the transfer to ensure that the proteins had successfully transferred. The membranes were

then blocked using SuperBlock™ (Thermo Scientific, UK) for 1 hour at room temperature on a shaker. The membranes were then transferred into 50ml falcon tubes and incubated with their primary antibody (Table 2.6) diluted in either 5% milk (GAPDH) or 5% BSA (NFE2L2) in TBST and rotated overnight at 4°C.

Table 2.6. Primary and secondary antibodies with their dilutions

Primary antibody	Primary Dilution	Secondary antibody	Secondary Dilution
GAPDH	1:50,000	Anti-mouse (IR800)	1:20,000
NFE2L2	1:100	Anti-rabbit (IR680)	1:20,000

2.5.6 Immunoblotting

Following primary antibody incubation, the membrane was then washed with TBST 3 x 15 minutes. The membrane was incubated with its corresponding secondary antibody (Table 2.6)in TBST for 1 hour at room temperature on a shaker. The membrane was then washed with TBST 3 x 15 minutes per wash. For fluorescent immunodetection, the membrane was scanned using the LI-COR Odyssey 9120 IR Imager (LI-COR Biosciences, Cambridge, UK). The same protocol was followed for the loading control using GAPDH primary antibody for RV protein.

2.5.7 Western blot analysis

Western blot results are represented as the ratio of the protein of interest (NFE2L2) to the housekeeper, GAPDH using the densitometry analysis method using the ImageJ software (National Institutes of Health, Bethesda, MD, USA).

2.6 Histology and immunohistochemistry

2.6.1 Tissue processing

Sectioned RV and lungs were stored in 10% formalin following *in vivo* work for more than 2 days. Each of the sectioned tissue was then placed into biopsy cassettes, which were placed into a tissue basket and washed under tap water. Here after, the tissue was processed using a Shandon citadel 1000 tissue processor (ThermoFisher, UK) to become dehydrated. Overnight, the tissue was taken through an ethanol gradient and then into histoclear and paraffin wax (Table 2.7). After the tissue was processed it was then embedded into paraffin wax blocks using the Shandon Histocenter 3 (ThermoFisher, UK). Prior to embedding into the wax, the tissue was carefully adjusted into the orientation of interest. The wax was then added, and the tissue wax blocks were placed onto a cooling machine set at -20 °C for 2-3 hours to allow the wax to fully set. Following this, the tissue was then stored at room temperature until further use.

Table 2.7. Tissue processor programme schedule

Station	Solution	Incubation period
1	10% NBF	pass
2	70% Ethanol	2 hours
3	80% Ethanol	2 hours
4	95% Ethanol	2 hours
5	95% Ethanol	2 hours
6	100% Ethanol	1 hour 30 mins
7	100% Ethanol	1 hour 30 mins
8	100% Ethanol	1 hour
9	HistoClear	1 hour 30 mins
10	HistoClear	1 hour
11	Paraffin wax	1 hour
12	Paraffin wax + vacuum	1 hour

2.6.2 Tissue sectioning

The microtome was used to cut the tissue embedded paraffin wax blocks. This was adjusted to cut the tissues at 5 μm using the Leica RM2125 microtome (Leica Microsystems, UK). Each of the cut sections were then placed into a paraffin section flotation mounting bath set at ~45°C for 1 minute to allow the tissue to stretch. The tissue was then mounted onto glass microscope slides.

2.6.3 Picrosirius red staining

The 5 μm sections of tissue were deparaffinized by washing them twice in xylene for 15 minutes followed by 10 minutes. The tissue was then rehydrated by washing them for 5 minutes each through an ethanol gradient (100% ethanol, 90% ethanol, 70% ethanol) followed by two final washes in distilled water. Sections were stained with picrosirius red (100%) for one hour followed by a rinse in distilled water. Sections were dehydrated in an ethanol gradient of 70% ethanol and 90% ethanol for one minute each and two washes of 100% ethanol with 5 minutes per wash followed by two washes in xylene for 5 minutes. The sections were then mounted using the DPX mounting medium and covered by a glass coverslip.

2.6.4 Haematoxylin and eosin staining

The 5 μm sections of tissue were deparaffinized and rehydrated following the same procedure mentioned in section 2.6.3. Haematoxylin (Abcam, ab245880) was applied to each tissue section and incubated for 5 minutes at room temperature. Sections were then rinsed with distilled water to remove any excess stain. Bluing reagent was then applied to each section and incubated for 10-15 seconds. The sections were then washed with distilled water and dipped in 100% ethanol. Eosin Y solution was added to each section and incubated for 2-3 minutes in room temperature. Slides were rinsed with 100% ethanol and dehydrated by passing them through an ethanol gradient (70%, 90% and 100% ethanol) and two washes in xylene. Finally, sections were mounted using DPX mounting medium and covered by a glass coverslip.

2.6.5 PCNA staining in RV tissue

The 5 μm sections of tissue were deparaffinized and rehydrated following the same procedure mentioned in section 2.6.3. For antibody staining, we used the heat-induced antigen retrieval method where slides were heated in citrate buffer (10 mM, pH 6.0) in a pressure cooker for 15 minutes set to full power. Slides were then left to cool for at least 30 minutes followed by a wash with distilled water for 10 minutes. Slides were blocked using BLOXall blocking solution for 10 minutes to reduce any background staining and then washed twice with PBS for 10 minutes. The tissue was then permeabilised using 1% BSA in PBS with 0.4% Triton X-100 and this was done twice, with 10 minutes incubations each time. The slides were then blocked to prevent any non-specific binding using 2.5% normal horse serum for 1 hour at room temperature. The primary antibody PCNA (Abcam, ab18197) (1:5000) in PBS with 1% BSA was incubated overnight at 4°C. On the second day, after two 10-minute PBS washes, sections were incubated with the secondary antibody (anti-rabbit) in 1% BSA in PBS for 1 hour at room temperature. This was then followed by another two 10-minute's washes with PBS and then incubated with an AEC substrate until the colour develops (between 2-10 minutes). Sections were washed with distilled water and then counterstained lightly with Carazzi haematoxylin for 5 mins. This was followed by incubation in lukewarm water for 4 minutes. Finally, Aquatex® mounting media was added to the slides followed by a glass coverslip. Sections were left to dry for at least 3 hours before imaging.

2.6.6 Analysis of interstitial collagen in RV

RV interstitial collagen images were taken using the Zeiss microscope, all at a 20x magnification. Images were quantified using a ratio of the area positive for collagen to the total tissue area. This was achieved by using the threshold method via ImageJ software (National Institutes of Health, Bethesda, MD, USA).

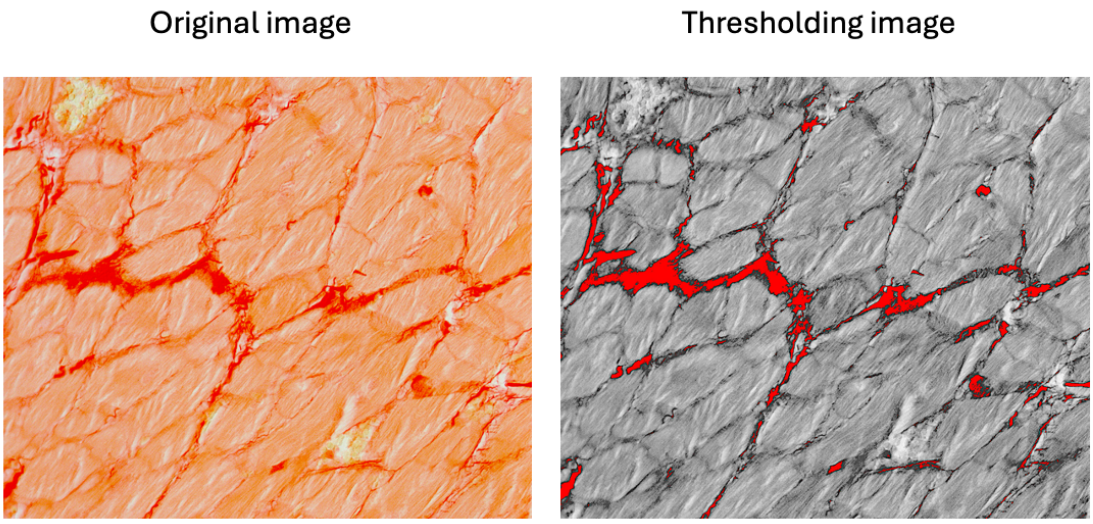

Figure 2.2. Example image of how thresholding was performed

RV tissue was stained with picrosirius red to assess interstitial collagen production and assessed on ImageJ (National Institutes of Health, Bethesda, MD, USA) using the thresholding method. Figure A) represents the original image taken from the Zeiss microscope at a 20x magnification Figure B) represents an example of how the thresholding technique was performed. The collagen areas were highlighted in red and then the area was obtained.

2.6.7 Analysis of perivascular collagen in right coronary artery

RCA vessels from the RV tissue which were pre-stained with picrosirius red were imaged using the Zeiss microscope, at both 20x and 40x magnification. Firstly, we measured the collagen area by measuring the collagen in the adventitial layer of the RCA using threshold method in ImageJ (National Institutes of Health, Bethesda, MD, USA). Then we traced the lumen perimeter which is assumed to be the perimeter of a circle. The diameter of this circle is thus calculated (by dividing the lumen perimeter by Pi) to indicate the size of the vessel and to calculate the lumen area. Then finally, we ratioed the collagen area to the lumen area (named as RCA collagen area fraction). We then measured the intima-media thickness, by drawing from the intima layer of the vessel to the outer of the media layer to gain the intima-media thickness. We then calculated this as a ratio of intima-media thickness to vessel diameter. For comparison of the two ratios between animal groups: RCA collagen area to lumen area and RCA intima-media thickness to diameter, RCA vessels were categorised into three different groups based on their diameter size: 15-50μm, 50-100μm and >100μm.

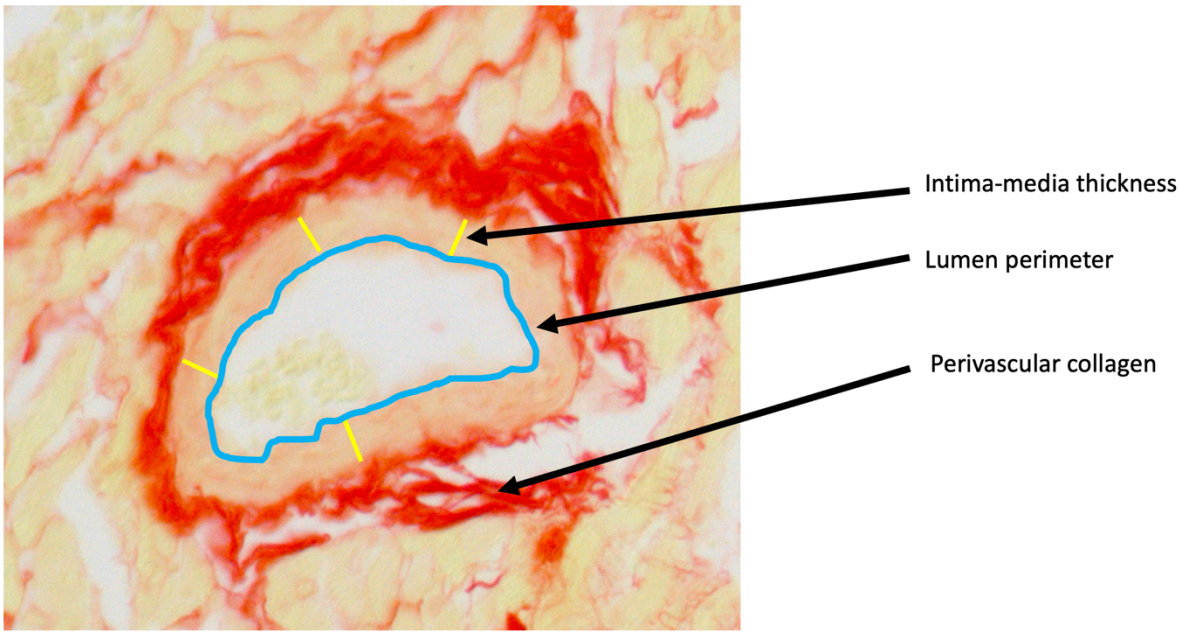

Figure 2.3. Example image of how the RCA analysis was performed

RV tissue was stained with picrosirius red to assess perivascular collagen production and assessed on ImageJ (National Institutes of Health, Bethesda, MD, USA) using the thresholding method. Images were taken using the Zeiss Axioplan microscope on the ZEN microscopy software at both 20x and 40x magnification. Representative images show a RCA vessel highlighting what was defined as the perivascular collagen area, how the lumen perimeter was traced and how to measure the thickness of the intima-media layers.

2.6.8 Analysis of myocyte size in RV

We used the RV images which were counterstained with picrosirius red or H&E to calculate the myocyte size. This was achieved by drawing directly around the area of the myocyte on the ImageJ software (National Institutes of Health, Bethesda, MD, USA). Between 10-20 myocytes from a single sample were measured and the sizes of these myocytes was averaged as the myocyte size for that sample.

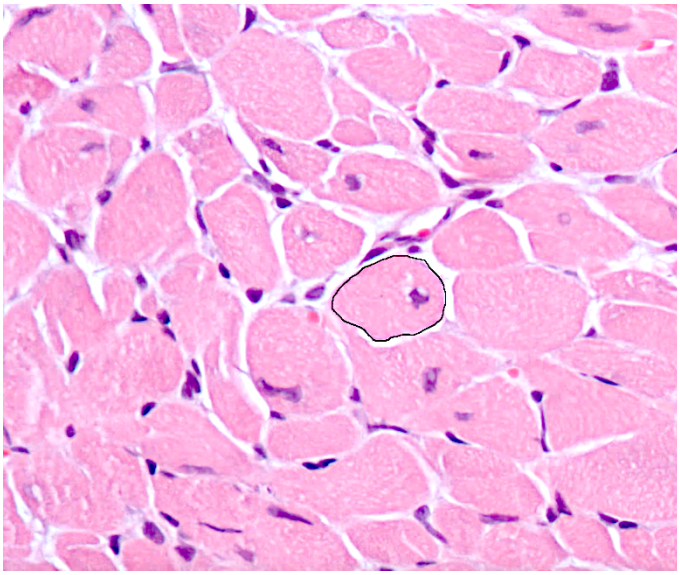

Figure 2.4. Example of how the RV myocyte area was obtained

RV tissue was either stained with picrosirius red or H&E to highlight the cell boundary. Images were captured on the Zeiss Axioplan microscope on the ZEN microscopy software at 40x magnification and analysed using ImageJ software (National Institutes of Health, Bethesda, MD, USA).

2.6.9 Analysis of PCNA in RV

The purpose of PCNA staining was to assess the cell proliferation status of the RV fibroblasts. The images of PCNA stained RV tissues were taken using the Zeiss Axioplan microscope and brightfield images were captured on the ZEN microscopy software. The PCNA analysis was achieved by calculating a PCNA score. The cells which are PCNA positive have a clear, distinct

brown nucleus. Therefore, the number of positive cells was ratioed to the total number of nucleus-stained cells ensuring to exclude the RV myocytes.

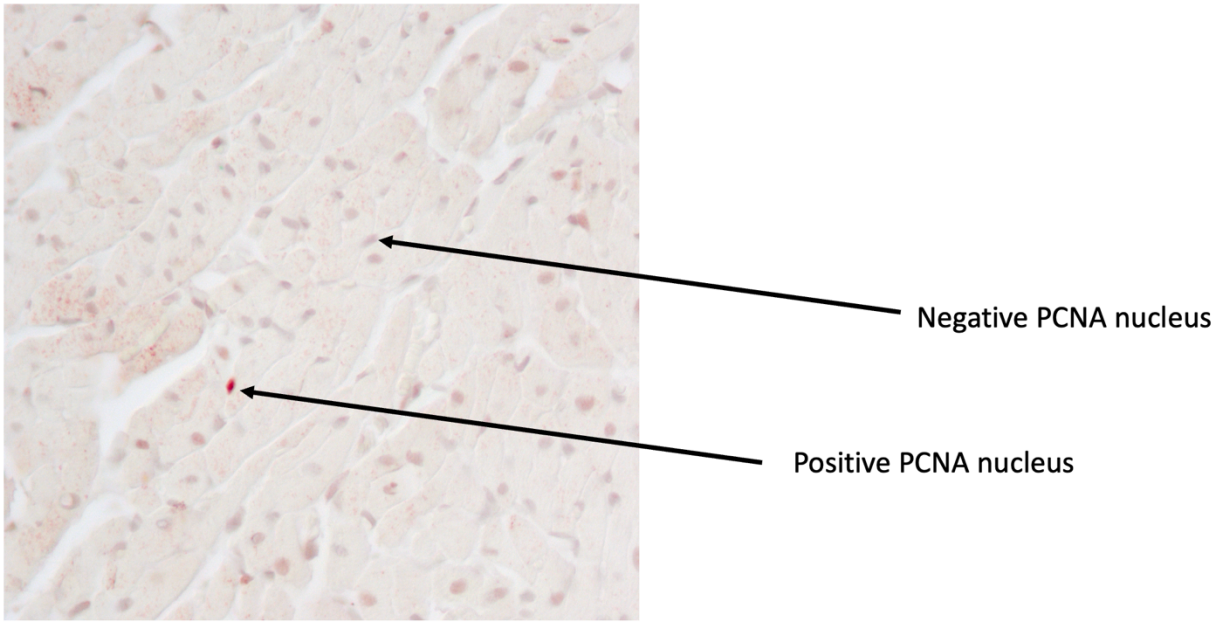

Figure 2.5. Example image of RV with arrows pointing to a PCNA positive and PCNA negative nuclei

2.7 Cell culture and biological study of human cardiac fibroblasts and MCT RV fibroblasts

All cell culture work was performed in a Class II biological safety cabinet.

2.7.1 Subculturing procedure

Male and female human cardiac fibroblast (HCF) isolated from the ventricles of patients with some heart diseases (C-12375, PromoCell, UK) and RV fibroblasts isolated from male MCT-treated rats (Kindly donated from the Archer Lab, Canada). Cells were grown in T-75 cm^2 culture flasks containing pre-warmed fibroblast growth medium 3 (C-23025, Promocell, UK) for the male and female HCF cells or DMEM for the male MCT RV fibroblasts and incubated at 37°C, 17-21% O_2 and 5% CO_2. The treatment for the male MCT can be referred to in Dr Lian

Tian study (Tian et al., 2020a). When cells were ready to be passaged, once they had reached 80-90% confluency, the media was aspirated, and cells were washed with sterile 1x phosphate buffered saline (PBS). Cells were then treated with 5ml of TrypLE^{TM} Express (Gibco, UK) and incubated at 37°C, 17-21% O_2 and 5% CO_2 for 2-3 minutes until all the cells had fully detached from the flask. Once all cells had fully detached, as observed via the microscope, they were resuspended with fibroblast growth medium 3 or DMEM and centrifuged at 150 xg for 8 minutes at room temperature. The supernatant was then discarded, and the cell pellet was resuspended with the required amount of media. Cells were then either seeded into their cell culture dishes (35mm, 60mm and 100mm) for downstream experiments or were placed into a fresh 75cm^2 culture flask to allow them to grow and then placed into the incubator at 37°C, 17-21% O_2 and 5% CO_2. Female HCF cells were ready to be split usually once every 7-10 days, meanwhile male HCF were ready to be split every 4-5 days, usually at a ratio of 1:2. For the HCF cells, cells were treated at passage numbers 4-9, meanwhile MCT RV fibroblasts cells were treated at passage 3 or 4.

2.7.2 Treatment on cells

Male and female HCF cells were seeded into 12x35mm cell culture dishes. 6 from the 12x35mm dishes were labelled as the normoxic group and the other 6 were labelled as the hypoxic group. 35mm dishes were labelled for either MitoSOX or Ki-67 staining. Within each of the normoxic and hypoxic groups, cells were either treated with ethanol (100%), E2 (10nM) or MitoQ (300nM) once they had reached 50% confluency. The dishes labelled for hypoxia, were then placed into a 1% O_2, 5% CO_2, Nitrogen 200bar hypoxic chamber to induce a hypoxic environment. The chamber was then placed into the incubator. Meanwhile, the other 6 dishes were placed into a normoxic environment in the incubator at 37°C, 17-21% O_2 and 5% CO_2. Approximately, one hour after the chamber was sealed, it was then flushed for 10 minutes to degas the media and then placed back into the incubator. At the 24-hour time point, the dishes were then re-exposed to ethanol (100%) which was used as the vehicle, E2 (10nM) or MitoQ (300nM) and sealed back into the hypoxic chamber for these hypoxic dishes and placed back into the incubator. Similarly, one hour later the chamber was flushed for 10 minutes, sealed and placed back to the incubator.

For male MCT RV fibroblasts, cells were seeded into 3x35mm cell culture dishes. Similarly, the cells were then treated with ethanol (100%), E2 (10nM) or MitoQ (300nM) once they had reached 50% confluency. Given that these cells were primary cultures from MCT treated rats, the cells were not placed into the hypoxic chambers, and instead were incubated in the normoxic environment at 37°C, 17-21% O_2 and 5% CO_2 overnight. At the 24-hour time point, the cells were then re-exposed to ethanol (100%), E2 (10nM) or MitoQ (300nM) and incubated overnight. The cells were then stained with MitoSOX or used for immunocytochemistry studies as described below at the 48-hour time point.

2.7.3 Imaging of MitoSOX-stained human cardiac fibroblasts and MCT RV fibroblasts and analysis

At the 48-hour time point, the media in the culture dish was aspirated and the treated samples were washed with sterile PBS and then incubated with 2.5μM MitoSOX along with two drops of NucBlue® Live ReadyProbes® Reagent to stain the nucleus for 30 minutes at 37°C, 17-21% O_2 and 5% CO_2 and in the absence of light. The cells were then imaged using the confocal microscope (Leica TCS SP8 microscope) on the Leica Application Suite X (LAS X) software at 63x magnification. Several images were taken from each sample. Images were then analysed on ImageJ software (National Institutes of Health, Bethesda, MD, USA) by drawing a rectangle box on the region of interest to obtain the mean fluorescent intensity value from an individual cell. A few cells from each sample were analysed and averaged.

2.7.4 Immunocytochemistry staining with Ki-67, PCNA, Col1a1, TFAM, NFE2L2 on cultured human cardiac fibroblasts and MCT RV fibroblasts

At the 48-hour time point, cells were washed with PBS and then fixed by adding 400μL of pre-chilled (-20°C) methanol (100%) for 5 minutes at room temperature. Cells were then washed three times with ice cold PBS for 5 minutes. Cells were then blocked using in 1% BSA, (0.3m glycine, 0.1% tween-20 and PBS) for 30 minutes at room temperature. Cells were then incubated with their appropriate primary antibody (NFE2L2, TFAM, PCNA, Ki-67 and Col1a1). All primary antibodies were used at a 1:100 dilution in PBS with 1% BSA with 0.1% Tween-20 overnight, except for PCNA (1:5000) and Ki-67 (1:50). On the following day, the cells were

washed with PBS three times at room temperature. The secondary antibody (488 goat anti-rabbit IgG in 1% BSA, 1:400) was then added, (except for Ki-67 which is conjugated to Alexa Fluor® 647) and cells were incubated for 1 hour hidden from light at room temperature. Following this, cells were washed 3 times with PBS in the dark. Prolong™ gold antifade mounting media was then added to counterstain for DAPI and this was followed by placing a coverslip on the dish. The dishes were left in the dark overnight at 4°C to be imaged the following day. The dishes were imaged using the confocal microscope (Leica TCS SP8 microscope) on the LAS X software at 20x magnification or with EVOS MC5000 microscope (Invitrogen, UK) at 20x magnification.

2.7.5 Image analysis on immunocytochemistry staining

For the immunocytochemistry on cells stained with Ki-67 or PCNA, the analysis was done by counting the number of positive cells over the total cell count to get the ratio. NFE2L2, was analysed by measuring only the nuclear intensity, while for TFAM and Col1a1, cytosolic intensity of cells was measured.

2.8 Statistical analysis

All statistical analysis was performed using GraphPad Prism (V 9.1.0). All data is represented as mean ± standard error of mean (S.E.M), with the n number denotating the number of samples which is either referring to an individual rat, individual cell or vessel. Data was analysed using either unpaired T-tests, one-way ANOVA, two-way ANOVA or three-way ANOVA where appropriate. A ROUT outlier test was performed if deemed appropriate to identify and remove any potential outliers. Simple linear regression analysis was performed between RCA collagen area fraction and RCA diameter, intima-media thickness and RCA diameter, PCNA and RV fibrosis and between Fulton index and RVSP. P values of <0.05 were deemed as statistically significant with *$p<0.05$, **$p<0.01$, ***$p<0.001$ and ****$p<0.0001$.

CHAPTER 3

3. Examining the sex differences in RV function, structural remodelling and fibrotic parameters in a SuHx rat model

3.1. Introduction

PAH predominately affects the females with a 4:1 female to male ratio, although the females with PAH display better RV function and survival than the males (Shapiro et al., 2012). Currently, research particularly on sex differences in RV within PAH is limited. Thus, understanding these sex differences with regards to the structural remodelling and functional changes taking place within the RV, will be essential in identifying potential targets and must also be considered in case these targets vary between the sexes. Hence, throughout this thesis we consistently explore both the males and females.

In PAH, remodelling of the RV is triggered by the increase in afterload as a result of pulmonary vasculature remodelling (Vonk Noordegraaf and Galiè, 2011). During the compensated stage, the RV will increase in muscle mass in an attempt to preserve cardiac function (Vélez-Rendón et al., 2018). At this stage, this increase in muscle mass may serve as beneficial in helping maintain the RV function whilst its dealing with the high pressures (Andersen et al., 2019). However, at the later stage or decompensated stage of PAH, it is inevitable that maladaptive remodelling will occur, with excessive fibrosis serving as one of the key drivers (Andersen et al., 2019). Fibrosis can be characterised by excessive activation and proliferation of the fibroblast cells (Egemnazarov et al., 2018). The fibroblasts serve as the main collagen producing cells, and excessive fibrosis leads to pathological alterations in the collagen network surrounding the cardiomyocytes and interstitium in the heart (Travers et al., 2016). The integrity of this network is crucial in maintaining cardiac structure and function and thereby remodelling of this only contributes to RV failure (Travers et al., 2016).

It was shown that the healthy RV has a higher collagen content than the LV (7.4% versus 5%) in the human myocardium, suggesting that remodelling of the collagen network within the RV may have more of a biomechanical impact on overall heart function (Oken and Boucek, 1957, Andersen et al., 2019). However, given the major structural differences between the

RV and LV as well as the differences in the responses to the PAH signals (that lead to predominant RV failure and not LV), it is not appropriate to compare findings between the RV and LV from this study. Due to this, we do not examine the scope of the LV.

Despite the plethora of research that has been done within PAH, all the current therapies only target the pulmonary vasculature component with no existing therapies available and effectively targeting the RV. To combat this, we decided to induce PH by utilising the gold standard SuHx model in male and female rats to examine the sex differences in RV structure and function. Male and female Sprague-dawley rats were grouped into either control or SuHx. Rats then either received a subcutaneous injection of Sugen (25mg/kg) and were then placed into a hypobaric hypoxic chamber for approximately 3 weeks. Following the end of their period in hypoxia, rats were placed into normoxia for up to 5 weeks in which the SuHx phenotype continues to worsen. Control rats received the vehicle (CMC) and were kept in normoxia for up to 8 weeks. In week 8 post injection, rats were haemodynamically assessed by PV loop via the open chest method then humanely killed with the RV dissected freely then cut into small pieces. Less than 1% of the overall RV tissue was cut into pieces of fresh RV tissue taken and stained for mitochondrial properties. The remainder of the heart (RV and LV+S) and lungs were collected and harvested for immunohistochemistry (IHC) staining and quantitative polymerase chain reaction (qPCR) experiments.

The objectives of this chapter were to:

- To characterise the SuHx model in both male and female rats by assessing their hemodynamic parameters and pathological alterations.
- To examine the sex differences in factors linked to and affecting RV collagen deposition and fibrosis.
- To examine the extent of RV hypertrophy by measuring RV myocyte size.
- To assess the changes in the RV genes that play a role in RV fibrosis.

3.2 SuHx affected only the body weight of male rats

At the start of the study all animal body weights were recorded. No significant differences were detected between male control versus male SuHx and female control and female SuHx groups (Figure 3.1 A). Although there were significant sex differences between the male control and female control group (211.2 ± 6.25g vs. 158.7 ± 4.41g, ****p<0.0001, n=10) and the male SuHx and female SuHx groups (208.2 ± 4.43g vs. 159.3 ± 2.55g, ****p<0.0001, n=10), confirming that the male groups were heavier than the female groups (Figure 3.1 A). The weights of the rats were recorded at the end of the study, with the same trend seen between the males and females. Male control rats were significantly heavier than the female controls (346.7 ± 6.93g vs. 228.9 ± 5.37g, ****p<0.0001, n=10) and the male SuHx versus the female SuHx (319.1 ± 9.11g vs. 223.4 ± 5.78g, ****p<0.0001, n=10) (Figure 3.1 B). There was also a significant decrease in body weight in the male SuHx group versus the male controls (319.1 ± 9.11g vs. 346.7 ± 9.11g, *p<0.05, n=10) with no differences found between the female control and female SuHx groups (Figure 3.1 B). As well as this, animal bodyweights were recorded weekly to monitor animal welfare (Figure 3.1 C, D and E), no differences were detected between the two female groups however bodyweight changed overtime in the male control vs. male SuHx groups, (week 8: 249.8 ± 5.69g vs. 209.3 ± 2.17g, ****p<0.0001, n= 10) (week 9: 278.6 ± 5.54g vs. 231.1 ± 2.88g, ****p<0.0001, n=10) (week 10: 298.5 ± 5.44g vs. 224.8 ± 3.89g, ****p<0.0001, n=10) (week 11: 313.9 ± 5.25g vs. 277.6 ± 4.86g, ***p<0.001, n=10) (week 12: 325.6 ± 6.38g vs. 297.7 ± 6.15g, *p<0.05, n=10) and (week 14: 346.7 ± 6.93g vs. 319.1 ± 9.11g, *p<0.05, n=10) (Figure 3.1 C, D and E).

A

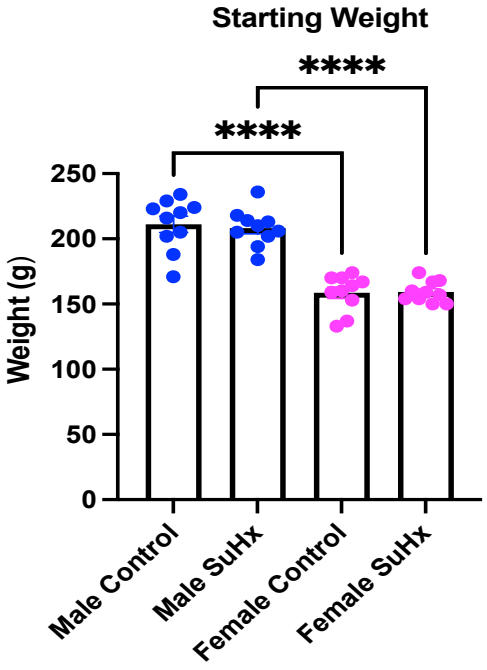
Starting Weight
****
****
Weight (g)
250
200
150
100
50
0
Male Control
Male SuHx
Female Control
Female SuHx

B

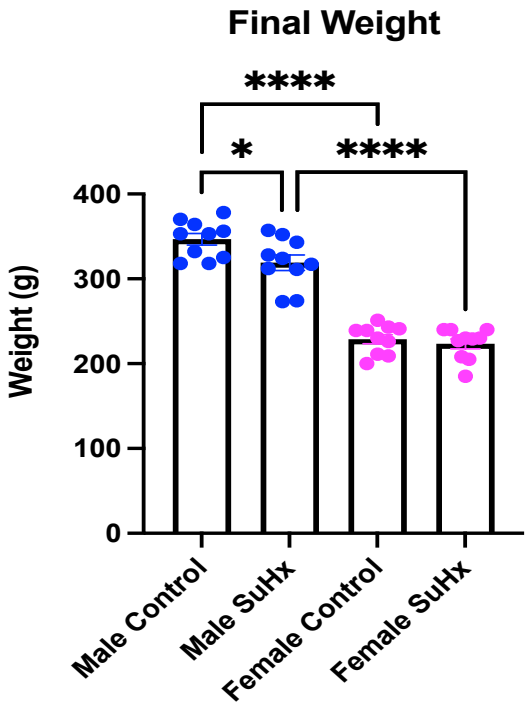
Final Weight
****
*
****
Weight (g)
400
300
200
100
0
Male Control
Male SuHx
Female Control
Female SuHx

C

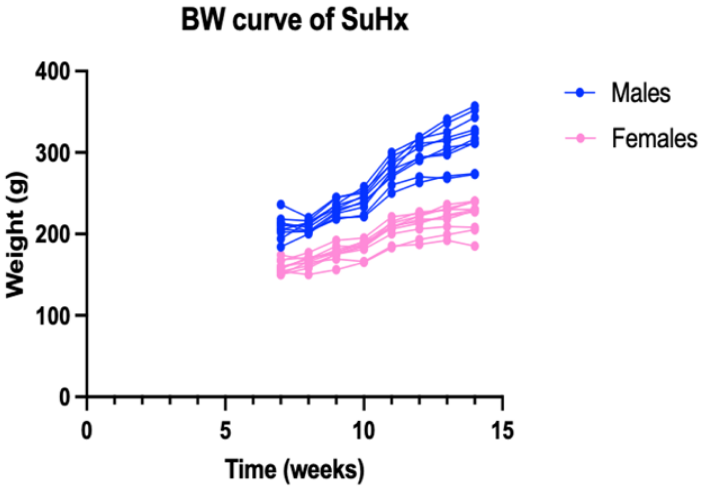
BW curve of SuHx
Weight (g)
400
300
200
100
0
0
5
10
15
Time (weeks)
Males
Females

D

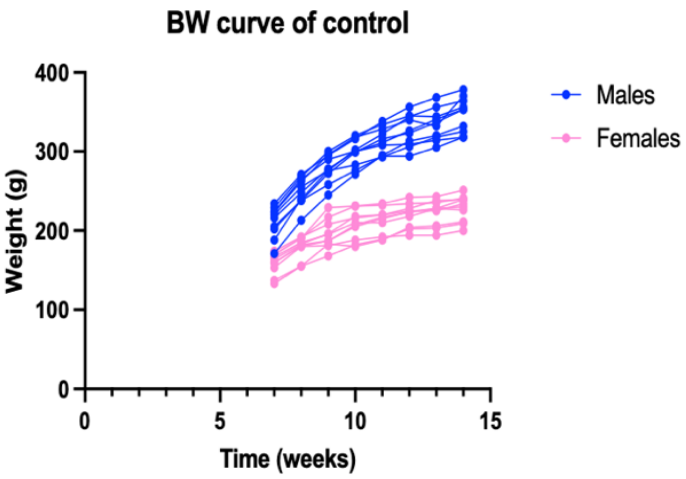
BW curve of control
Weight (g)
400
300
200
100
0
0
5
10
15
Time (weeks)
Males
Females

E

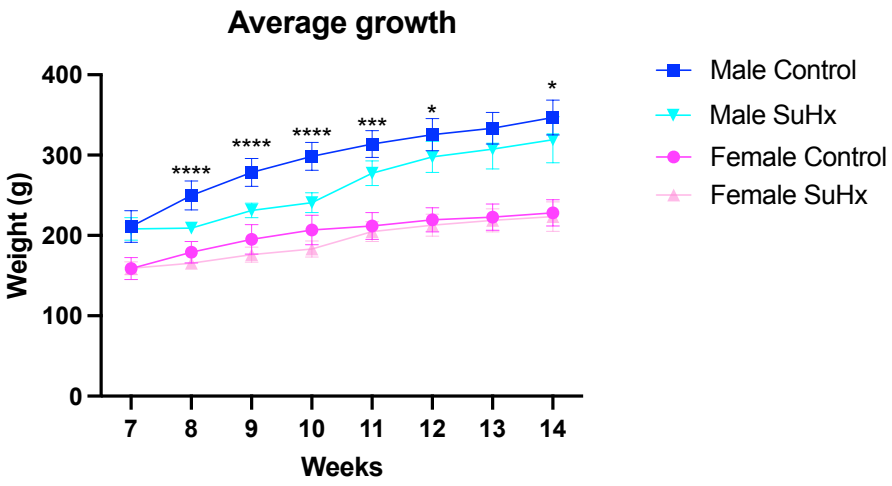

Figure 3.1. Bodyweight of male and female control and Sugen-hypoxia (SuHx) treated animals

A) and B) represent each individual rat's body weight measurement at the start and end of the study protocol. C), D) and E) represent animal body curves throughout the duration of the study. Statistical analysis was performed using two-way ANOVA for figures A and B and three-way ANOVA for figure E. In figure E, statistical significance only compares male control vs. male SuHx and female control vs. female SuHx groups at their given time point. Statistical significance is shown as *p<0.05, *** p<0.001, **** p<0.0001, with n=10 per group.

3.3 RV, LV + Septum and Fulton index were affected by SuHx

After the rats' bodyweights were recorded following the end of their 3 weeks in hypoxia and 5-week period in normoxia, the hemodynamic parameters were recorded. The animals were then culled with the RV and LV + septum dissected and weighed prior to being harvested. There was a significant increase in RV weight in the male control versus male SuHx group (0.51 ± 0.02g vs. 0.21 ± 0.01g, ****p<0.0001, n=10) and female control versus female SuHx group (0.38 ± 0.04g vs. 0.15 ± 0.01g, ****p<0.0001, n=10), with the male SuHx RV being notably heavier than the female SuHx groups (0.51 ± 0.02g vs. 0.38 ± 0.04g, **p<0.01, n=10) (Figure 3.2 A). Whilst there was only a significant increase in LV + Septum weight in the female SuHx group versus the female control (0.68 ± 0.03g vs. 0.56 ± 0.01g, **p<0.01, n=10) (Figure 3.2 B). The male control LV + septum weighed more than the female control group (0.80 ± 0.02g vs. 0.56 ± 0.11g, ****p<0.0001, n=10) and the same was seen for the male SuHx versus the female SuHx group (0.83 ± 0.02g vs. 0.68 ± 0.03g, ***p<0.001, n=10). The Fulton Index (RV/LV+S) ratio was then calculated, and this was significantly increased in both male SuHx versus male control (0.61 ± 0.02g vs. 0.25 ± 0.01g, ****p<0.0001, n=10) and female SuHx versus female control groups (0.55 ± 0.05g vs. 0.26 ± 0.01g, ****p<0.0001, n=10) (Figure 3.2 C).

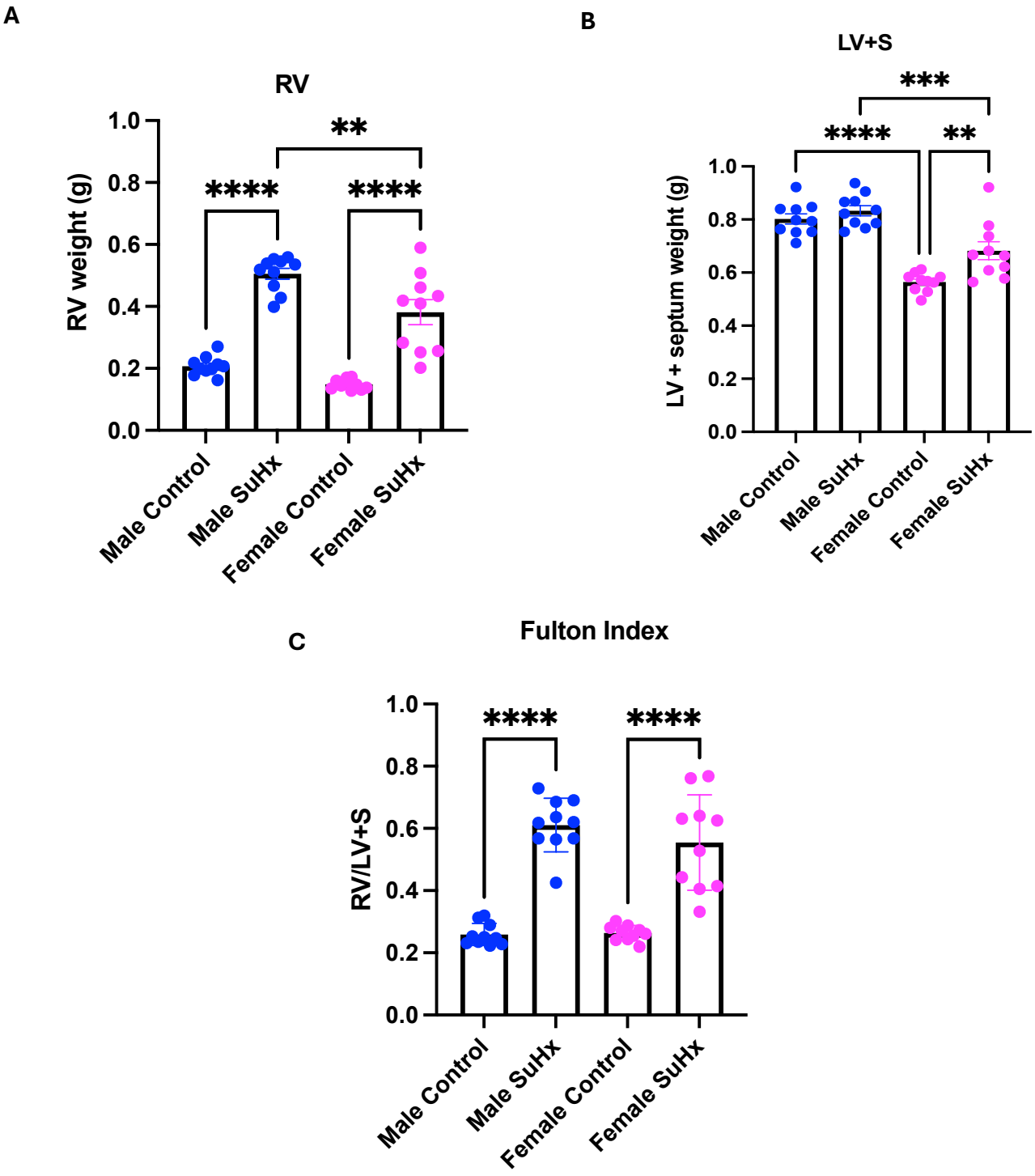

Figure 3.2. RV, LV+S and Fulton index in male and female control and SuHx rats

Figure A) and B) male and female right ventricle (RV) and left ventricle + septum (LV + S) weights were recorded after their PV loop surgery. C) The Fulton index (RV/LV+S) was measured at the end of the study as an indicator of RV hypertrophy. n=7-10 per group. *p<0.05, ** p<0.01, **** p<0.0001. Statistical analysis was performed using two-way ANOVA. All data represent mean ± standard error of the mean (S.E.M). (SuHx) Sugen-hypoxia.

3.4 RVSP was increased in both male and female SuHx rats, whilst RVEDP was only increased in male SuHx rats

RVSP was recorded at the end of the rat's period in normoxia (Figure 3.3). There was a significant increase in RVSP in the male SuHx versus male control group (86.13 ± 5.05 mmHg vs. 30.10 ± 1.61mmHg, ****p<0.0001, n=8-10) and female SuHx versus female control group (85.14 ± 6.31mmHg vs. 30.67 ± 1.31mmHg, ****p<0.0001, n=7-9), highlighting no sex differences (Figure 3.4 A). Meanwhile, RVEDP was only increased in the male SuHx versus male control group (4.16 ± 0.44mmHg vs. 2.01 ± 0.31mmHg, *p<0.05, n=8-10) suggesting that the males could be more severely affected than the females (Figure 3.4 B). Meanwhile, there were no significant differences in the heart rates across all the four groups (Figure 3.4 C). Thus, implying that the changes detected in RVSP and RVEDP are not associated or linked to increases in heart rate.

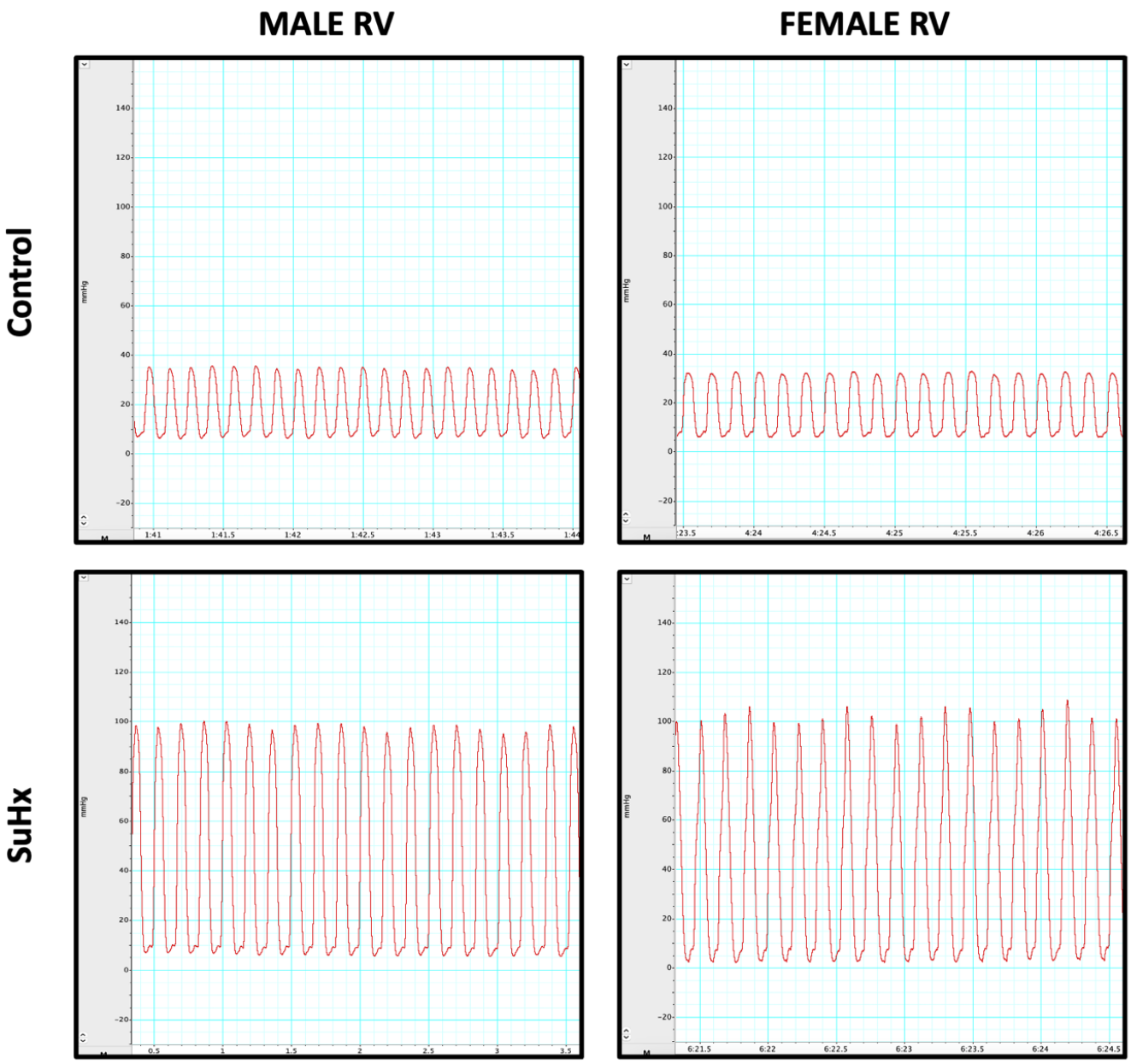

Figure 3.3. Diagram of RV pressure traces from the PV loop recordings

Traces of right ventricular (RV) pressures from male and female control and Sugen-hypoxia (SuHx) rats to highlight the differences visually between the control RV trace and the pulmonary hypertensive RV trace. Each pressure trace was recorded for between 10-15 minutes. A clean trace indicates correct placement of the catheter within the chamber.

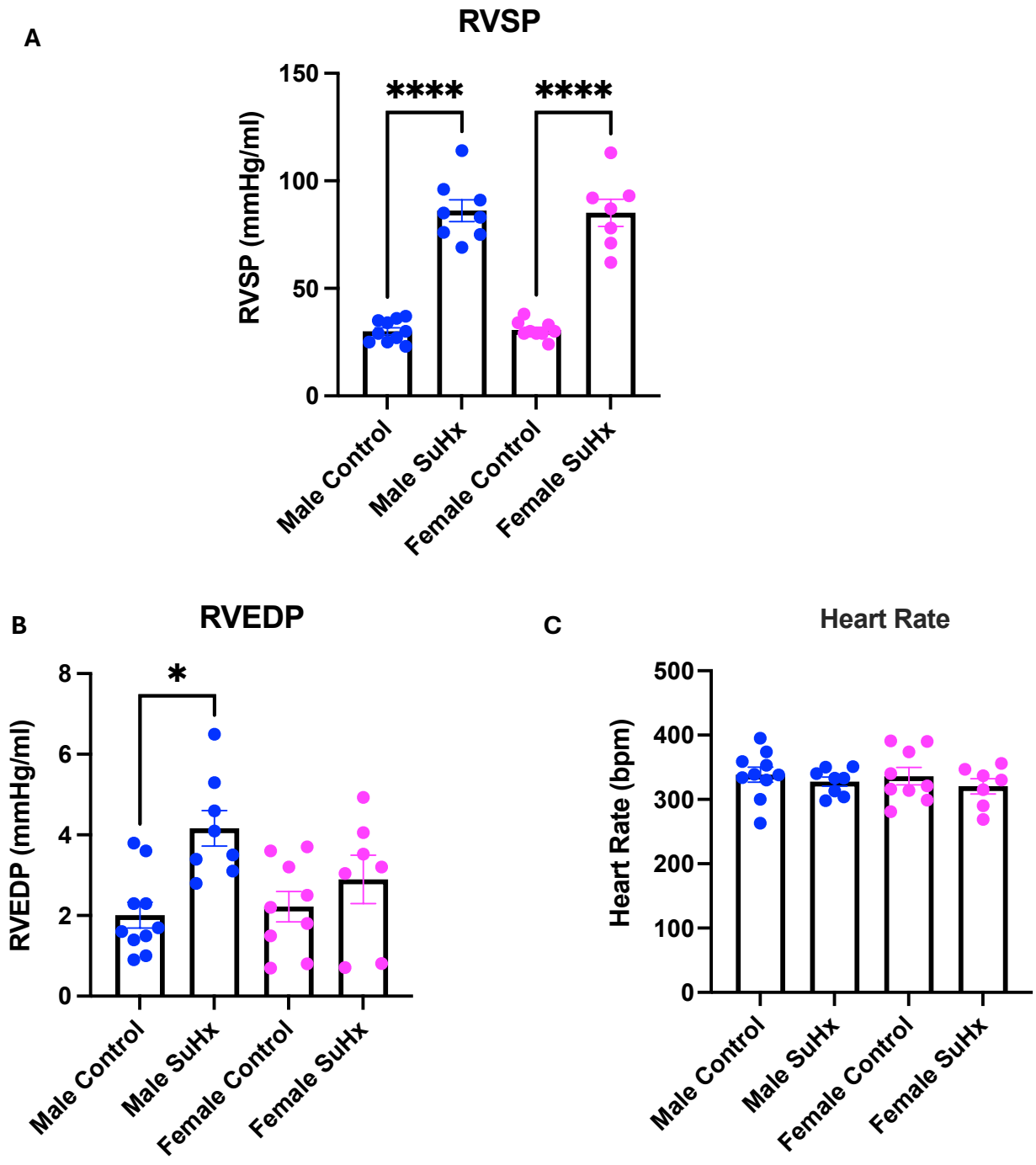

Figure 3.4. SuHx increases RVSP in both male and female rats, meanwhile RVEDP is only increased in male Sugen-hypoxia (SuHx) rats

A) right ventricular systolic pressure (RVSP) (mmHg/ml) B) right ventricular end diastolic pressure (RVEDP) (mmHg/ml). C) Heart rate (bpm) taken during PV loop recordings, n=7-10 per group. *p<0.05, **** p<0.0001. Statistical analysis was performed using two-way ANOVA. Data represents the mean ± standard error of the mean (S.E.M).

3.5 SuHx had no effect on LVSP and LVEDP in male and female rats

Male and female rats left systolic pressure (LVSP) and left ventricular end diastolic pressure (LVEDP) was assessed at the end of their period in normoxia (Figure 3.5). No significant differences were detected in both LVSP and LVEDP measurements in male and female SuHx groups versus their counterpart controls (Figure 3.6 A and B). Thus, implying that SuHx effects seen are not influencing LV function and hence, we propose the model to be RV specific.

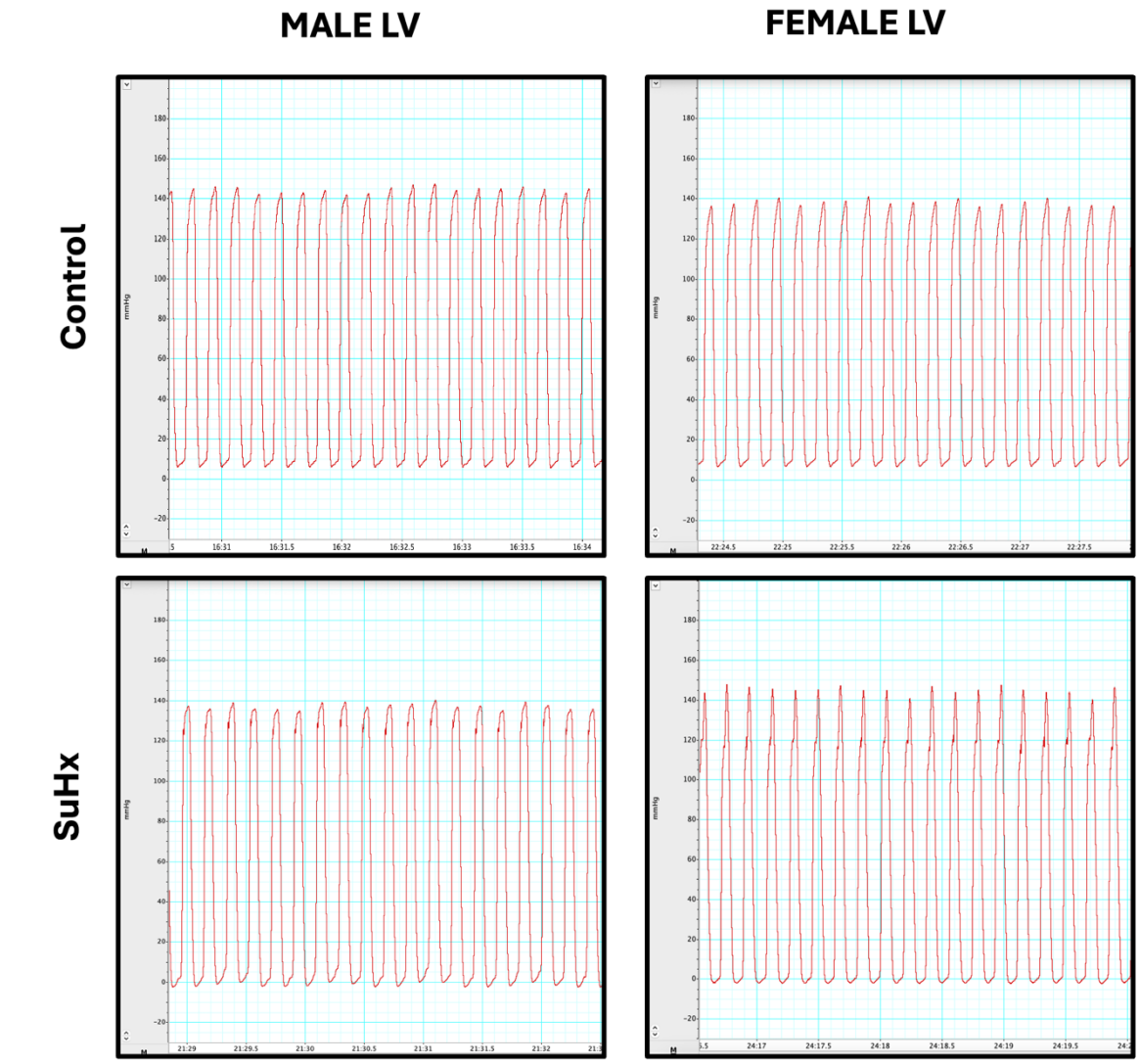

Figure 3.5. Diagram of LV pressure traces from the PV loop recordings.

Traces of left ventricle (LV) pressures from male and female control and Sugen-hypoxia (SuHx) rats to show visually that there was no difference between the control LV trace and the pulmonary hypertensive LV trace. Each pressure trace was recorded for between 10-15 minutes. A clean trace indicates correct placement of the catheter.

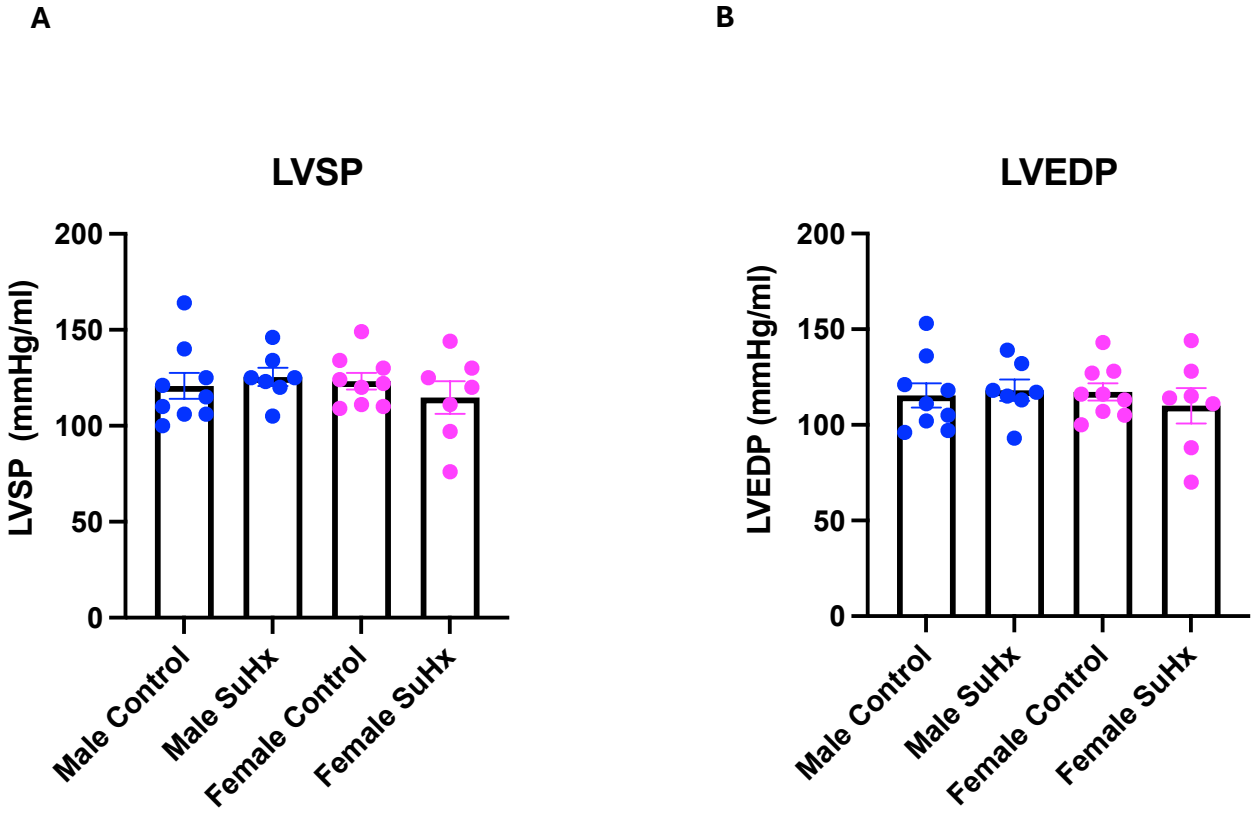

Figure 3.6. LV hemodynamic parameters

The following left ventricle (LV) parameters were measured via PV loop by open chest method. A) Left ventricular systolic pressure (LVSP) (mmHg/ml). B) Left ventricular end diastolic pressure (LVEDP) (mmHg/ml). n=7-9 per group. All statistical analysis was performed using two-way ANOVA. All data represent mean ± standard error of the mean (S.E.M).

3.6 SuHx reduced right ventricular-pulmonary artery coupling in male rats but not in female rats

Figure 3.7 shows the representative RV PV loops based on which the RV-pulmonary artery coupling was calculated using the single-beat method. The pulmonary effective arterial elastance (Ea), a measurement of RV afterload was significantly increased in both male SuHx versus male control groups (1.66 ± 0.16 mmHg vs. 0.56 ± 0.08 mmHg, ****p<0.0001, n=9-10) and female SuHx versus female control groups (1.76 ± 0.29 mmHg vs. 0.61 ± 0.08 mmHg, ****p<0.0001, n=7-8) (Figure 3.8 A) whilst RV end-systolic elastance (Ees) was not affected in either male and female groups by SuHx (Figure 3.8 B). The RV adaptation to alterations in RV contractility can be defined by the ratio of Ees/Ea, which revealed a significant reduction in the male SuHx versus male control group (0.39 ± 0.05 mmHg vs. 0.78 ± 0.08 mmHg, ***p<0.001, n=9-10) with no significant differences seen in the female groups (Figure 3.8 C).

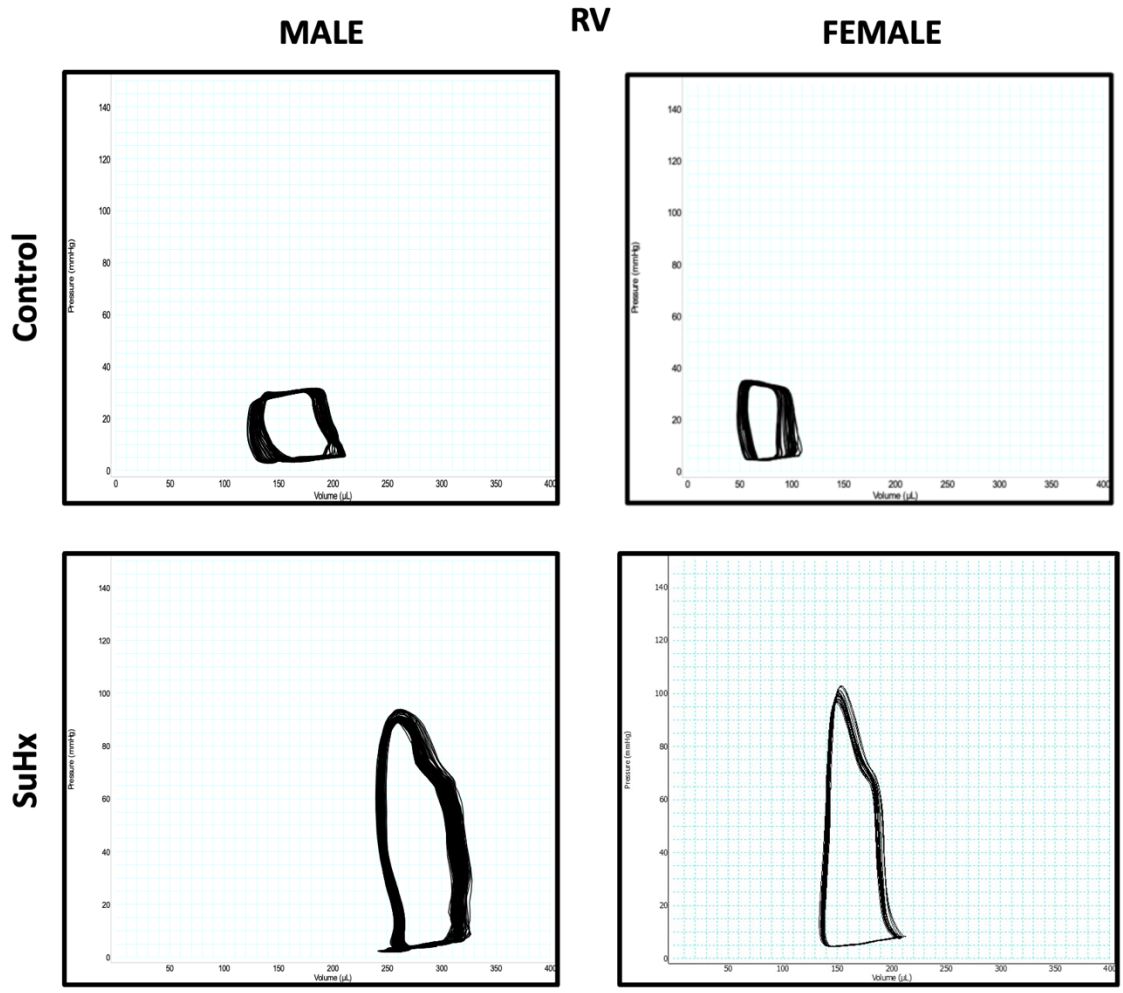

Figure 3.7. Diagram of right ventricular (RV) pressure volume loops recordings from male and female control and SuHx rats

Representative pressure volume (PV) loops. In the right ventricle (RV) of the Sugen-hypoxia (SuHx) rats, the shape of the PV loop changed due to the increases in RV pressure.

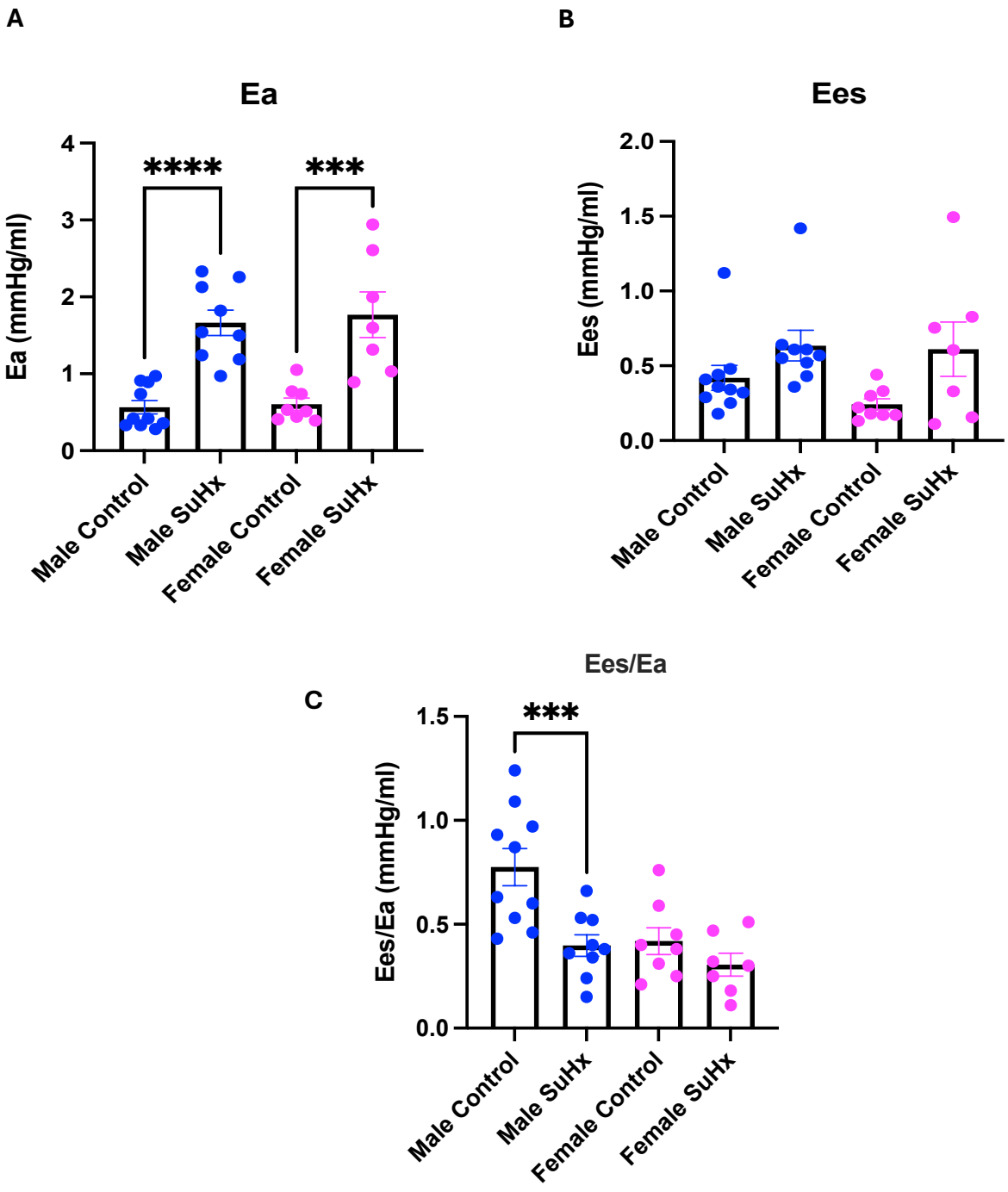

Figure 3.8. Right ventricular (RV) hemodynamic parameters

The following right ventricle (RV) parameters were measured via pressure-volume (PV) loop by open chest method. A) Pulmonary effective arterial elastance (Ea) (mmHg/ml) B) Right ventricular end-systolic elastance (Ees) (mmHg/ml) C) The ratio of right ventricular end systolic elastance (Ees) to pulmonary arterial elastance (Ea), often referred to as right ventricular-pulmonary arterial (RV-PA) coupling (mmHg/ml), with n= 7-10 per group. All data represent mean ± standard error of the mean (S.E.M). Statistical analysis was performed using two-way ANOVA. *** p<0.001, ****p<0.0001.

3.7 The effect of SuHx on collagen deposition in the RV in both male and females

A key feature of RV failure is excessive collagen formation, alterations in the collagen cross linking and imbalances in collagen turnover which correlates positively with increased fibrosis (Andersen et al., 2019). Therefore, we examined sections of the RV from the tissue harvested from the male and female control and SuHx rats by counterstaining them with picrosirius red to detect total collagen production (Figure 3.9 A). The collagen area fraction was calculated as a ratio of the area positive for collagen to the total tissue area. It was detected that collagen deposition was increased in only the male SuHx versus male control groups RV tissue (20.05 ± 1.78 % vs. 9.41 ± 0.38 %, ****$p<0.0001$, n=7-8), with mild increase but no significant difference detected in the females RV tissue (Figure 3.9 B). Thus, suggesting that males may be experiencing a greater degree of fibrosis than the females.

A

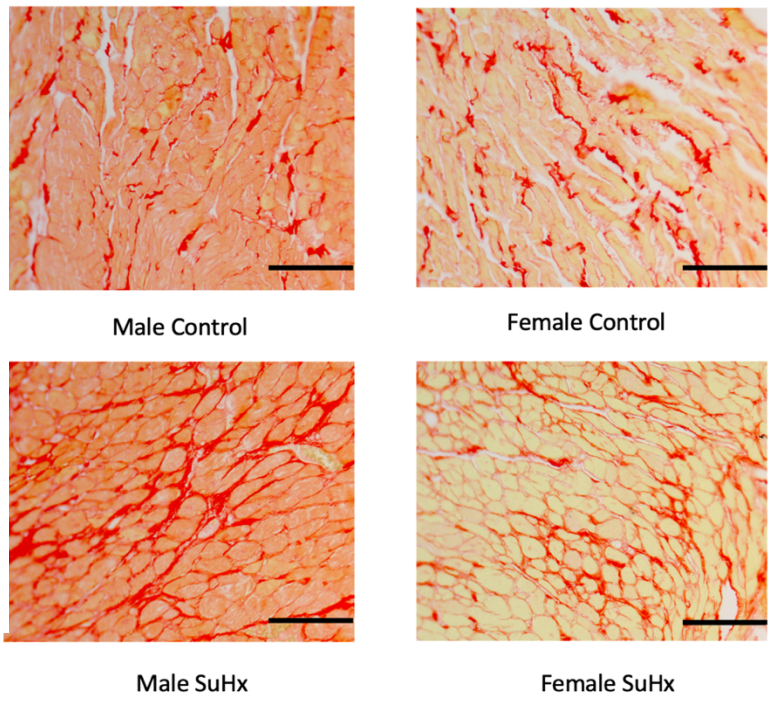

B

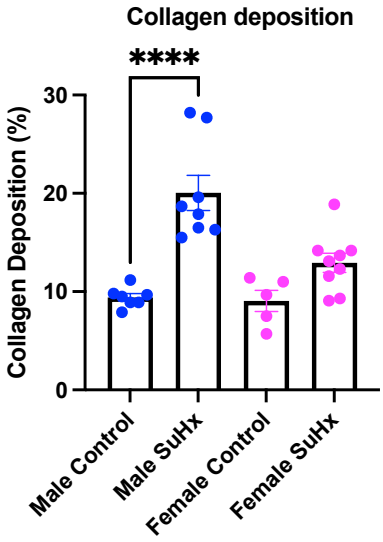

Figure 3.9. RV collagen deposition

Right ventricle (RV) tissue section from male and female Sugen-hypoxia (SuHx) and control rats were counterstained with picrosirius red to stain for areas positive for collagen. (A) Representative images for male and female control and SuHx RV. (B) Summary of the percentage of collagen positive area, with n=5-9 per group. All data represent mean ± standard error of the mean (S.E.M). Statistical analysis was performed using the two-way ANOVA. ****p<0.0001. Scale bar represents 100µm.

3.8 The effect of SuHx on the RV expression of genes linked to fibrosis and cardiac remodelling

The effect of SuHx on RV gene expression linked to fibrosis and cardiac remodelling was assessed in both male and female rats. Interestingly, we detected an upregulation in collagen type 1 alpha 1 chain (Col1a1) in the female SuHx rats versus their controls (4.49 ± 1.22 vs. 1.04 ± 0.10, *p<0.05, n=10) (Figure 3.10 A). The same was found for collagen type 3 alpha 1 chain (Col 3a1) in the female control versus the female SuHx (2.37 ± 0.48 vs. 1.03 ± 0.08, *p<0.05, n=10) which was not seen in the males (Figure 3.10 B). Instead, the male SuHx rats demonstrated an increase in transforming growth factor β 1 versus the male controls (3.32 ± 0.58 vs. 1.04 ± 0.04, ***p<0.001, n=10) (TGFβ1), a key promoter of fibrosis, which was not seen in the females (Figure 3.10 C). TSC-22 (TGF β stimulated clone 22) (TSC22D1), which enhances TGFβ1 signalling by increasing receptor stability via antagonising Smad 7 was also similarly found to be upregulated in only the male SuHx rats (2.30 ± 0.36 vs. 1.09 ± 0.19, **p<0.01, n=10) (Figure 3.10 D). The plasma biomarker, latent transforming growth factor β binding protein 2 (LTBP-2), which is intimately connected to cardiac fibrosis, was found to be upregulated in only the female SuHx group when compared with the female control group (38.48 ± 15.85 vs. 1.03 ± 0.08, *p<0.05, n=10) (Figure 3.10 E). Meanwhile, both male control versus male SuHx (10.97 ± 1.89 vs. 1.03 ± 0.08, **p<0.01, n=10) and female control versus female SuHx (11.46 ± 3.02 vs. 1.05 ± 0.11, **p<0.01, n=10) demonstrate an increase in connective tissue growth factor (CTGF) (Figure 3.10 F).

A

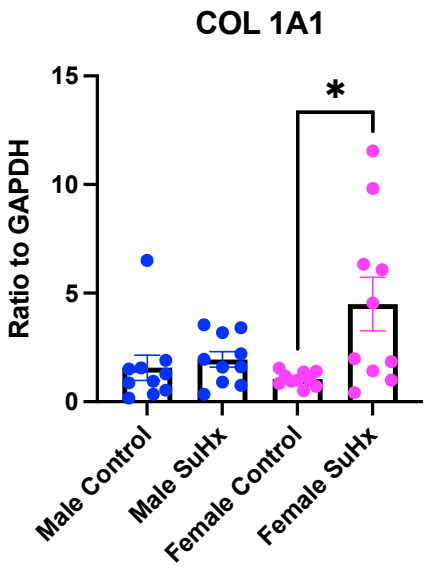
COL 1A1
Ratio to GAPDH
15
10
5
0
*
Male Control
Male SuHx
Female Control
Female SuHx

B

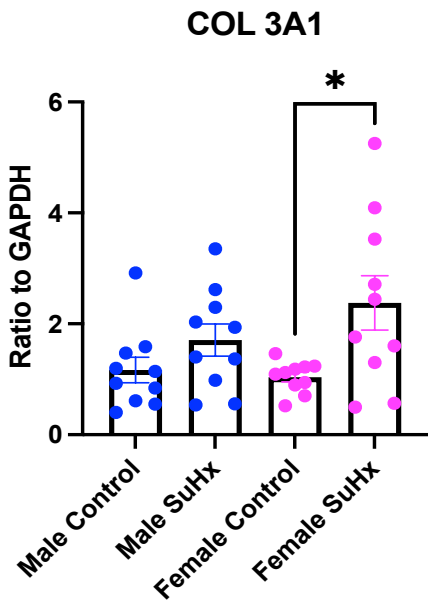
COL 3A1
Ratio to GAPDH
6
4
2
0
*
Male Control
Male SuHx
Female Control
Female SuHx

C

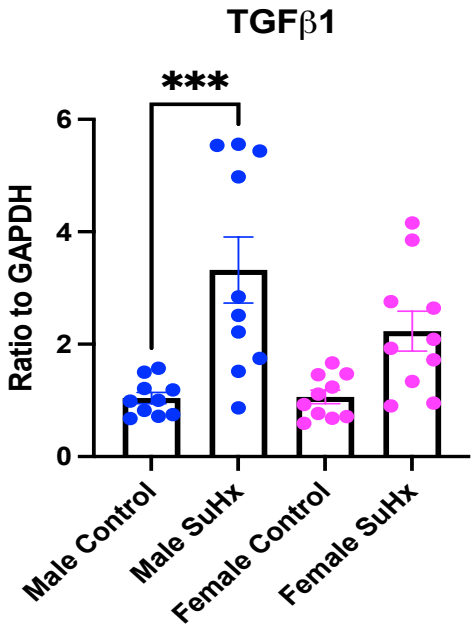
TGFβ1
Ratio to GAPDH
6
4
2
0
***
Male Control
Male SuHx
Female Control
Female SuHx

D

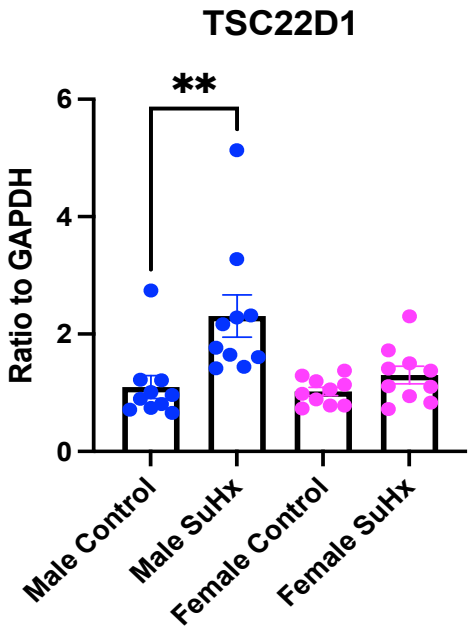
TSC22D1
Ratio to GAPDH
6
4
2
0
**
Male Control
Male SuHx
Female Control
Female SuHx

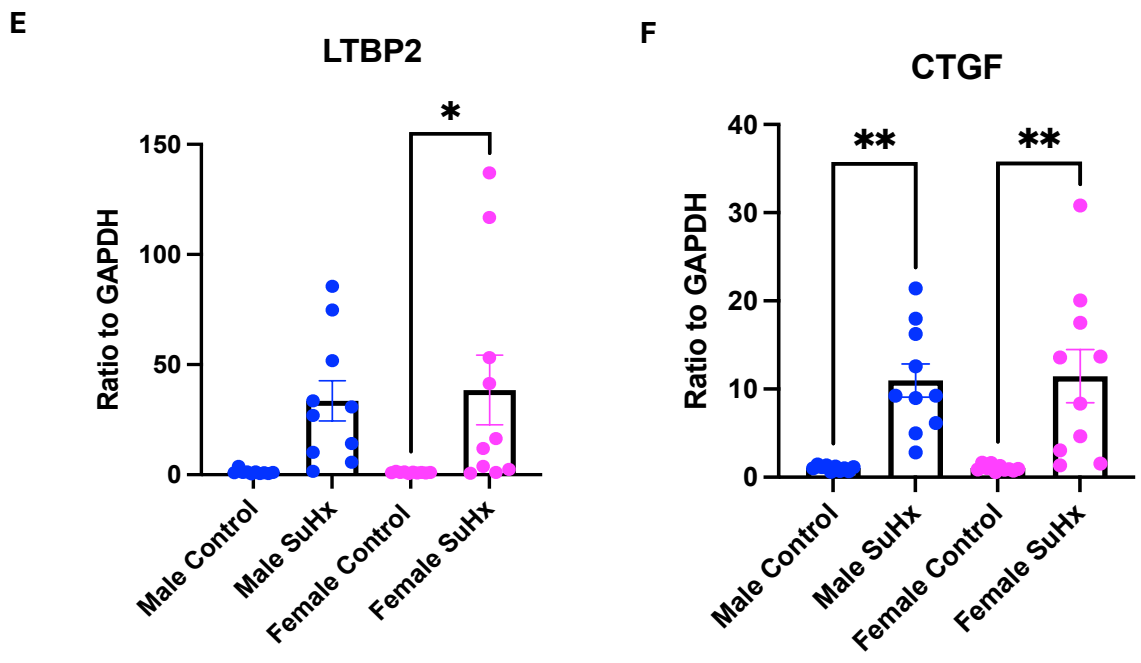

Figure 3.10. The effect of SuHx on RV gene expression linked to fibrosis and cardiac remodelling

Quantitative polymerase chain reaction (qPCR) was performed on right ventricular (RV) tissue harvested from the male and female control and Sugen-hypoxia (SuHx) rats. A) collagen type 1 alpha 1 chain col1a1 gene expression B) collagen type 3 alpha 1 chain col3a1 gene expression C) transforming growth factor β 1 TGFβ1 gene expression D) transforming growth factor β 1 stimulated clone 22, TSC22D1 gene expression E) latent transforming growth factor β binding protein 2, LTBP2 gene expression F) connective tissue growth factor, CTGF gene expression. All values represent the mean ΔΔCT value ± standard error of the mean (S.E.M). All data was normalized to the housekeeper, glyceraldehyrde-3-phosphate dehydrogenase (GAPDH) gene expression with n=10 per group. Samples were performed in triplicates and data was analysed using the two-way ANOVA with *p<0.05, **p<0.01 and ***p<0.001.

3.9 Proliferating cell nuclear antigen is upregulated by SuHx in both male and female SuHx rats

Proliferating cell nuclear antigen (PCNA) is an important factor involved in DNA replication and repair (González-Magaña and Blanco, 2020). Using IHC, we stained the RV tissue from male and female control and SuHx rats with an anti-PCNA antibody to target the highly proliferating cells which can be identified as bright red in colour (Figure 3.11 A). We found that there was an increase in PCNA protein expression in both the male SuHx versus male control (18.59 ± 3.04 % vs. 2.31 ± 0.71 %, ****$p<0.0001$, n=7-9) and female SuHx versus female control rats (11.96 ± 1.87 % vs. 2.12 ± 0.75%, **$p<0.0019$, n=7-8) (Figure 3.11 B). We then directly compared the collagen deposition in terms of area fraction (%) versus the PCNA (%) (Figure 3.11 C). We found that in the male SuHx and female SuHx rats as PCNA increases, there is an increase in collagen deposition (Figure 3.11 C). Meanwhile, male control and female control rats which represent a lower PCNA (%) are associated with lower levels of collagen deposition (%) (Figure 3.11 C). In addition, the linear regression line for female is below the male, which implies that at the same proliferation rate (PCNA) in response to SuHx, female RV displays less fibrosis, indicating that the female RV responds better in terms of fibrosis than the males.

A

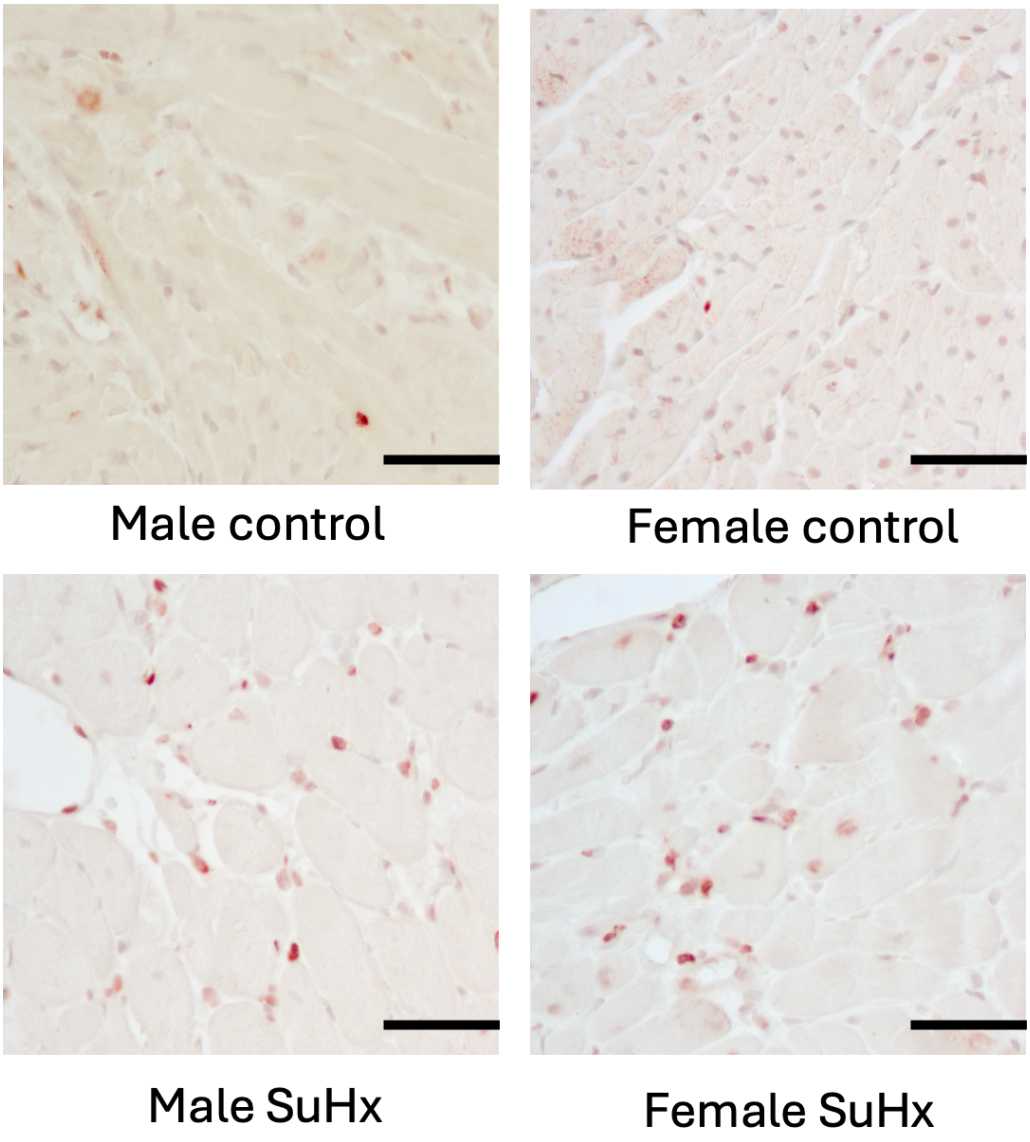
Male control
Female control
Male SuHx
Female SuHx

B

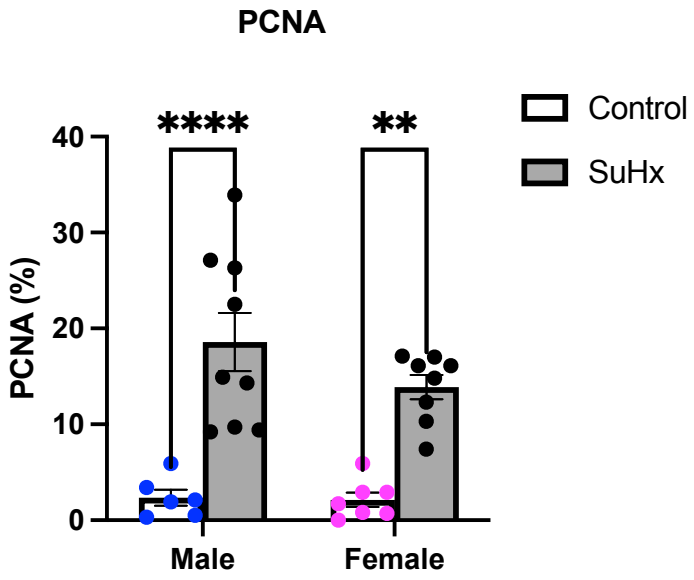
PCNA
PCNA (%)
40
30
20
10
0
****
**
Male
Female
Control
SuHx

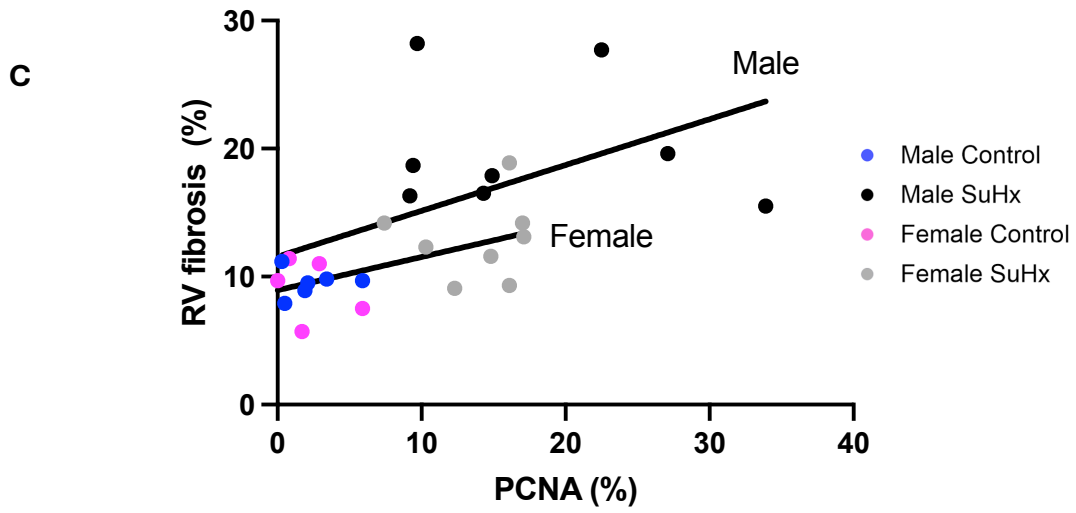

Figure 3.11. Proliferation marker PCNA was significantly upregulated in RV tissue from male and female control and SuHx rats

Immunohistochemistry (IHC) was performed using an anti-proliferating cell nuclear antigen (PCNA) antibody (1:5000) on right ventricle (RV) tissue to detect the expression of PCNA protein from male and female control and SuHx rats. PCNA positive cells can be detected as they appear bright red in colour versus negative cells which appear as a dull/light red. A) PCNA representative images B) quantification of PCNA positive cell count, which was ratioed to the total cell count and represented as a percentage. C) Simple-linear regression of PCNA (%) versus collagen deposition (%) was performed for male and female control and SuHx rats. Each data point represents an individual rat. Between 2-10 images were analysed for each rat, with n=7-9 across the groups. Statistical analysis was performed using a two-way ANOVA. Images were captured at 40x. Scale bar represents 100μm.

3.10 Myocyte area is increased by SuHx in both male and female rats

Hypoxia induced cardiac hypertrophy is associated with increases in myocyte size (Johnson et al., 2023). Therefore, we assessed cross sections of RV tissue, which was pre-stained with picrosirius red to determine myocyte size from the male and female SuHx rats. The myocyte size was measured by drawing around the myocyte and obtaining its area, which was repeated for several myocytes from the one rat. The area of the myocytes was then averaged to obtain the overall mean myocyte area from the one rat (Figure 3.12 A). Here, we found that the myocyte area (μm^2) was increased for both male SuHx versus male control (375 ± 30.08μm^2 vs. 169.7 ± 14.63μm^2, ****p<0.0001, n=7-9) and female SuHx versus female control rats (396.0 ± 37.07μm^2 vs. 114.5 ± 2.71$\mu m^{2,}$ ****p<0.0001, n=6-9) (Figure 3.12 B). When we compared only the male and female control groups, we found that there was also a reduction in the female control group (114.5 ± 2.71μm^2 vs. 169.7 ± 14.63μm^2, **p<0.01, n=6-7) (Figure 3.12 C).

A

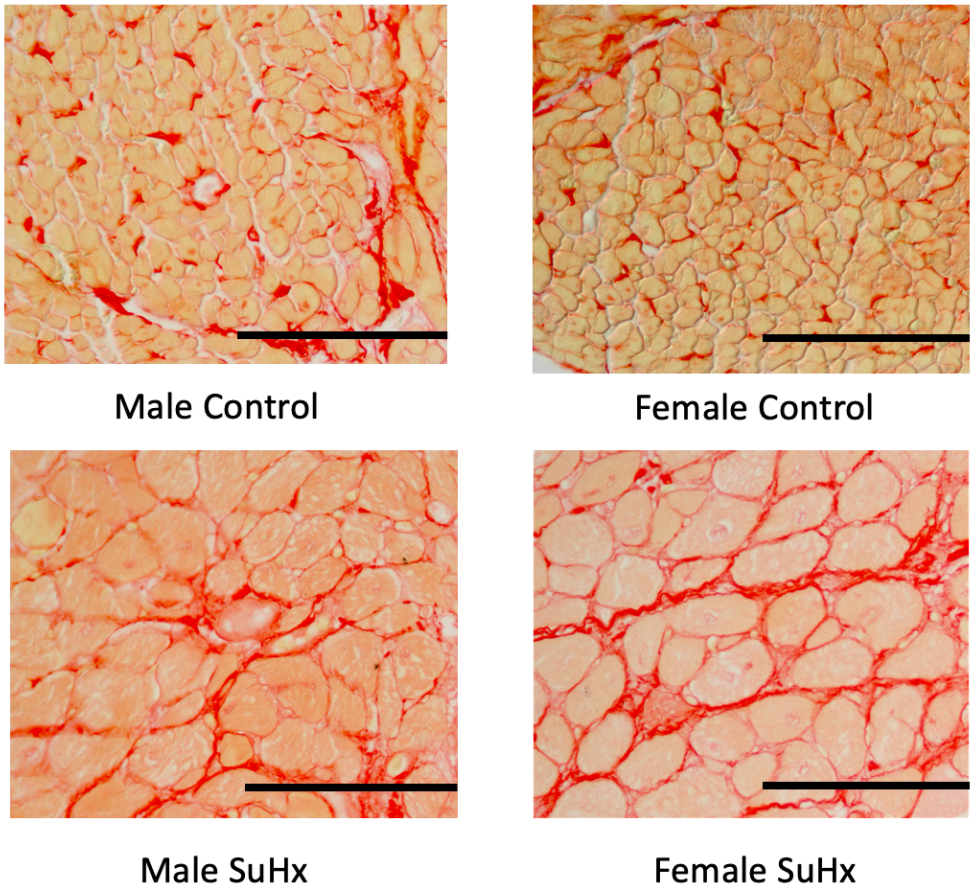
Male Control
Female Control
Male SuHx
Female SuHx

B

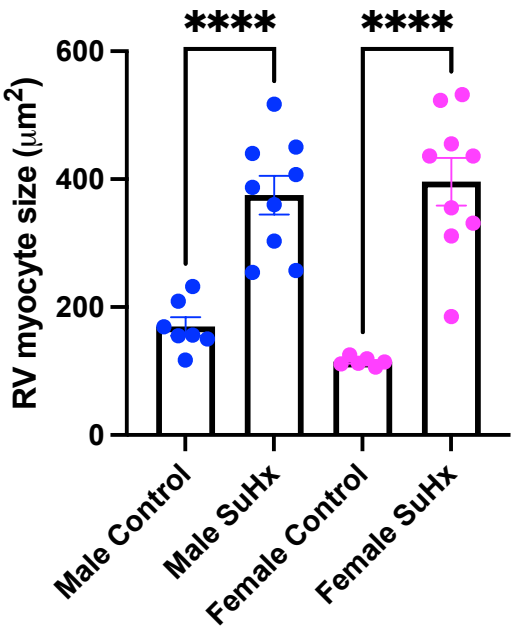
RV myocyte area
****
****
RV myocyte size (μm²)
600
400
200
0
Male Control
Male SuHx
Female Control
Female SuHx

C

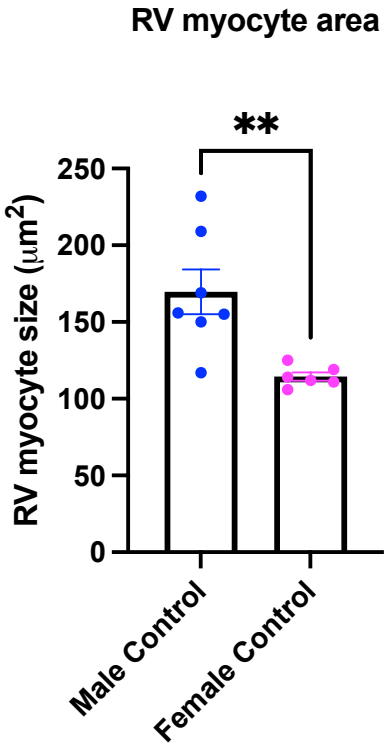
RV myocyte area
**
RV myocyte size (μm²)
250
200
150
100
50
0
Male Control
Female Control

Figure 3.12. The effect of SuHx on myocyte area in male and female rats

A) representative images of picrosirius red stained right ventricle (RV) tissue from male and female control and SuHx rats. B) Quantification of the myocyte area which was calculated by drawing around the area of a single myocyte. C) Quantification of the myocyte area but only comparing the control groups. The area was obtained for several myocytes (10-20 myocytes) from the one rat, which was then averaged to obtain the overall mean area of a myocyte from the one rat (μm^2). One data point represents one rat. n=6-10. Scale bar represents 100μm. All data represent mean ± standard error of the mean (S.E.M). Statistical analysis was performed using the two-way ANOVA for figure B and unpaired t test for figure C. **p<0.01 and ****p<0.0001.

3.11 Pulmonary arteries in the male and female SuHx rats

To further characterise the SuHx model, we examined lung sections from the male and female control and SuHx rats, which were stained with Millars elastin stain and Haematoxylin and Eosin (H&E) which allowed us to visualise some of the PA. Millars elastin stain will stain the elastin layers in the PA as a brown-black colour (Figure 3.13 A), and it is known that within PH the PA vessels will become muscularised in which they will develop a double elastic lamina. Meanwhile, H&E stains the cytoplasm as pink and the nuclei blue, enabling for visualisation of the PA vessel structure (Figure 3.11 B).

A

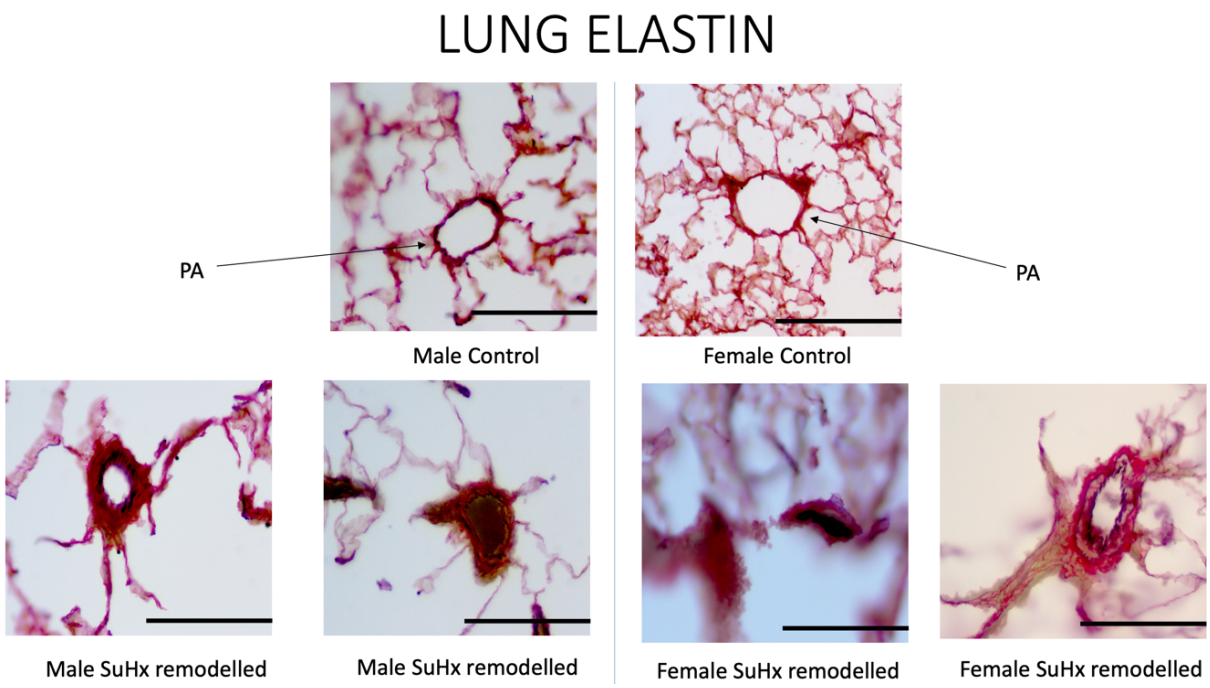
LUNG ELASTIN
PA
PA
Male Control
Female Control
Male SuHx remodelled
Male SuHx remodelled
Female SuHx remodelled
Female SuHx remodelled

B

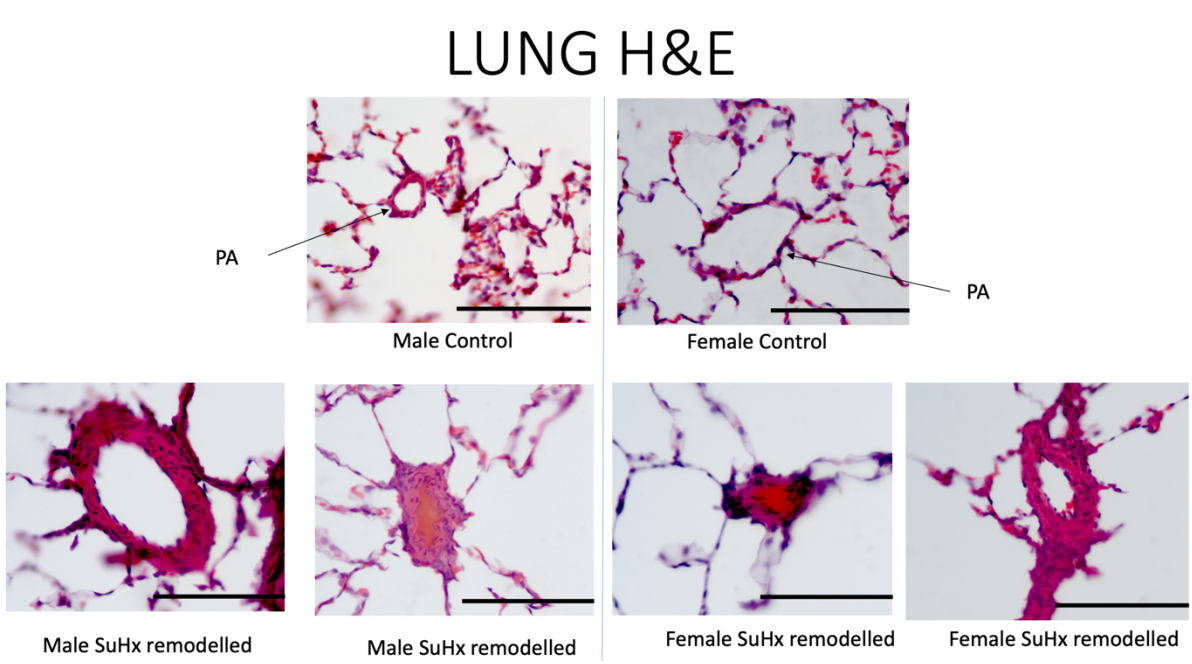
LUNG H&E
PA
PA
Male Control
Female Control
Male SuHx remodelled
Male SuHx remodelled
Female SuHx remodelled
Female SuHx remodelled

Figure 3.13. Male and female control and SuHx pulmonary artery vessels

Male and female control and SuHx rat's lung tissue was counterstained with (A) Elastin and (B) H&E. Vessels stained with H&E and elastin to examine the PA vessel structure. Arrows point to the location of the pulmonary artery. Scale bar represents 100μm.

3.12 Discussion

The aim of chapter 3 was to characterise the SuHx rat model by assessing the rats haemodynamics, pathological changes within the pulmonary vasculature and the functional and structural remodelling changes within the RV. Firstly, we are able to report that we were able to successfully replicate the SuHx model as described by Nicolls and colleagues by producing a PH phenotype (Nicolls et al., 2012). The choice of rats as the model species was primarily due to the fact that the SuHx model was originally developed in rats (Taraseviciene-Stewart et al., 2001). Gomez-Arroyo has also reported multiple failed attempts using a mouse SuHx model (Gomez-Arroyo et al., 2012). As well as this, the mouse SuHx models exhibit a much less severe PAH phenotype and do not show the same characteristics which can be found in the rat models, such as the occluded vessels and obliterative angiopathy (Vitali, 2019). It has also been reported that once the mice enter their normoxia period, the RV hypertrophy will return to normal, hence they will not progress into RV failure, which are key features of human PAH that must be presented in the models to allow for them to be targeted (Vitali, 2019). The SuHx rat model has since been used extensively amongst different research groups (Vitali et al., 2014, Mamazhakypov et al., 2020, Hamberger et al., 2022). Majority of the studies carried out using the SuHx model use only the male sex, and given the sexual dimorphism within PAH (Rafikova et al., 2015), we realised the importance of investigating both the sexes and thereby incorporated both male and females in our study.

We firstly looked at the bodyweights at the start of the study, where we did not find any differences between the control and SuHx groups for both male and female. However, we did find the male rats to be significantly heavier than the females as expected due to the differences in their natural growth rate, food intake and gonadal hormones secretions. At their final weight, we found this sex difference between the males and female weight remained the same, with the males being significantly heavier. We also found there was a significant reduction in the male SuHx weight versus its control. There is an overwhelming amount of evidence showing the trend in sick animals and their reduced food-motivated behaviour, which could be mediated by the infiltration of inflammatory cytokines in the SuHx rats (Johnson, 1998). It is interesting that there was no reduction in the female SuHx

bodyweight given that these animals are also sick. The preservation of the female bodyweight could be due to the protective activity of estrogen or differences in the stress response making them less vulnerable to weight loss.

The hemodynamic parameters confirmed the development of SuHx induced PH. It is worth noting that we did use the open-chest method to record our hemodynamic parameters and given that this is a highly invasive technique it can cause disruption to the cardiac and respiratory system potentially affecting the PV loop data. Therefore, it is more suitable to use the close chest method. We firstly examined the RV function by recording the RVSP. Here we found, that SuHx significantly increased RVSP in both male and female SuHx rats, whilst it had no effect on LVSP. Interesting, we did find that the RVEDP was only increased in the male SuHx group. Increases in RVEDP has been associated with worse mortality and positively correlates with ventricular structural remodelling (Imamura and Kinugawa, 2017). Similarly, when we assessed LVEDP we found no differences, indicating that the effects we will see will be subject to the changes within the RV. When we looked at the effective pulmonary effective arterial elastance (Ea), which is an indicator of the RV afterload, we found that SuHx increased this in both male and female. The coupling between the cardiac contractility and arterial system can be analysed using the ratio of Ees to Ea, also known as RV-PA coupling which is able to give an overall indication of the cardiovascular function and efficiency. Here, we found the RV-PA coupling was reduced in only the male SuHx rats, suggesting that females have better RV function in response to the SuHx. We did also examine the PA vessel structure to further characterise the model, however given that we did not quantify the images we cannot confirm whether remodelling has occurred within the PA which is a limitation of this study.

The RV hypertrophy was measured by the Fulton index, which is the RV weight scaled to the LV+S weight and here we found that there was a significant increase in both male and female SuHx groups, confirming the development of RV hypertrophy, as a result of the increases in RV afterload. We did, however, see that there was a significant increase in LV+S weight in the female SuHx group, which can influence the ratio. It is now recommended that RV hypertrophy should be measured by ratioing the RV weight to the tibia length to avoid any biases due to changes in LV+S weight/potential LV remodelling and also bodyweight (Hagdorn

et al., 2019). Nevertheless, this increase in Fulton index does suggest that the male and female SuHx rats did undergo a significant degree of RV hypertrophy.

Following these findings, we then measured the size of the myocyte area within the RV tissue. Here we found, the female control baseline myocyte area to be significantly smaller versus the males. However, the female SuHx rats show that it does increase to the same size as the male SuHx rats, suggesting that the female rats underwent a greater increase in myocyte size in response to SuHx. This may explain why there was preservation in RV-pulmonary artery coupling in female only but not in male.

We then investigated the interstitial collagen deposition within the RV tissue. Collagen is synthesised predominately by the fibroblasts and plays an important role in maintaining cardiac structure and function (Andersen et al., 2019). In PAH, there is excessive activation and proliferation of the collagen-producing fibroblasts, that eventually leads to excessive fibrosis within the RV, which is one of the main hallmarks of PAH induced RV failure. RV fibrosis has been measured in human patients with PAH, where they detected higher levels when compared with their respective controls; (9.6 ± 0.7% vs. 7.2 ± 0.6%, $p<0.01$ n=9-11) (Rain et al., 2013), (4.1 ± 0.6% vs. 2.3 ± 0.7%, $p<0.01$, n=5-6) (Bruggen et al., 2016). When we measured the collagen deposition within the RV tissue, we detected a significant increase in collagen content in only the male SuHx rats, which points towards male SuHx undergoing worse RV fibrosis. We propose that the increases in RVEDP that we see in only the male SuHx could be associated with this higher degree of RV interstitial fibrosis, which we also only detect in the male SuHx rats. In addition, the increase in RV myocyte size in the female SuHx rats may explain why the female RV developed the same degree of hypertrophy (indicated by Fulton index) as the males in response to the SuHx. When examined at the gene expression level, we found the opposing effects in which we seen a significant increase in Col1a1 and Col3a1 in the female SuHx rats. Although, it has been reported that Col1a1 and Col3a1 are highly time dependent (Marlovits et al., 2004). The increase in Col1a1 and Col3a1 gene expression but not protein detected by PSR staining in the female SuHx, could be as a result of the genes not having enough time to translate into protein. Alternatively, at the time we

measured the RV interstitial fibrosis, perhaps enough of the protein in the male SuHx had been made causing the genes to be downregulated through negative feedback.

We then had a look at the expression of genes which play a key role in tissue fibrosis including TGF-β1, which was found to be increased in only the male SuHx rat. The same was seen for TSC22D1, a facilitator of TGF-β1 signalling (Yan et al., 2011). Given these genes play a role in activating the fibroblasts and contributing towards fibrosis, reduced expression could be associated with a reduction in RV hypertrophy and mass. Consistent with the increased RV hypertrophy that we see in both sexes, we found that CTGF, another marker of fibrosis was upregulated in both the male and female SuHx rats. However, LTBP2, a novel gene member that belongs to the TGF-β family and plays a role in fibrosis, was found to be increased in only the female SuHx rats. We did also examine these genes at the protein expression level, but due to antibody complications we were not able to retrieve any clear data.

The RV tissue from the male and female SuHx showed increased levels of PCNA protein expression detected by IHC. PCNA positive cells were present in the myocytes from the RV, however we only counted the PCNA positive fibroblasts cells as a direct measurement of fibroblasts proliferation. This increase in PCNA positive cells was expected in the male SuHx rats as they also illustrate an upregulation in their interstitial collagen deposition. We did not detect this increase in collagen deposition in the female SuHx rats, but as we did see that the females had underwent significant RV hypertrophy (measured by Fulton Index) alongside increased RV myocyte size, we presume that fibroblast proliferation may have contributed to the RV hypertrophy, which we have confirmed by the PCNA staining. We then directly measured PCNA versus collagen deposition, and as expected, for both male and female SuHx rats as PCNA increased, there was also an increase in collagen deposition.

Overall, to summarise the findings from chapter 3, we illustrate that the male SuHx rats have worse RV-pulmonary artery coupling, as seen by reduced Ees/Ea compared to the females. We show that the males SuHx demonstrate increased RVEDP, which could be connected to the higher degree of RV interstitial fibrosis as increased fibrosis would contribute to a stiffer RV and thereby increase the RVEDP, which was also only observed in only the male SuHx rats.

We found the increase in interstitial fibrosis in the males to be associated with upregulated expression of the pro-fibrotic genes: TGF-β1, TSC22D1 and CTGF. We show that both male and female myocyte sizes are increased as a result of RV hypertrophy, although the myocyte area appears to undergo a larger increase in size in the female SuHx rats. While it is known that male PAH patients tend to have worse RV function and that male and female PAH patients do undergo more fibrosis in their RV when compared to healthy controls, it has not yet been investigated whether this fibrosis is worse in the male patients. Currently, there are no treatments targeting the RV fibrosis in PAH patients. Therefore, there is a need for more research to investigate the mechanisms driving this fibrosis and the associated sex differences to identify potential targets.

3.13 Summary

Overall, chapter 3 demonstrates that we were able to reproduce the SuHx model phenotype in both male and female Sprague-Dawley rats. We confirmed the SuHx model by specifically showing the rats' haemodynamics profiles, which confirmed an increased RVSP, and by measuring several different parameters linked to fibrosis, hypertrophy, pulmonary remodelling, and proliferation. We highlight key sex differences in the male SuHx rats, which exhibit worse RV interstitial fibrosis and elevated RVEDP. We targeted a fibrosis pathway by measuring the gene expression of Col1a1, Col3a1, TGF-β1, TSC22D1, and LBTP2 in RV tissue for the first time, and found key sex differences in the male and female SuHx rats. Many studies using the SuHx rat model have variabilities in their protocols, with the main differences in their hypoxia and normoxia exposure periods. We achieved the SuHx model by using a single subcutaneous Sugen (25mg/kg) injection followed by 3-weeks in hypoxia (10% O_2) and 5 weeks in normoxia. Given that we are able to successfully mimic key features seen in human PAH patients (remodelled PA vessels and increased RVSP), we propose that this protocol could be utilised for future studies.

CHAPTER 4

4. Sex differences in mitochondrial related gene expression in the RV and lungs

4.1 Introduction

Mitochondria are the energy powerhouses of all eukaryotic cells, as they are responsible for providing the cells with adenosine triphosphate (ATP) via oxidative phosphorylation (Brand et al., 2013). However, in pulmonary arterial hypertension (PAH), there is a reprogramming of the cell metabolism, which shifts it over to an aerobic glycolytic state leading to a reduction in the amount of ATP produced (Riou et al., 2023). Within PAH, there is excessive proliferation of both myocardial right ventricular (RV) fibroblasts and pulmonary artery smooth muscle cells (PASMCs), therefore the ATP demand begins to exceed the ATP supply which can then offset detrimental cellular processes such as, apoptosis within both the RV and pulmonary vasculature (Ryanto et al., 2023). This impaired metabolism has also been demonstrated to reduce RV myocyte contractility during systole in the heart (Tian et al., 2020b).

Mitochondria quickly adapt to their conditions via a number of mechanisms referred to as biogenesis (the formation of new mitochondria), fusion and fission (division) (Bonnet et al., 2006). They are normally tightly regulated by a series of fusion and fission events allowing the mitochondria to exist in a highly dynamic filamentous network. However, in PAH there is a favourable shift towards excessive fission which leads to the mitochondria losing its filamentous structure and becoming fragmented, which further reduces ATP production and has been shown to promote reactive oxygen species (ROS) in the RV (Breault et al., 2023). Within PAH, overexpression of fission proteins has been identified in RV fibroblasts and in the PASMCs (Bonnet et al., 2007, Marsboom et al., 2012, Tian et al., 2017, Tian et al., 2018). An inhibitor of the fission protein dynamin related protein 1 (Drp1) known as Drpitor1a was found to reduce mitochondrial fission, cell proliferation and inhibit apoptosis in human PAH PASMCs (Wu et al., 2023). In monocrotaline (MCT) induced PH rats, Drpitor1a reduced pulmonary artery (PA) obstruction, lowered pulmonary vascular resistance and overall improved RV function (Wu et al., 2023). Thus, the results demonstrated by Wu et al., shine light on the potential impact that excessive mitochondrial fission may have on PAH patients. Limited research has been done examining the sex differences in the mitochondrial dynamics

gene expression profile within the RV, therefore we aim to examine this in the Sugen-hypoxia (SuHx) rat model.

Beside that females demonstrate preserved RV function in PAH, there is growing evidence to suggest that females also have better mitochondrial capacity than the males (Cardinale et al., 2018). Previous studies have shown that the female mitochondria, have higher antioxidant capacity and produce less ROS when compared with males, which is proposed to be predominately due to the protective actions of the estrogens (Vina et al., 2011, Görlach et al., 2015). Hence, the current evidence under healthy conditions points towards females exhibiting better mitochondrial function. However, whether this sex differences exists in a PAH environment remains unknown. The data from PAH models suggests that restoring mitochondrial metabolism, by decreasing fatty acid oxidation, increasing PDH activity, glucose oxidation and ATP production in PAH may lead to improved RV function by increasing RV contractile function, reducing cell proliferation and collagen production in the RV fibroblasts (Fang et al., 2012). This has been found in pulmonary artery banding (PAB), MCT, Fawn-Hooded and SuHx rat models of PH in both RV myocytes and RV fibroblasts (Piao et al., 2010, Fang et al., 2012, Piao et al., 2013a, Piao et al., 2013b, Frump et al., 2015, Drozd et al., 2017, Tian et al., 2017).
Although, it must be noted that these studies mentioned above examine only the male sex and not the female, therefore the sex differences remain unknown.

It was previously reported that ischemia induced injury may be responsible for the detrimental mitochondrial changes which take place within the RV in PAH (Ryan et al., 2015a). Ischemia has been found to occur in the RV in rodent models of PAH including male MCT rats, male SuHx rats and in male and female human PAH patients (Dasgupta et al., 2020, Wu et al., 2021). It was also found that restoring right coronary perfusion via supra-aortic banding in MCT-induced PAH in male rats improves oxidative metabolism and RV function (Tian et al., 2020b).

Therefore, the aims of this investigation were to assess the effect of SuHx-induced PH on RV right coronary artery (RCA) remodelling and mitochondrial function. We investigate the RCA

remodelling including vessel wall remodelling in the intima and media layers and perivascular collagen deposition and whether there were any sex differences, as this has never been done before in a SuHx rat model. As well as this, we examined MitoSox, mitochondrial membrane potential and mitochondrial morphology in the RV. We also investigate the RV and lung expression of genes linked to mitochondrial dynamics and function and their sex differences. Indeed, we hypothesise that mitochondrial function in terms of biogenesis, dynamics and oxidative stress is better preserved in the RV of females and that sex is involved in the mitochondrial abnormalities in PAH associated RV failure. Due to this, we propose that more intact mitochondrial function will be positively correlated with less severe RCA remodelling in the females. In order to determine this, using the SuHx rat model, we used immunohistochemistry to stain and examine the RCA collagen deposition. Similarly, using the SuHx rat model, we stained fresh pieces of RV tissue for mitochondrial properties which were then imaged using the confocal microscope. We then followed this up by using qPCR to examine mitochondrial gene expression in both the RV and lung tissues.

The objectives of this chapter were to:

- Examine the degree of RCA vessel remodelling and RCA collagen deposition
- Examine mitochondrial membrane potential via TMRM, mitochondrial superoxide via MitoSOX, and mitochondrial morphology via MitoTracker Green in male and female control and SuHx rats
- Assess gene expression linked to hypoxia, mitochondrial biogenesis, mitochondrial dynamics, and mitochondrial oxidative stress in control and SuHx RV and lung tissue

4.2 The effect of SuHx on RCA remodelling in male and female rats

It has been found that in PAH, there is a reduction in systolic RCA flow due to an increase in RV pressure and RV mass (van Wolferen et al., 2008). RCA remodelling may contribute to the change in RCA flow. Due to this, we measured the perivascular collagen deposition and intima-media thickness from the RCA vessels from both male and female control and SuHx rats to determine the sex differences as this has yet to be reported. The vessels were subcategorised into groups based on their diameter sizes (15-50μm, 50-100μm and >100μm). Vessels below 15μm were excluded in case they were mistaken for a capillary. Figure 4.1 shows representative images of the RCA from both male and female control and SuHx rats.

Firstly, we analysed the perivascular collagen area by ratioing the perivascular collagen area to lumen area, and here we found that in the male control, as diameter decreases, there is a slight increase in the ratio (R^2=0.09 and p<0.12) (Figure 4.2 A). In male SuHx, as diameter increases there is a greater reduction in the collagen ratio (R^2=0.23 and p<0.0002) (Figure 4.2 A). We found there was a significant difference between the two slopes (p<0.0129) (Figure 4.2 A). We then directly compared the differences in the collagen ratio with the vessels separated into three different size groups. This showed that the greatest increase and remodelling in collagen content took place in the male SuHx vessels which had a vessel diameter between 15-50μm (1.45 ± 0.13 vs. 0.90 ± 0.11, *p<0.05, n=12-21) (Figure 4.2 B). In the female, as diameter decreases no differences in the ratio were detected for both female SuHx and control rats (Figure 4.2 C). Similarly, when the three RCA vessel size groups were compared, no differences were detected (Figures 4.2 D).

Next, we analysed the intima-media thickness (ratioed to the vessel diameter mentioned above). In male control, as diameter decreases there is an increase in the intima-media thickness (R^2=0.28 and p<0.0059) (Figure 4.3 A). In male SuHx, as the diameter increases, the ratio is also reduced ($R^{2=}$0.21 and p<0.0004) (Figure 4.3 A). There was no differences found between the slopes (Figure 4.3 A). As described above, the vessels were subcategorised into the same groups based off their diameter size. This revealed no changes across the different vessel diameters for the male rats (Figure 4.3 B). Meanwhile, as the female control diameter

decreases there is an increase in the intima-media thickness (R^2=0.30 and p<0.0037) (Figure 4.3 C). In female SuHx, we found that as diameter increases there is a reduction in the intima-media thickness (R^2=0.0002 and p<0.9167) and there was a significant difference between the slopes (p<0.0174) (Figure 4.3 C). When we compared the vessels by size, we detected a significant, though slight, reduction in the ratio in the female SuHx rats, in the vessels belonging to the 50-100μm group (Figure 4.3 D) (0.10 ± 0.01 vs. 0.15 ± 0.01, *p<0.05, n=12-14).

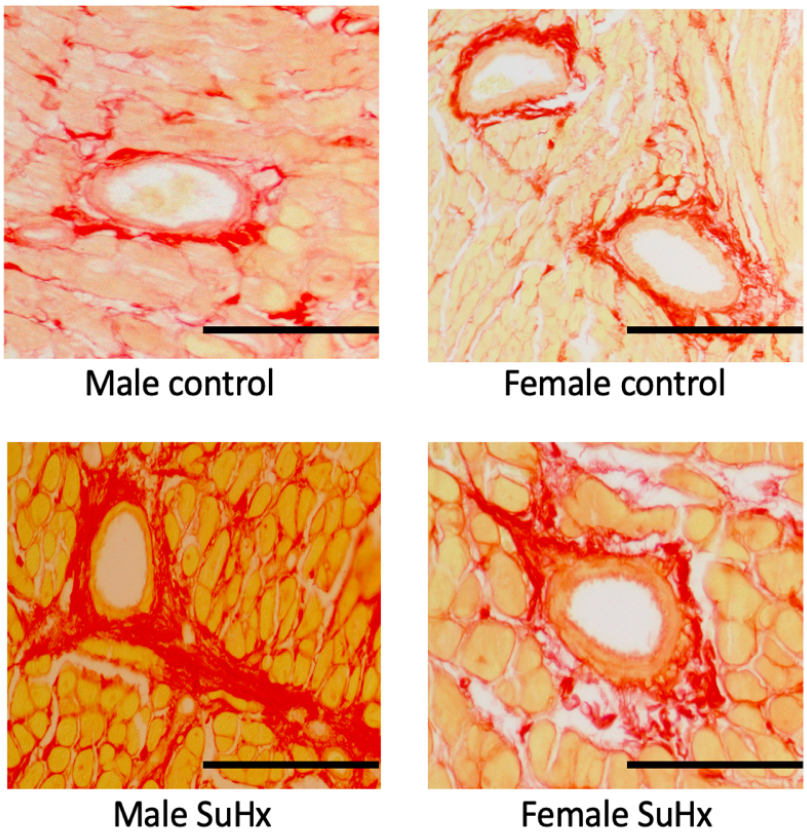

Figure 4.1. SuHx induces RCA vessel remodelling in the male RCA vessels

Male and female control and SuHx right coronary artery (RCA) vessels were stained with picrosirius red to aid for RCA vessel detection within the male and female control and SuHx RV tissue. Images shown were taken at 20x magnification. Scale bar represents 100μm.

A

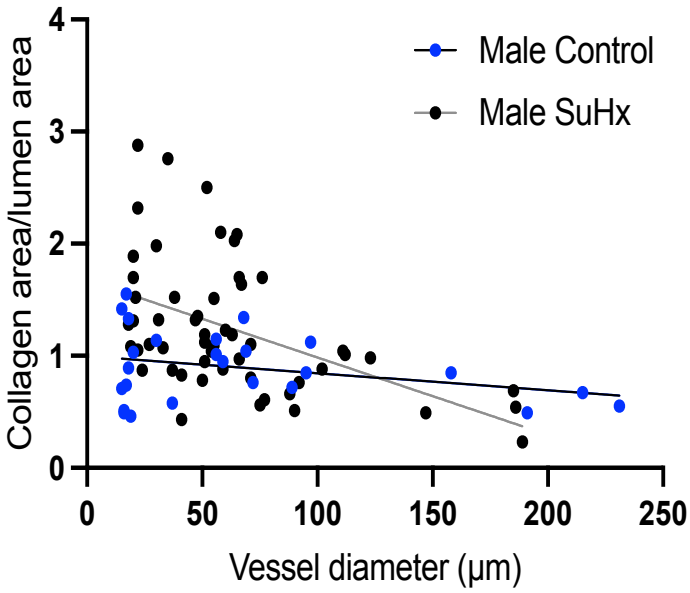
Male Control
Male SuHx
Collagen area/lumen area
0
1
2
3
4
0
50
100
150
200
250
Vessel diameter (μm)

B

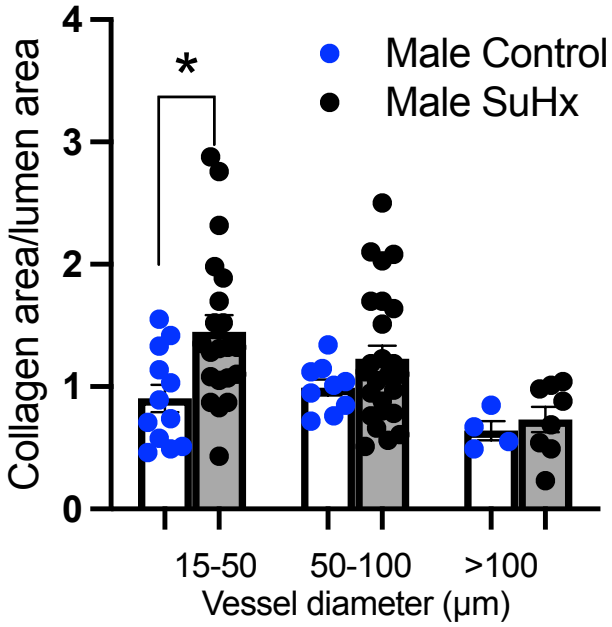
*
Male Control
Male SuHx
Collagen area/lumen area
0
1
2
3
4
15-50
50-100
>100
Vessel diameter (μm)

C

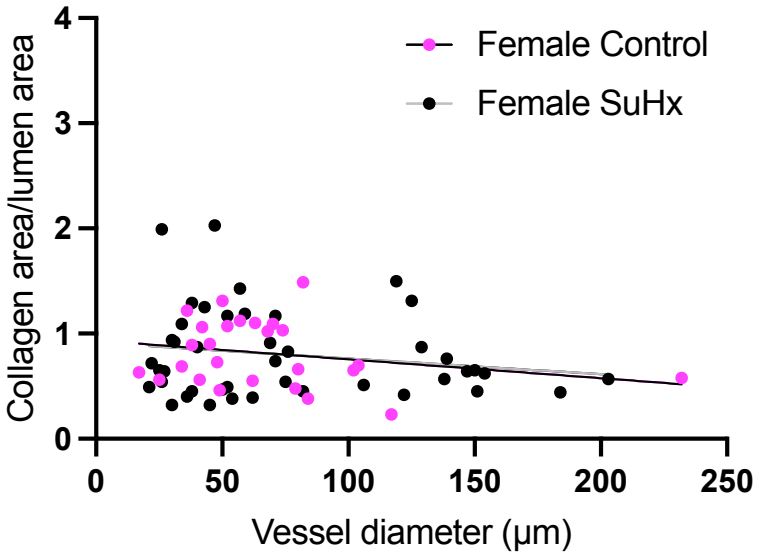
Female Control
Female SuHx
Collagen area/lumen area
0
1
2
3
4
0
50
100
150
200
250
Vessel diameter (µm)

D

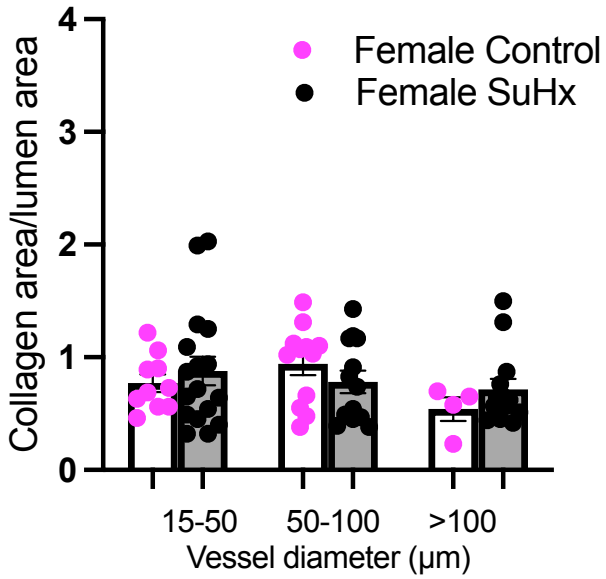
Female Control
Female SuHx
Collagen area/lumen area
0
1
2
3
4
15-50
50-100
>100
Vessel diameter (µm)

Figure 4.2. SuHx induces RCA collagen remodelling in the male RCA vessels

Male and female control and SuHx right coronary artery (RCA) vessels were stained with picrosirius red to detect the collagen area. The collagen area was then measured and ratioed to the lumen area. Figure A and B show the quantification for the male rats, whilst figure C and D show the female quantification. The areas were obtained using ImageJ software (National Institutes of Health, Bethesda, MD, USA) analysing images taken at both 20x and 40x magnification. Simple-linear regression was performed across all the vessels. The RCA vessels were categorised based on their vessel size (15-50μm, 50-100μm and >100μm). Results shown represent the mean ± SEM. Male n= 4-25 and female n= 4-17. The n number represents the number of RCAs from each group. All data represent the standard error of the mean (S.E.M). Statistical analysis was performed by using an unpaired t-test, with *$p<0.05$.

A

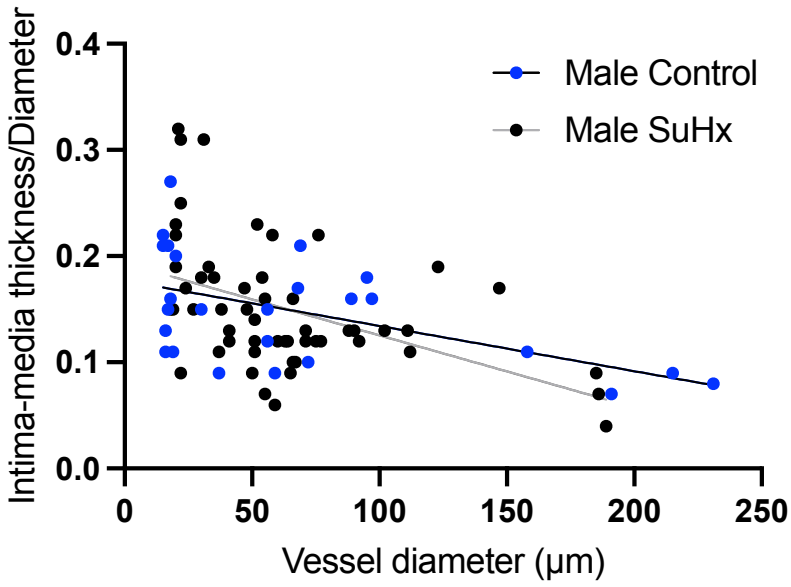
Intima-media thickness/Diameter
0.4
0.3
0.2
0.1
0.0
0
50
100
150
200
250
Vessel diameter (μm)
Male Control
Male SuHx

B

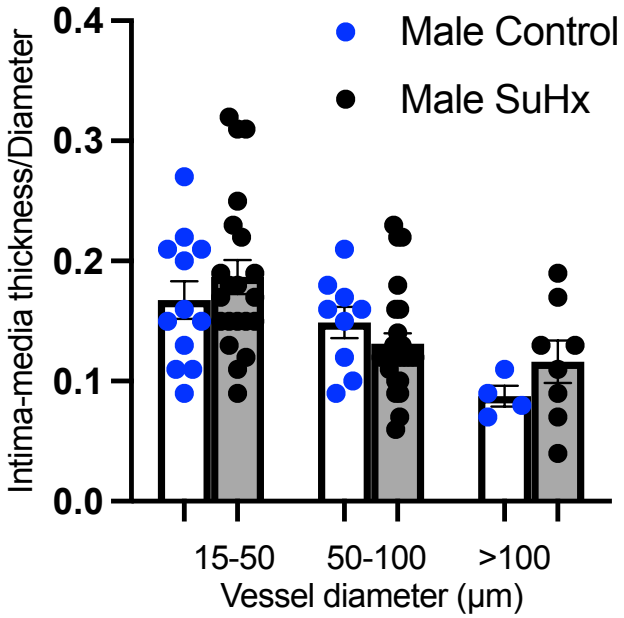
Intima-media thickness/Diameter
0.4
0.3
0.2
0.1
0.0
15-50
50-100
>100
Vessel diameter (μm)
Male Control
Male SuHx

C

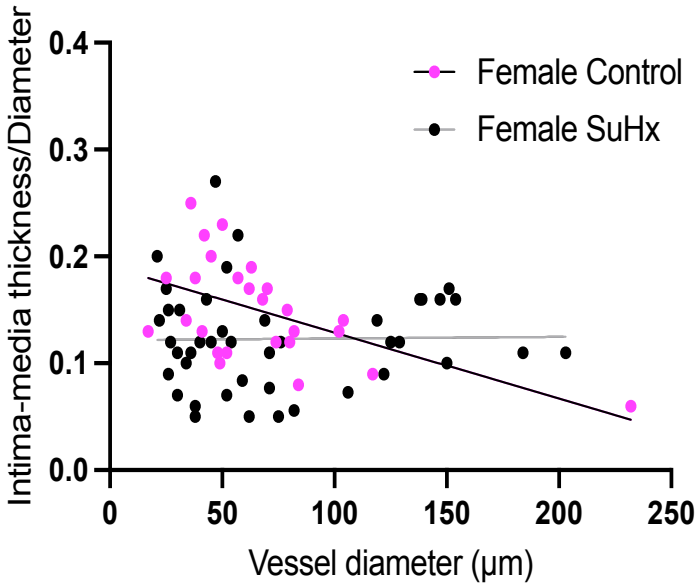
Intima-media thickness/Diameter
0.4
0.3
0.2
0.1
0.0
0
50
100
150
200
250
Vessel diameter (μm)
Female Control
Female SuHx

D

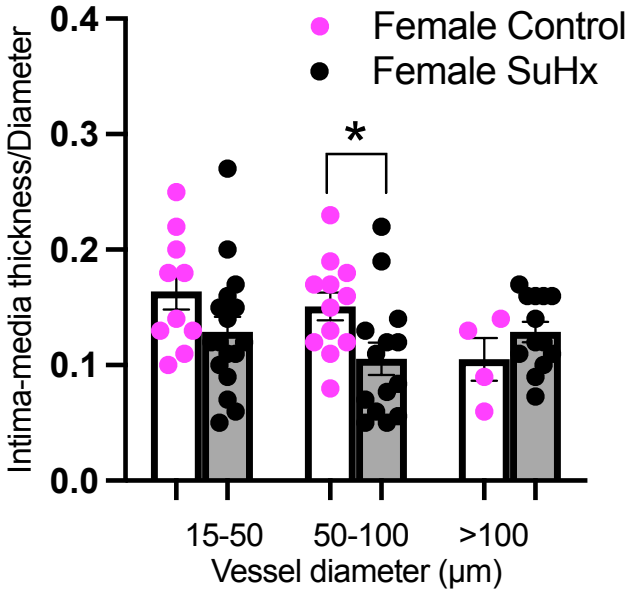
Intima-media thickness/Diameter
0.4
0.3
0.2
0.1
0.0
*
15-50
50-100
>100
Vessel diameter (μm)
Female Control
Female SuHx

Figure 4.3. SuHx induces an increase in RCA intima-media thickness in the female RCA vessels

Male and female control and SuHx right coronary artery (RCA) vessels were stained with picrosirius red to help identify the vessel layers and structure. The intima-media area was then measured and ratioed to the vessel's diameter. Figure A and B show the quantification for the male rats, whilst figure C and D show the female quantification. The areas were obtained using ImageJ software (National Institutes of Health, Bethesda, MD, USA) analysing images taken at both 20x and 40x magnification. Simple-linear regression was performed across all the vessels. The RCA vessels were categorised based on their vessel size (15-50μm, 50-100μm and >100μm). Male n= 4-21 and female n= 4-17. The n number represents the number of RCAs from each group. Statistical analysis was performed by using an unpaired t-test, with *$p<0.05$. All data represent the standard error of the mean (S.E.M).

4.3 The effect of SuHx on mitochondrial superoxide levels, mitochondrial membrane potential and mitochondrial morphology in male and female RV tissues

Fresh RV tissue from rats was incubated with the following stains: DAPI, MitoSox, Mito green tracker and TMRM at 37°C, 17-21% O_2 and 5% CO_2. The blue fluorescent dye, DAPI, is a widely employed nuclei stain to confirm the presence of a live cell which was used as a control on all RV tissues. The tissue was then co-incubated with TMRM, MitoTracker green or MitoSOX. TMRM acts as a measurement of mitochondrial membrane potential which fluoresces as red in colour. It is a lipophilic cationic dye, which is positively charged and able to accumulate within the mitochondria in an inverse manner to the mitochondrial membrane potential (Creed and McKenzie, 2019). MitoTracker green will accumulate within the mitochondrial matrix where it selectively binds to the mitochondrial proteins and fluoresces as green in colour (Presley et al., 2003). Meanwhile, MitoSOX which is also lipophilic and positively charged, will accumulate within the mitochondrial matrix where it becomes oxidized by mitochondria superoxide causing it to produce a strong red signal (Roelofs et al., 2015). It must be noted that MitoSOX will not become oxidized by the other ROS and RNS species.

The SuHx reduced mitochondrial membrane potential in only male SuHx rats compared to the male control (22.19 ± 2.33 vs. 52.20 ± 17.29, *p<0.05, n=5-8) (Figure 4.4 A and B). Additionally, there was a significant reduction in the mitochondrial fusion grade assessed on MitoTracker green-stained tissues in the male SuHx rats versus their control (2.36 ± 0.16 vs. 3.0 ± 0.00, **p<0.01, n=5-8) (Figure 4.5 A and B). Mitochondrial fusion grades were ranked from either 0 to 3, with 3 representing the most intact mitochondria which exhibits minor fragmentation. Although, the RV mitochondrial fusion grade from female SuHx rats appeared to be slightly reduced compared to their control, this did not reach significance and was significantly higher in the females SuHx versus male SuHx (2.79 ± 0.12 vs. 2.36 ± 0.16, *p<0.05, n=8-9) (Figure 4.5 A and B). While SuHx had no significant effect on MitoSox signal across all groups, although there was a strong trend toward reduction in male SuHx group compared to male control group (p=0.13) (Figure 4.6 A and B).

A

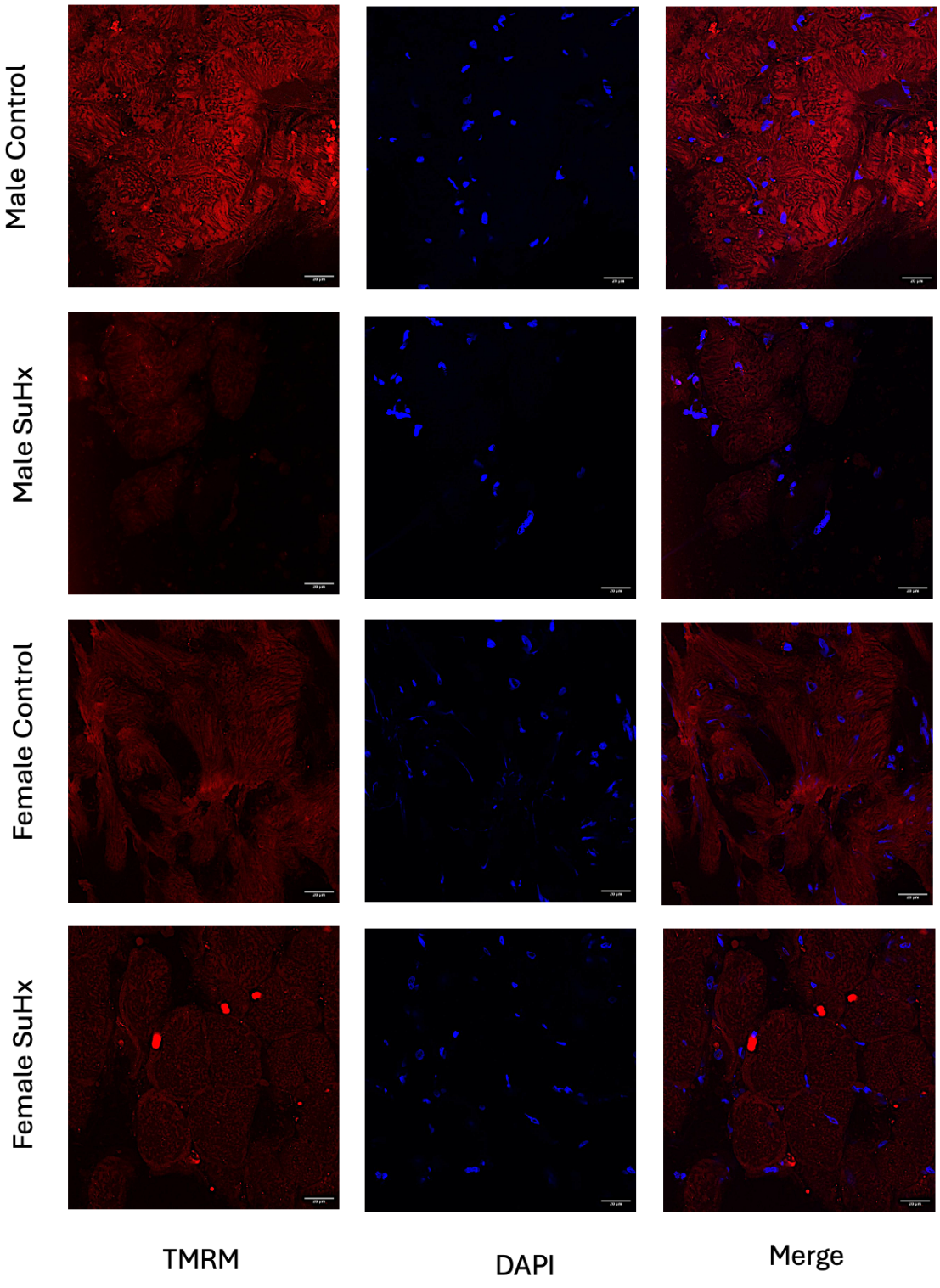
Male Control
Male SuHx
Female Control
Female SuHx
TMRM
DAPI
Merge

B

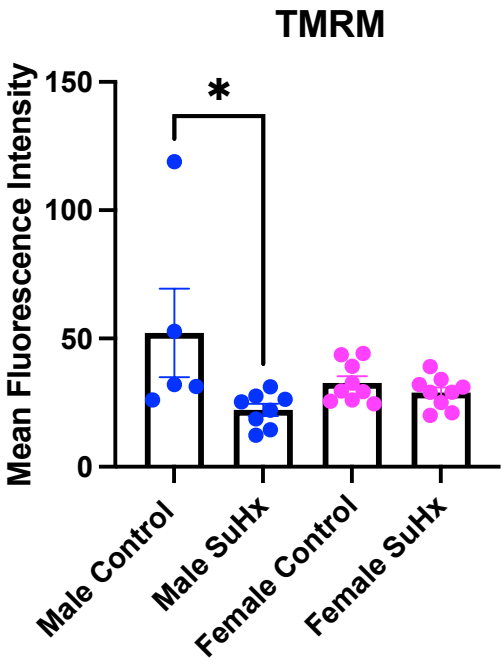

Figure 4.4. SuHx reduces mitochondrial membrane potential in the male SuHx rats

A) confocal microscopy images representing right ventricle (RV) tissue stained with DAPI for the nuclei and TMRM for mitochondrial membrane potential. B) Quantification of mitochondrial membrane potential. n=5-9. All statistical analysis was performed using two-way ANOVA. *$p<0.05$. Images were captured at 63x magnification. Scale bar represents 20μm. All data represent the standard error of the mean (S.E.M).

A

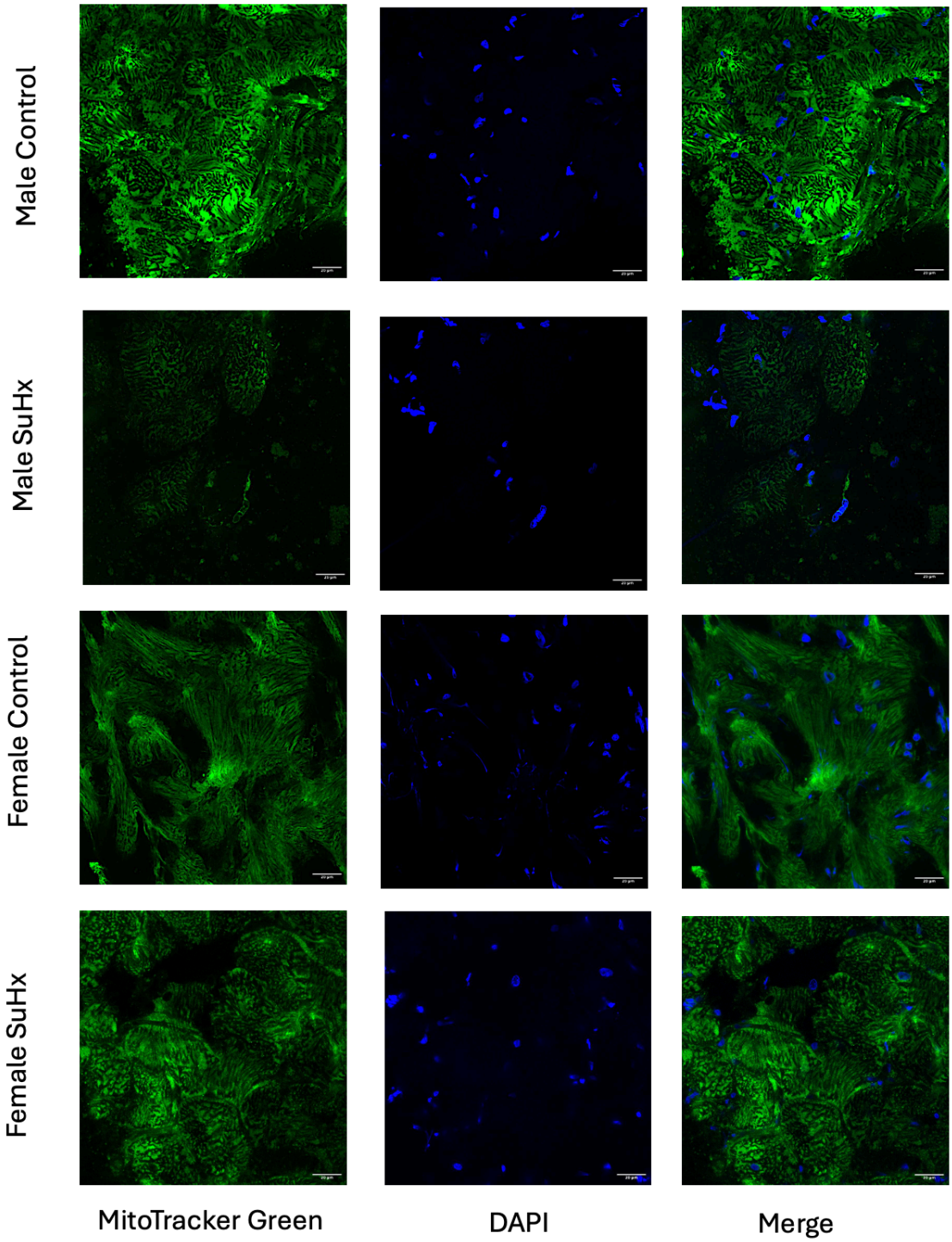
Male Control
Male SuHx
Female Control
Female SuHx
MitoTracker Green
DAPI
Merge

B

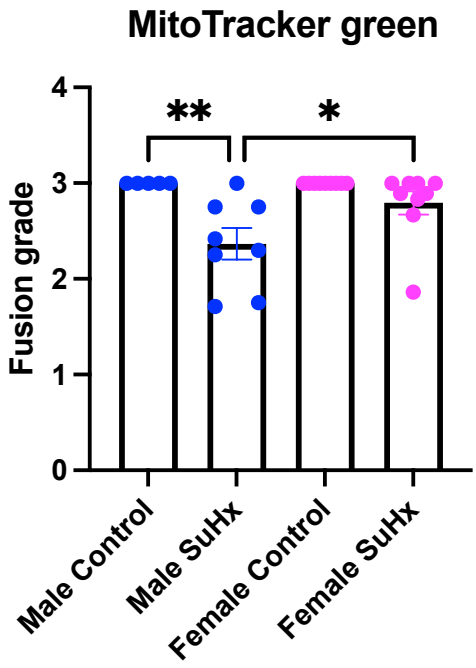

Figure 4.5. SuHx reduced mitochondrial fusion in both male and female SuHx rats

A) confocal microscopy images representing (right ventricle) RV tissue stained with DAPI for the nuclei and MitoTracker green for mitochondrial morphology. B) Quantification of mitochondrial fusion grade. n=5-9. All statistical analysis was performed using two-way ANOVA. *p<0.05, **p<0.01. Images were captured at 63x magnification. Scale bar represents 20μm. All data represent the standard error of the mean (S.E.M).

A

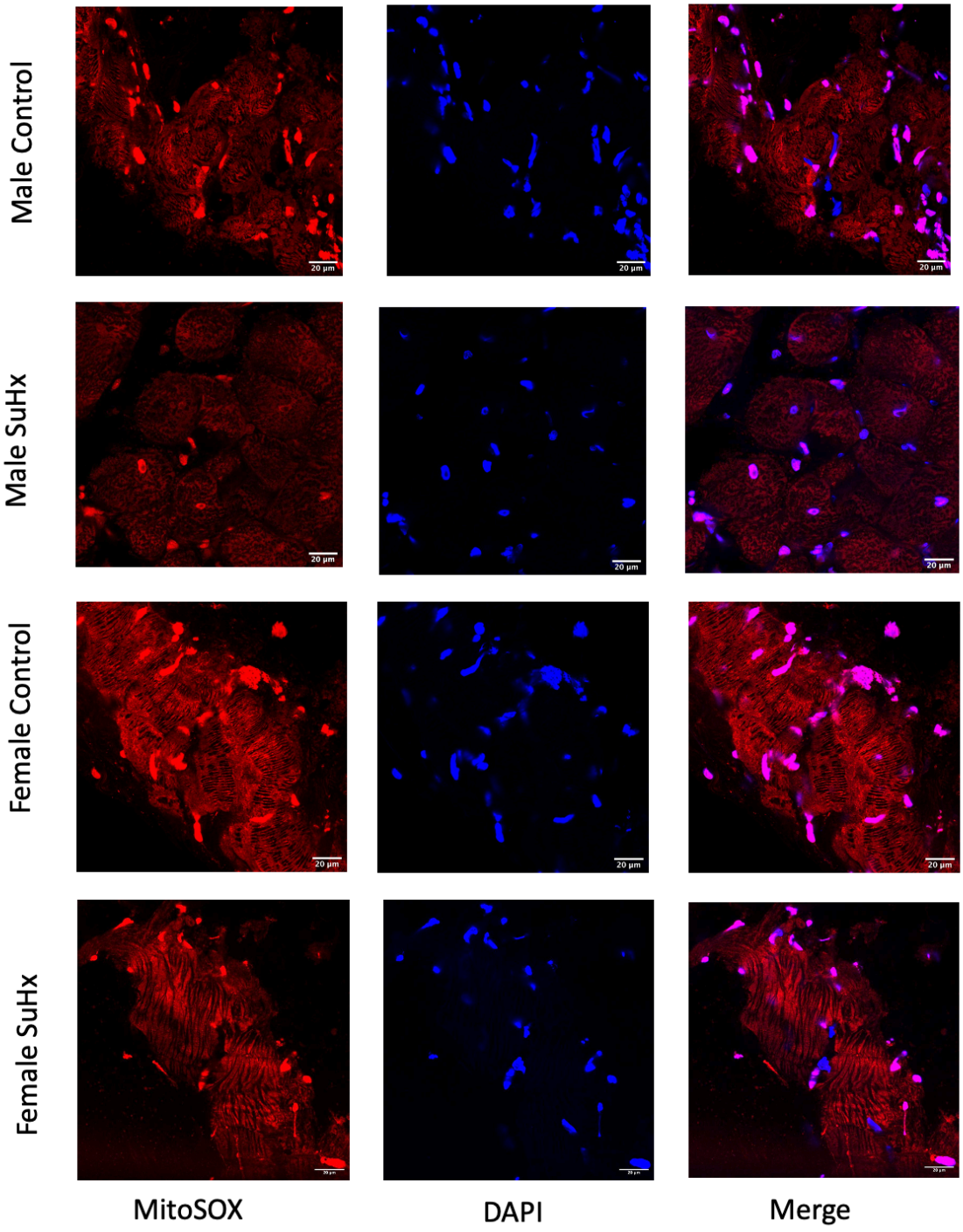
Male Control
Male SuHx
Female Control
Female SuHx
MitoSOX
DAPI
Merge

B

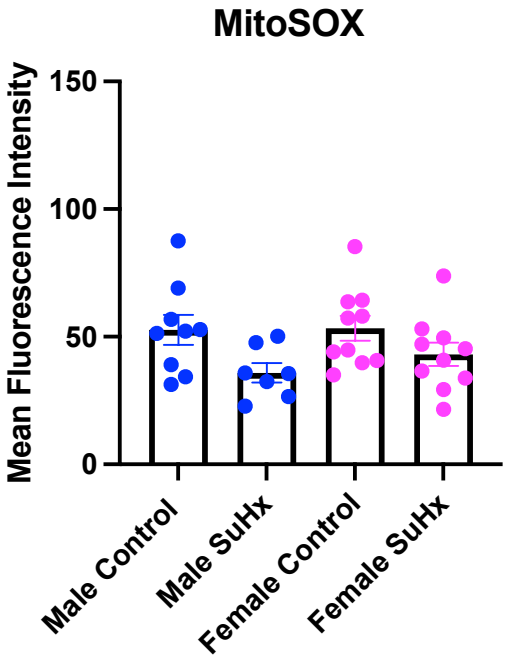

Figure 4.6. SuHx did not affect MitoSOX intensity

A) Confocal microscopy images representing right ventricle (RV) tissue stained with DAPI for the nuclei and MitoSOX (red) for mitochondrial superoxide intensity. B) Quantification of MitoSOX. n=7-10. All statistical analysis was performed using two-way ANOVA. Images were captured at 63x magnification. Scale bar represents 20μm. All data represent the standard error of the mean (S.E.M).

4.4 The expression of a hypoxia marker gene, HK2 was upregulated in the RV tissue in both male and female but reduced in the lung tissue

There are four isoforms of hexokinase (HK 1-4), which play a role in the glycolytic pathway, with HK2 serving as the most predominate isoform in cardiac tissue (Heikkinen et al., 2000). Under hypoxic conditions, it is known that HK2 will become upregulated through hypoxia inducible factor 1 alpha (HIF1α) activation, thereby serving as a marker of hypoxia. The expression of HK2 was measured by qRT-PCR which showed that SuHx did indeed increase HK2 expression in the RV for male SuHx versus male control (1.46 ± 0.13 vs. 1.02 ± 0.07, *p<0.05, n=10) and female SuHx versus female control (1.64 ± 0.16 vs. 1.02 ± 0.07, **p<0.01, n=10) (Figure 4.7 A). However, the opposite effect was seen in the lung tissue, in which HK2 was reduced in the male SuHx versus male control (0.62 ± 0.08 vs. 1.06 ± 0.11, *p<0.05, n=10) and female SuHx versus female control (0.67 ± 0.09 vs. 1.10 ± 0.14, *p<0.05, n=10) (Figure 4.7 B).

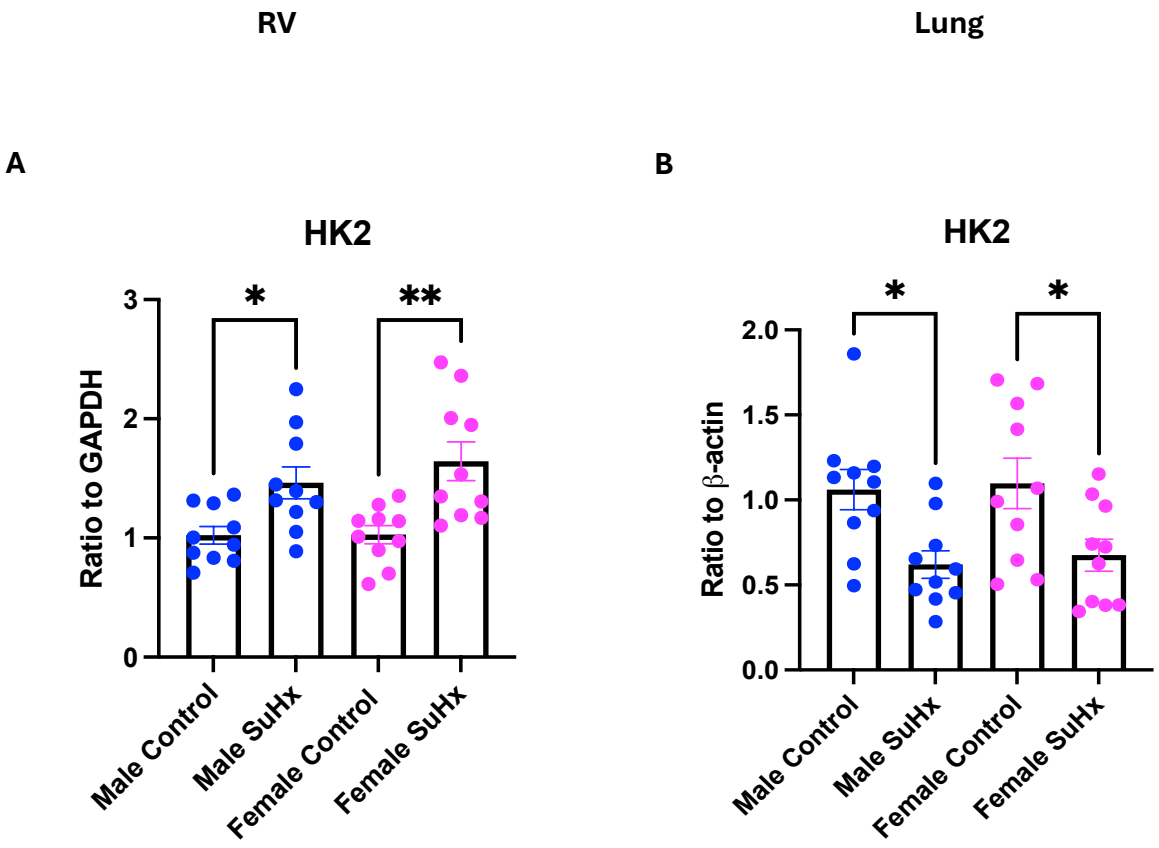

Figure 4.7. SuHx increased HK2 gene expression within the RV but reduced HK2 in the lungs

Quantitative polymerase chain reaction (qPCR) was performed on right ventricle (RV) tissue harvested from the male and female control and Sugen-hypoxia (SuHx) rats. A) Hexokinase 2 (HK2) expression in RV tissue. B) HK2 expression from lung tissue. All values represent the mean ΔΔCT value ± standard error of the mean (S.E.M). RV gene expression data was normalized to the glyceraldehyrde-3-phosphate dehydrogenase (GAPDH) gene expression, whilst lung tissue was normalised to β-actin, with n=10 per group. Samples were performed in triplicates and data was analysed using the two-way ANOVA with *p<0.05, **p<0.01, ***p<0.001 and ****p<0.0001.

4.5 The effect of SuHx on the expression of genes involved in the mitochondrial biogenesis pathway in RV tissue

Mitochondrial biogenesis is regulated by the peroxisome proliferator activated receptor gamma co activator 1 alpha (PCG-1α), nuclear respiratory factor 1 and 2 (NRF 1 and 2) and mitochondrial transcription factor A (TFAM) pathway. The PCG-1α-NRF1/2-TFAM signalling pathway is critical in the maintenance of mitochondrial metabolic capacity. Therefore, we decided to examine the effect of SuHx on this pathway by using quantitative polymerase chain reaction (qRT-PCR) in the RV tissue. qRT-PCR results showed that SuHx did not influence NRF1 activity (Figure 4.8 C) but did increase NRF2 expression in the male SuHx rats versus male control (2.24 ± 0.40 vs. 1.12 ± 0.20, *$p<0.05$, n=10) (Figure 4.8 D). No significant differences were detected in PCG-1α (PPARGC1A) expression (Figure 4.8 A). Meanwhile, there was a significant increase in TFAM expression in the male SuHx rats versus male control (1.90 ± 0.25 vs. 1.11 ± 0.18, *$p<0.05$, n=10) (Figure 4.8 B).

A

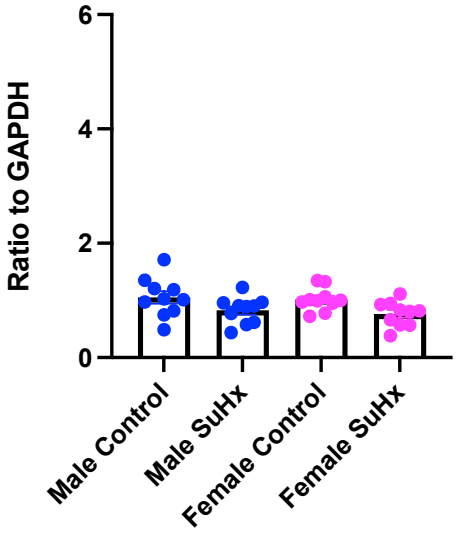
PPARGC1A
Ratio to GAPDH
0
2
4
6
Male Control
Male SuHx
Female Control
Female SuHx

B

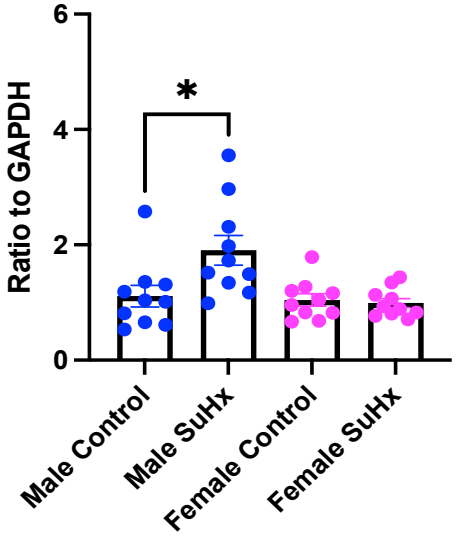
TFAM
Ratio to GAPDH
*
0
2
4
6
Male Control
Male SuHx
Female Control
Female SuHx

C

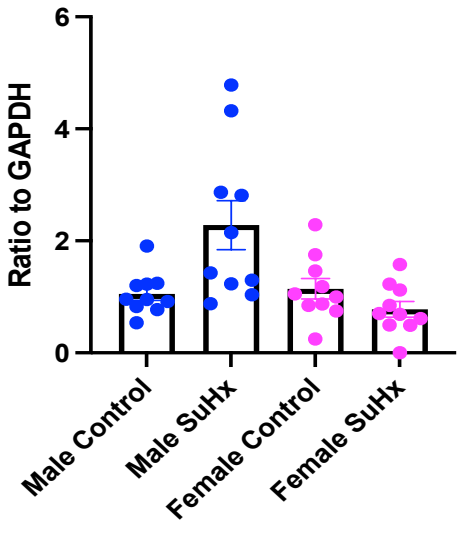
NRF1
Ratio to GAPDH
0
2
4
6
Male Control
Male SuHx
Female Control
Female SuHx

D

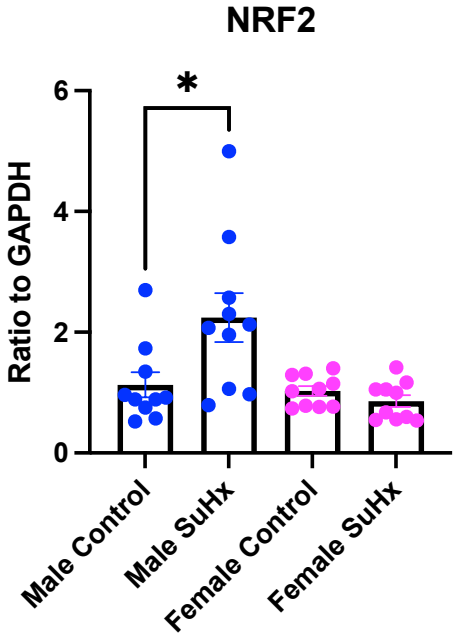
NRF2
Ratio to GAPDH
*
0
2
4
6
Male Control
Male SuHx
Female Control
Female SuHx

Figure 4.8. The effect of SuHx on RV gene expression linked to mitochondrial biogenesis

Quantitative polymerase chain reaction (qPCR) was performed on RV tissue harvested from the male and female control and SuHx rats. A) Peroxisome proliferator activated receptor gamma co activator 1 alpha, PPARGC1A, also referred to as PGC1α gene expression B) Mitochondrial transcription factor A, TFAM gene expression C) Nuclear respiratory factor 1, NRF1 gene expression D) Nuclear respiratory factor 2, NRF2 gene expression. All values represent the mean ΔΔCT value ± S.E.M. All data was normalized to the Glyceraldehyrde-3-phosphate dehydrogenase (GAPDH) gene expression, with n=10 per group. Samples were performed in triplicates and data was analysed using the two-way ANOVA with *$p<0.05$.

4.6 The effect of SuHx on the expression of genes involved in the mitochondrial dynamics in RV tissue

Assessment of the genes involved in mitochondrial dynamics was performed using qRT-PCR on the male and female RV tissue. There were no significant differences in Mitofusin 1 and 2 (MFN1/2) across the groups which plays a crucial role in mitochondrial fusion (Figure 4.9 A and B). Also, no differences were detected in dynamin 2 (DNM2) which is involved in mitochondrial fission (Figure 4.9 C). Similarly, no differences were found in optic atrophy-1 (OPA1) which is involved in mitochondrial fusion (Figure 4.9 D).

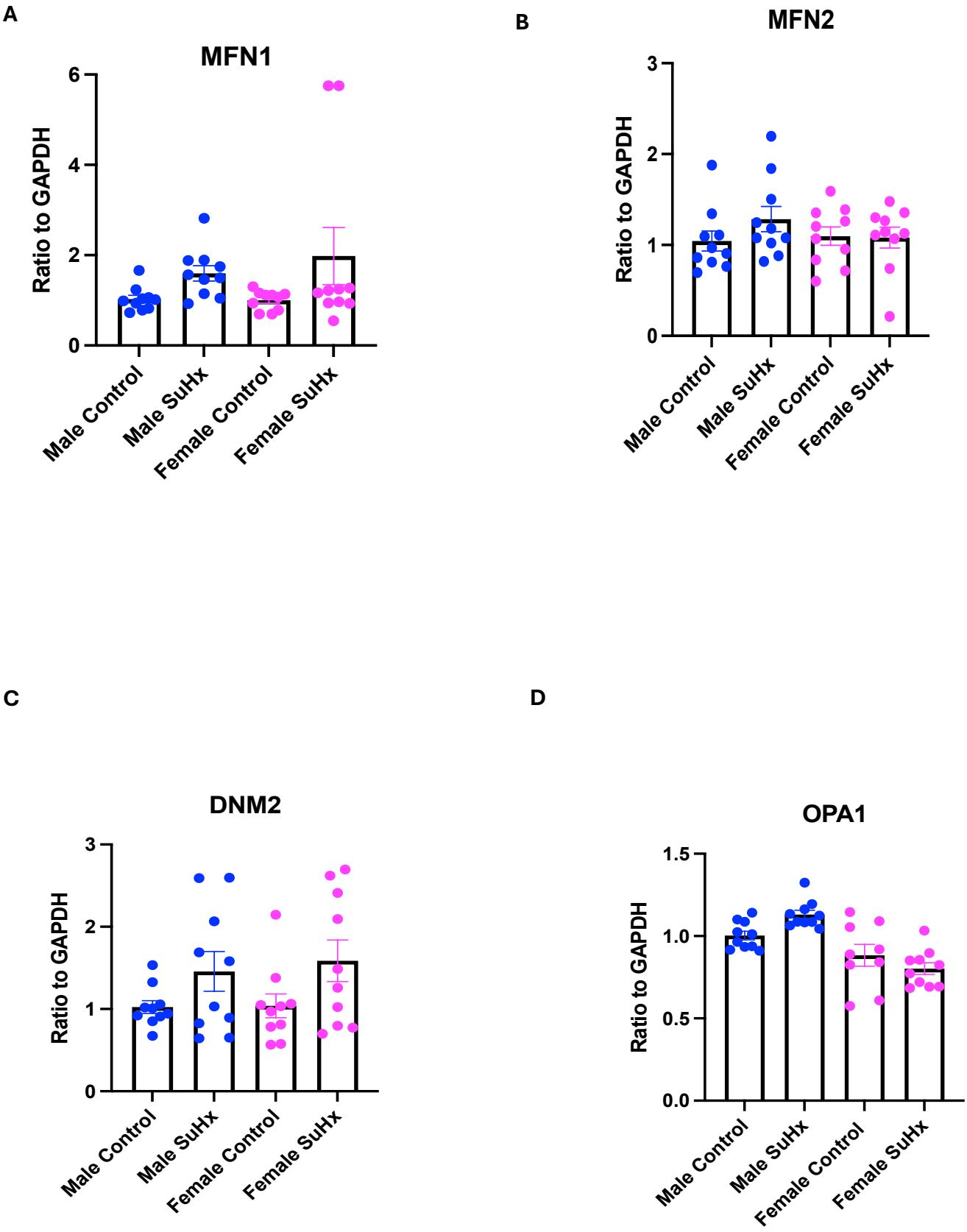
A
MFN1
Ratio to GAPDH
0
2
4
6
Male Control
Male SuHx
Female Control
Female SuHx
B
MFN2
Ratio to GAPDH
0
1
2
3
Male Control
Male SuHx
Female Control
Female SuHx
C
DNM2
Ratio to GAPDH
0
1
2
3
Male Control
Male SuHx
Female Control
Female SuHx
D
OPA1
Ratio to GAPDH
0.0
0.5
1.0
1.5
Male Control
Male SuHx
Female Control
Female SuHx

Figure 4.9. The effect of SuHx on RV gene expression linked to mitochondrial dynamics

Quantitative polymerase chain reaction (qPCR) was performed on RV tissue harvested from the male and female control and SuHx rats. A) Mitofusin 1, MFN1 gene expression B) Mitofusin 2, MFN2 gene expression C) Dynamin 2, DNM2 gene expression D) Optic atrophy 1, OPA1 gene expression. All values represent the mean ΔΔCT value ± S.E.M. All data was normalized to the Glyceraldehyrde-3-phosphate dehydrogenase (GAPDH) gene expression, n=10 per group. Samples were performed in triplicates and data was analysed using the two-way ANOVA.

4.7 The effect of SuHx on the expression of genes involved in mitochondrial oxidative stress in RV tissue

Transcriptional activator, nuclear factor erythroid 2-related factor 2 (NFE2L2) which plays a crucial role in regulating cellular resistance to reactive oxidants, demonstrated no significant differences across the groups (Figure 4.10 A). The same was seen for a downstream target of NFE2L2, known as NAD(P)H dehydrogenase (quinone 1) (NQO1) (Figure 4.10 B). No differences were found in superoxide dismutase (SOD2) which plays a role in reducing ROS (Figure 4.10 C). Whilst one of the major mitochondrial enzymes, monoamine oxidase A (MAO-A) that generates ROS, was found to be upregulated in only the female SuHx versus female control rats (9.94 ± 3.47 vs. 1.16 ± 0.22, **p<0.01, n=10) (Figure 4.10 D). Heat shock protein 90 alpha family class A member 1 (HSP90AA1) which is known to play a role in reducing oxidative stress was found to be upregulated in the male SuHx versus the male control rats (4.28 ± 0.76 vs. 1.10 ± 0.18, ****p<0.0001, n=10) (Figure 4.10 E). At the same time, a significant reduction in HSP90AA1 was detected in the female SuHx rats versus the male SuHx rats (2.16 ± 0.31 vs. 4.28 ± 0.76, **p<0.01, n=10) (Figure 4.10 E).

A

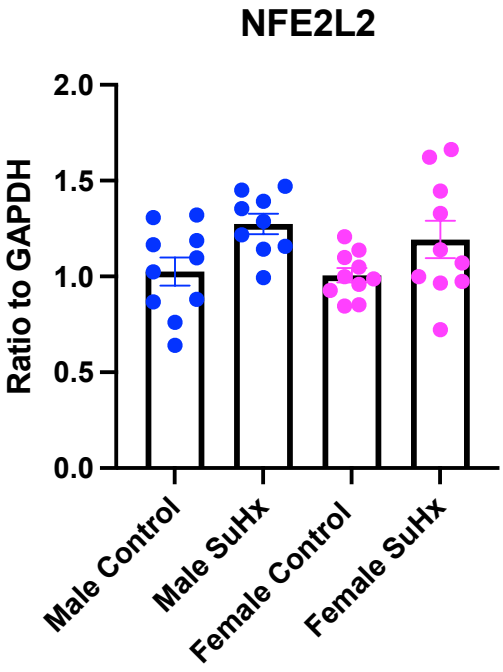
NFE2L2
Ratio to GAPDH
2.0
1.5
1.0
0.5
0.0
Male Control
Male SuHx
Female Control
Female SuHx

B

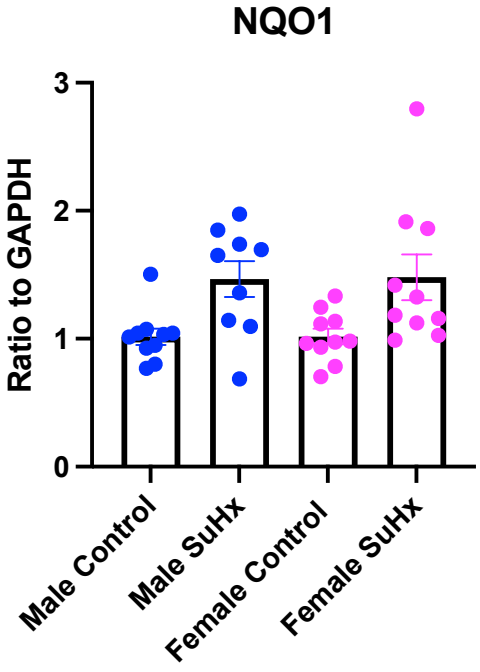
NQO1
Ratio to GAPDH
3
2
1
0
Male Control
Male SuHx
Female Control
Female SuHx

C

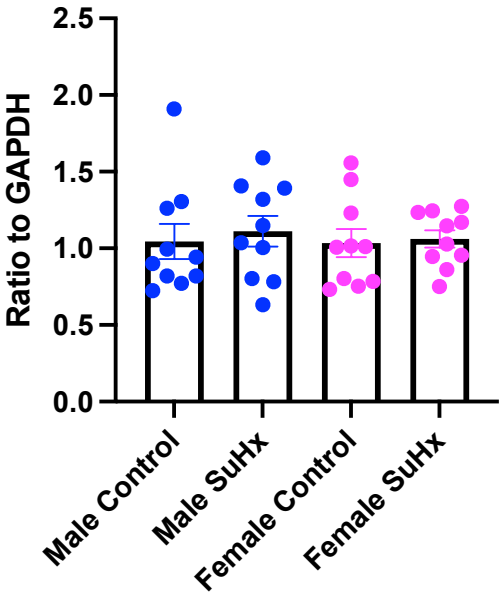
SOD2
Ratio to GAPDH
2.5
2.0
1.5
1.0
0.5
0.0
Male Control
Male SuHx
Female Control
Female SuHx

D

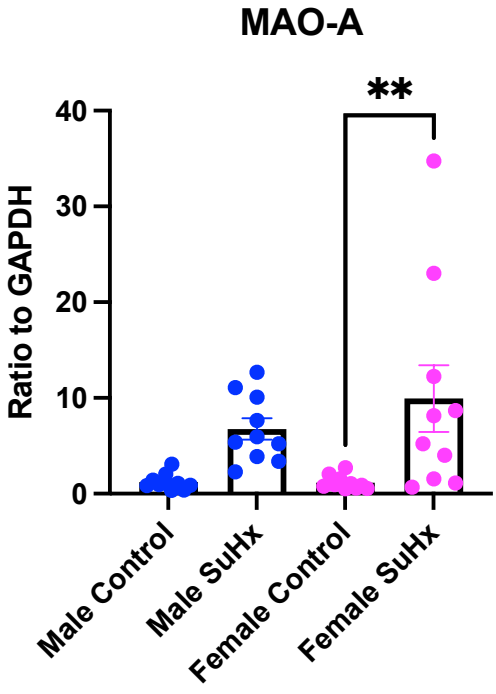
MAO-A
**
Ratio to GAPDH
40
30
20
10
0
Male Control
Male SuHx
Female Control
Female SuHx

E

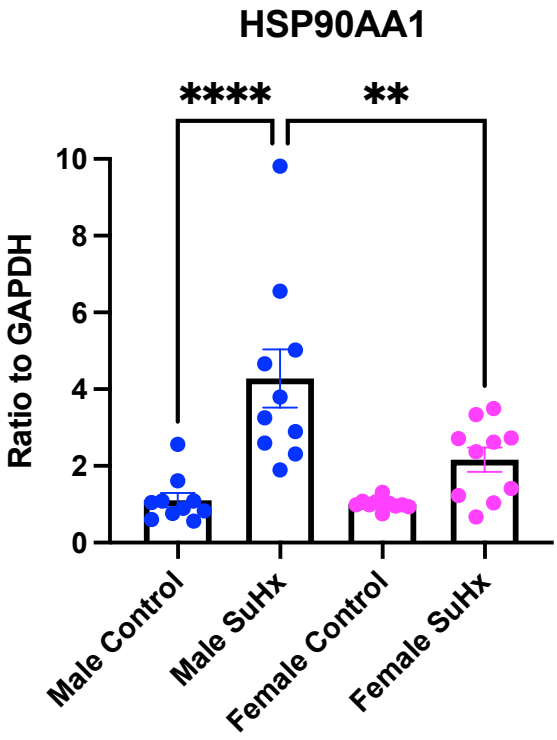

Figure 4.10. The effect of SuHx on RV gene expression linked to mitochondrial oxidative stress

Quantitative polymerase chain reaction (qPCR) was performed on RV tissue harvested from the male and female control and SuHx rats. A) Nuclear factor erythroid 2-related factor 2, NFE2L2 gene expression B) NAD(P)H dehydrogenase (quinone 1), NQO1 gene expression C) superoxide dismutase 2, SOD2 gene expression D) monoamine oxidase A, MAO-A gene expression E) Heat shock protein 90 alpha family class A member 1, HSP90AA1 gene expression. All values represent the mean ΔΔCT value ± standard error of the mean (S.E.M). All data was normalized to the Glyceraldehyrde-3-phosphate dehydrogenase (GAPDH) gene expression, with n=9-10 per group. Samples were performed in triplicates and data was analysed using the two-way ANOVA with *p<0.05 and **p<0.01. A ROUT outlier test was performed on NFE2L2 and NQO1 gene expression which identified one outlier in the male SuHx group, for both genes which was removed.

4.7.1 The effect of SuHx on RV NFE2L2 protein expression

To follow up on the RV qPCR, NFE2L2 RV protein expression was measured. Densitometric analysis of the western blot revealed a significant reduction in the male SuHx group versus male control (0.57 ± 0.06 vs. 1.00 ± 0.07, **p<0.01, n=4-5) (Figure 4.11 A and C). Meanwhile no significant differences were detected in the in the female groups (Figure 4.11 B and D).

A

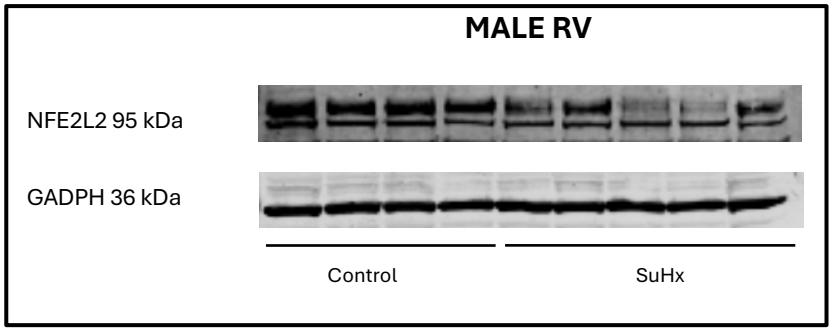

B

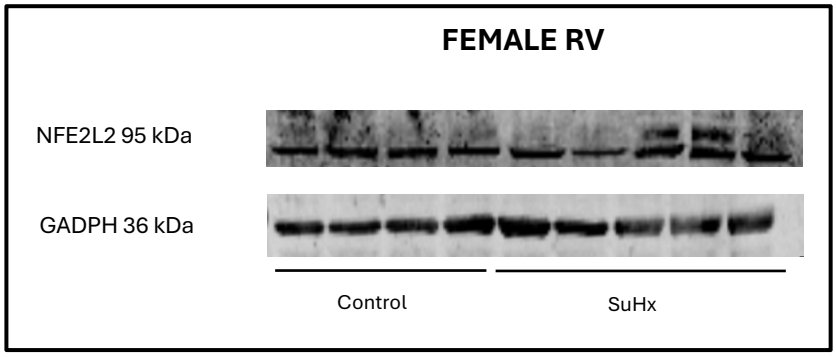

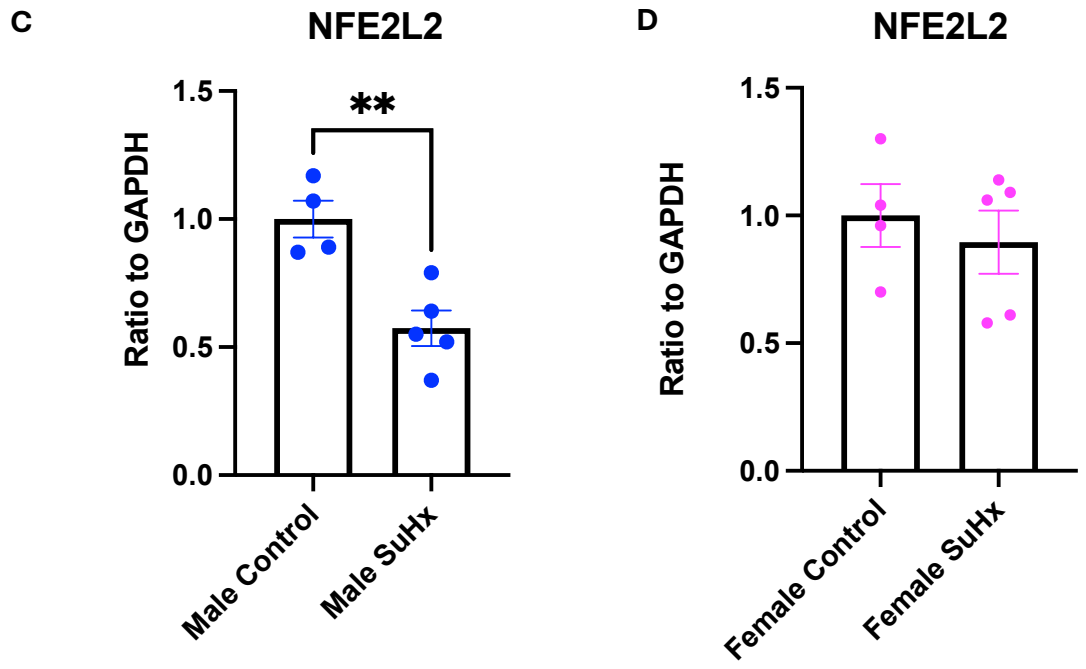

Figure 4.11. NFE2L2 protein expression in male and female control and SuHx RV tissue

Protein expression was assessed by western blot. A) Representative image of male right ventricle (RV) nuclear factor erythroid 2-related factor 2 (NFE2L2) expression normalized to glyceraldehyrde-3-phosphate dehydrogenase (GAPDH) B) Representative image of female RV NFE2L2 expression normalized to GAPDH C) Quantitative analysis of NFE2L2 expression ratioed to housekeeper, GAPDH for male rats D) Quantitative analysis of NFE2L2 expression ratioed to housekeeper, GAPDH for female rats, with n=4 for male and female control rats and n=5 for male and female SuHx rats. Data represents mean + standard error of the mean (S.E.M) value. Statistical analysis was performed using an unpaired t test with **p<0.01.

4.8 The effect of SuHx on the expression of estrogen receptor genes in RV tissue

Estrogen will couple to one of its estrogen receptors: ERα, ERβ or GPER to mediate its signalling (Fuentes and Silveyra, 2019). ESR1 is the gene that encodes for the ERα receptor, meanwhile ESR2 encodes for the ERβ receptor (Fuentes and Silveyra, 2019). ESR1 and ESR2 have been found to reside in the nucleus, mitochondria and cytoplasm or as an extra-nuclear receptor at the plasma membrane (Fuentes and Silveyra, 2019). Sex differences have been found in ESR1 protein expression, with ESR1 expression significantly higher in the female cardiomyocytes compared with the males (Sun et al., 2021b). Meanwhile, ESR2 protein expression is similar in both male and female cardiomyocytes (Grohé et al., 1998, Sun et al., 2021b). Due to this, we examined the ESR1 and ESR2 gene expression in the RV tissue from the male and female SuHx rats. We found there was a significant reduction in the ESR1 gene expression in the female SuHx rats versus the male SuHx rats (0.47 ± 0.03 vs. 1.33 ± 0.30, *$p<0.05$, $n=10$) (Figure 4.12 A) whilst no differences were found in ESR2 gene expression (Figure 4.12 B).

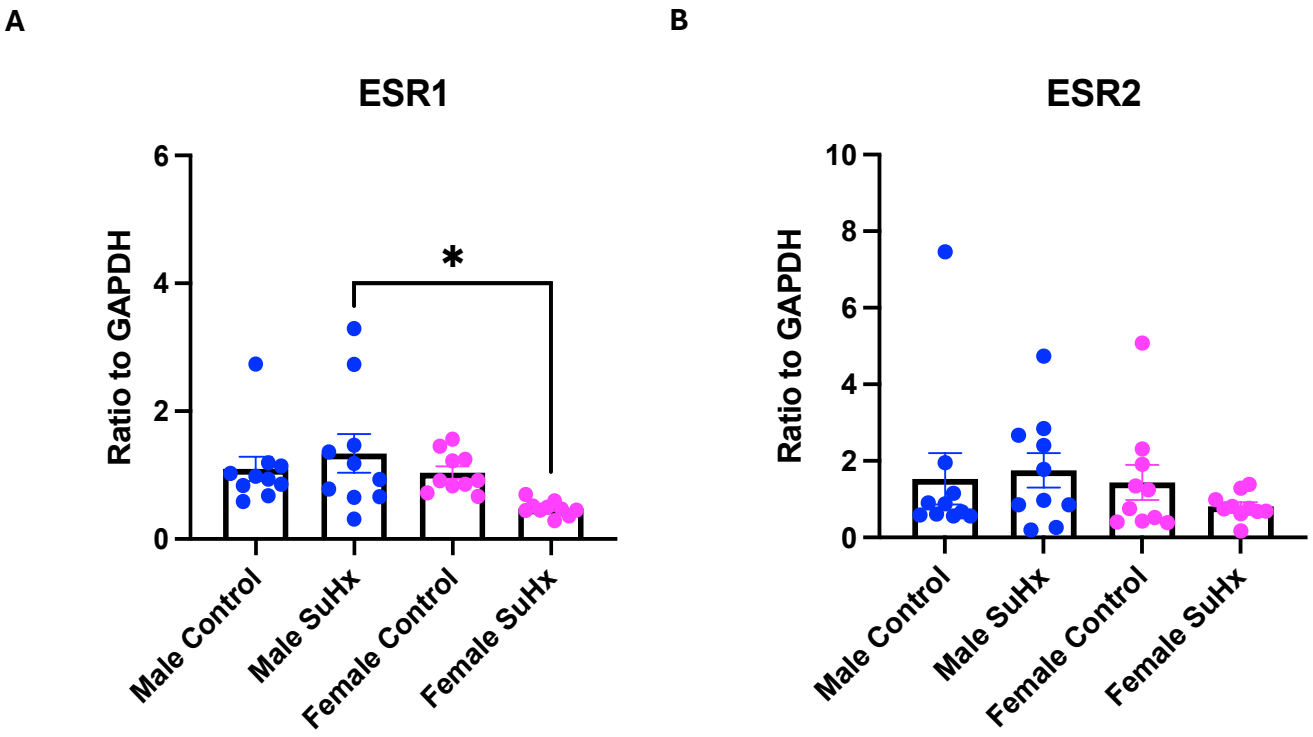

Figure 4.12. The effect of SuHx on RV estrogen receptor gene expression

Quantitative polymerase chain reaction (qPCR) was performed on RV tissue harvested from the male and female control and SuHx rats. A) estrogen receptor 1, ESR1 gene expression B) estrogen receptor 2, ESR2 gene expression. All values represent the mean ΔΔCT value ± standard error of the mean (S.E.M). All data was normalized to the Glyceraldehyde-3-phosphate dehydrogenase (GAPDH) gene expression, with n=10 per group. Samples were performed in triplicates and data was analysed using the two-way ANOVA with *p<0.05.

4.9 The effect of SuHx on lung gene expression linked to mitochondrial biogenesis

We decided to examine the effect of SuHx on the same mitochondrial biogenesis genes that were investigated in the RV tissue but now in the lung tissue. The qRT-PCR results showed that SuHx did not alter PCG-1α (PPARGC1A) or nuclear respiratory factor 2 (NRF2) gene expression (Figure 4.13 A and D). However, it did reduce mitochondrial transcription factor A (TFAM) expression in the male SuHx versus male control group (0.52 ± 0.09 vs. 1.05 ± 0.12, *p<0.05, n=10) (Figure 4.13 B). Similarly, SuHx reduced NRF1 expression in the male SuHx versus male control rats (0.62 ± 0.08 vs. 1.01 ± 0.04, *p<0.05, n=10) (Figure 4.13 C).

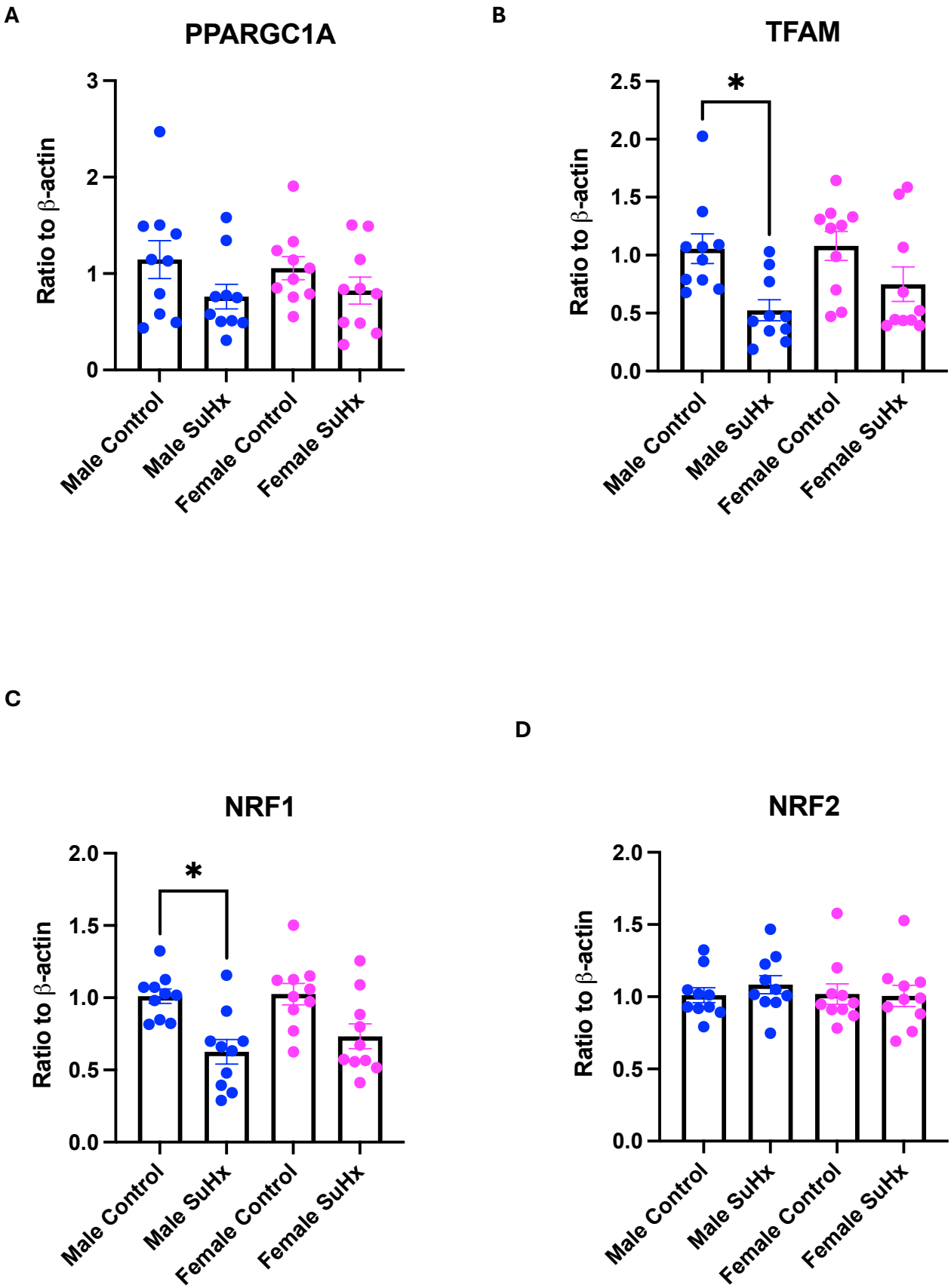
A
PPARGC1A
Ratio to β-actin
3
2
1
0
Male Control
Male SuHx
Female Control
Female SuHx
B
TFAM
*
Ratio to β-actin
2.5
2.0
1.5
1.0
0.5
0.0
Male Control
Male SuHx
Female Control
Female SuHx
C
NRF1
*
Ratio to β-actin
2.0
1.5
1.0
0.5
0.0
Male Control
Male SuHx
Female Control
Female SuHx
D
NRF2
Ratio to β-actin
2.0
1.5
1.0
0.5
0.0
Male Control
Male SuHx
Female Control
Female SuHx

Figure 4.13. The effect of SuHx on lung gene expression linked to mitochondrial biogenesis

Quantitative polymerase chain reaction (qPCR) was performed on the lung tissue harvested from the male and female control and SuHx rats. A) Peroxisome proliferator activated receptor gamma co activator 1 alpha, PPARGC1A, also known as PGC1α gene expression B) Mitochondrial transcription factor A, TFAM gene expression C) Nuclear respiratory factor 1, NRF1 gene expression D) Nuclear respiratory factor 2, NRF2 gene expression. All values represent the mean ΔΔCT value ± standard error of the mean (S.E.M). All data was normalized to the β-actin gene expression with n= 10 per group. Samples were performed in triplicates and data was analysed using the two-way ANOVA with *$p<0.05$.

4.10 The effect of SuHx on lung gene expression linked to mitochondrial dynamics

When we examined the genes linked to mitochondrial dynamics in the lung, we found a significant reduction in MFN1 in the male SuHx versus male control group (0.67 ± 0.07 vs. 1.00 ± 0.03, *p<0.05, n=10) (Figure 4.14 A). Whilst a significant reduction in MFN2 was detected in both male SuHx versus male control and female SuHx versus female control groups, highlighting no sex differences (males: 0.65 ± 0.09 vs. 1.02 ± 0.07, *p<0.05, n=10; females: 0.67 ± 0.08 vs. 1.04 ± 0.09, *p<0.05, n= 10) (Figure 4.14 B). Similarly, when we looked at DNM2 expression this was found to be reduced in both male SuHx versus male control and female SuHx versus female control groups (males: 0.62 ± 0.05 vs. 1.00 ± 0.04, *p<0.05, n=9-10; females: 0.72 ± 0.09 vs. 1.06 ± 0.13, *p<0.05, n=10) (Figure 4.14 C). Whilst no differences were detected in OPA1 expression (Figure 4.14 D).

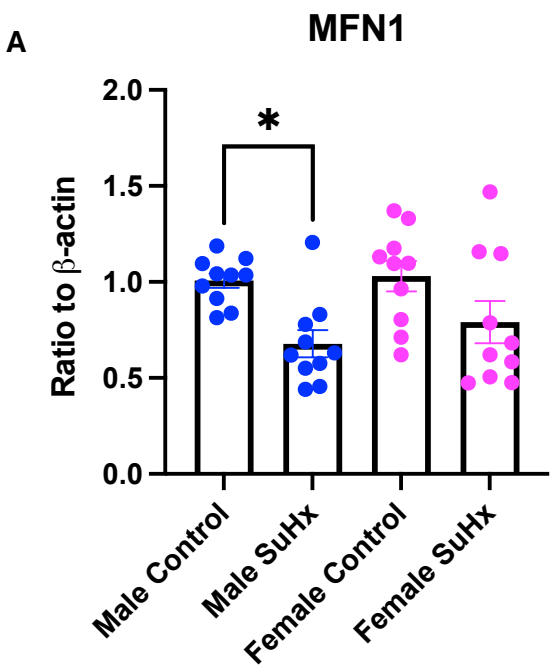
A
MFN1
Ratio to β-actin
2.0
1.5
1.0
0.5
0.0
*
Male Control
Male SuHx
Female Control
Female SuHx

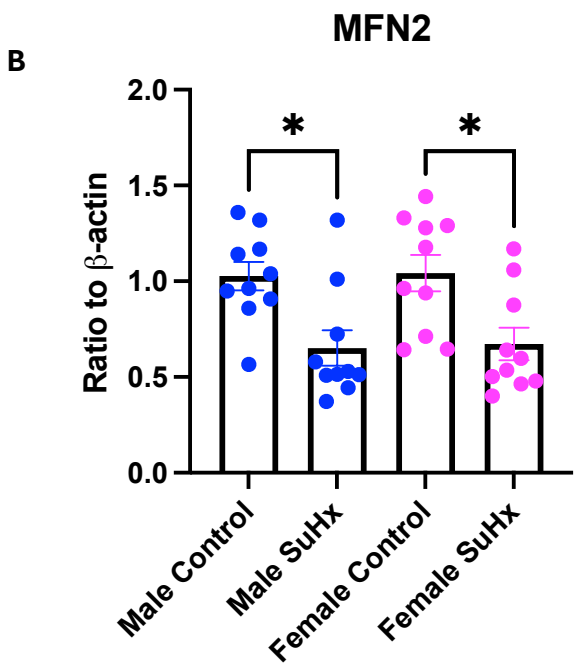
B
MFN2
Ratio to β-actin
2.0
1.5
1.0
0.5
0.0
*
*
Male Control
Male SuHx
Female Control
Female SuHx

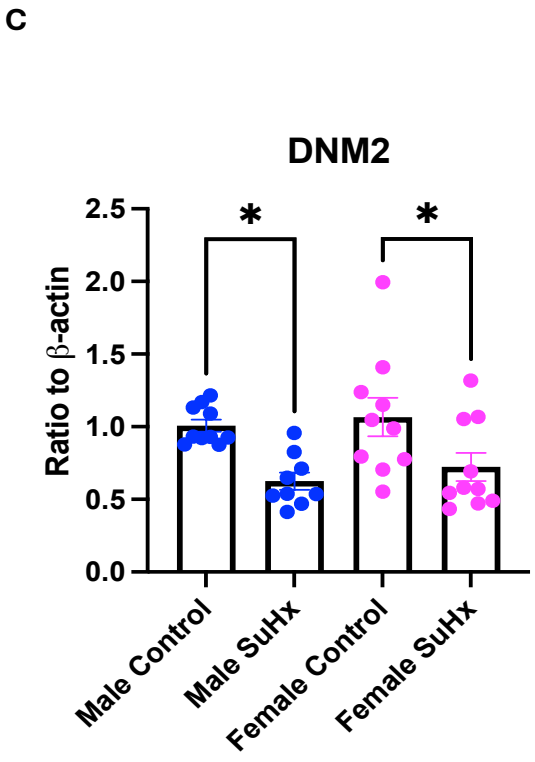
C
DNM2
Ratio to β-actin
2.5
2.0
1.5
1.0
0.5
0.0
*
*
Male Control
Male SuHx
Female Control
Female SuHx

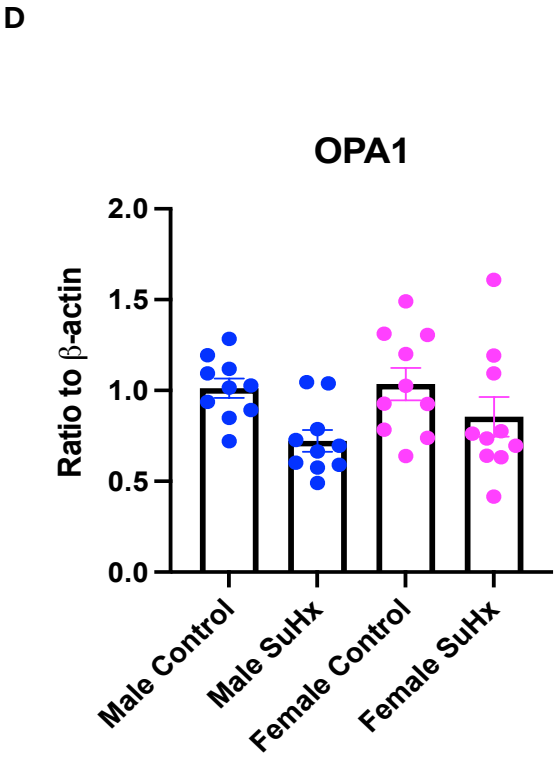
D
OPA1
Ratio to β-actin
2.0
1.5
1.0
0.5
0.0
Male Control
Male SuHx
Female Control
Female SuHx

Figure 4.14. The effect of SuHx on lung gene expression linked to mitochondrial dynamics

Quantitative polymerase chain reaction (qPCR) was performed on lung tissue harvested from the male and female control and Sugen hypoxia (SuHx) rats. A) Mitofusin 1, MFN1 gene expression B) Mitofusin 2, MFN2 gene expression C) Dynamin 2, DNM2 gene expression D) Optic atrophy 1, OPA1 gene expression. All values represent the mean ΔΔCT value ± standard error of the mean (S.E.M). All data was normalized to the β-actin gene expression with n=9-10 per group. Samples were performed in triplicates and data was analysed using the two-way ANOVA with *p<0.05. A ROUT outlier test was performed on DNM2 gene expression which identified one outlier in the male SuHx group which was removed.

4.11 The effect of SuHx on lung gene expression linked to mitochondrial oxidative stress

The same qPCR was performed on the lung tissue examining the same mitochondrial oxidative stress linked genes which were tested in the RV. No changes were detected across the groups in NFE2L2 gene expression (Figure 4.15 A). We did detect a significant increase in NQO1 expression in male SuHx versus male control and female SuHx versus female control rats (males: 3.76 ± 0.54 vs. 1.05 ± 0.10, ****$p<0.0001$, n= 10; females: 2.39 ± 0.25 vs. 1.02 ± 0.06, *$p<0.05$, n= 10) (Figure 4.15 B). No changes were seen in SOD2, MAO-A and HSP90AA1 gene expression across the male and female control and SuHx groups (Figure 4.15 C, D and E).

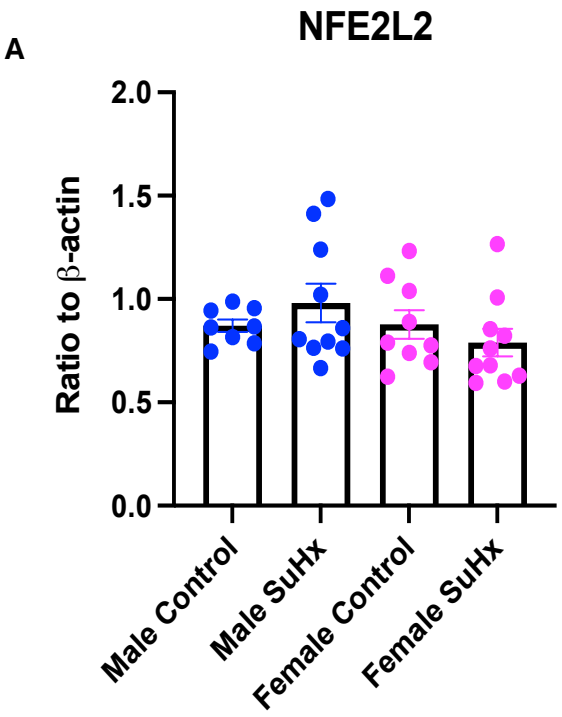
A
NFE2L2
Ratio to β-actin
2.0
1.5
1.0
0.5
0.0
Male Control
Male SuHx
Female Control
Female SuHx

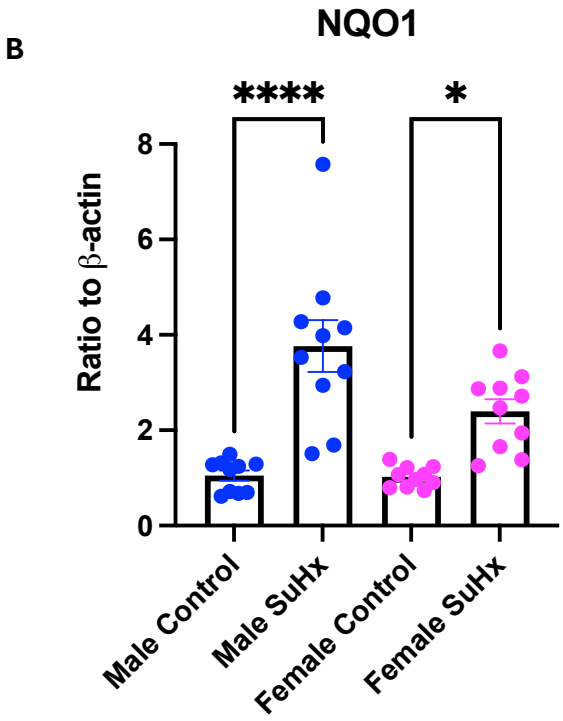
B
NQO1
****
*
Ratio to β-actin
8
6
4
2
0
Male Control
Male SuHx
Female Control
Female SuHx

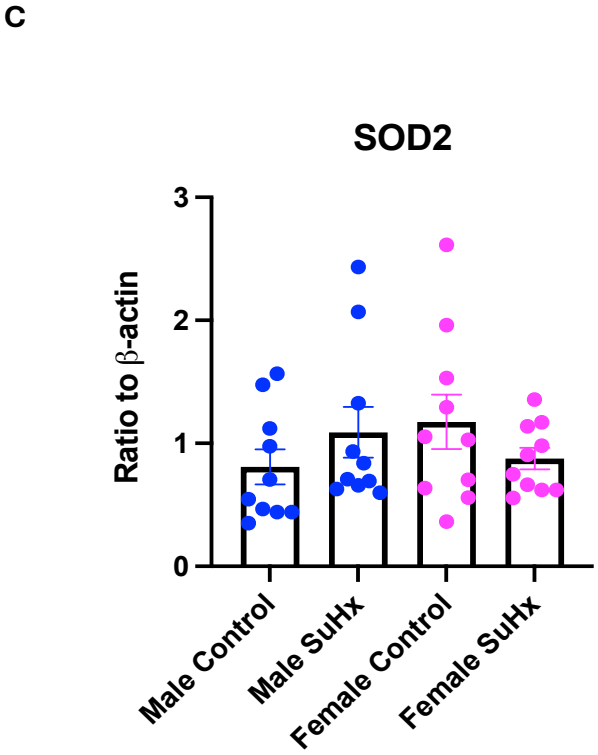
C
SOD2
Ratio to β-actin
3
2
1
0
Male Control
Male SuHx
Female Control
Female SuHx

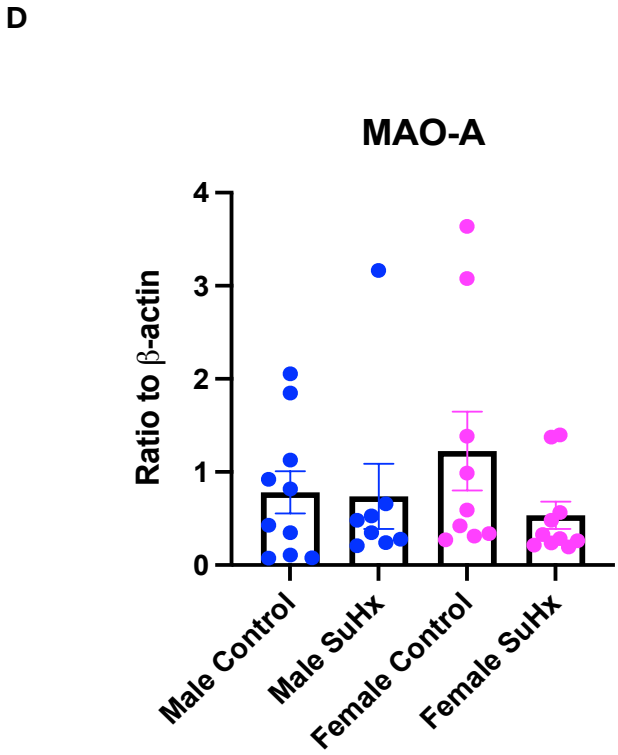
D
MAO-A
Ratio to β-actin
4
3
2
1
0
Male Control
Male SuHx
Female Control
Female SuHx

E

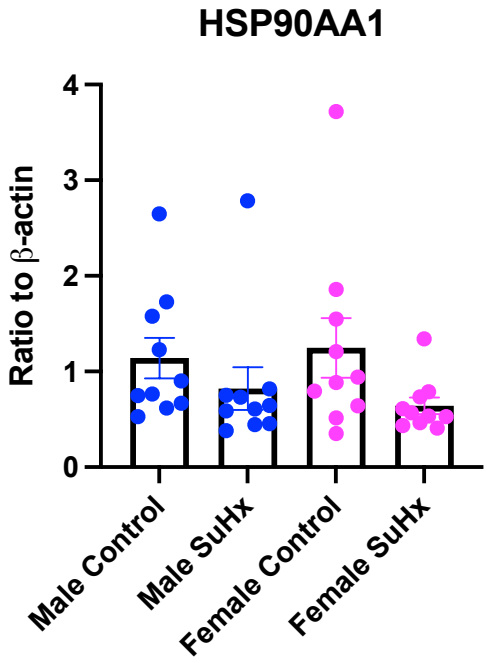

Figure 4.15. The effect of SuHx on lung gene expression linked to mitochondrial dynamics

Quantitative polymerase chain reaction (qPCR) was performed on lung tissue harvested from the male and female control and SuHx rats. A) Nuclear factor erythroid 2-related factor 2, NFE2L2 gene expression B) NAD(P)H dehydrogenase (quinone 1), NQO1 gene expression C) Superoxide dismutase 2, SOD2 gene expression D) Monoamine oxidase A, MAO-A gene expression. E) Heat shock protein 90 alpha family class A member 1, HSP90AA1 gene expression. All values represent the mean ΔΔCT value ± standard error of the mean (S.E.M). All data was normalized to the β-actin gene expression, with n=8-10 per group. Samples were performed in triplicates and data was analysed using the two-way ANOVA with *p<0.05 and ****p<0.0001. A ROUT outlier test was performed on NFE2L2 and MAO-A genes which identified 1-2 outliers which were excluded.

4.12 The effect of SuHx on the expression of estrogen receptor genes in lung tissue

The estrogen receptors, ESR1 and ESR2 were examined in the RV tissue from the male and female rats. To follow up on this, we examined ESR1 and ESR2 gene expression in the lung tissue. Here, we found no significant differences across any of the male and female groups for ESR1 (Figure 4.16 A) and ESR2 (Figure 4.16 B) gene expression.

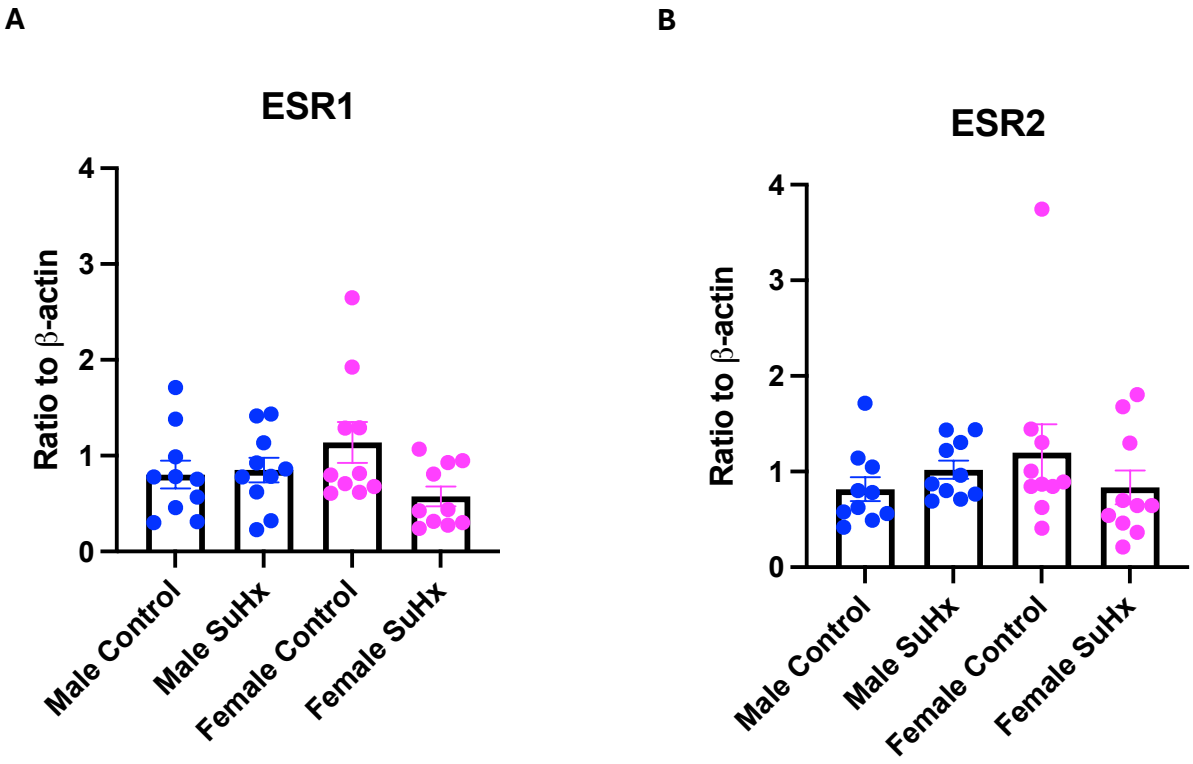

Figure 4.16. The effect of SuHx on estrogen receptor gene expression in the lung tissue

Quantitative polymerase chain reaction (qPCR) was performed on lung tissue harvested from the male and female control and SuHx rats. A) estrogen receptor 1 (ESR1) gene expression B) estrogen receptor 2 (ESR2) gene expression. All values represent the mean ΔΔCT value ± standard error of the mean (S.E.M). All data was normalized to the housekeeper, β-actin gene expression, with n=10 per group. Samples were performed in triplicates and data was analysed using the two-way ANOVA.

4.13 Discussion

The aim of chapter 4 was to examine the effect of SuHx on the remodeling of the RCA across a range of RCA diameter sizes. In addition, we aimed to examine the mitochondrial properties (mitochondrial superoxide production, membrane potential and mitochondrial morphology) in the RV tissue, and mitochondrial-linked gene expression in both the RV and lung tissues. Throughout chapter 4, we consistently aimed to examine the sex differences which are taking place within the SuHx rat model. Several studies have shown impaired mitochondrial function within the SuHx rat model, but it is not clear whether there are any sex differences in these mitochondrial targets. As well as this, to date there has been no data reported on the structural remodeling/fibrosis within the RCAs in the SuHx model and whether there are any sex differences.

The RCA supplies blood to the RV, however given the increased intracavity pressures in PAH, this causes remodeling of the RCA that eventually leads to a reduction in the RCA flow, leading to an impairment in coronary perfusion (RV ischemia) and microvascular rarefaction (van Wolferen et al., 2008, Bogaard et al., 2009, Archer et al., 2013). Abnormal RCA flow reserve has been shown through MRI imaging in human PAH patients and is generally well documented in PAH patients (Vogel-Claussen et al., 2011). Increasing RCA perfusion pressure and flow has shown to support the RV and provide the capability for the RV to increase its contractility in an attempt to adapt to the increased PAP (van Wolferen et al., 2008). As well as this, increasing RCA perfusion pressure through the supra-coronary aortic banding model in MCT rats led to an improvement in RV function by reducing RV hypertrophy, RV fibrosis and enhancing contractile function (Tian et al., 2020b). It also produced an overall improvement in cardiac output by improving perfusion of both the heart and lung, thereby highlighting the importance of the RCA status in contributing to improved RV function (Tian et al., 2020b). There have been limited reports on RCA function in the SuHx model, with only one study recorded, which found that using an endothelin-1 receptor antagonist, macitentan improved RCA endothelin cell function (Inagaki et al., 2021). Hence, we will be the first to report RCA remodeling in the SuHx rats.

When we examined the collagen deposition around the RCA vessels, we found that the male SuHx rats had significantly more perivascular fibrosis, particularly in their smaller vessels (15-50μm) than the females. When we measured the intima-media thickness in the RCA vessels, we did not detect any differences in the males, but did see a significant reduction in the females (50-100μm) RCA vessels. This suggests that the males RCA vessels are undergoing a higher degree of structural remodelling, particularly in their smaller vessels which is not seen in the females. It can be confirmed that this remodelling is due to perivascular collagen formation and not due to an increase in intima-media thickness. This does align with the concept that males have worse RV status, which may also be explained/linked to worse RCA remodelling. In a larger context, we predict that this remodelling could contribute to RCA vessel stiffness, potentially leading to a reduction in RCA flow and hence, contributing to ischemia within the RV. Ischemia induced by microvascular rarefaction has been linked to mitochondrial dysfunction, including a shift to the Warburg metabolism in the RV in multiple animal models of PAH (Sutendra and Michelakis, 2014, Lahm et al., 2018, Tian et al., 2020a). Therefore, we predict that the RCA remodelling in the male SuHx rats could be contributing to the impairment of mitochondrial function and promoting RV dysfunction.

Pressure overload exerted on the RV can lead to an increase in reactive oxygen species (ROS) that eventually produces a ROS imbalance (Wong et al., 2013). This imbalance induces cell proliferation and plays a significant role in RV hypertrophy and fibrosis that ultimately leads to RV remodeling and disrupts the pulmonary vasculature by promoting vasoconstriction (Nozik-Grayck and Stenmark, 2007, Tabima et al., 2012, Aggarwal et al., 2013, Wong et al., 2013, Voelkel et al., 2013). Isolated mitochondria from MCT induced failing RV was also found to have elevated ROS production (Redout et al., 2007). As well as this, microvascular endothelial cells (MVEC) harvested from SuHx rats demonstrate upregulated mitochondrial reactive oxygen species (mtROS) production which promoted increases in migration, proliferation and mitochondrial fragmentation (Suresh et al., 2019). The antioxidant defence systems has been shown to fail at the early stages in pressure overloaded RVs in comparison to pressure overload LV which is able to offer a stronger antioxidant defence system (Reddy and Bernstein, 2015). Major antioxidant SOD2 was reported to not be activated at all in a pulmonary hypertensive stressed RV leaving the RV at greater risk of ROS induced damage

(Ecarnot-Laubriet et al., 2003). We determined mitochondrial superoxide production by staining the RV tissue with MitoSOX and also by examining RV and lung tissue gene expression linked to oxidative stress. A previous study by Germande and colleagues, found an increase in mitochondrial superoxide production in human pulmonary artery endothelin cells (HPAECs) extracted from a female's main pulmonary artery branch which was exposed to hypoxia (Germande et al., 2022). However, we found RV mitochondrial superoxide production to be unaltered in both male and female control and SuHx rats. This is interesting given we would have expected to see an increase in the SuHx groups as oxidative stress is majorly involved in the pathophysiology of PAH. We then examined the genes linked to mitochondrial oxidative stress – NFE2L2, NQO1, SOD2, MAO-A and HSP90AA1 in both RV and lung tissue. Here, we found no changes in NFE2L2, NQO1, SOD2 and MAO-A gene expression in the male SuHx RV. However, we found a significant increase in MAO-A gene expression in the female SuHx RV, but not in the lung tissue. MAO-A which belongs to a class of enzymes situated on the outer mitochondrial membrane is a major source of ROS and has a well-established role of contributing to vascular dysfunction (Kaludercic et al., 2014). MAO-A protein expression was found to be increased within the intimal and medial layers of the pulmonary vasculature in human PAH patients (Sun et al., 2021a). It has also been detected to be increased in the RV and pulmonary vasculature of male SuHx rat (Sun et al., 2021a). Thus, it is surprising that we did not detect this increase in MAO-A gene expression in the male SuHx rats in neither RV or lung tissue. We did find a significant reduction in NFE2L2 RV protein expression in the male SuHx rats, whilst no differences were found in the female SuHx rats. In contrast, antioxidant gene, heat shock protein 90 alpha family class A member 1 (HSP90AA1) was found to be upregulated in the male SuHx RV. We detected a key sex difference here, in which the male SuHx RV tissue illustrated a higher expression of HSP90AA1 when compared with the female SuHx RV. Within the lungs tissue, there was an increase in NQO1 gene expression in both male and female SuHx rats. NQO1 acts downstream of transcriptional regulator NFE2L2 which plays an important role in cellular defence against oxidative stress (Xiong et al., 2015). Together, NFE2L2 and NQO1 establish a redox balance and lower stress-induced injury and tend to be activated by the presence of ROS. As we did not detect an increase in mitochondrial superoxide levels in the RV tissue for both male and female SuHx rats, this could explain why we did not find any differences in NFE2L2 and NQO1 RV gene expression. However, current

research in PH has revealed decreased NFE2L2 expression and suggest that NFE2L2 and NQO1 upregulation could remarkably improve RV and pulmonary vasculature remodeling (Qin et al., 2022). Therefore, the decrease in NFE2L2 RV protein expression in the male SuHx rats is in line with the current literature and perhaps could indicate that the antioxidant system within the RV is failing. This is also suggestive that the male SuHx are illustrating a more progressive PH status which is also described in Chapter 3.

The mitochondria play a crucial role in the production of ATP which is generated via the mitochondrial membrane potential (MMP) (Zorova et al., 2018). A study by Germande and colleagues using HPAECs stained with a MMP probe (TMRM) found a significant reduction in MMP in the HPAECs which were exposed to hypoxia (Germande et al., 2022). Similarly, in the male SuHx rats we also found a loss of MMP, which strongly suggests that there will be a depletion in the amount of ATP produced. At the same time, reduced TMRM also serves as an indicator of poorer mitochondrial health and injury. Germande research group then measured mitochondrial fission and fusion using the MitoTracker green probe and this was found to also be reduced in the HPAECs exposed to hypoxia (Germande et al., 2022). Similarly, we found a reduction in MitoTracker green in the male SuHx rats. We are also the first to report SuHx induced decrease in TMRM and MitoTracker green in male rats.

We then decided to examine the gene expression of the mediators responsible for mitochondrial fusion and fission within both RV and lung tissue. Hence, we would suspect to see an increase in the fission mediator, DNM2 and downregulation of the fusion mediators: MFN1, MFN2 and OPA1. Within the RV, we detected no differences across any of the genes. Meanwhile, in the lung we found a downregulation of MFN1 in only the male rats and MFN2 in both male and female SuHx rats. Previous studies have confirmed that in human PASMC and lung tissue of PAH patients, that there is indeed a deficiency in MFN2 protein expression (Lu et al., 2016b). This produces a pro-proliferative and pro-apoptotic environment whilst driving excessive mitochondrial fission and reduced fusion. These effects were then attenuated upon restoration of MFN2 (Lu et al., 2016b, Zhu et al., 2017). No differences were found in OPA1 in the lung which relies on MFN1, but not MFN2 to mediate mitochondrial fusion (Cipolat et al., 2004, Dasgupta et al., 2020) Surprisingly, we detected a reduction in

DNM2 in the lungs in both male and female SuHx groups which suggest there is a reduction in mitochondrial fission. Perhaps, this could be a compensatory effect of the mitochondria attempting to regain its fusion-fission balance.

We then examined the genes linked to mitochondrial biogenesis. Firstly, we examined PGC1α, which is located in the cell nucleus and cytoplasm and is a versatile transcription coactivator (Liang and Ward, 2006). PGC1α has been shown to be expressed in tissues in which the mitochondria are most abundant such as the RV (Lin et al., 2005). Here, it acts with a variety of transcription factors that play a role in many responses including those involved in mitochondrial biogenesis. The mechanism by which PGC1α achieves this is still being studied however it has been shown to iinduce MFN2 transcription via binding the ERRα to regulate mitochondrial biogenesis (Koves et al., 2005). Loss of MFN2 has also been shown to reduce PGC1α activity (Soriano et al., 2006, Ryan et al., 2013). PGC1α also works predominately with the NRF system, where it directly modulates NRF1/2 and its downstream gene, TFAM in a collaborative manner to stimulate mitochondrial biogenesis (Picca and Lezza, 2015). Due to this, we would have predicted a decrease in all mitochondrial biogenesis genes in the SuHx groups. However, in the RV, we found an increase in TFAM and NRF2 in the male SuHx rats, meanwhile in the lungs we detected a decrease in TFAM and NRF1 in the male SuHx group. The decrease we see in the lungs, would correlate with a reduction in mitochondrial biogenesis, and hence mitochondrial mass.

We decided to measure the gene expression of hexokinase 2 (HK2) which is a stable marker of hypoxia that is regulated in a HIF-1α dependent manner. HIF-1α becomes stabilised only under hypoxic conditions and then will increase the expression of HK2 (Docherty et al., 2019). To date, there has been limited research done investigating the presence of the hypoxic genes within the RV in a PAH model. Here, we found that HK2 was significantly upregulated in the RV in both male and female SuHx rats, which will likely be as a result of the activation of HIF-1α during the 3 weeks of hypoxia. Thus, HK2 expression remained increased/stable despite the animal's re-exposure to normoxia for 5 weeks, and we propose that this likely because the rats are in a PAH status. This suggest that the RV is in a hypoxic state, potentially as a result of the restricted perfusion due to RCA remodelling and fibrosis, especially in the male

SuHx rats. However, when we measured this within the lung tissue, we found that this had decreased even when compared to the controls. This could perhaps be due to an increased expression of rescue genes that over-compensate to reduce HK2 expression. Similar to the RV, we did not detect any sex differences. This is interesting as previous studies have found the females hPASMCs to have significantly higher HIF-1α levels (Docherty et al., 2019). As far as we are aware, HK2 expression has not been assessed in RV tissue from SuHx rats, therefore, we show for the first time, that HK2 expression is increased in both male and female SuHx rats.

Finally, we examined the estrogen receptor 1 (ESR1) and 2 (ESR2) gene expression in both the RV and lung tissue. Within the RV, we highlighted a key sex difference in which there was increased ESR1 expression in the male SuHx rats when compared to the female SuHx rats. This goes against a previous studies which detects ESR1 to be more highly expressed in the female cardiomyocytes compared with the males (Grohé et al., 1998, Sun et al., 2021b). As well as this, loss of ESR1 function in female rats was correlated with uncoupling of the RV-pulmonary system, diastolic dysfunction and fibrosis (Cheng et al., 2020). Whilst we detected the lower ESR1 gene expression with better RV status and less fibrosis in our female SuHx rats as discussed in Chapter 3. Meanwhile, we detected no differences in both ESR1 and ESR2 expression in the lung tissue for both male and female rats.

Overall, our results highlight several key sex differences which point towards the male SuHx having a worse PH status. Firstly, the male SuHx demonstrate worse mitochondrial status than the females. This can be seen in the form of reduced MMP and a reduction in their mitochondrial mass as detected by TMRM and MitoTracker green, respectively. The SuHx males also illustrate reduced gene expression in the mitochondrial fusion markers, MFN1 and MFN2 in their lung tissue, suggesting that they are more exposed to a fusion-to-fission imbalance. Additionally, the male SuHx also have a reduction in their lung mitochondrial biogenesis markers, TFAM and NRF1 gene expression. Although we did not detect this in the RV of the males, we did see contrasting effects that TFAM and NRF2 were upregulated, which we propose to be compensatory. In addition, the males illustrate worse perivascular fibrosis in their smaller RCA vessels, which we did not see in the females. An increase in RCA fibrosis

could contribute to RV stiffening and ischemia within the RV, leading to impaired RV mitochondrial properties as observed in the male SuHx rats.

4.14 Summary

This is the first study to directly compare the perivascular fibrosis and intima-media thickness vessel wall remodelling that takes place within the RCA vessels in both male and female SuHx rats. We discovered that the male SuHx illustrated worse RCA remodelling as a result of increased perivascular collagen deposition. We show that the male SuHx rats also have a worse mitochondrial status, and we propose that this could be connected to the RCA remodelling that we detected in the males. Therefore, it would be useful to target the RCA remodelling and fibrosis within PAH, and then directly assess the mitochondrial properties to determine RCA link with mitochondrial status. The knowledge of such link may provide insight into therapies for RV in PAH.

CHAPTER 5

5. Examining the sex dependent effects of estradiol and MitoQ and their influence on mitochondrial and fibrotic parameters *in vitro* and *in vivo*

5.1 Introduction

Oxidative stress occurs when there is an abundance of reactive oxygen species (ROS). Excess ROS can then initiate mutations in the mitochondrial DNA (mtDNA), mitochondrial respiratory chain, membrane permeability and induce overall mitochondrial dysfunction and hence, poor outcomes in affected patients (Guo et al., 2013). Once mtDNA is damaged, it can start to amplify with decreased/increased expression of its critical proteins, thereby worsening the oxidative stress state (Guo et al., 2013). When the right ventricle (RV) is exposed to pressure overload, it has been correlated with increased levels of ROS that have been linked to increases in collagen formation and hence, fibrosis (Mikhael et al., 2019).

As the mitochondria are considered as the major source of ROS they are especially vulnerable to ROS-induced injury. Due to this, Michael Murphy developed what is now known as Mitoquinone (MitoQ) (Murphy, 1997). MitoQ originated as a coenzyme Q (CoQ) analogue which is attached to a triphenylphosphonium cation (TPP) and can be characterised as a selective mitochondrial antioxidant drug that works to lower mitochondrial ROS (mtROS) (Liberman et al., 1969, Murphy, 1997). It has been shown to lower ROS production and thereby inhibit oxidative damage (Gottwald et al., 2018). It does this by being able to rapidly migrate into the mitochondrial membrane, where it delivers ubiquinone, and then accumulates within the mitochondria up to 100-1000 fold (Gan et al., 2018, Gottwald et al., 2018). Therefore, it is able to neutralise the ROS at the site in which it is formed. Given its promising results, MitoQ has been utilised in a number of clinical trials (see chapter 1, section 1.6.2 for more details). To date, MitoQ has been tested in PH animal models including the pulmonary arterial banding and chronic hypoxia (Pak et al., 2018, Yan et al., 2023, Li et al., 2024b). These studies produced promising results which showed that treatment with MitoQ was able to inhibit acute hypoxia-induced increase in superoxide production in the pulmonary artery smooth muscle cells (PASMCs) and decrease the progression of RV hypertrophy and dilatation following chronic hypoxia exposure (Pak et al., 2018). As well as this, MitoQ was able to prevent RV dysfunction after pulmonary artery banding (PAB) by attenuating RV

hypertrophy and RV dilatation as well as reduce RV superoxide accumulation (Pak et al., 2018). Another study which treated microvascular endothelial cells (MVECs) harvested from male SuHx rats with MitoQ found that MitoQ attenuated basal $[Ca^{2+}]_i$ via inhibiting the transient receptor potential vanilloid-4 (TRPV4) channels, and reduced SuHx-MVEC migration and proliferation (Suresh et al., 2018, Suresh et al., 2019). MitoQ quenching of mtROS and reduction of TRPV4 was also found to reduce mitochondrial fragmentation (Suresh et al., 2019). Interestingly, these effects were found to occur only in the SuHx-MVECs but not in normoxic-MVECS, suggesting that MitoQ is specific and able to directly modify the PAH induced dysfunctional pathways (Suresh et al., 2019). Given the promising results of MitoQ from Suresh's et al., and Pak et al., studies, we decided to examine MitoQ effect on RV function and fibrosis in the SuHx animal model, as this has never been reported.

Additionally, estradiol (E2) has been known to inhibit RV fibrosis within the SuHx rat model via reducing interstitial collagen deposition within the myocardium (Liu et al., 2014, Lahm et al., 2016). Thereby, suggesting that E2 may also play a protective role within the RV by reducing RV stiffness and increasing compliance. There are limited studies regarding the link between oxidative stress / ROS following E2 treatment in the RV. Nonetheless the link with oxidative stress leading to detrimental factors within the RV has been discussed. Particularly, in a SuHx model, oxidative stress was shown to promote cardiomyocyte deterioration and perivascular remodelling leading to RV remodelling (Woo et al., 2017). It has also been mentioned that the females had less RV fibrosis and it was proposed to be due to a better oxidative response (Woo et al., 2017). The response was detected by greater levels of caveolin-1, and decreased endothelial nitric oxide synthase-derived superoxide when compared with the males (Rafikova et al., 2015). Given that E2 can both directly and indirectly affect the mitochondria, E2 is speculated to affect ROS and thus cellular function.

Therefore, the aims of this investigation were to examine the benefits of reducing ROS on RV fibrosis and RV function in PAH using both *in vitro* cell culture and the SuHx rat model.

The objectives of this chapter were to:

- To examine the effects of MitoQ and E2 on cell proliferation and collagen production in male and female human cardiac fibroblasts (HCF) in culture with and without hypoxia.

- To examine the effects of MitoQ and E2 on cell proliferation and collagen production in RV fibroblasts isolated from male monocrotaline (MCT) rats in culture.

- To examine the effects of MitoQ on RV fibrosis and function in the SuHx rat model of PH.

5.2 E2 and MitoQ reduced MitoSOX production in both male and female human cardiac fibroblasts under both normoxia and hypoxia conditions

MitoSOX production was measured by assessing the fluorescence intensity as described in methods section chapter 2, section 2.7.9. In the male HCFs, there was a significant increase in MitoSOX production in the hypoxia vs. normoxia groups (68.89 ± 3.14 AU vs. 40.05 ± 1.45 AU, ****p<0.001, n=14) (Figure 5.1 A and C). MitoSOX was lowered by E2 + normoxia when compared with the normoxia group (23.61 ± 1.99 AU vs. 40.05 ± 1.45 AU, ****p<0.0001, n=14-17) (Figure 5.1 A and C). The same reduction was detected for the normoxia + MitoQ versus the normoxia group (15.46 ± 1.71 AU vs. 40.05 ± 1.45 AU, ****p<0.0001, n=13-14) (Figure 5.1 A and C). In the male HCF, hypoxia + E2 similarly reduced MitoSOX levels in comparison to the hypoxia group (23.51 ± 2.20 AU vs. 68.89 ± 3.14 AU, ****p<0.001, n=14-20) (Figure 5.1 A and C). Again, the same outcome was seen for hypoxia + MitoQ versus hypoxia (16.38 ± 1.12 AU vs. 68.89 ± 3.14 AU, ****p<0.0001, n=14-18) (Figure 5.1 A and C).

In the female HCFs we did not find an increase in MitoSOX production in the hypoxia vs. normoxia. Although, we did see that MitoSOX production was lowered in the normoxia + E2 versus normoxia group (28.95 ± 5.01 AU vs. 81.28 ± 8.09 AU, ****p<0.001, n=11-15) (Figure 5.1 B and D). The same result was detected in the hypoxia + E2 versus hypoxia group (15.57 ± 1.59 AU vs. 81.32 ± 6.76 AU, ****p<0.0001, n=15-17) (Figure 5.1 B and D). A similar outcome was seen in the MitoQ treated groups in which MitoSOX intensity was lowered by MitoQ in the normoxia + MitoQ versus normoxia group (26.37 ± 2.38 AU vs. 81.28 ± 8.09 AU, ****p<0.0001, n=11-18) (Figure 5.1 B and D). Similarly, hypoxia + MitoQ vs. hypoxia group also reduced MitoSOX intensity (44.28 ± 1.96 AU vs. 81.32 ± 6.76 AU, ****p<0.0001, n=15-20) (Figure 5.1 B and D).

A

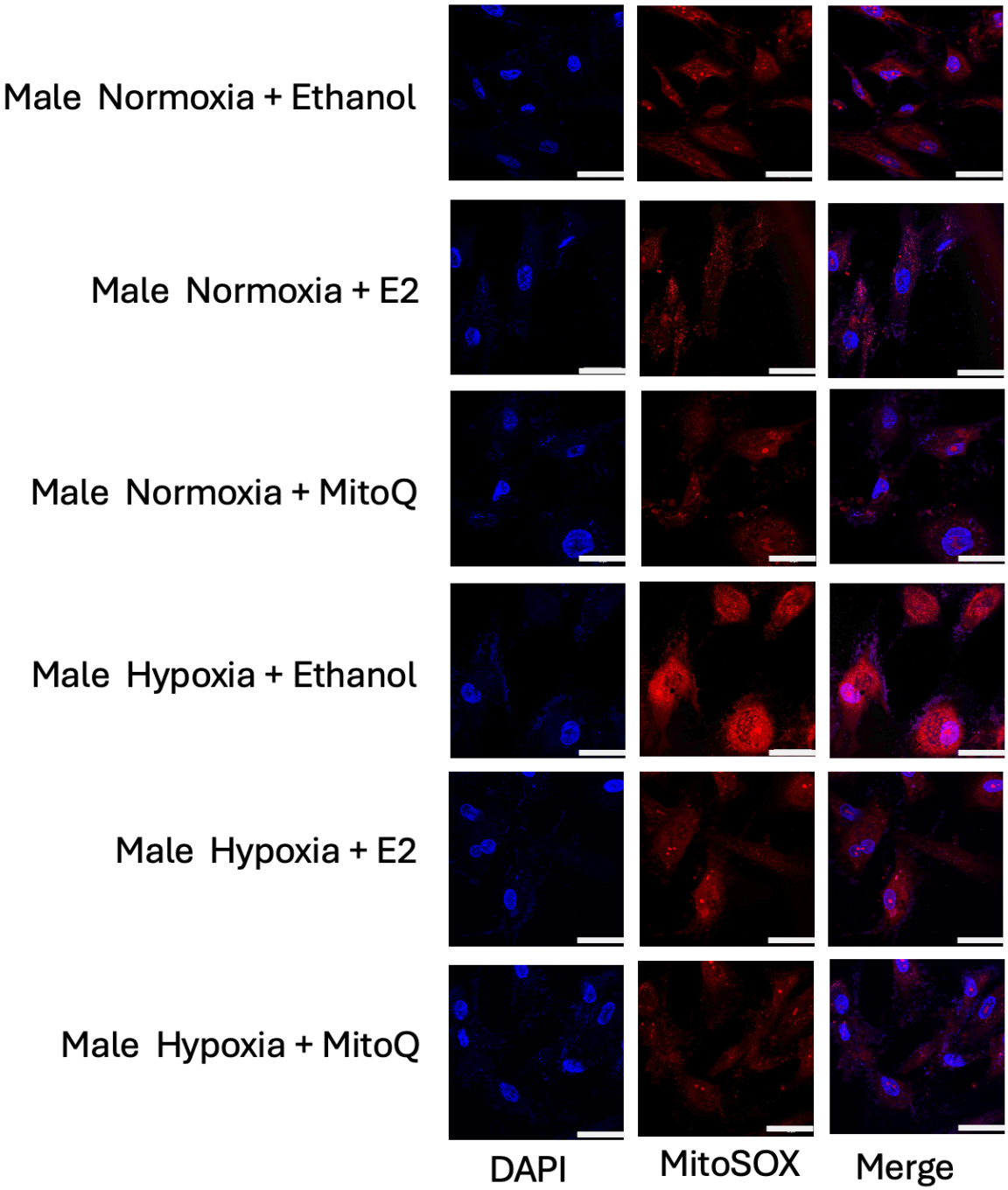
Male Normoxia + Ethanol
Male Normoxia + E2
Male Normoxia + MitoQ
Male Hypoxia + Ethanol
Male Hypoxia + E2
Male Hypoxia + MitoQ
DAPI
MitoSOX
Merge

B

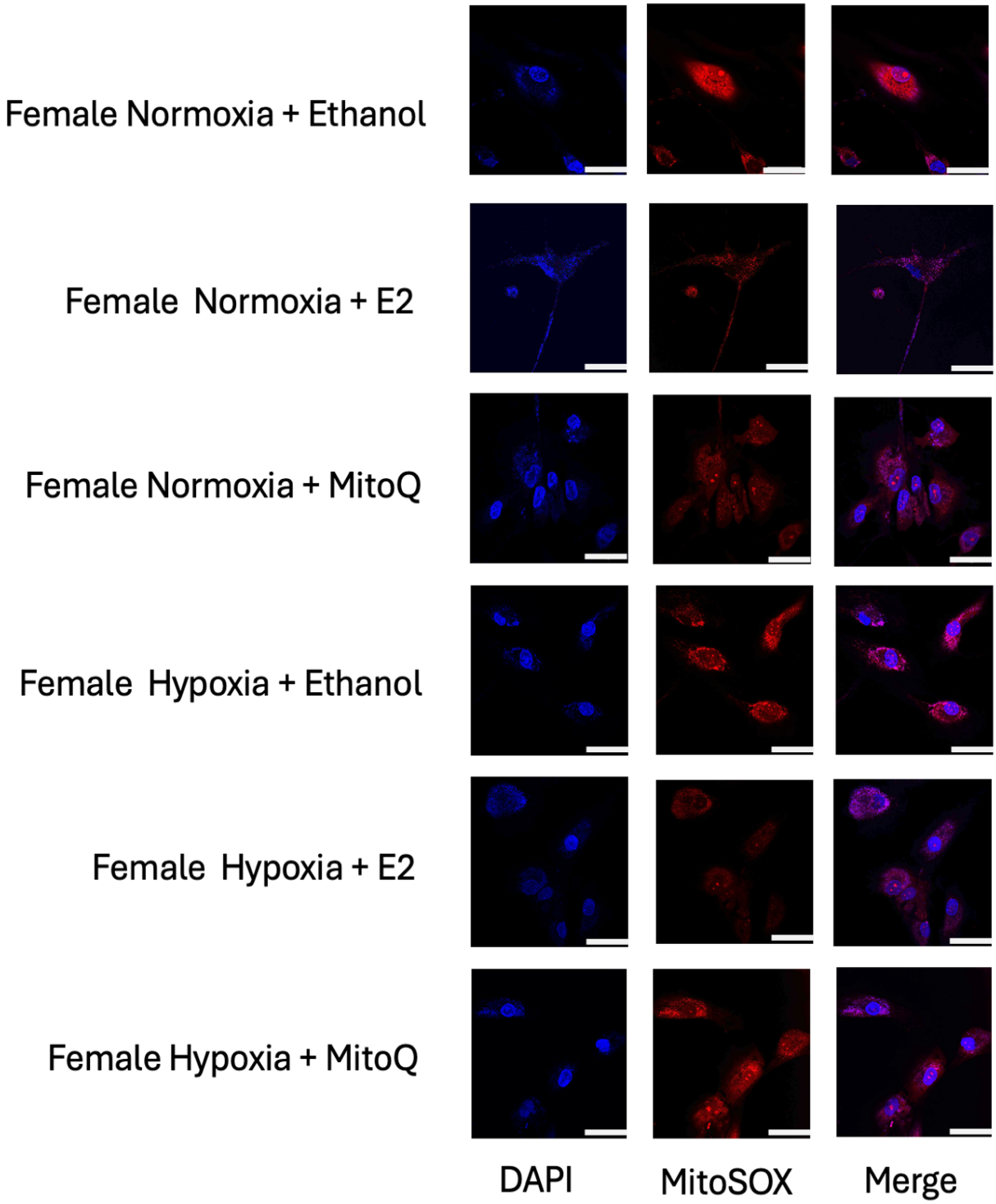
Female Normoxia + Ethanol
Female Normoxia + E2
Female Normoxia + MitoQ
Female Hypoxia + Ethanol
Female Hypoxia + E2
Female Hypoxia + MitoQ
DAPI
MitoSOX
Merge

C

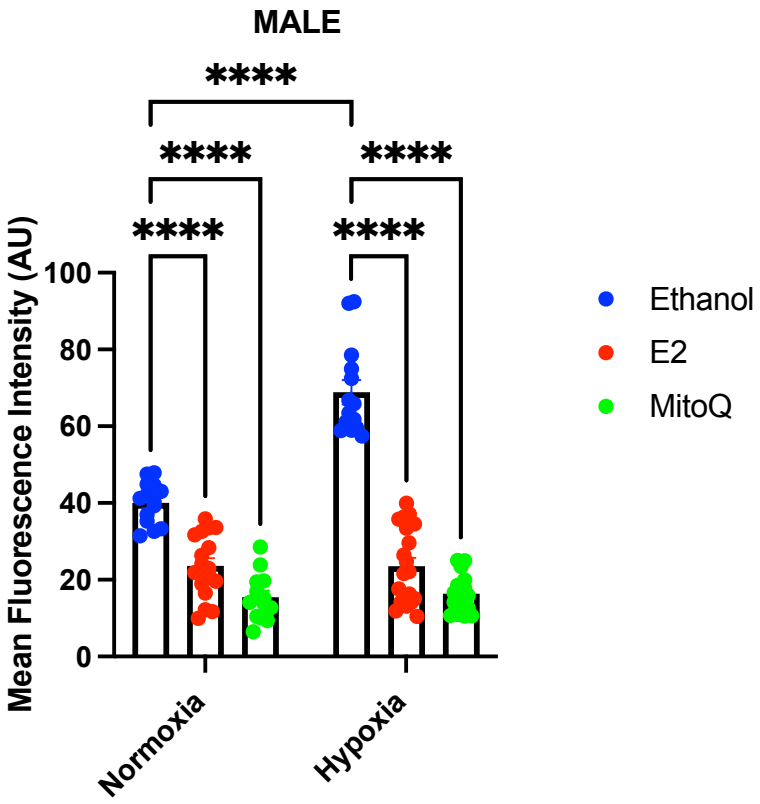
MALE
****
****
****
****
****
Mean Fluorescence Intensity (AU)
100
80
60
40
20
0
Normoxia
Hypoxia
Ethanol
E2
MitoQ

D

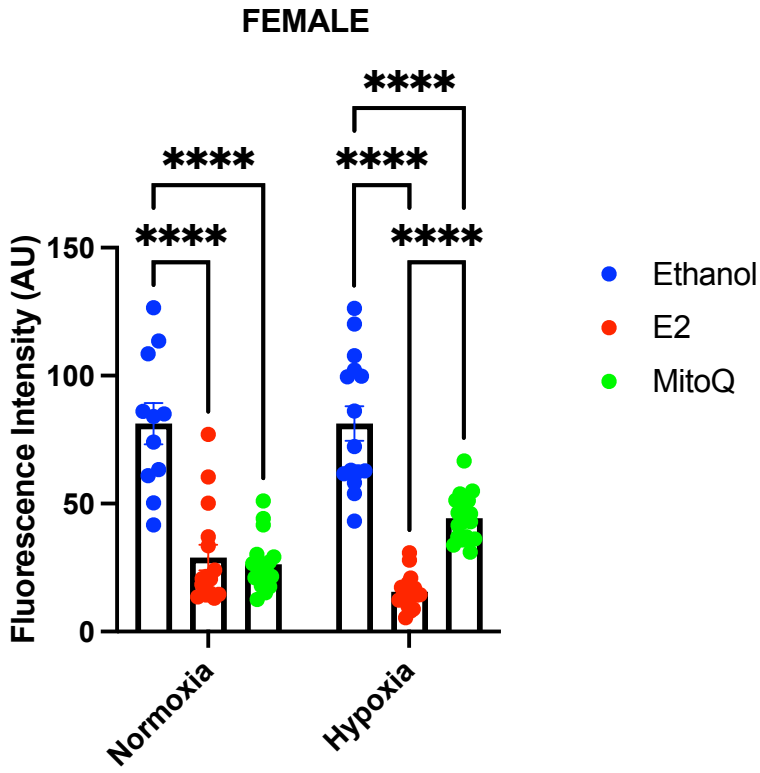
FEMALE
****
****
****
****
****
Fluorescence Intensity (AU)
150
100
50
0
Normoxia
Hypoxia
Ethanol
E2
MitoQ

Figure 5.1. The effect of E2 and MitoQ on MitoSOX intensity in the male and female HCF with and without hypoxia

Male and female human cardiac fibroblasts (HCF) cells were exposed to either normoxia or hypoxia and then treated with either ethanol, estradiol (E2) (10nM) or MitoQ (300nM). Male representative images (Figure A) and male quantification (Figure C) female representative images (Figure B) and female quantification (Figure D). All cells were stained with DAPI (blue) for nuclei and then MitoSOX (red) for mitochondrial superoxide production. Images were taken at 63x magnification. Scale bar represent 50μm. Cells were quantified by measuring their fluorescence intensity. n= represents the number of cells, with n=11-20. All statistical analysis was performed using a two-way ANOVA. *p<0.05, **p<0.01, ****p<0.0001.

5.3 The effect of E2 and MitoQ on proliferation of male and female HCF *in vitro* with and without hypoxia

Ki-67 plays a crucial role in cell proliferation (Soliman and Yussif, 2016), therefore we employed this marker as an indicator of how the male and female HCF isolated from the human ventricles were dividing under normoxic and hypoxic conditions in either the presence of ethanol (100%), E2 (10nM) or MitoQ (300nM). The cells positive for Ki-67 fluoresced as red in color and then were assessed by counting the number of positive cells over the total cell count, which was then represented as a percentage.

In the male HCF cells treated with hypoxia did not seem to increase the percentage of Ki-67 positive cells. However, treatment with MitoQ reduced the percentage of Ki-67 positive cells in the normoxia + MitoQ vs. normoxia group (43.46 ± 4.29% vs. 78.39 ± 3.83%, ****p<0.0001, n=6-8) (Figure 5.2 A and C). The same was seen in the hypoxia + MitoQ vs. hypoxia group (41.51 ± 3.84% vs. 73.88 ± 2.51%, ****p<0.0001, n=6) (Figure 5.2 A and C). Meanwhile, no differences were detected in the E2 groups under both normoxia and hypoxia conditions when compared with their respective control group. However, there was a significant reduction in the percentage of Ki-67 positive cells in the normoxia + E2 vs. normoxia + MitoQ groups (43.46 ± 4.29% vs. 76.23 ± 3.19%, ****p<0.0001, n=6-9) (Figure 5.2 A and C). The same was also seen in the hypoxia + E2 vs. hypoxia + MitoQ group (41.51 ± 3.84% vs. 73.85 ± 3.27%, p<0.0001, n=6) (Figure 5.2 A and C).

In the female HCF cells, no differences were detected by E2 and MitoQ across the normoxia groups. However, under hypoxic conditions MitoQ significantly reduced percentage of Ki-67 positive cells in the hypoxia + MitoQ vs. hypoxia treated group (15.51 ± 2.38% vs. 39.33 ± 4.33%, ***p<0.001, n=7-10) (Figure 5.2 B and D). E2 was also able to significantly reduce the percentage of Ki-67 positive cells in the hypoxia + E2 vs. hypoxia treated group (23.33 ± 3.84% vs. 39.33 ± 4.33%, *p<0.05, n=7-10) (Figure 5.2 B and D).

A

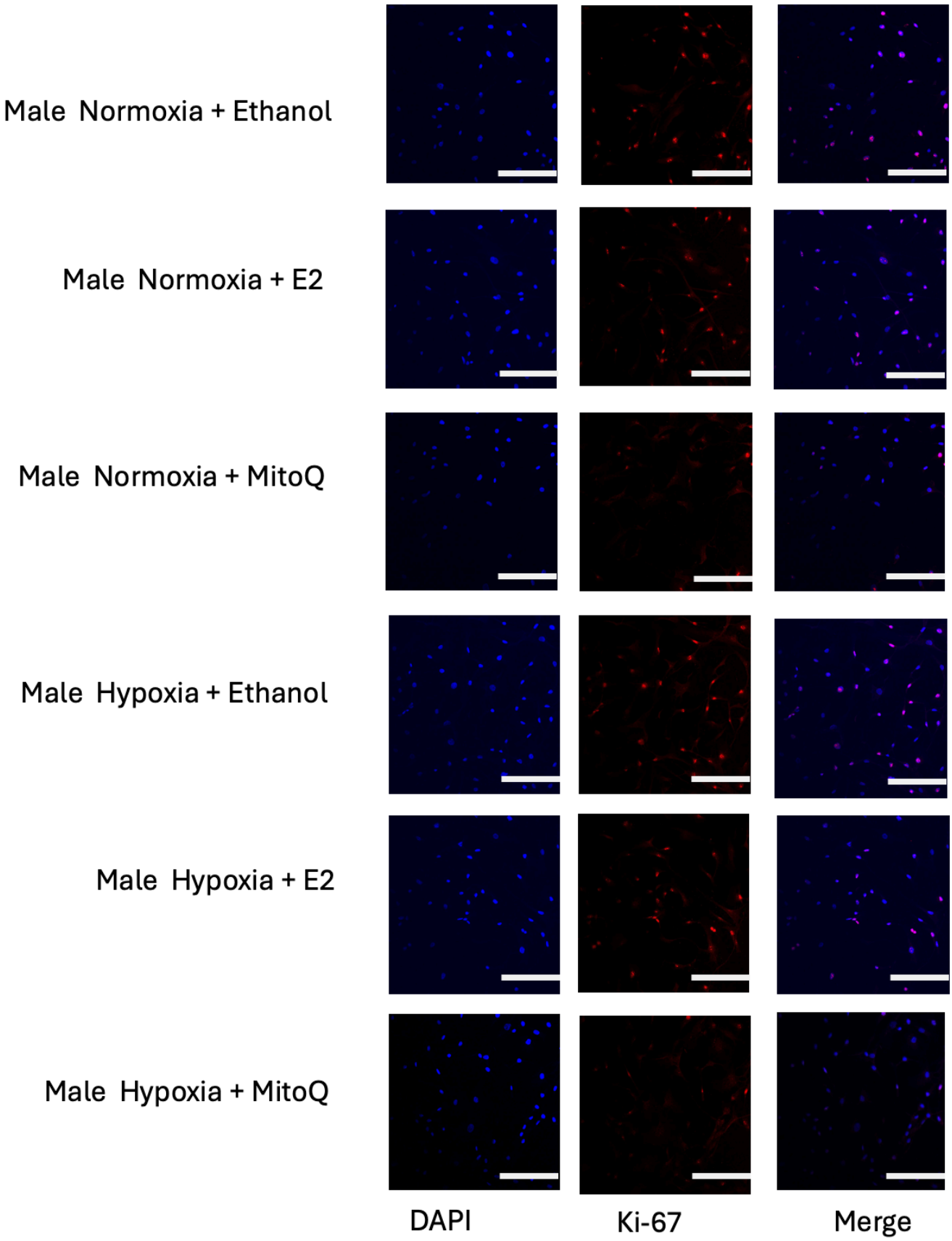
Male Normoxia + Ethanol
Male Normoxia + E2
Male Normoxia + MitoQ
Male Hypoxia + Ethanol
Male Hypoxia + E2
Male Hypoxia + MitoQ
DAPI
Ki-67
Merge

B

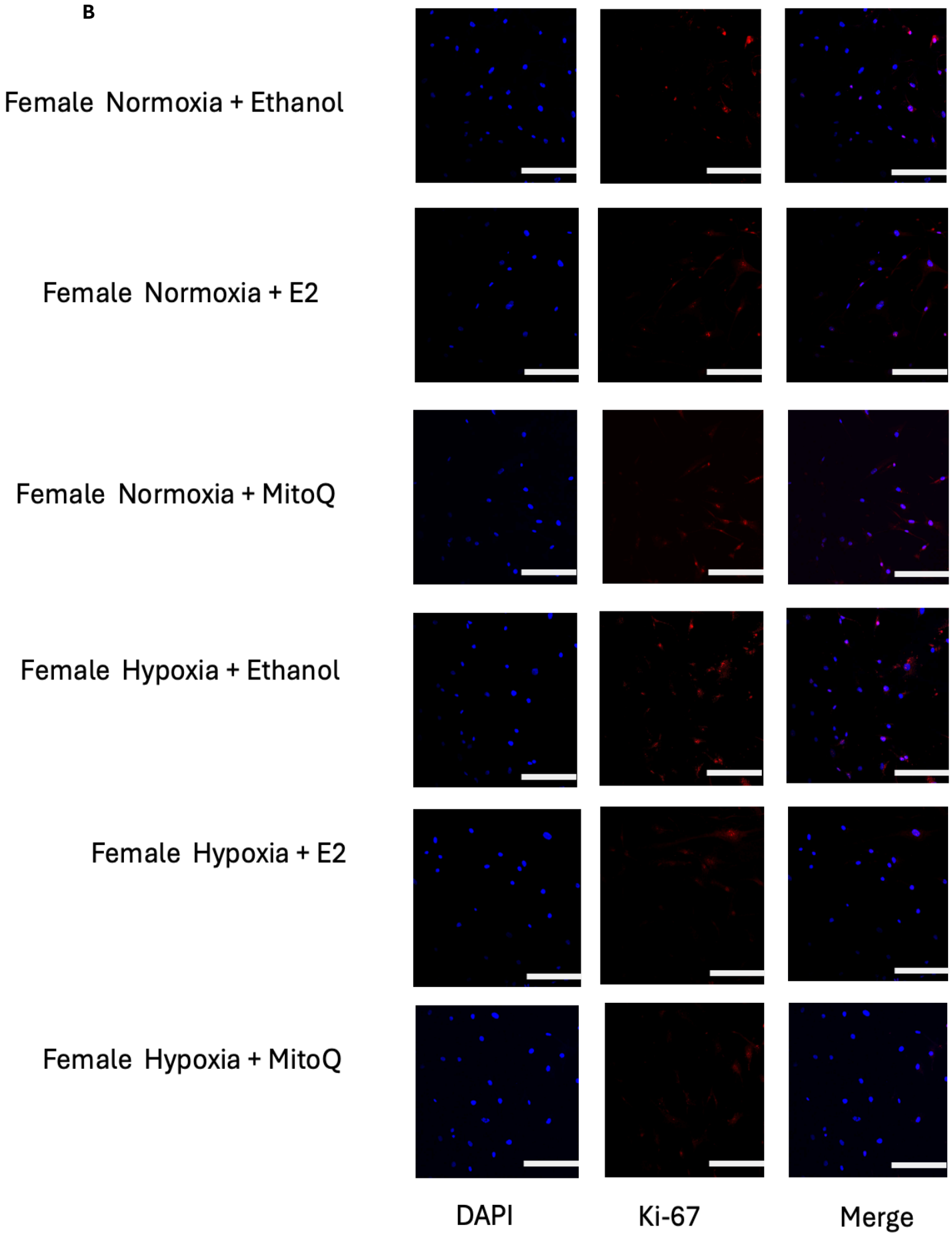
Female Normoxia + Ethanol
Female Normoxia + E2
Female Normoxia + MitoQ
Female Hypoxia + Ethanol
Female Hypoxia + E2
Female Hypoxia + MitoQ
DAPI
Ki-67
Merge

C

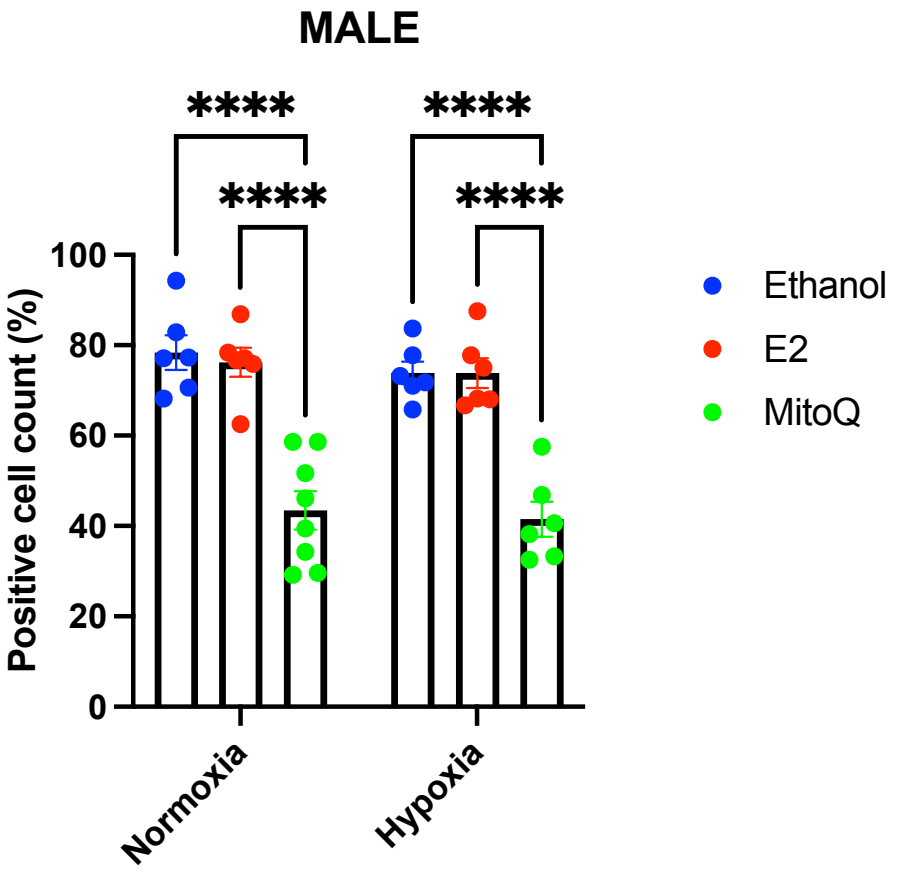
MALE
****
****
****
****
Positive cell count (%)
100
80
60
40
20
0
Normoxia
Hypoxia
Ethanol
E2
MitoQ

D

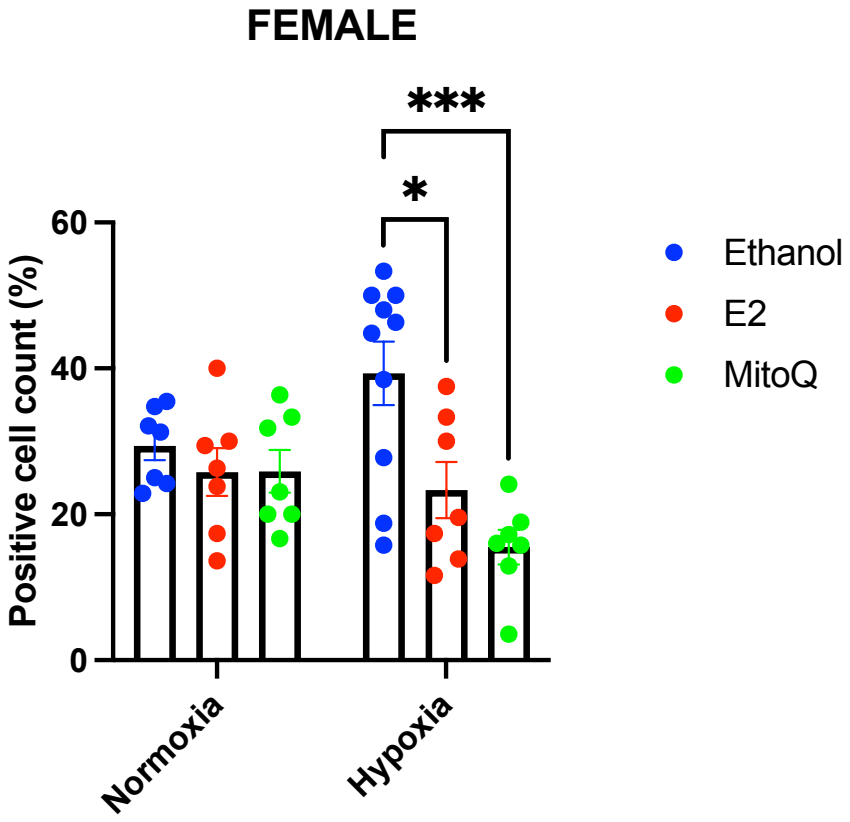
FEMALE
***
*
Positive cell count (%)
60
40
20
0
Normoxia
Hypoxia
Ethanol
E2
MitoQ

Figure 5.2. The effect of E2 and MitoQ on Ki-67 positive cell count in the male and female HCF with and without hypoxia

Male and female human cardiac fibroblasts (HCF) cells were exposed to either normoxia or hypoxia and then treated with either ethanol, estradiol (E2) (10nM), or MitoQ (300nM). Representative images are shown in figures A for male and figure B for female. All cells were stained with DAPI for nuclei (blue) and Ki-67 (red) for cell proliferation. Images were captured at 20x magnification. Scale bar represent 200μm. Cells were quantified by calculating the positive cell count over the total cell count and represented as a percentage (figures C and D). 7-10 images per group were analysed, with n representing the number of cells, with n=6-10. All statistical analysis was performed using a two-way ANOVA with *$p<0.05$, ***$p<0.001$, ****$p<0.0001$.

5.4 E2 and MitoQ altered the protein expression of TFAM, NFE2L2 and Col1a1 in male and female HCF cells

The effects of Col1a1, NFE2L2 and TFAM were examined as Col1a1 is responsible for regulating the collagen type 1 protein which contributes to vessel / RV wall stiffness in a PAH setting (Kakaletsis et al., 2023). Meanwhile NFE2L2 is one of the main pathways activated by MitoQ and TFAM serves as a crucial marker for mitochondrial activity (Hu et al., 2018, Ma et al., 2023). These proteins were tested on both male and female HCF cells which were treated with E2 and MitoQ in the presence of either normoxia or hypoxia.

In the male HCF no differences were detected in Col1a1 expression between normoxia and normoxia + E2 group. However, hypoxia + E2 vs. hypoxia was found to reduce Col1a1 expression (27.65 ± 1.08 AU vs. 60.90 ± 2.93 AU, ****p<0.0001, n=24) (Figure 5.3 A and B). Meanwhile, MitoQ reduced Col1a1 expression as seen in the normoxia + MitoQ vs. normoxia group (11.36 ± 0.65 AU vs. 53.10 ± 2.69 AU, ****p<0.0001, n=24-36). The same was seen in the hypoxia + MitoQ vs. hypoxia group (14.74 ± 0.88 vs. 60.90 ± 2.93, ****p<0.0001, n=24) (Figure 5.3 A and B). MitoQ reduced Col1a1 expression even when compared with E2 as seen in the normoxia + MitoQ vs. normoxia + E2 group (11.36 ± 0.65 AU vs. 54.65 ± 3.67 AU, ****p<0.00001, n=24-36). The same was also seen in the hypoxia groups, hypoxia + MitoQ vs. hypoxia group (14.74 ± 0.88 AU vs. 27.65 ± 1.08 AU, *p<0.05, n=24) (Figure 5.3 A and B).

In the female HCF, E2 was not able to reduce Col1a1 expression under normoxia conditions but was able to do so in the presence of hypoxia as seen in the hypoxia + E2 vs. hypoxia groups (38.39 ± 2.16 AU vs. 66.59 ± 4.32 AU, ****p<0.0001, n=32-38) (Figure 5.3 C and D). Meanwhile, MitoQ was able to reduce Col1a1 in the presence of normoxia as seen in the normoxia + MitoQ vs. normoxia group (17.77 ± 1.11 AU vs. 72.48 ± 4.18 AU, ****p<0.0001, n=33-35). The same was seen in the hypoxia + MitoQ vs. hypoxia group (12.16 ± 0.63 AU vs. 66.59 ± 4.32 AU, ****p<0.0001, n=33-35) (Figure 5.3 C and D). MitoQ was also able to reduce Col1a1 greater than E2 in both normoxia + MitoQ versus normoxia + E2 group (17.77 ± 1.11 AU vs. 60.84 ± 2.41 AU, ****p<0.0001, n=32-36) and in

the hypoxia + MitoQ vs. hypoxia + E2 groups (12.16 ± 0.63 AU vs. 38.39 ± 2.16 AU, ****p<0.0001, n=38) (Figure 5.3 C and D).

In the male HCF, nuclear NFE2L2 intensity was increased in the normoxia + E2 vs. normoxia group (31.52 ± 1.06 AU vs. 22.24 ± 0.50 AU, ****p<0.0001, n=42). The same increase was also seen in the hypoxia + E2 vs. hypoxia groups (34.43 ± 0.90 AU vs. 27.43 ± 0.56 AU, ****p<0.0001, n=28-42) (Figure 5.3 E and F). MitoQ also increased NFE2L2 intensity in the normoxia + MitoQ vs. normoxia group (31.98 ± 0.93 AU vs. 22.24 ± 0.50 AU, ****p<0.0001, n=40-42). The same increase was detected in the hypoxia + MitoQ vs. hypoxia group (35.42 ± 0.73 AU vs. 27.43 ± 0.56 AU, ****p<0.0001, n=42-43) (Figure 5.3 E and F).

Similarly, in the female HCF NFE2L2 was increased in the normoxia + E2 vs. normoxia group (31.25 ± 0.63 AU vs. 21.72 ± 0.79 AU, ****p<0.0001, n=28-39) and in the hypoxia + E2 vs. hypoxia groups (31.71 ± 0.67 AU vs. 23.52 ± 0.94 AU, ****p<0.0001, n=28-42) (Figure 5.3 G and H). The same outcome was also produced by MitoQ as seen in the normoxia + MitoQ vs. normoxia groups (34.82 ± 1.18 AU vs. 21.72 ± 0.79 AU, ****p<0.0001, n=28-39) and in the hypoxia + MitoQ vs. hypoxia groups (31.14 ± 0.72 AU vs. 23.52 ± 0.94 AU, ****p<0.0001, n=42) (Figure 5.3 G and H).

In the male HCF, cytosolic TFAM intensity was significantly increased in the normoxia + E2 vs. normoxia groups (22.32 ± 0.50 AU vs. 14.36 ± 0.43 AU, ****p<0.0001, n=28) and in the hypoxia + E2 vs. hypoxia groups (23.32 ± 0.89 AU vs. 14.89 ± 0.44 AU, ****p<0.0001, n=28) (Figure 5.3 I and J). MitoQ also produced an increase in TFAM in the normoxia + MitoQ vs. normoxia groups (20.57 ± 0.73 AU vs. 14.36 ± 0.43 AU, ****p<0.0001, n=28) and in the hypoxia + MitoQ vs. hypoxia (21.04 ± 0.85 AU vs. 14.89 ± 0.44 AU, ****p<0.0001, n=28) (Figure 5.3 I and J).

The same outcome was seen for the females in which E2 increased TFAM intensity in the normoxia + E2 vs. normoxia groups (28.07 ± 0.59 AU vs. 15.43 ± 0.65 AU, ****p<0.0001, n=28) and in the hypoxia + E2 vs. hypoxia groups (21.50 ± 0.79 AU vs. 17.50 ± 0.57 AU,

**p<0.01, n=28). MitoQ also increased TFAM intensity as seen in the normoxia + MitoQ vs. normoxia group (23.79 ± 0.94 AU vs. 15.43 ± 0.65 AU, ****p<0.0001, n=28) and in the hypoxia + MitoQ vs. hypoxia groups (21.14 ± 0.62 AU vs. 17.50 ± 0.57 AU, **p<0.01, n=28) (Figure 5.3 K and L).

A

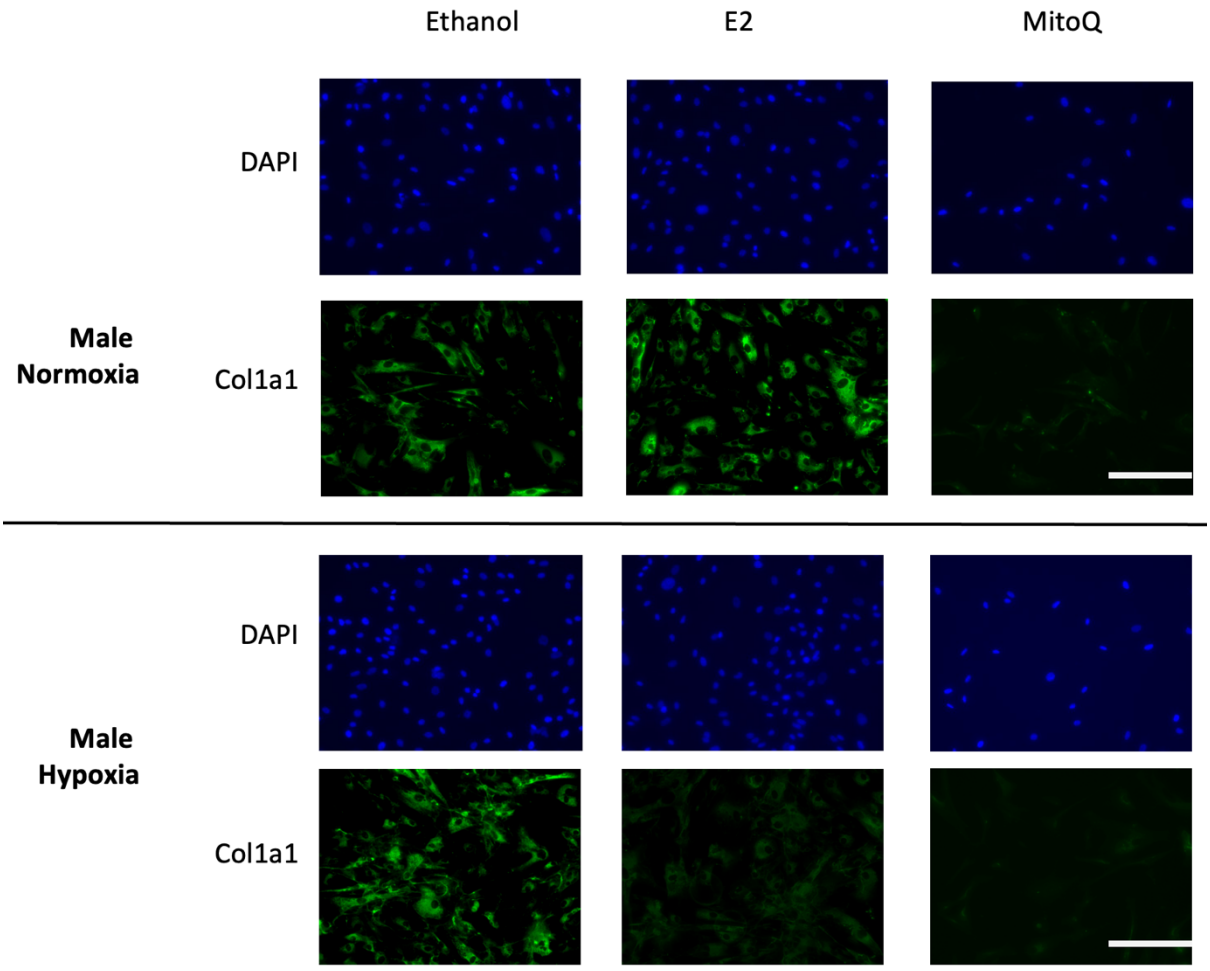
Ethanol
E2
MitoQ
DAPI
Male
Normoxia
Col1a1
DAPI
Male
Hypoxia
Col1a1

B

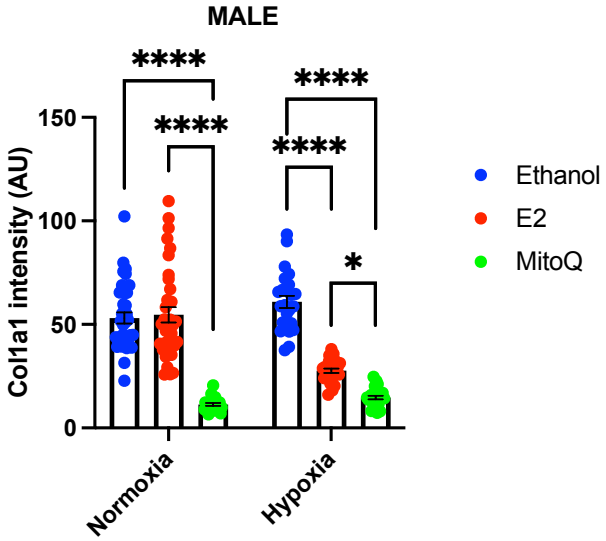
MALE
Col1a1 intensity (AU)
150
100
50
0
****
****
****
****
*
Normoxia
Hypoxia
Ethanol
E2
MitoQ

C

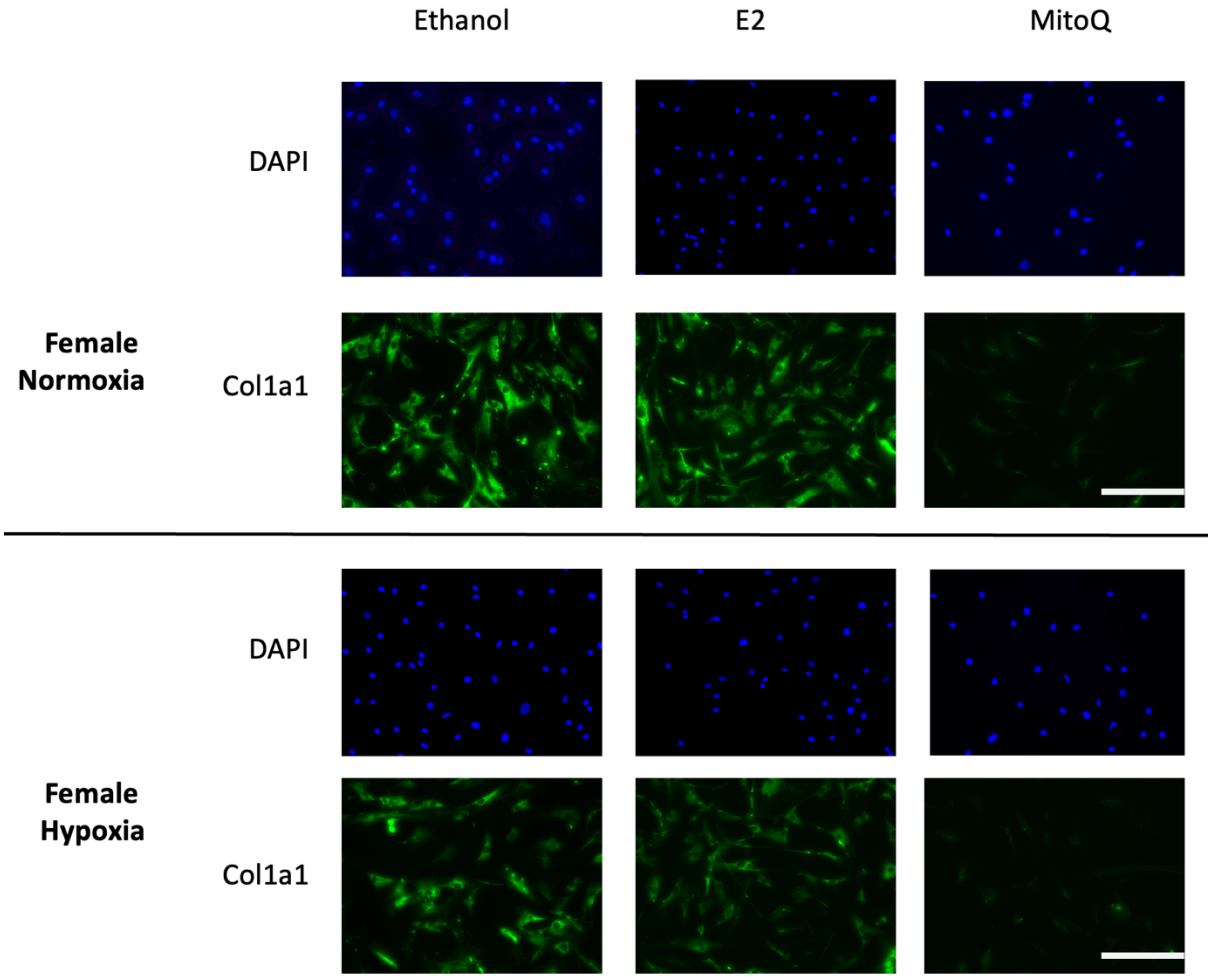
Ethanol
E2
MitoQ
DAPI
Female Normoxia
Col1a1
DAPI
Female Hypoxia
Col1a1

D

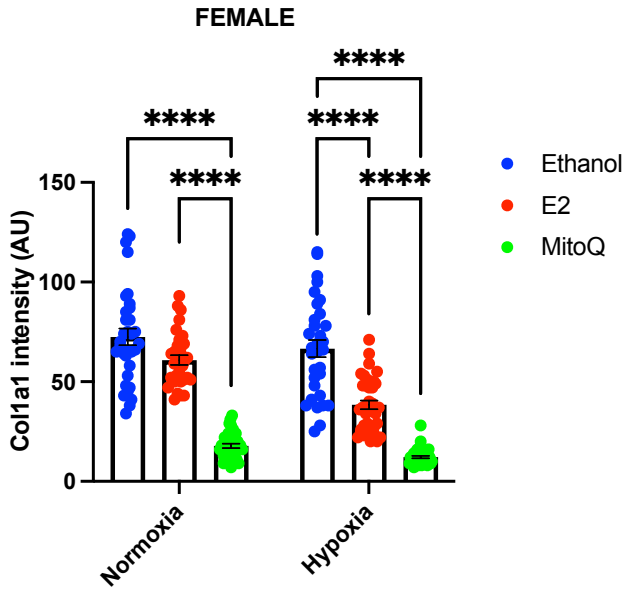
FEMALE
****
****
****
****
****
150
100
50
0
Col1a1 intensity (AU)
Normoxia
Hypoxia
Ethanol
E2
MitoQ

E

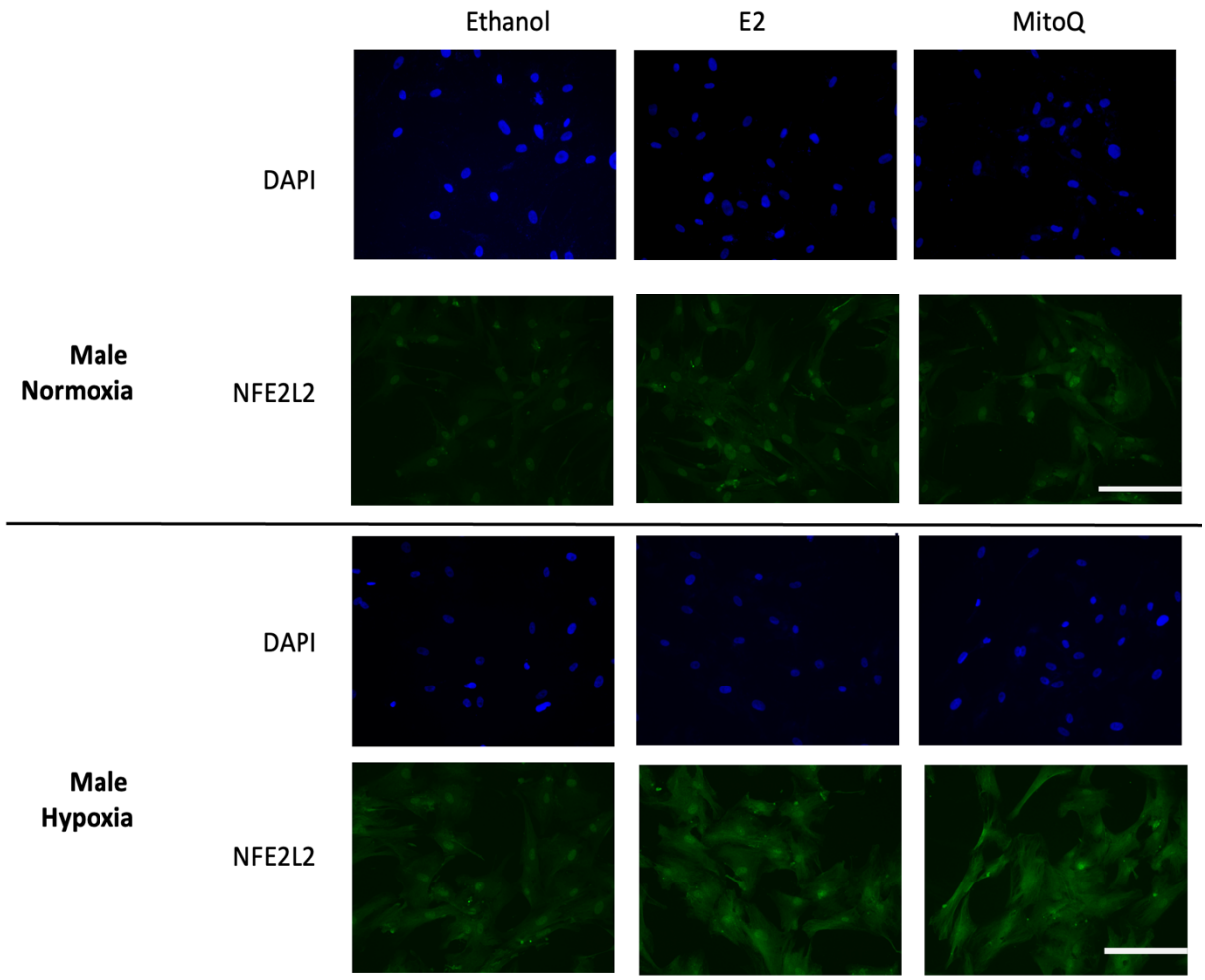
Ethanol
E2
MitoQ
DAPI
Male
Normoxia
NFE2L2
DAPI
Male
Hypoxia
NFE2L2

F

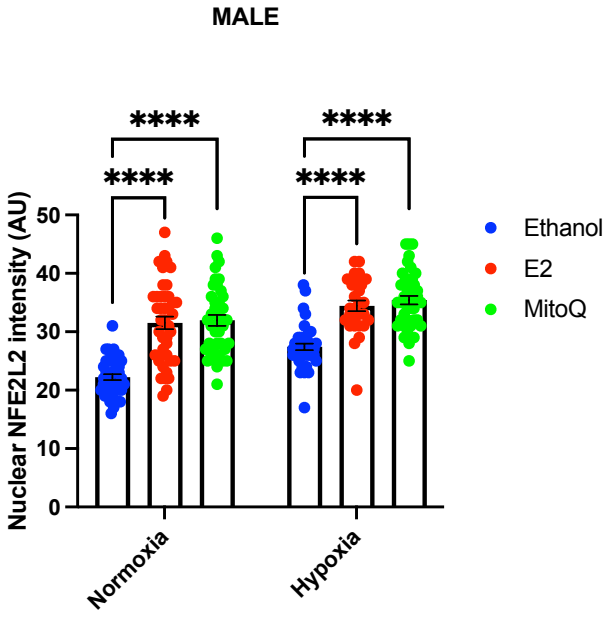
MALE
****
****
****
****
Nuclear NFE2L2 intensity (AU)
0
10
20
30
40
50
Normoxia
Hypoxia
Ethanol
E2
MitoQ

G

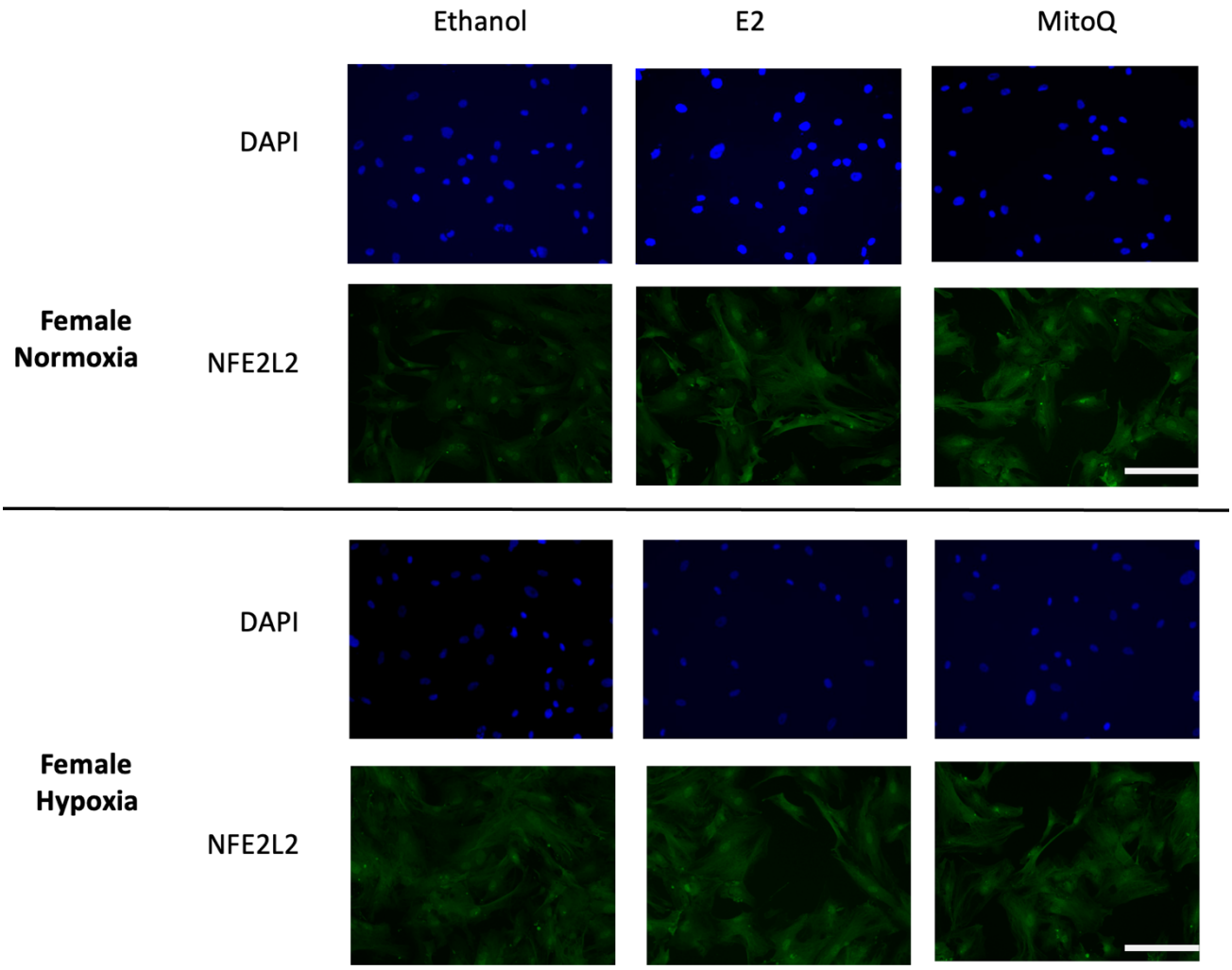
Ethanol
E2
MitoQ
DAPI
Female Normoxia
NFE2L2
DAPI
Female Hypoxia
NFE2L2

H

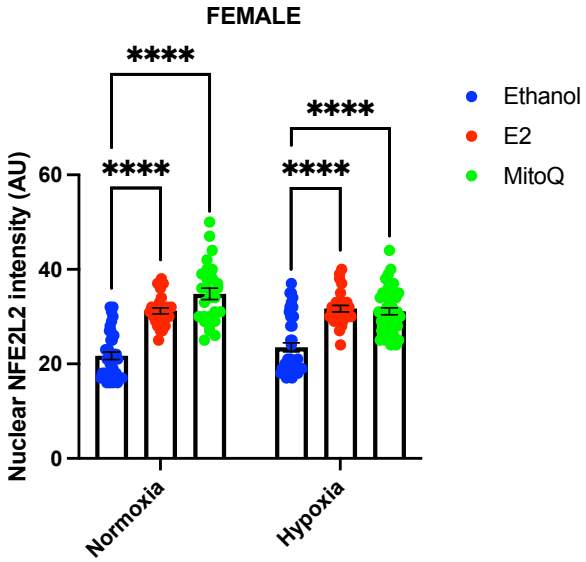
FEMALE
****
****
****
****
Nuclear NFE2L2 intensity (AU)
60
40
20
0
Normoxia
Hypoxia
Ethanol
E2
MitoQ

I

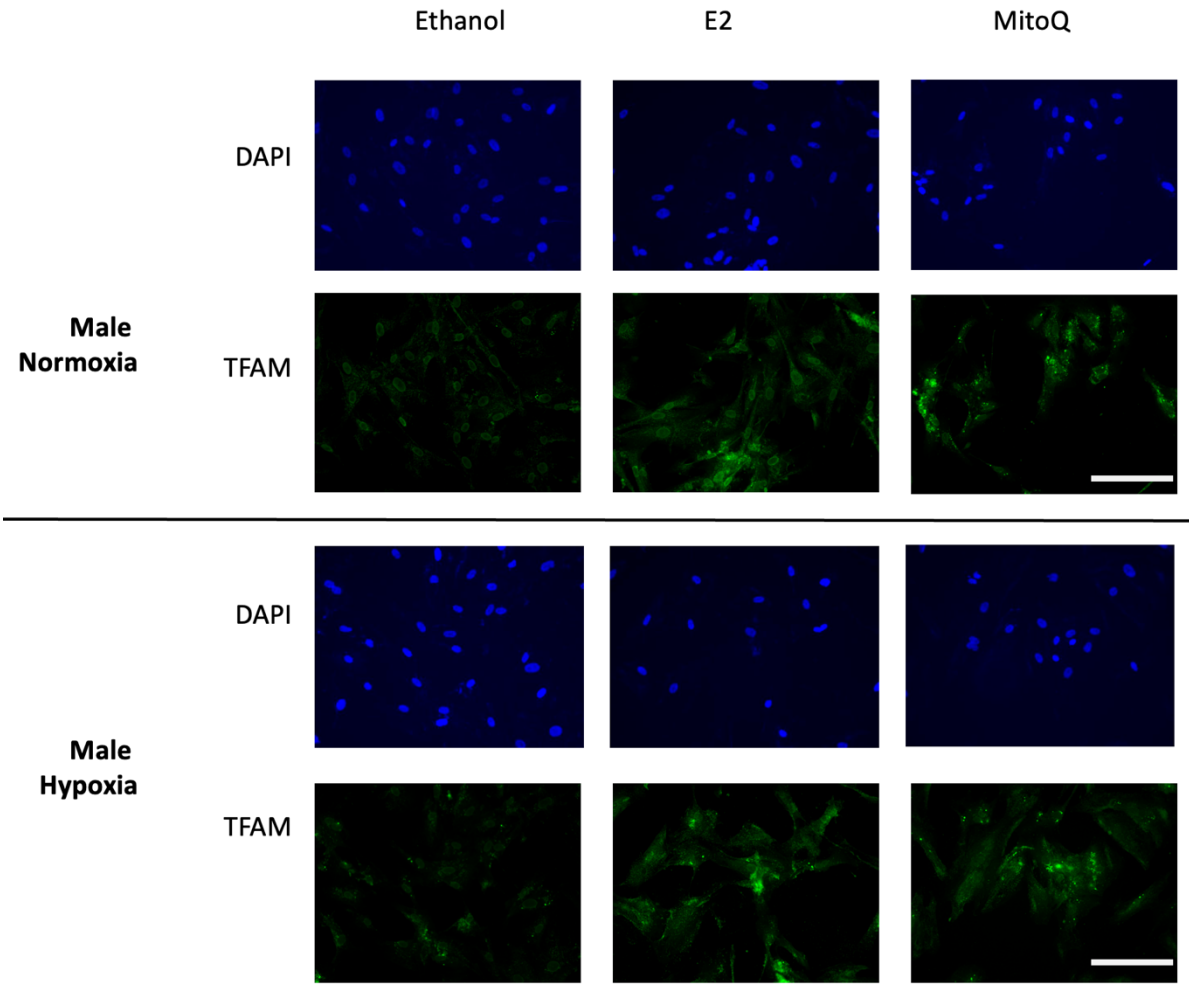
Ethanol
E2
MitoQ
DAPI
TFAM
Male
Normoxia
DAPI
TFAM
Male
Hypoxia

J

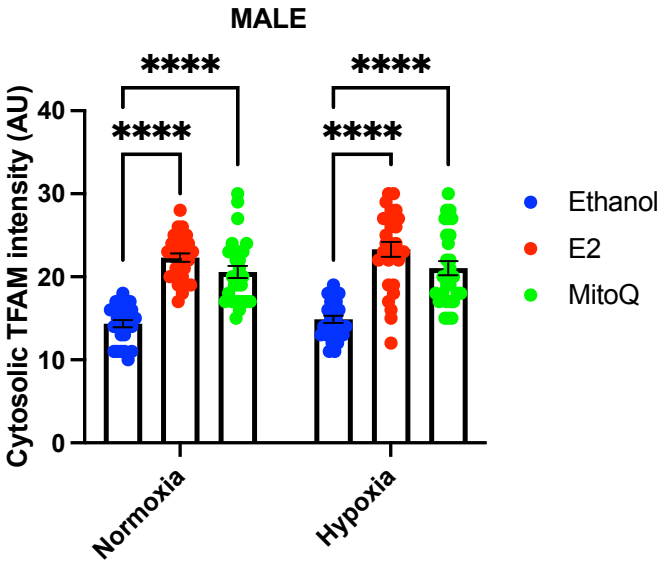
MALE
Cytosolic TFAM intensity (AU)
0
10
20
30
40
****
****
****
****
Normoxia
Hypoxia
Ethanol
E2
MitoQ

K

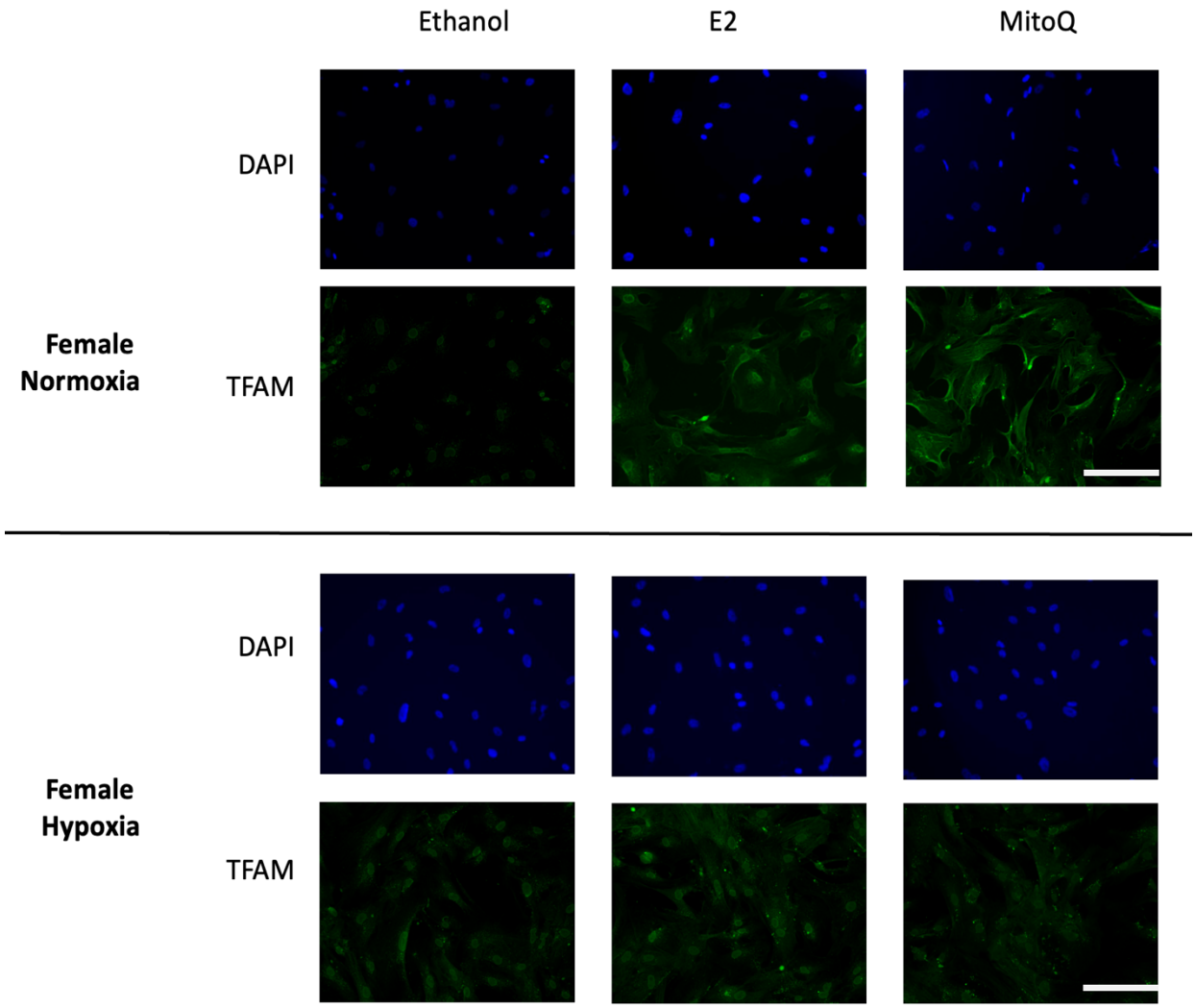
Ethanol
E2
MitoQ
DAPI
Female
Normoxia
TFAM
DAPI
Female
Hypoxia
TFAM

L

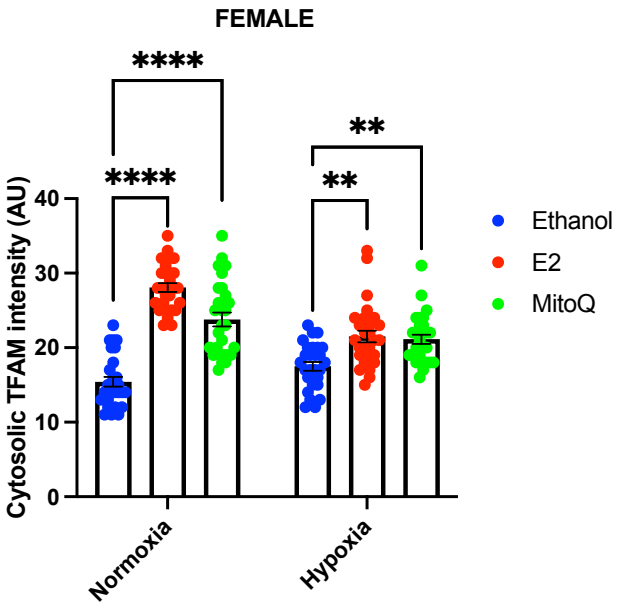
FEMALE
****
****
**
**
Cytosolic TFAM intensity (AU)
0
10
20
30
40
Normoxia
Hypoxia
Ethanol
E2
MitoQ

Figure 5.3. E2 and MitoQ altered Col1a1, nuclear NFE2L2 and cytosolic TFAM intensity under normoxia and hypoxia conditions in male and female HCF cells

Male and female human cardiac fibroblasts (HCF) cells were treated with either ethanol, estradiol (E2) (10nM) or MitoQ (300nM) and then exposed to either normoxia or hypoxia for 48 hours. All cells were stained with DAPI for nuclei (blue). Representative images showing collagen type 1 alpha 1 chain (Col1a1) (green), nuclear factor erythroid 2-related factor 2 (NFE2L2) (green) and mitochondrial transcription factor A (TFAM) (green) are shown in figures A, C, E, G, I and K, and cell quantification is shown in figures B, D, F, H, J and L. All quantification analysis was performed using the ImageJ software (National Institutes of Health, Bethesda, MD, USA). Images were captured at 20x magnification. Scale bar represents 200μm. Each n number represents an individual cell, with n=24-43. Statistical analysis was performed using a two-way ANOVA with *p<0.05, **p<0.01, ****p<0.0001.

5.5 Both E2 and MitoQ reduced MitoSOX production in male MCT RV fibroblasts

To follow up from the human HCF analysis, male MCT RV fibroblasts were treated with ethanol, E2 (10nM) and MitoQ (300nM) and stained with MitoSOX. Given that these cells were isolated from MCT-PAH RV, they did not need to be further exposed to hypoxic conditions. Indeed, we found that E2 reduced MitoSOX levels in MCT RV fibroblasts when compared with ethanol treatment (36.11 ± 7.35 AU vs. 85.74 ± 13.62 AU, *$p<0.05$, n=5) (Figure 5.4 A and B) and the same reduction was seen in the MCT RV fibroblasts treated with MitoQ (43.79 ± 8.47 AU vs. 85.74 ± 13.62 AU, *$p<0.05$, n=5) (Figure 5.4 A and B).

A

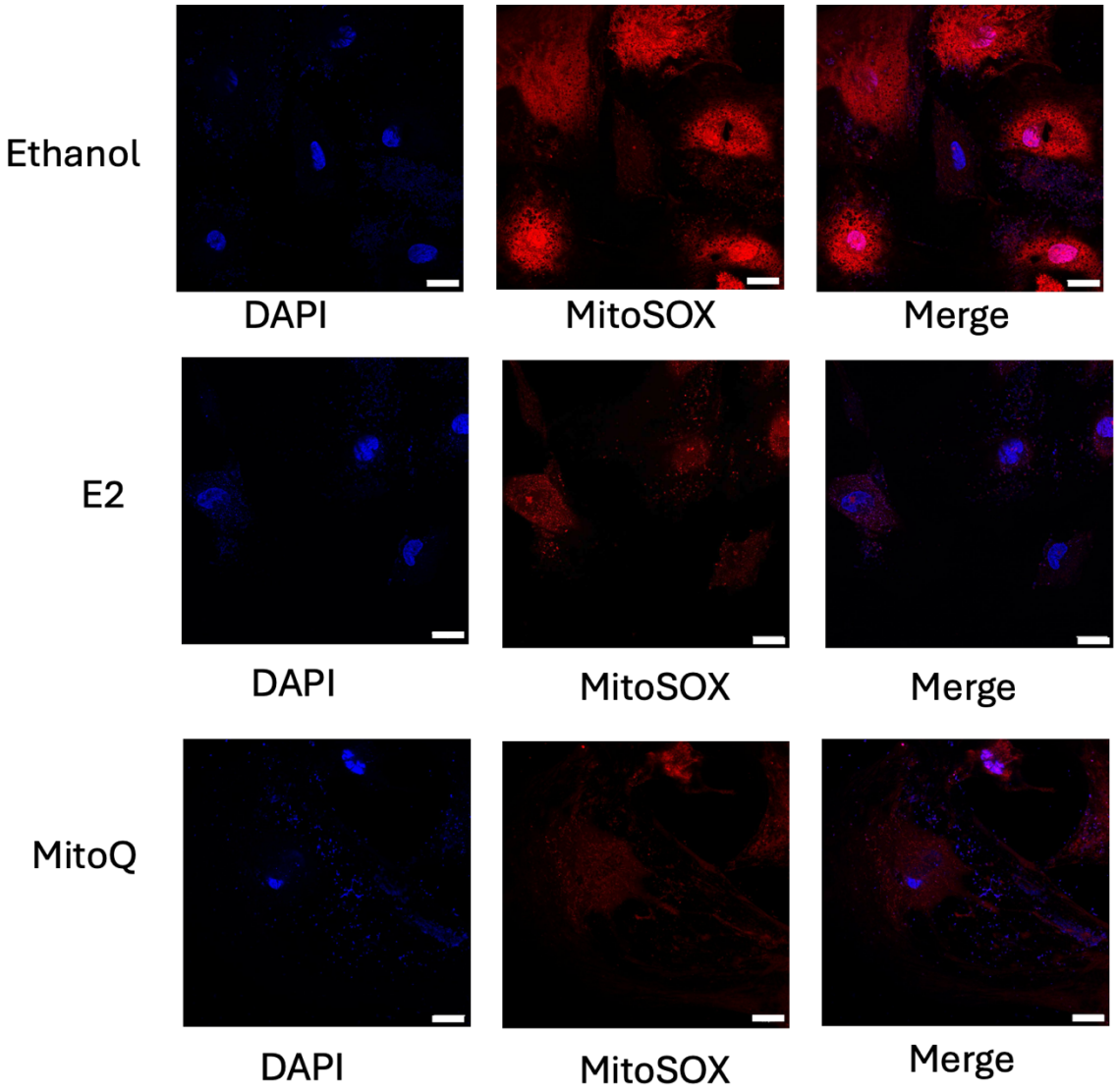
Ethanol
DAPI
MitoSOX
Merge
E2
DAPI
MitoSOX
Merge
MitoQ
DAPI
MitoSOX
Merge

B

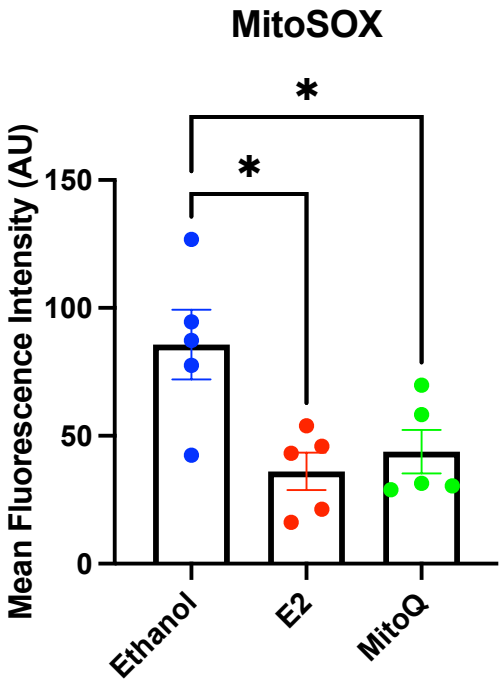

Figure 5.4. MitoSOX signal is reduced by E2 and MitoQ

Male monocrotaline (MCT) right ventricle (RV) fibroblasts were treated with either ethanol, estradiol (E2) (10nM) or MitoQ (300nM) and then stained with DAPI for nuclei localization (blue) and MitoSOX for mitochondrial superoxide production (red). A) MitoSOX representative images B) quantification of MitoSOX. Each data point represents cells from an individual rat, with n=5 per group. Images were captured at 63x magnification. Scale bar represents 20μm. Statistical analysis was performed using a one-way ANOVA. *p<0.05.

5.6 E2 and MitoQ reduced PCNA positive cell count in the MCT RV fibroblasts

Having confirmed that MitoSOX was reduced by E2 and MitoQ in the male MCT RV fibroblasts, the next aim was to investigate whether E2 and MitoQ play a role in modifying cell proliferation through measuring the PCNA count. PCNA count was found to be reduced by E2 versus ethanol (10.44 ± 1.02% vs. 20.00 ± 1.34%, **p<0.01, n=5). The same was also detected by MitoQ versus ethanol (10.40 ± 1.01% vs. 20.00 ± 1.34%, **p<0.01, n=5) (Figure 5.5 A and B).

A

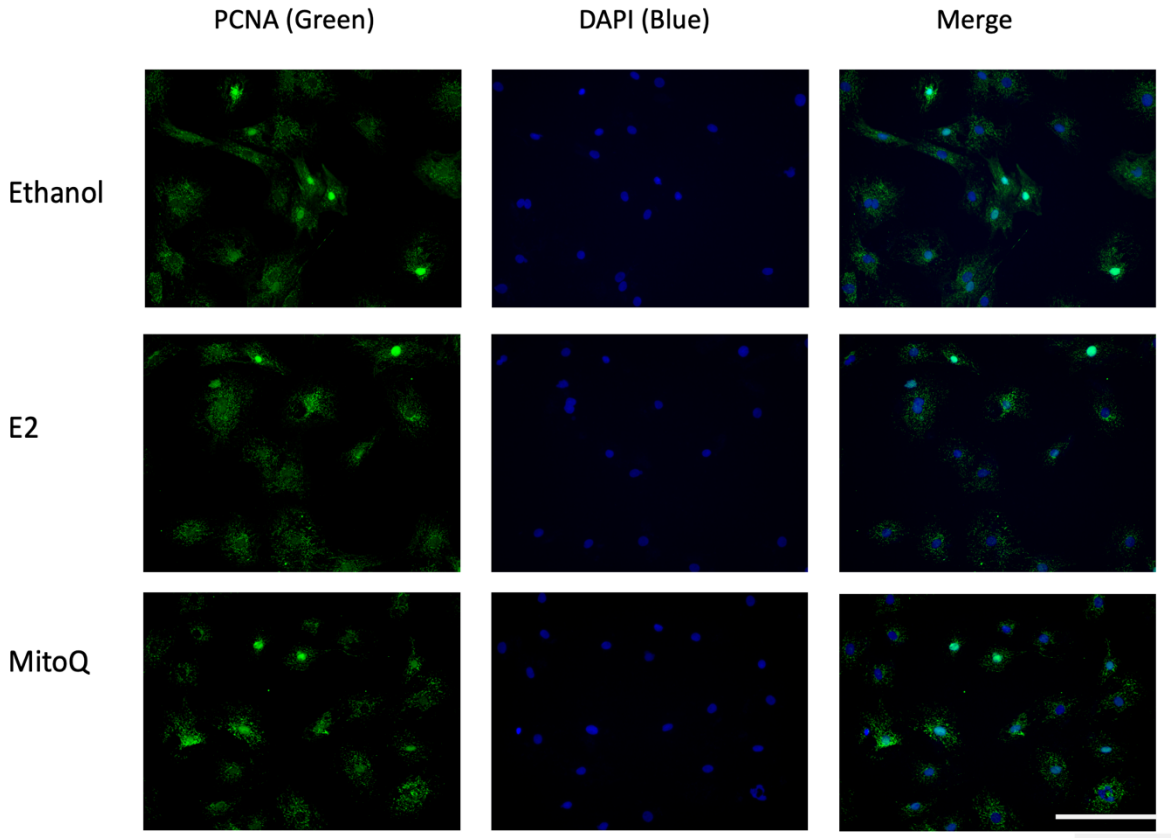
PCNA (Green)
DAPI (Blue)
Merge
Ethanol
E2
MitoQ

B

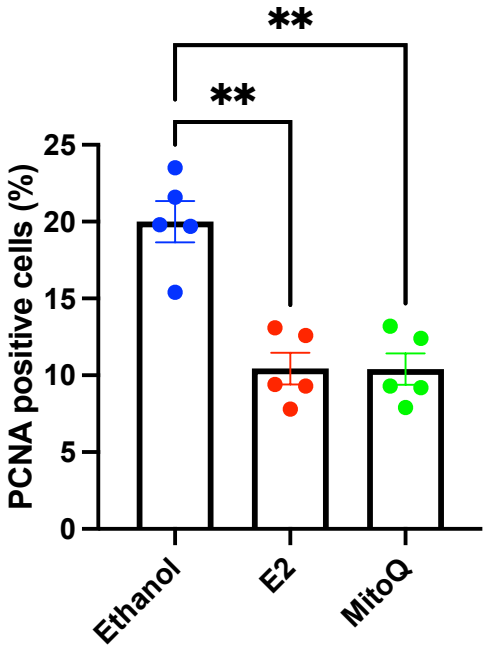
**
**
PCNA positive cells (%)
25
20
15
10
5
0
Ethanol
E2
MitoQ

Figure 5.5. E2 and MitoQ reduced proliferating cell nuclear antigen (PCNA) positive cell count in the male MCT RV fibroblasts

Male monocrotaline (MCT) right ventricle (RV) fibroblasts were treated with either ethanol, estradiol (E2) (10nM) or MitoQ (300nM) and then stained with DAPI for nuclei (blue) and proliferating cell nuclear antigen (PCNA) (1:500) for cell proliferation (green). Figure A) representative PCNA images and Figure B) represents PCNA quantitative analysis. Cells were imaged using Image J software and quantified by counting the number of positive cells which was ratioed to the total cell count and represented as a percentage. Statistical analysis was performed using a one-way ANOVA, with **$p<0.01$. Images were taken at 20x magnification. Scale bar represents 200μm. Each data point represents cells from an individual rat, with n=5 per group.

5.7 E2 and MitoQ played a role in altering the protein expression of Col1a1, NFE2L2 and TFAM in male MCT RV fibroblasts

Following the same conditions, we then examined whether nuclear NFE2L2, cytosolic TFAM and Col1a1 expression was altered following treatment with E2 (10nM) or MitoQ (300nM). Col1a1 intensity was found to be reduced by E2 versus ethanol (33.75 ± 2.86 AU vs. 39.75 ± 3.35 AU, *p<0.05, n=4) and MitoQ versus ethanol (31.75 ± 2.65 AU vs. 39.75 ± 3.35 AU, *p<0.05, n=4) (Figure 5.6 A and B). E2 increased nuclear NFE2L2 intensity versus ethanol (49.00 ± 1.78 AU vs. 38.75 ± 2.01 AU, *p<0.05, n=4) and the same increase in NFE2L2 intensity was also detected by MitoQ versus ethanol (58.50 ± 1.55 AU vs. 38.75 ± 2.01 AU, **p<0.01, n=4) (Figure 5.6 C and D). TFAM intensity was also increased by E2 versus ethanol (46.50 ± 1.04 AU vs. 35.75 ± 1.65 AU, *p<0.05, n=4) and MitoQ versus ethanol (49.25 ± 1.25 AU vs. 35.75 ± 1.65 AU, *p<0.05, n=4) (Figure 5.6 E and F).

A

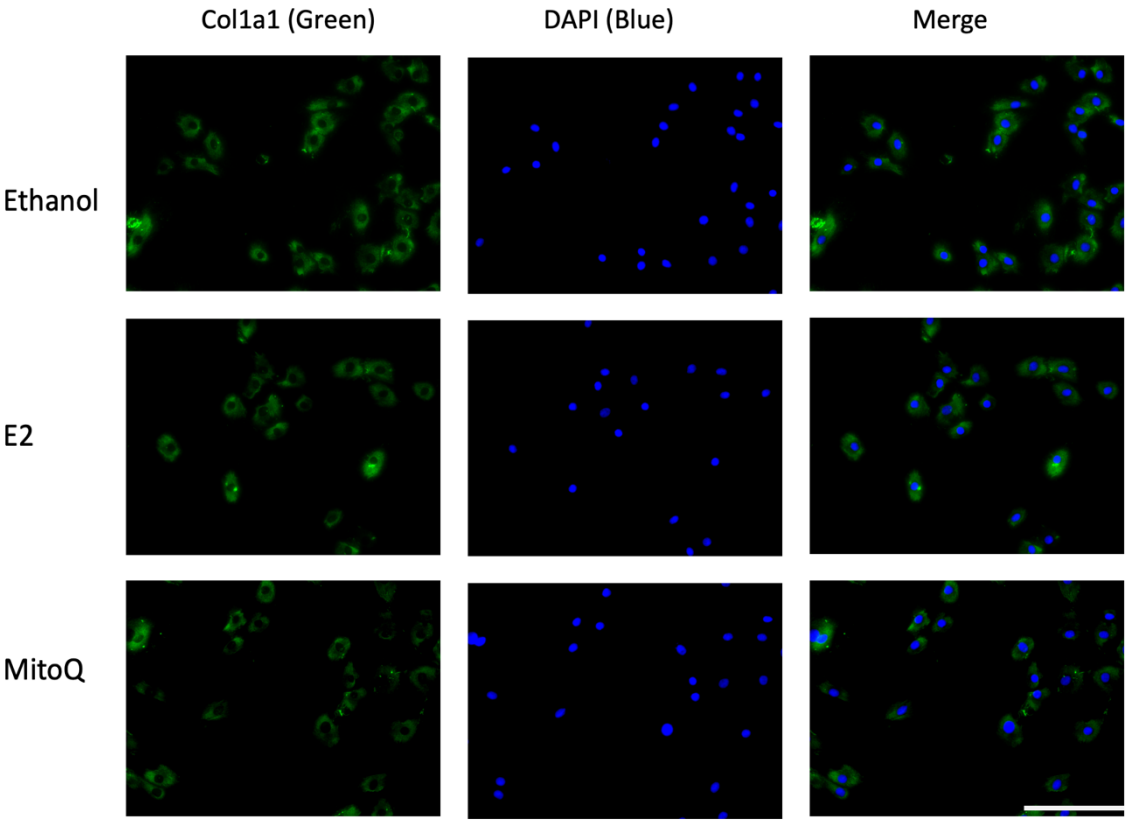
Col1a1 (Green)
DAPI (Blue)
Merge
Ethanol
E2
MitoQ

B

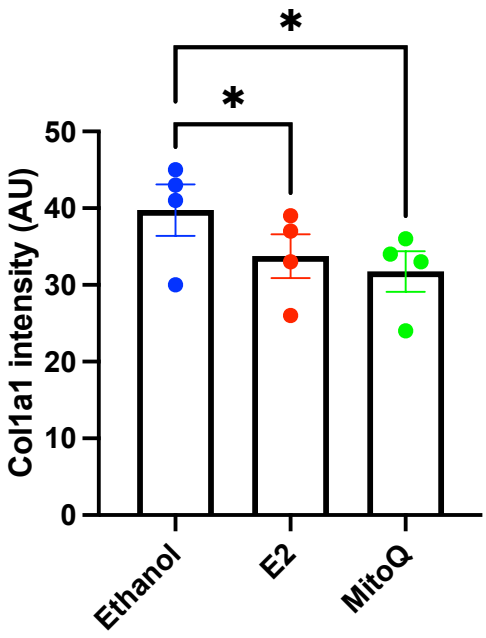
*
*
Col1a1 intensity (AU)
50
40
30
20
10
0
Ethanol
E2
MitoQ

C

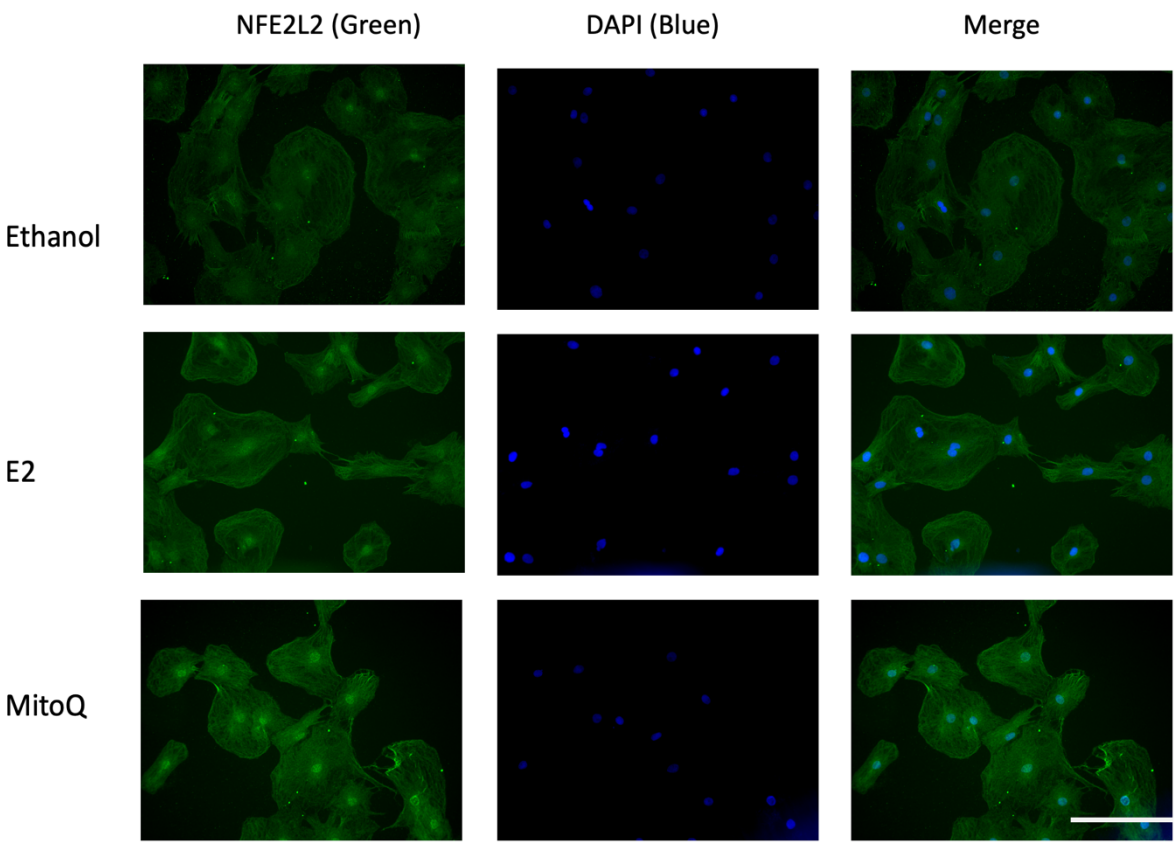
NFE2L2 (Green)
DAPI (Blue)
Merge
Ethanol
E2
MitoQ

D

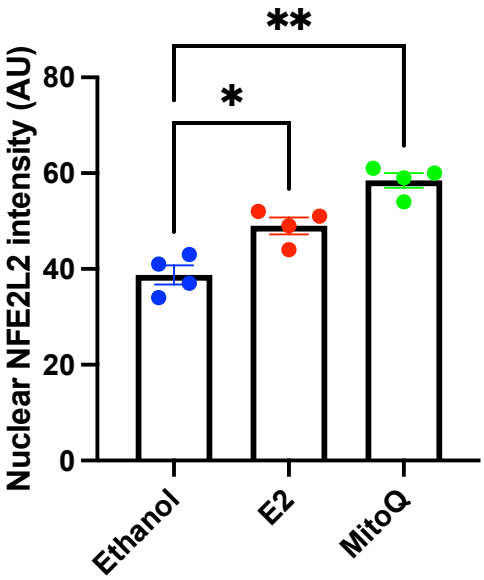
**
*
Nuclear NFE2L2 intensity (AU)
80
60
40
20
0
Ethanol
E2
MitoQ

E

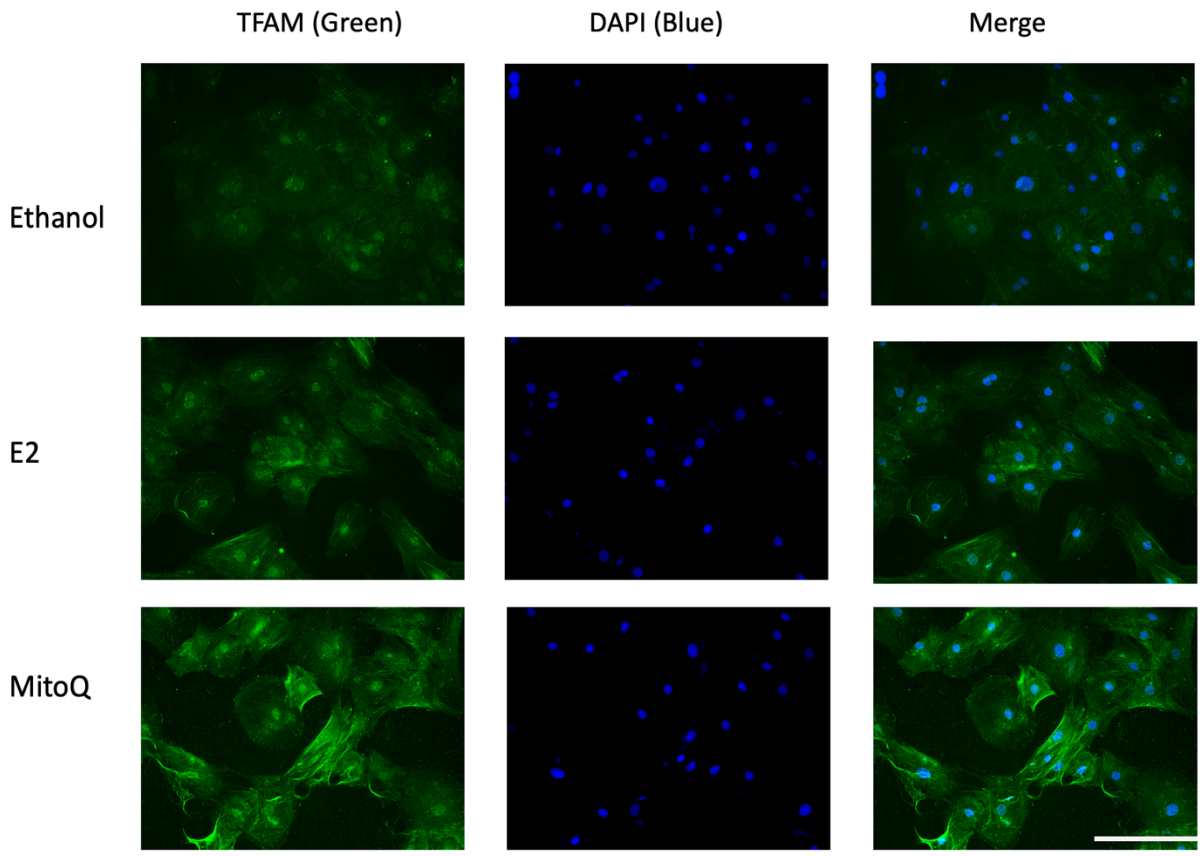
TFAM (Green)
DAPI (Blue)
Merge
Ethanol
E2
MitoQ

F

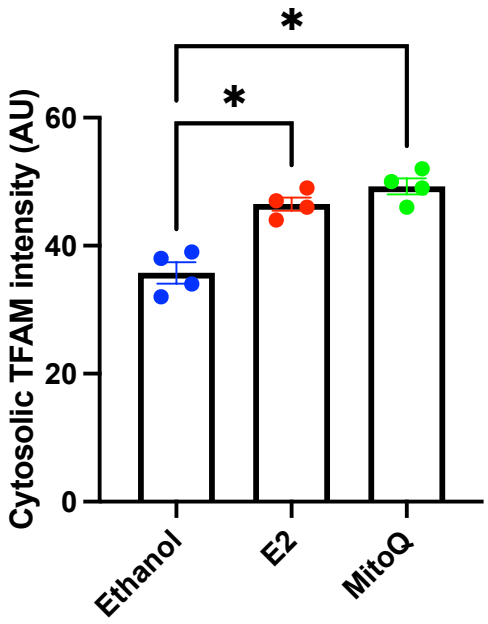
*
*
Cytosolic TFAM intensity (AU)
60
40
20
0
Ethanol
E2
MitoQ

Figure 5.6. E2 and MitoQ alter the protein expression of Col1a1, NFE2L2 and TFAM in MCT RV fibroblasts

Male monocrotaline (MCT) right ventricle (RV) fibroblasts were treated with either ethanol, estradiol (E2) (10nM) or MitoQ (300nM) and stained with DAPI for nuclei (blue) and then either nuclear factor erythroid 2-related factor 2 NFE2L2 (NFE2L2) (1:100), collagen type 1 alpha 1 chain (Col1a1) (1:100) and mitochondrial transcription factor A (TFAM) (1:100) which appear as green in colour. Figure A and B represent Col1a1 images and Col1a1 quantification. Figure C and D represent NFE2L2 images and NFE2L2 quantification. Figure E and F represent TFAM images and TFAM quantification. Cells were imaged and quantified by measuring their intensity using ImageJ software (National Institutes of Health, Bethesda, MD, USA). Statistical analysis was performed using a one-way ANOVA. *$p<0.05$, **$p<0.01$. Images were captured at 20x magnification. Scale bar represents 200μm. Each data point represents cells from an individual rat, with n=4 per group.

5.8 The effect of MitoQ on the body weights of SuHx rats

Male and female Sprague-dawley rats followed a similar protocol as described in chapter 3, in which they received a subcutaneous injection of Sugen (25mg/kg) and were exposed to hypoxia for 3 weeks (10%) and then placed into normoxia for 4 weeks. During the normoxia period, rats then either received an IP injection of vehicle (5% DMSO) or MitoQ (5mg/kg) twice weekly. Once the rats had reached the end of their period in normoxia, they were then PV looped via the open chest method and humanely sacrificed with their RV tissue harvested for future downstream experiments.

The bodyweight of the rats was recorded over the duration of the study to monitor the animals' health and also ensure that MitoQ was not adversely affecting the animals' welfare. At the start of the study, no significant differences were detected between the male SuHx and male SuHx + MitoQ group, and the female SuHx and female SuHx + MitoQ group. However, there was a significant increase between the male SuHx and female SuHx group at the start of the experiment, i.e., at the time of the injection of SU5416 (214.8 ± 8.68g vs. 172.7 ± 6.30g, ****p<0.0001, n=6) (Figure 5.7 A). The same significant increase was detected between both the male SuHx + MitoQ and female SuHx + MitoQ group at the start of the experiment (219.0 ± 10.07g vs. 163.8 ± 5.59g, ****p<0.0001, n=6) (Figure 5.7 A). The rats body weights were then recorded at the end of the study, in which there was a significant increase in the male SuHx vs. female SuHx groups (326.8 ± 5.85g vs. 205.2 ± 3.46g, ****p<0.0001, n=5) (Figure 5.7 B). A significant increase was then detected between the male SuHx + MitoQ and female SuHx + MitoQ group (313.2 ± 12.62g vs. 205.2 ± 3.46g, ****p<0.0001, n=6) (Figure 5.7 B). As well as this, there was a significant reduction in body weight found in the female SuHx + MitoQ rats versus the female SuHx rats (205.2 ± 3.46g vs. 230.2 ± 5.39g, *p<0.05, n=5-6) (Figure 5.7 B). Whilst, no differences were detected between the male SuHx vs. male SuHx + MitoQ group. The body weights of the rats were monitored weekly during the normoxia period, in which no significant changes were detected across the groups (Figure 5.7 C).

A

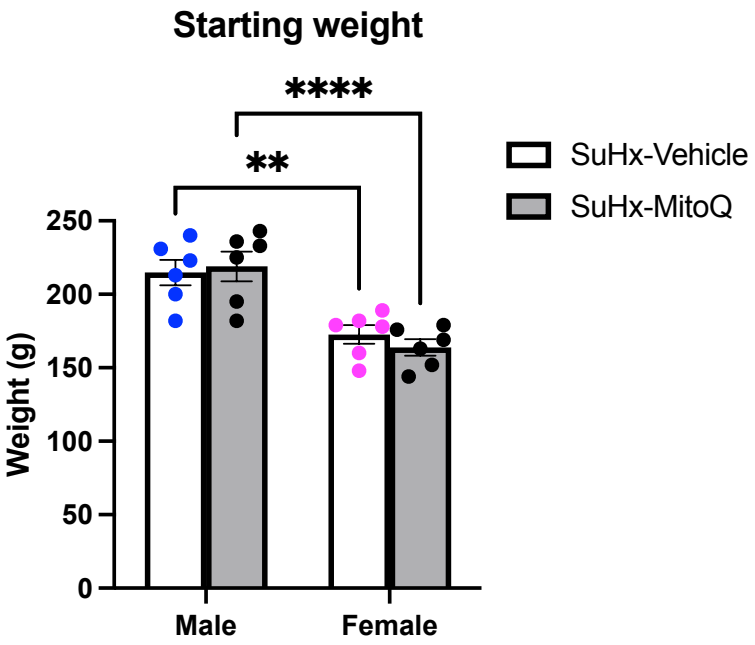
Starting weight
****
**
SuHx-Vehicle
SuHx-MitoQ
250
200
150
100
50
0
Weight (g)
Male
Female

B

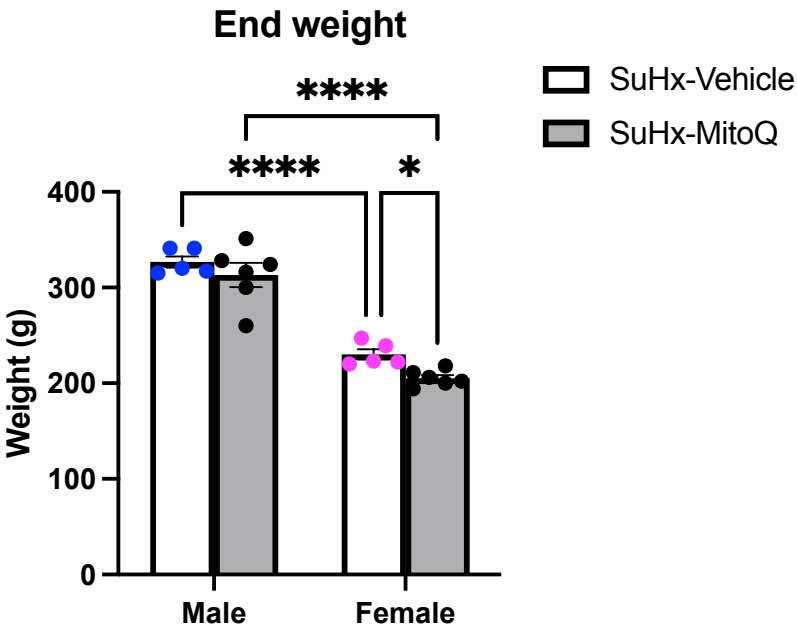
End weight
****
****
*
SuHx-Vehicle
SuHx-MitoQ
400
300
200
100
0
Weight (g)
Male
Female

C

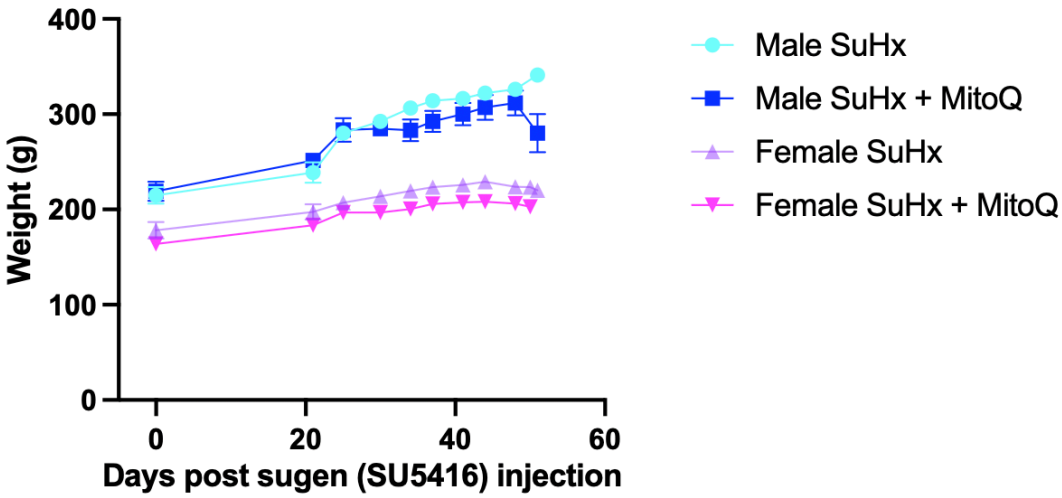

Figure 5.7. Bodyweight of the male and female SuHx and SuHx + MitoQ rats

Figure A and B represents the individual rat bodyweight at the start and end of the study. Figure C shows the average growth curve from day 0 and then once the rats came out of hypoxia (day 21) and until the end of the study. Statistical analysis was performed using a two-way ANOVA with significance represented as *p<0.05, *** p<0.001, **** p<0.0001. n=5-6 rats per group. SuHx = Sugen-hypoxia.

5.9 The effect of MitoQ on RV, LV + Septum and Fulton index in SuHx rats

The rats RV and LV+S weights were recorded to determine whether SuHx and MitoQ had any effect on these parameters. This was then followed up by measuring the RV hypertrophy using the Fulton index. It was found that there were no significant differences in RV, LV+S and Fulton index for MitoQ vs. Vehicle treatment in both male and female rats (Figure A-C), although there is a trend toward decrease in the Fulton index in male SuHx-MitoQ vs. male SuHx-Vehicle group (P=0.10).

A

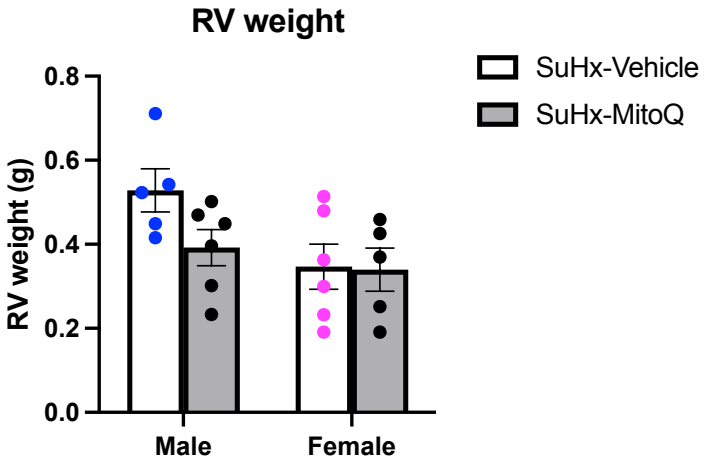
RV weight
SuHx-Vehicle
SuHx-MitoQ
RV weight (g)
0.8
0.6
0.4
0.2
0.0
Male
Female

B

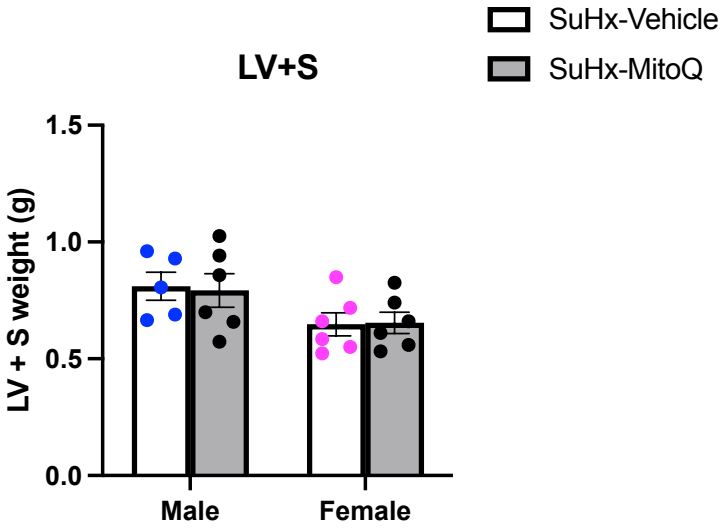
SuHx-Vehicle
SuHx-MitoQ
LV+S
LV + S weight (g)
1.5
1.0
0.5
0.0
Male
Female

C

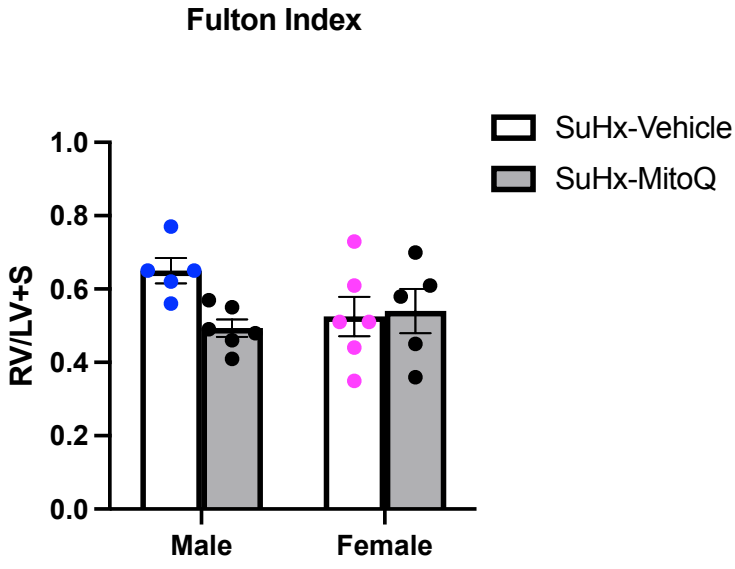
Fulton Index
SuHx-Vehicle
SuHx-MitoQ
RV/LV+S
1.0
0.8
0.6
0.4
0.2
0.0
Male
Female

Figure 5.8. The effect of SuHx and MitoQ on male and female RV weight, LV+S weight and the Fulton index

Male and female rats were treated twice weekly with either MitoQ (5mg/kg) via intraperitoneal (IP) injection or vehicle (5% DMSO in PBS). Figure A and B) Male and female right ventricle (RV) and left ventricle + septum (LV + S) weights were recorded at the end of the study. C) The Fulton index was then calculated using RV/LV+S ratio as an indicator of RV hypertrophy. Data represent the mean ± standard error of the mean (S.E.M). Statistical analysis was performed using two-way ANOVA with n=5-6 per group. SuHx = Sugen-hypoxia.

5.10 The effect of MitoQ on RVSP, RVEDP and heart rate in SuHx rats

Hemodynamic parameters were recorded to determine whether MitoQ treatment twice weekly (5mg/kg) via IP injection affected the rats RVSP, RVEDP and heart rate. No differences across any of the parameters (RVSP, RVEDP and heart rate) (Figure A-C) were detected in both male and female groups.

A

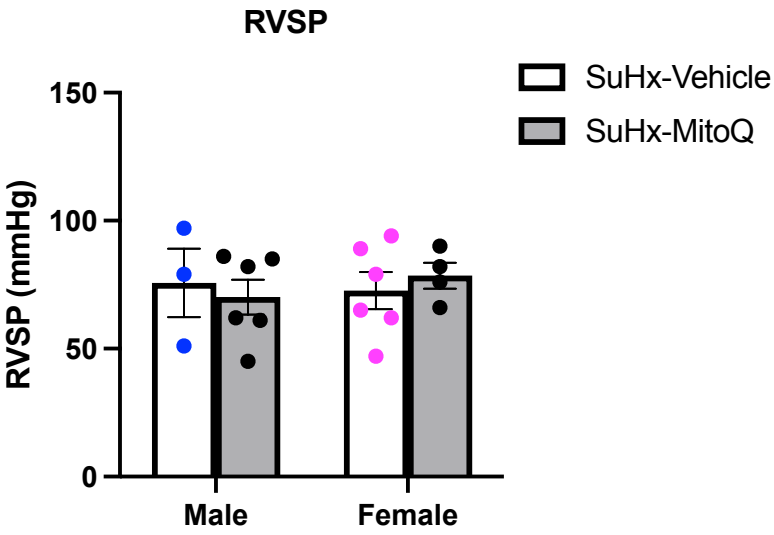
RVSP
SuHx-Vehicle
SuHx-MitoQ
RVSP (mmHg)
150
100
50
0
Male
Female

B

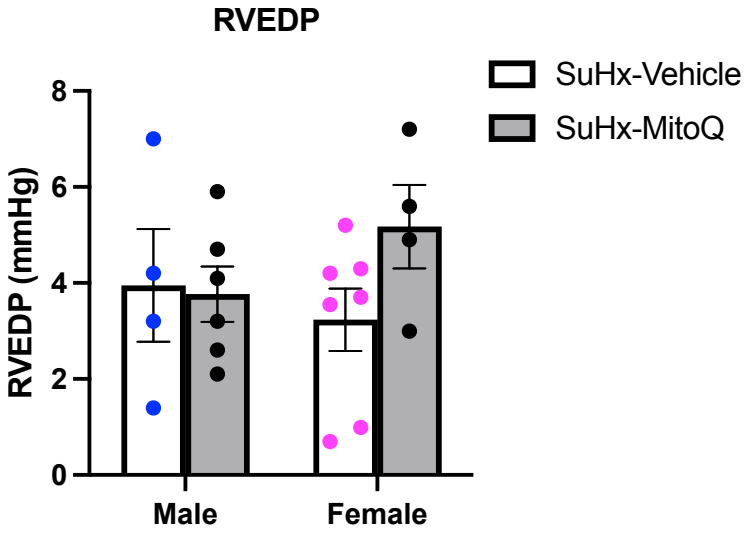
RVEDP
SuHx-Vehicle
SuHx-MitoQ
RVEDP (mmHg)
8
6
4
2
0
Male
Female

C

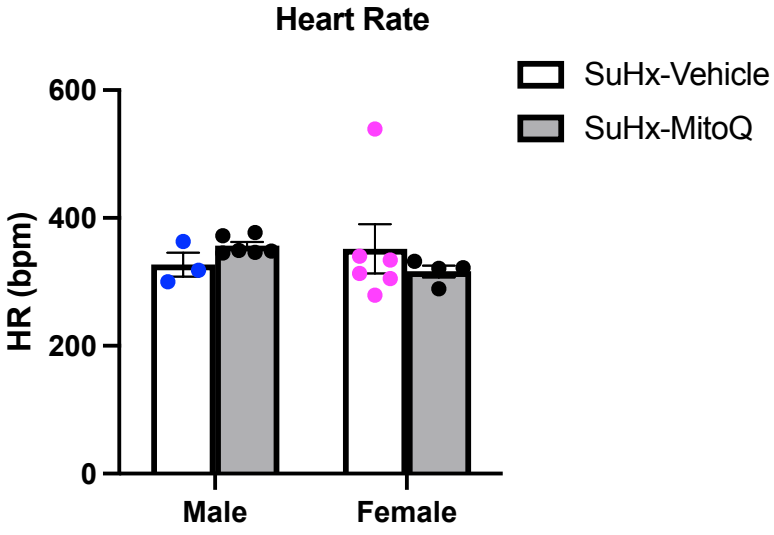
Heart Rate
SuHx-Vehicle
SuHx-MitoQ
HR (bpm)
600
400
200
0
Male
Female

Figure 5.9. MitoQ treatment does not affect RVSP, RVEDP and HR in male and female SuHx rats

Male and female rats were treated twice weekly with either MitoQ (5mg/kg) via intraperitoneal (IP) injection or vehicle (5% DMSO in PBS). Hemodynamic parameters were recorded via pressure-volume (PV) loop using the open chest method. A) right ventricular systolic pressure (RVSP) (mmHg) B) right ventricular end diastolic pressure (RVEDP) (mmHg) C) heart rate (HR) (bpm), n=3-6 per group. Statistical analysis was performed by using a two-way ANOVA. Data represent the mean ± standard error of the mean (S.E.M). SuHx = Sugen-hypoxia.

5.11 The relationship between RVSP and the Fulton index in SuHx rats

An increase in RVSP tends to be associated with an increase in RV hypertrophy index. Due to this, we decided to measure the relationship between both factors. Firstly, we examined the relationship between the male SuHx rats versus the male SuHx + MitoQ rats. This showed that as the RVSP increased there was an increase in the Fulton index detected in the male SuHx group (R^2 = 0.35, p<0.59) (Figure 5.10 A). A similar result was detected in the male SuHx + MitoQ group but with a slightly smaller increase in the Fulton index as RVSP increased (R^2 = 0.09, p<0.55) (Figure 5.10 A). Since, all these rats are from SuHx with elevated RVSP and there are limited data points, we further examined the relationship between RVSP and the Fulton index within a larger range of RVSP by including a data point from the healthy control rats from chapter 3. The healthy control point represents the average control value from the 10 rats in chapter 3. This showed that in the male SuHx group as RVSP increases, there is a greater increase in the Fulton index (R^2 = 5.622, p<0.14) (Figure 5.10 B). The same was detected in the male SuHx + MitoQ treated rats (R^2 =5.24, p<0.07) (Figure 5.10 B). Although, the slope of the correlation line is smaller though not significant in SuHx-MitoQ vs. SuHx-Vehicle groups regardless of including the healthy control point or not.

The same was performed for the female rats, and it was found that as RVSP increased, a similar outcome was detected in which there was also an increase in the Fulton index (Female SuHx: R^2 = 0.80, p<0.01, female SuHx + MitoQ: R^2 = 0.66, p<0.18) (Figure 5.10 C). When the healthy control data point was added, this demonstrated that as RVSP increased there was a positive increase in the Fulton index for both female SuHx and female SuHx + MitoQ group (female SuHx: R^2 = 0.88, p<0.0017, female SuHx + MitoQ: R^2 = 0.72, p<0.06) (Figure 5.10 D). Similar to the males, the slope of the correlation line is smaller or greater though not significant in SuHx-MitoQ vs. SuHx-Vehicle groups when the healthy control point is included or not respectively.

A

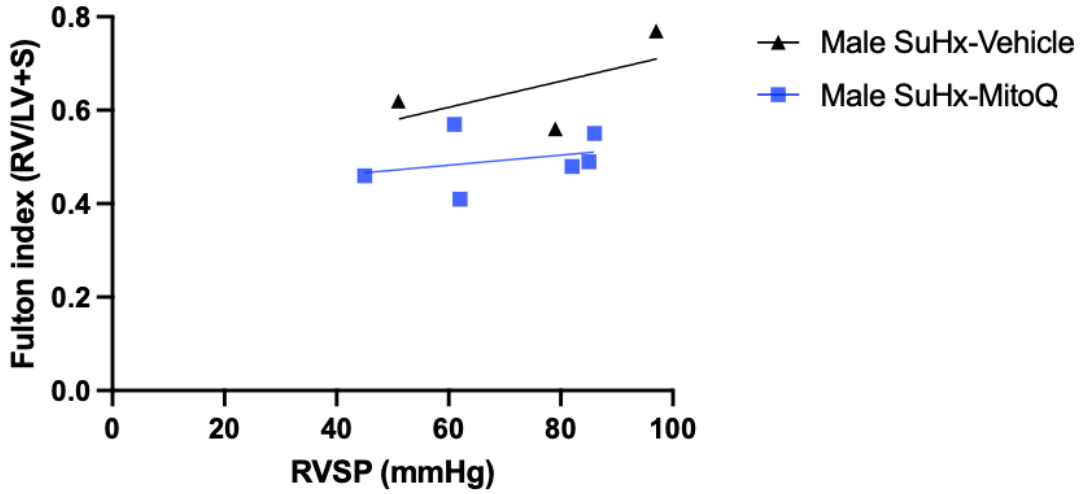
Fulton index (RV/LV+S)
0.0
0.2
0.4
0.6
0.8
0
20
40
60
80
100
RVSP (mmHg)
Male SuHx-Vehicle
Male SuHx-MitoQ

B

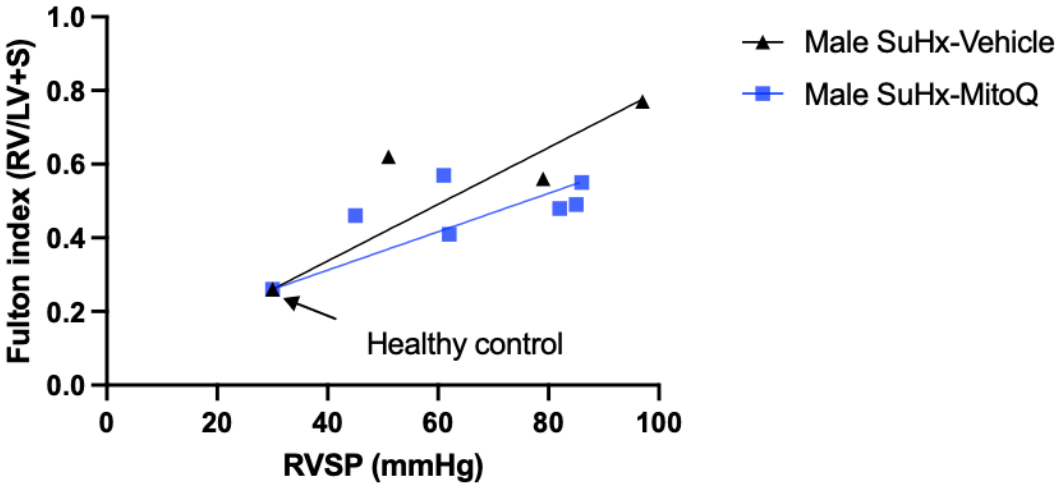
Fulton index (RV/LV+S)
0.0
0.2
0.4
0.6
0.8
1.0
0
20
40
60
80
100
RVSP (mmHg)
Healthy control
Male SuHx-Vehicle
Male SuHx-MitoQ

C

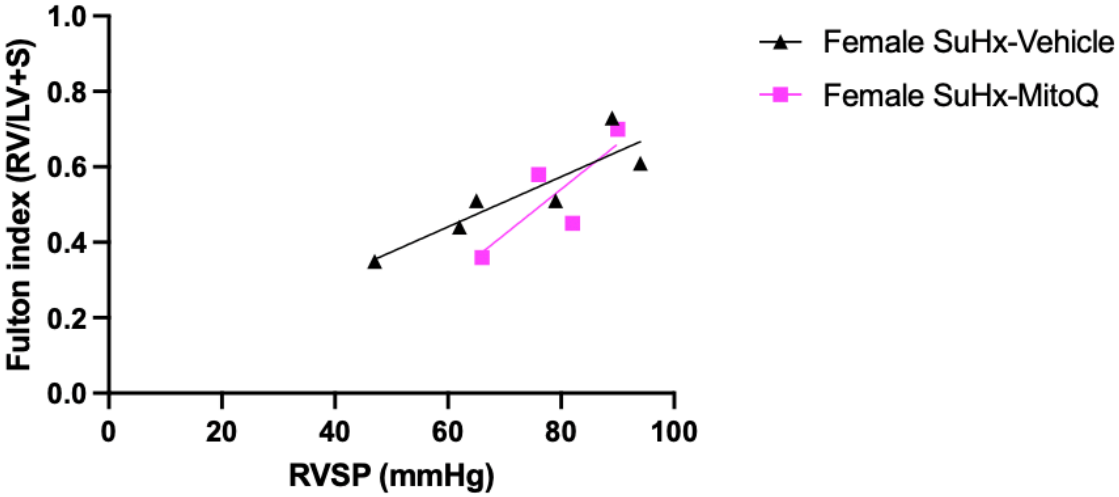
Fulton index (RV/LV+S)
1.0
0.8
0.6
0.4
0.2
0.0
0
20
40
60
80
100
RVSP (mmHg)
Female SuHx-Vehicle
Female SuHx-MitoQ

D

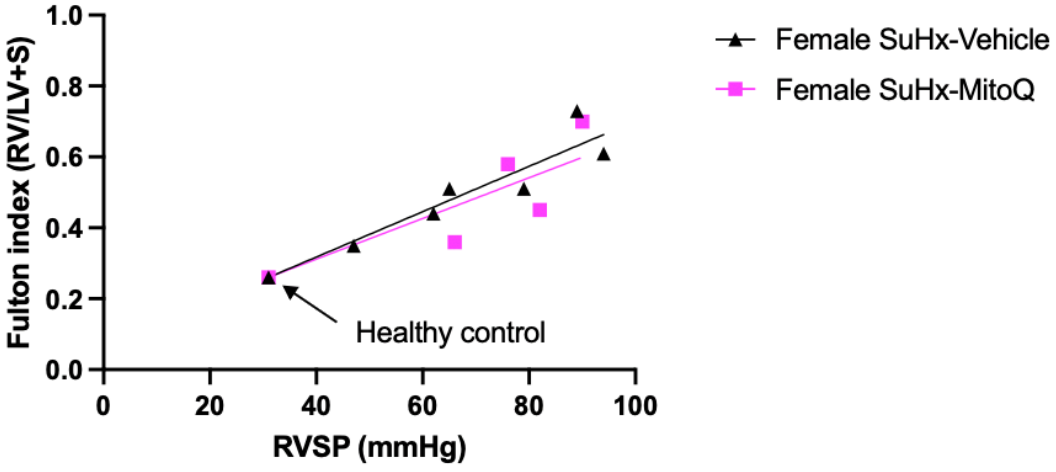
Fulton index (RV/LV+S)
1.0
0.8
0.6
0.4
0.2
0.0
0
20
40
60
80
100
RVSP (mmHg)
Healthy control
Female SuHx-Vehicle
Female SuHx-MitoQ

Figure 5.10. SuHx induced increases in RVSP is associated with an increase in RV hypertrophy, which is slightly alleviated by MitoQ treatment

A) Correlations between the right ventricle systolic pressure (RVSP) and the Fulton index in the male Sugen-hypoxia (SuHx) versus male SuHx MitoQ rats. B) An average male healthy control point from the rats in chapter 3 (averaged across the 10 rats) was included into the correlation. C) Correlation between RVSP and Fulton index for female SuHx versus female SuHx + MitoQ D) An average female healthy control point from the rats in chapter 3 (averaged across the 10 rats) was included into the correlation. Fulton index was obtained by weighing the RV and left ventricle (LV+S) and performing a RV/LV+S ratio. RVSP was obtained during pressure volume (PV) loop recordings. Simple-linear regression was performed across all the groups. Each data point shown for male and female SuHx and SuHx + MitoQ represents an individual rat, meanwhile the healthy data point is an average across the 10 rats. Male n= 3-7, female n=4-7.

5.12 The effect of MitoQ treatment on pulmonary effective arterial elastance, RV end systolic elastance and RV-pulmonary artery coupling in SuHx rats

The pulmonary effective arterial elastance (Ea) serves as a measurement of right ventricle (RV) afterload and was found to be unaltered by MitoQ treatment in both male and female SuHx rats (Figure 5.11 A). RV end systolic elastance (Ees) was also found to be unaltered by MitoQ in both male and female SuHx rats (Figure 5.11 B). The efficiency between RV contractility and the pulmonary arterial system can be measured by using the Ees/Ea ratio to give an overall indication of RV-pulmonary artery coupling. Here, we found that this was increased in the male SuHx + MitoQ rats versus male SuHx + vehicle rats (0.88 ± 0.05 vs. 0.63 ± 0.08, *$p<0.05$, n=3-5) (Figure 5.11 C) and a mild but not significant increase in female SuHx + MitoQ vs. female SuHx + vehicle rats (P=0.30).

A

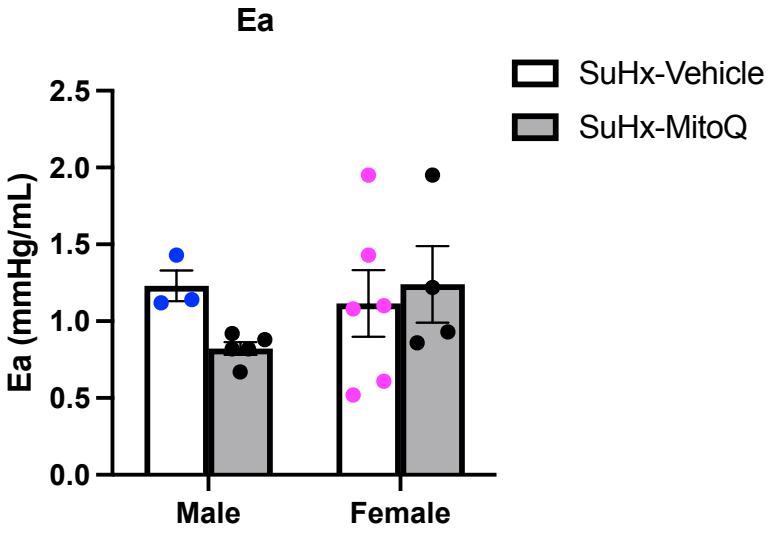
Ea
SuHx-Vehicle
SuHx-MitoQ
Ea (mmHg/mL)
2.5
2.0
1.5
1.0
0.5
0.0
Male
Female

B

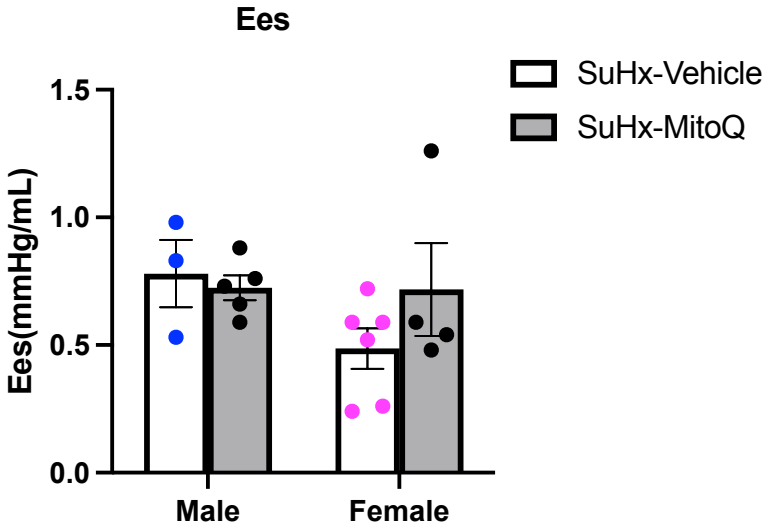
Ees
SuHx-Vehicle
SuHx-MitoQ
Ees(mmHg/mL)
1.5
1.0
0.5
0.0
Male
Female

C

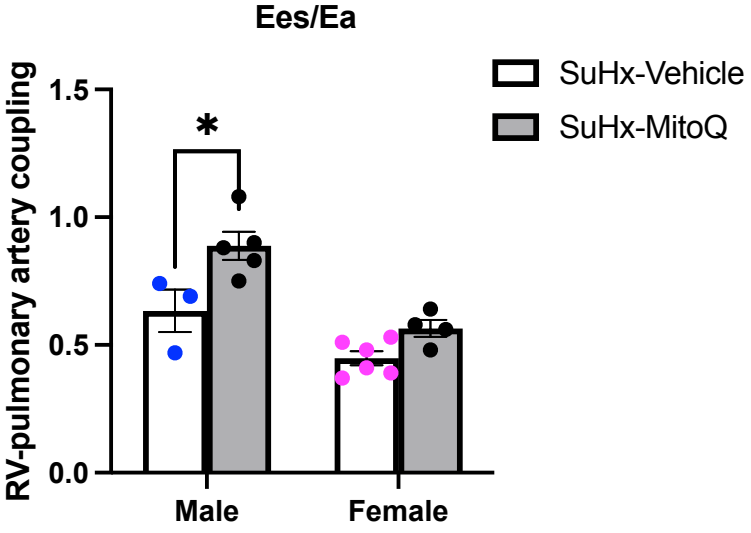
Ees/Ea
SuHx-Vehicle
SuHx-MitoQ
RV-pulmonary artery coupling
1.5
1.0
0.5
0.0
*
Male
Female

Figure 5.11. MitoQ treatment did not affect Ea and Ees in male and female SuHx but did increase RV-pulmonary artery coupling in only male SuHx rats

The right ventricle (RV) parameters were obtained via pressure volume (PV) loop using the open chest method. A) Pulmonary effective arterial elastance (Ea) B) RV end systolic elastance (Ees) C) The ratio of the RV end systolic elastance to effective arterial elastance (Ees/Ea) known as RV-pulmonary artery coupling, n=3-6 per group. All data represent the mean ± standard error of the mean (S.E.M). Statistical analysis was performed using two-way ANOVA, *$p<0.05$. SuHx = Sugen-hypoxia.

5.13 The effect of MitoQ treatment on collagen deposition in RV in SuHx rats

SuHx showed a significant increase in collagen deposition in the male SuHx rats (Chapter 3, section 3.1.6). Following the same protocol as chapter 3, we examined the interstitial collagen deposition in the RV of the male and female SuHx + vehicle and SuHx + MitoQ treated rats. It was detected that collagen deposition was reduced in the male SuHx + MitoQ rats versus male SuHx + vehicle rats (8.40 ± 0.49% vs. 13.08 ± 1.21%, **p<0.01, n=5-6) (Figure 5.12 A and B). Whilst, no differences were detected in the female rats with MitoQ treatment.

A

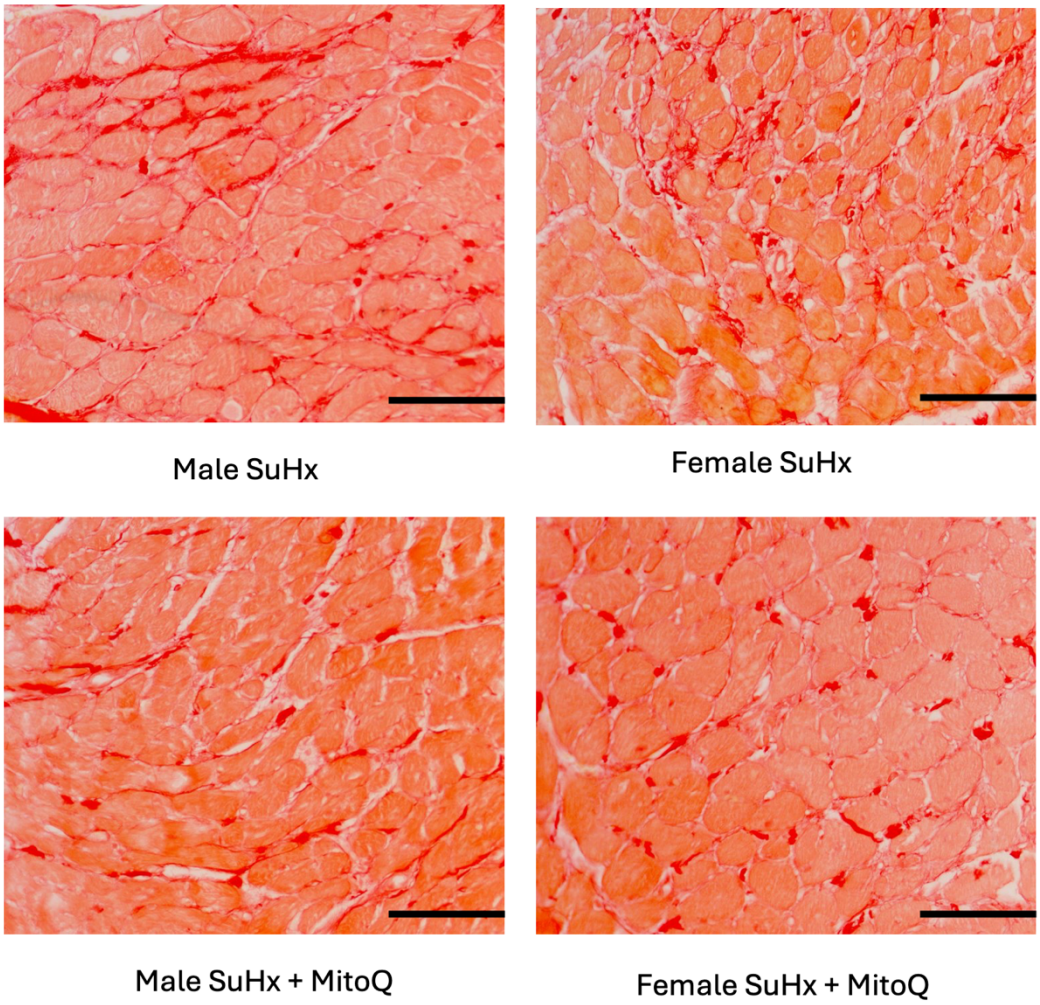
Male SuHx
Female SuHx
Male SuHx + MitoQ
Female SuHx + MitoQ

B

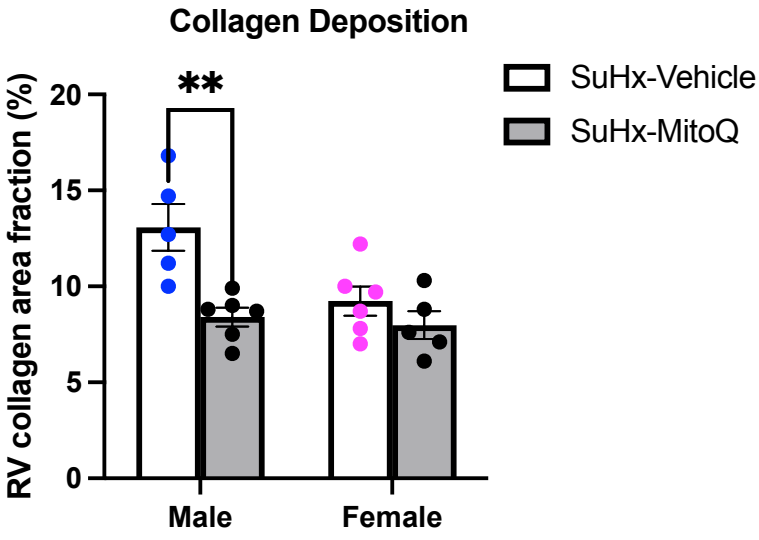
Collagen Deposition
RV collagen area fraction (%)
20
15
10
5
0
**
Male
Female
SuHx-Vehicle
SuHx-MitoQ

Figure 5.12. MitoQ reduces collagen deposition in the male SuHx rats

Right ventricle (RV) tissue was stained with picrosirius red to highlight the areas positive for collagen production. A) Representative images for male and female Sugen-hypoxia (SuHx) + vehicle and SuHx MitoQ rats. B) Summary of the percentage positive for collagen production, n= 5-6 per group. All data represent the mean ± standard error of the mean (S.E.M). Statistical analysis was performed using the two-way ANOVA, **p<0.01. Scale bar represents 100μm.

5.14 The effect of MitoQ treatment on myocyte area in male and female rats

In chapter 3 (section 3.1.9) we detected that there was a significant increase in myocyte size in the male and female SuHx rats. Therefore, we decided to repeat this for the rats which had been exposed to SuHx + MitoQ treatment to determine whether MitoQ was able to reduce this. The same protocol was followed by drawing around the area of a single myocyte and repeating this for several myocytes (10-20 myocytes) from the one rat. This was then averaged to achieve an overall mean myocyte area for an individual rat. Here, we found that there were no significant differences across any of the groups, although there was trend towards a decrease in myocyte size in male SuHx-MitoQ vs. male SuHx-vehicle rats ($p=0.59$) (Figure 5.13 A and B).

A

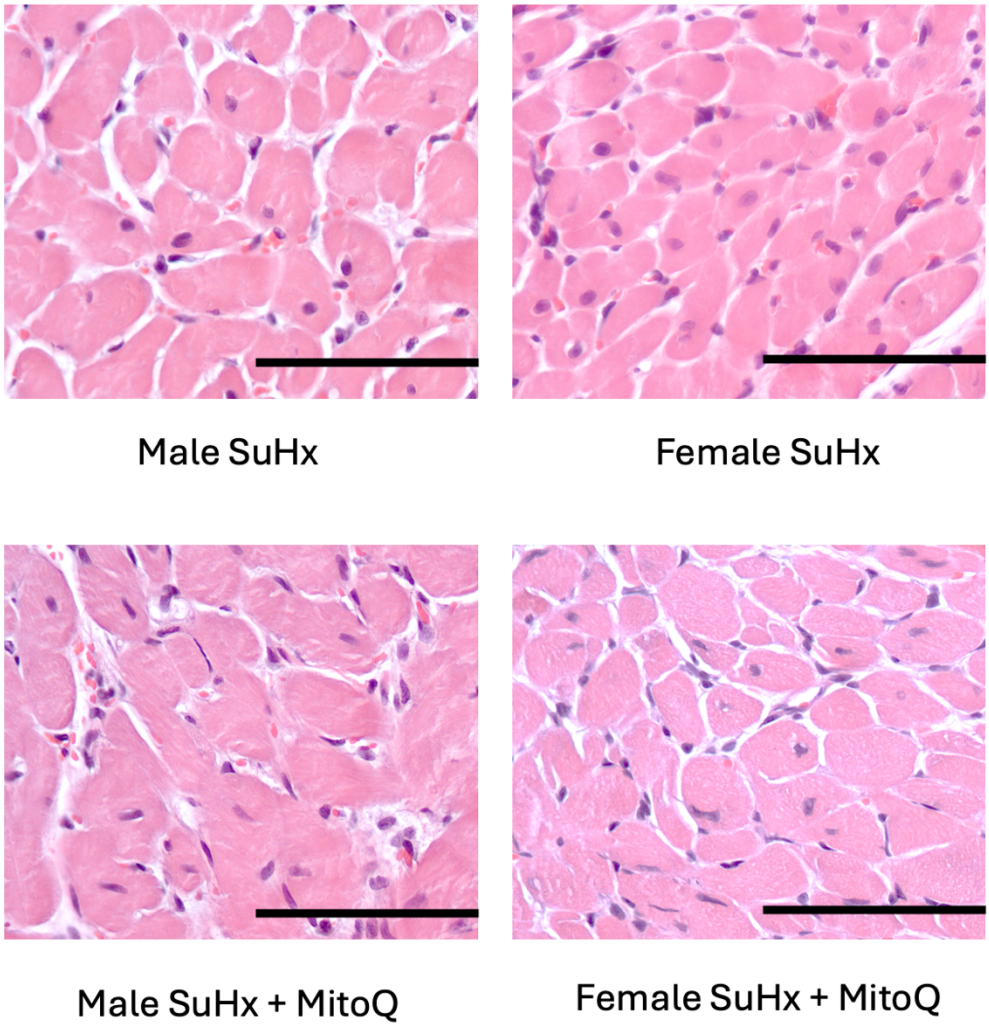
Male SuHx
Female SuHx
Male SuHx + MitoQ
Female SuHx + MitoQ

B

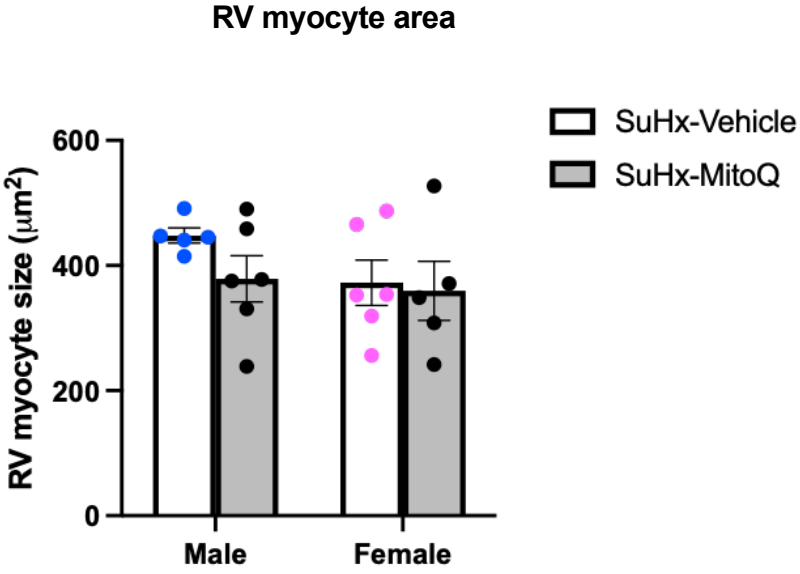
RV myocyte area
SuHx-Vehicle
SuHx-MitoQ
RV myocyte size (μm²)
600
400
200
0
Male
Female

Figure 5.13. The effect of SuHx + MitoQ on myocyte area in male and female rats

A) Representative images (40x magnification) of hematoxylin and eosin (H&E) stained right ventricle (RV) tissue from male and female rats. B) Quantification of the myocyte area which was calculated by drawing around the area of a single myocyte. The area was obtained for several myocytes (10-20 myocytes) from one rat which was then averaged to obtain the overall mean area of the myocyte (μm^2). One data point represents one rat. All data represent the mean + standard error of the mean (S.E.M), with n=5-6 per group. Scale bar represents 100μm. Statistical analysis was performed using the two-way ANOVA. SuHx = Sugen-hypoxia.

5.15 Discussion

The first aim of chapter 5 was to examine the effect of MitoQ and E2 on HCF and MCT RV fibroblast cells. HCF were exposed to hypoxia to deprive the cells of oxygen and recapitulate the PH proliferative environment. Whereas, as MCT RV fibroblasts were already treated, therefore these cells did not undergo further exposure to hypoxia. We measured the proliferation of the male and female HCF cells via measuring Ki-67 intensity. Interestingly, we found that there were no differences in the cell count in both male and female normoxia versus hypoxia groups which goes against our prediction. We believe that this may be as a result of the cells failing to proliferate as an increased number of cells would only lead to an increase in O_2 demand which would further aggravate the hypoxia stress. Another potential reason is that these HCF were isolated from patients with some heart diseases. These cells already grow in a fast proliferation rate even under normoxia condition and the hypoxic stimulus may not further increase the proliferation rate. However, we did find that MitoQ induced a significant decrease in the positive cell count under both normoxia and hypoxia conditions in the male HCF. This decrease was confirmed to be even further than E2. In the female HCF, the same reduction was detected in E2 and MitoQ treated cells, but only under hypoxic conditions. Using the male MCT RV fibroblast cells, we measured the cell proliferation by staining the cells with proliferating cell nuclear antigen (PCNA). It was found that both E2 and MitoQ reduced the cell count. We propose that MitoQ and E2 may be achieving this by targeting the mitochondria as both drugs are directly involved with the mitochondria, but whether it is through the same mechanism remains unknown. It could be that MitoQ and E2 may be able to sense a defect in the mitochondrial metabolism which is triggered by either the hypoxia or MCT. MitoQ and E2 are then able to inhibit one of the four protein complexes in the mitochondrial electron transport chain (ETC). A previous study suggest that MitoQ was able to potently inhibit complex I proliferation in breast cancer cells and that it is this inhibition of oxidative phosphorylation that is primarily responsible for the anti-proliferative effect of MitoQ (Cheng et al., 2023). E2 treatment has also been found to interact with the ETC complexes, by either restoring or decreasing their activity depending on the location and condition (Torres et al., 2018a, Torres et al., 2018b). Another study demonstrated that E2 is

able to slow the phosphorylation rate in isolated hepatic mitochondrial by inhibiting and destabilizing ATP synthase (Torres et al., 2018a).

We then discovered that there was an increase in mitochondrial superoxide production in the male HCF following hypoxia exposure. MitoQ and E2 were able to reduce mitochondrial superoxide levels under both normoxic and hypoxic conditions in the male HCF. However, in the female HCF, we did not detect a rise in mitochondrial superoxide accumulation under the hypoxia conditions. The male and females oxidative stress response will differ, and it is believed that the males tend to have a higher production of ROS with less antioxidant mechanisms available (Martínez de Toda et al., 2023). However, we find that under normoxic conditions, the female group mitochondrial superoxide levels are higher compared to the male HCF normoxia mitochondrial superoxide levels. The reason as to why we did not find this increase in mitochondrial superoxide under hypoxia conditions in the females could be a result of them already maxing out their mitochondrial superoxide response. Additionally, the female HCF could have a higher basal level of mitochondrial superoxide as these cells may have been isolated from a patient with more severe heart disease than the males and the mitochondrial superoxide levels are not further enhanced by hypoxia. In addition, similar to better preservation of RV function in females versus males in PAH, female cardiac cells may also have its protective role in response to hypoxia *in vitro*, which prevents them from further increasing their mitochondrial superoxide response under hypoxia. We did find that both E2 and MitoQ were able to reduce mitochondrial superoxide levels under both normoxia and hypoxia conditions for both male and female HCF, confirming that both drugs are not sensitive to hypoxic conditions and work effectively in both the normoxia and hypoxia environment. The same outcome was found by E2 and MitoQ in the male MCT RV fibroblasts. This is also in line with previous studies which show that MitoQ reduced superoxide levels detected by MitoSOX in non-PAH models (Escribano-Lopez et al., 2016, Fortner et al., 2020, Huang et al., 2022, Zhang et al., 2022b). This is not surprising as it is widely suggested that MitoQ predominately exerts its effects by altering the mitochondrial superoxide pathway (Jurkuvenaite et al., 2015).

MitoQ has been proposed to work through a NFE2L2 dependent mechanism, in which studies have found that NFE2L2 inhibition reverses the protective effects of MitoQ (Hu et al., 2018). Treatment with MitoQ has also been reported on numerous occasions to inhibit NFE2L2 degradation and increase NFE2L2 nuclear translocation and its downstream targets, NQO1 in the presence of ROS (Dinkova-Kostova et al., 2002, Cen et al., 2021). Due to this, we examined whether treatment with MitoQ and E2 alter the protein expression of NFE2L2 in the male and female HCF cells and male MCT RV fibroblasts. We found that NFE2L2 nuclear intensity was increased by E2 and MitoQ. These results are consistent with those of previous reports where MitoQ works through the NFE2L2 pathway. We did not detect any differences between the normoxic and hypoxic environment for both the male and female HCFs. As mitochondrial superoxide production remained unchanged in the female HCF, this could be the reason for this but unlikely as in the male HCF mitochondrial superoxide was increased by hypoxia. Here, we seen the NFE2L2 expression did increase by hypoxia but this did not reach significance. We would have predicted an increase in NFE2L2 as it has been reported to be increased and stabilized by the release of mtROS (Ngo and Duennwald, 2022). Instead, we show that this increase of NFE2L2 by MitoQ and E2 is occurring in a mtROS independent manner. The mechanism by which E2 increases NFE2L2 expression has been studied previously and was found to occur through the PI3K-AKT pathway (Gorrini et al., 2014, Ishii and Warabi, 2019). In this study, we propose that E2 may be acting through this pathway to increase NFE2L2 nuclear intensity, but we are not able to confirm this.

We then determined whether MitoQ and E2 were able to alter cytosolic TFAM intensity. TFAM plays a crucial role in maintaining mtDNA copy number by regulating mtDNA transcription and replication (Kang et al., 2018). TFAM has also been reported to play a role in protecting mtDNA from oxidative injury, suggesting that there may be some cross talk between them both (Hu et al., 2018). We found that MitoQ and E2 increased TFAM levels in both normoxic and hypoxic conditions and this result was seen in both the males and female HCFs and in the male MCT RV fibroblasts. Our data also suggest that there is a crosstalk between mtROS and TFAM. Previous studies have also detected that MitoQ was able to increase TFAM gene and protein expression (Yin et al., 2016, Hu et al., 2018). As well as this, it has been found that E2 treatment is also able to increase TFAM protein levels (Chen et al.,

2015). Overall, suggesting that MitoQ and E2 are able to drive transcription and replication of mtDNA which would enhance and support mitochondrial biogenesis activity.

Hypoxia has been implicated as a pro-fibrogenic stimulus that triggers the increase of collagen production. Therefore, we decided to examine whether we could detect any changes in the male and female HCFs and in primary male MCT RV fibroblasts treated with MitoQ and E2. Unexpectedly, we found that there were no increases in the male normoxia versus male hypoxia group, and the same was seen for the females. We propose that the hypoxic exposure may not be long enough (48 hours) to induce an increase in Col1a1 levels. Similarly, there was also no increase in male and female HCF proliferation by hypoxia either, which could also be the reason as to why the hypoxia stimulus did not induce an increase in Col1a1 expression. We did find that, under both normoxia and hypoxia conditions, MitoQ was able to reduce Col1a1 levels in the male and female HCF and male MCT RV fibroblasts. This reduction in Col1a1 was confirmed to be far greater a response than E2. Meanwhile, E2 was only able to reduce Col1a1 levels under hypoxic exposure in both the male and female HCF. MitoQ and E2 reducing Col1a1 is in agreement with previous studies which also find the same result (Alencar et al., 2018, Turkseven et al., 2020, Zhang et al., 2022b, Nataraj et al., 2024). Overall, we did not detect any sex differences on the influence of MitoQ and E2 on NFE2L2, TFAM and Col1a1 expression.

Although previous studies find that MitoQ and E2 treatment are able to increase NFE2L2, TFAM and reduce Col1a1, it must be noted that these are in various models, cell types, conditions and with varying doses of MitoQ and E2. Hence, we are the first to report that 300nM MitoQ treatment and 10nM of E2 is able to induce these changes in NFE2L2, Col1a1 and TFAM protein intensity in male and female HCF cells which have been exposed to normoxia and hypoxia and in male primary MCT RV fibroblasts. We are also the first to directly compare the sex differences.

The final aim of this chapter was a preliminary study investigating the effects of MitoQ on the SuHx rat model. MitoQ has been tested within PAH models including: pulmonary arterial banding (PAB) and chronic hypoxia (Pak et al., 2018, Yan et al., 2023, Li et al., 2024a) and

finally, one study tested on SuHx primary endothelin cells extracted from male SuHx rats (Suresh et al., 2019). However, to date no study has directly tested the effect of MitoQ in the SuHx rat model.

We examined the effect of MitoQ (5mg/kg twice weekly via IP injection) on the rat's bodyweight, hemodynamic parameters, collagen deposition and myocyte size. It must be noted that we did not test MitoQ in normoxic control male and female rats due to time constraints and ongoing construction work taking place in the BPU. This presents as one of the major limitations in this project as there was no control group to compare the data with. MitoQ has been previously tested on control rats in which it had no effect on the rats bodyweight and RV function (Yan et al., 2023), however the dose, route of administration and frequency of MitoQ was different compared to our study. Therefore, we strongly recommend going forward that it would be essential to examine the role of MitoQ in control rats.

To begin, the weight of the rats was kept in line with the animal study in chapter 3. This can be seen as the rats' average starting weight in chapter 3 was around ~159g for females and ~209.7g for males, whilst in this study female rats started around ~168g and males around ~243g. Overtime, male and female rats gained weight, however there were no significant differences between the normoxia and hypoxia groups when comparing the same sexes at the start of the study. No differences were detected in the male SuHx-MitoQ versus male SuHx -Vehicle rats at the end of the study, however there was a small reduction in the female SuHx + MitoQ bodyweight. Yan et al., who examined chronic hypoxia induced PH rats, reported similar findings that MitoQ does not affect bodyweight (Yan et al., 2023). In the same study, Yan et al., reported that MitoQ was able to reduce RVSP and Fulton index following chronic hypoxia but not in the Vehicle-MitoQ rats, suggesting that it does not affect the healthy RV (Yan et al., 2023). We demonstrated that treatment with MitoQ had no significant effect on the RV weight, LV weight, Fulton index, RVSP, RVEDP and the heart rate when compared with the SuHx alone rats. Instead, we find there is a very mild decrease in RV weight and hypertrophy (Fulton index) in the male rats, which did not reach significance. Hence, this suggests that MitoQ was not able to alter pulmonary vascular remodeling especially in female SuHx rats, resulting in no change in RV afterload and thus RVSP and RV remodeling. We then examined the RV afterload (Ea) and RV contractility (Ees) which we found no differences.

Instead, there was a mild decrease in Ea in male SuHx rats with MitoQ treatment which indicates that MitoQ may have slightly improved pulmonary vascular remodeling, which is consistent with the mild decrease in RV weight and hypertrophy (Fulton index) in the male SuHx-MitoQ rats. Typically, in a case of RV failure, Ees is reduced and Ea is increased. The relationship between the cardiac contractility and arterial system can be analyzed using the Ees/Ea ratio. Progressive RV failure will result in the RV-pulmonary arterial system becoming uncoupled which will then lead to a decline in the Ees/Ea ratio, which was also seen in the male SuHx in chapter 3 (Hsu, 2019). We found that there was a significant increase in the RV-pulmonary artery coupling (Ees/Ea) in the male SuHx + MitoQ rats, which was not seen in the females highlighting a key sex difference. As seen in Chapter 3, SuHx did not change Ees/Ea in the female versus the female control, indicating a preservation of RV function. Therefore, it is not surprising that MitoQ did not further increase Ees/Ea or RV function in female SuHx rats. Therefore, this suggests that MitoQ could potentially preserve mitochondria function in a manner that helps promote better RV function in the male SuHx rats.

We then followed this up by measuring the RV myocyte size and interstitial collagen deposition, as increases in cell size serves as a widely known key characterize of hypertrophy (Frey et al., 2004) and collagen deposition also contributes to hypertrophy. However, there were no significant differences in myocyte size in both male and female SuHx rats with MitoQ treatment. We found no significant differences in interstitial collagen deposition in the female SuHx rats with MitoQ treatment, which is consistent with the no significant changes seen in RV weight and Fulton index. However, we detected that there was a significant reduction in RV interstitial collagen deposition in the male SuHx + MitoQ rats, which is consistent with the mild reduction in RV weight and hypertrophy and increased RV-PA coupling in the male SuHx + MitoQ rats. As well as this, the reduction in collagen deposition in the male SuHx + MitoQ rats agrees with the literature in that MitoQ works in a protective manner and reduces collagen production (Méndez et al., 2020).

Finally, to summarize our findings, we show that both E2 and MitoQ are able to reduce HCF cell proliferation under normoxic and hypoxic conditions in the male HCF cells. Meanwhile, E2 and MitoQ are only able to reduce cell proliferation in the hypoxia environment in the

female HCF cells. We show that MitoQ and E2 were able to reduce cell proliferation in the male MCT RV fibroblast cells. We observed that MitoQ and E2 were able to reduce mitochondrial superoxide levels in both normoxia and hypoxia for the male and female HCF cells. Similarly, mitochondrial superoxide was reduced by E2 and MitoQ in the male MCT RV fibroblasts. When we examined nuclear NFE2L2, cytosolic TFAM, and Col1a1 expression in the male MCT RV fibroblasts, E2 and MitoQ upregulated NFE2L2 and TFAM levels and reduced Col1a1. In the male and female HCF cells, we found that Col1a1 intensity was reduced by MitoQ in both normoxia and hypoxia, while, E2 only reduced Col1a1 levels in the hypoxic environment. Nuclear NFE2L2 intensity was increased by MitoQ and E2 in both normoxia and hypoxia for both male and female HCF cells. Lastly, cytosolic TFAM intensity was increased by MitoQ and E2 under normoxic and hypoxic conditions for both male and female HCF cells.

The results from the preliminary *in vivo* study examining the effect of MitoQ in SuHx rats revealed that MitoQ did not affect the bodyweight of the male and female rats. MitoQ was not able to reduce RV and LV+S weight, and hence did not affect the RV hypertrophy (Fulton index) for both male and female SuHx rats. It also did not lower RVSP or RVEDP or affect RV myocyte cell size in either male or female rats. However, it did enhance the RV-pulmonary artery coupling (Ees/Ea) in the male SuHx + MitoQ rats. The improvement in Ees/Ea was also associated with reduced interstitial collagen deposition in the male SuHx + MitoQ rats.

5.16 Summary

Overall, Chapter 5 demonstrates that both E2 and MitoQ are able to mediate protective effects *in vitro*. This was illustrated by a reduction in MitoSOX, cell proliferation, and Col1a1 expression in both male MCT RV fibroblasts and male and female HCF cells. Both E2 and MitoQ were also able to increase TFAM and NFE2L2 protein expression in both the male MCT RV fibroblasts and male and female HCF cells. Using our SuHx rat model, we did not find any major significant changes in RV hypertrophy, remodeling, RVSP, RVEDP and RV function upon MitoQ treatment in the female SuHx rats. However, in the male SuHx rats, whilst MitoQ had no effect on RV myocyte size, it was able to significantly reduce RV interstitial collagen deposition, slightly reduce RV hypertrophy and significantly improve RV-pulmonary artery

coupling. This suggests that the effect of MitoQ treatment *in vivo* may be sex specific. These results add to the complexity of MitoQ as a potential PAH antioxidant drug, and we suggest that further work is needed, particularly with a range of PAH models, before any conclusions are made regarding MitoQ's therapeutic value.

CHAPTER 6

6. Discussion

6.1 General discussion

Pulmonary arterial hypertension (PAH) is a progressive condition and its mortality relies on the status of the right ventricle (RV). RV dysfunction in PAH has been associated with mitochondrial dysfunction, including a change in the mitochondrial metabolism from oxidative phosphorylation to aerobic glycolysis, known as the Warburg effect (Piao et al., 2010, Ryan and Archer, 2014, Peng et al., 2016). As well as this, there are also disruptions in the mitochondrial fusion and fission proteins which are normally tightly regulated. Whilst in PAH, there is a shift towards excessive mitochondrial fission (Culley and Chan, 2018). Additionally, there is a strong sexual dimorphism in PAH, in which it predominately affects the females, with a ~4:1 female: male ratio (Walker et al., 2006, Badesch et al., 2010, Shapiro et al., 2012, Mair et al., 2014b). However, the female PAH patients demonstrate better RV function and less mortality rate than the males (Keen et al., 2020, Dignam et al., 2023, Ventetuolo et al., 2023). This has prompted investigations into the role of sex hormones, particularly estradiol (E2), on mitochondrial activity, which is still not well understood. E2 has been shown to influence mitochondrial functions both directly by targeting the mitochondria themselves and indirectly through the nucleus (Velarde, 2014). Whereby, it can regulate mitochondrial biogenesis activity, influence mtDNA replication and repair as well as influence the balance of the mitochondrial fusion and fission proteins (Velarde, 2014). The mitochondria also serve as the major source of reactive oxygen species (ROS), and in PAH there has been evidence of upregulated ROS which contributes to mitochondrial damage (Ryanto et al., 2023). E2 has been found to reduce ROS levels and hence, protect the mitochondria from oxidative damage (Velarde, 2014). There has also been the development of mitochondrial targeted antioxidant drugs, such as Mitoquinone (MitoQ) which have shown promising results in protecting the mitochondria in a left ventricle pressure overload by ascending aortic constriction (non-PAH) model (Goh et al., 2019, Kim et al., 2020). In addition, MitoQ has also illustrated protective activity in several animal models of PH including chronic hypoxia and pulmonary artery banding models (Pak et al., 2018, Yan et al., 2023, Li et al., 2024a) through improving mitochondria associated redox signalling (Pak et al., 2018, Yan et al., 2023, Li et al., 2024b). Indeed, MitoQ can lead to attenuation of some of the key

pathological PAH features, including mitochondrial fragmentation (Suresh et al., 2019). Therefore, we proposed that MitoQ may be able to offer the possibility to protect RV function via the targeting mtROS and improving mitochondrial function.

The key aims of this project were to characterise the sex differences in mitochondria and RV function using the gold-standard animal model of PAH, Sugen-hypoxia (SuHx) in male and female rats. We established that there was a need to identify whether there were any clear sex differences in these genes and protein linked to mitochondrial function and fibrosis, as there is limited research within this area. Following this, we examined whether there were any sex differences in right coronary artery (RCA) remodelling in the SuHx rat model. We propose that the remodelling could contribute to RCA stiffness and worsen ischemia. We then examined the effects of MitoQ and E2 treatment on cell proliferation, mtROS production via mitochondrial superoxide (MitoSOX), and mitochondria- and fibrosis-linked proteins *in vitro*. Lastly, this project examined the effect of MitoQ *in vivo* in male and female SuHx rats to determine whether it influences RV hypertrophy, collagen deposition and RV function. To my knowledge, this is the first study to examine the effects of MitoQ in the SuHx rat model *in vivo* in both sexes.

6.2 Summary of findings and conclusion

In chapter 3, we were able to successfully characterise the SuHx rat model. We propose that the SuHx rat model was the most appropriate model for our study as it targets both the pulmonary vasculature and the RV, whilst best representing the key PAH characteristics. This then allowed us to measure all the PAH phenotype parameters including the RV hypertrophy and gene changes that have taken place within the RV and lungs. SuHx rat model is now also one of the most extensively used PH models, therefore allowing for a comparison of our findings with those published. We illustrated a rise in right ventricular systolic pressure (RVSP) from the SuHx rats (>70mmHg vs. ~30mmHg in the control rats) which was also combined with an increase in RV hypertrophy. Although we must note that when we measured the RV hypertrophy, we ratioed RV to the LV+S weight. LV+S weight was increased by SuHx in the female rats which would have affected the RV/LV+S ratio. Therefore, it would have been

better to ratio the RV weight to the tibia length instead which would remain unchanged by SuHx and provide a more accurate measurement. Both male and female SuHx rats demonstrated an increase in cell proliferation within their RV and also an increase in RV myocyte cell size. Both the enlargement in cell size and increase in cell proliferation are in alignment with hypertrophic growth. Although we did not find sex differences in RVSP, RV hypertrophy, cell proliferation and myocyte size in response to SuHx, we detected a sexual dimorphism in that the male SuHx rats had a higher increase in RV interstitial collagen deposition, which was associated with worse RV-pulmonary artery coupling (Ees/Ea) compared to the females. Interestingly, this was also correlated with increased pro-fibrotic TGFβ1 signalling and TGFβ1 positive regulator, TSC22D1 gene expression in the male SuHx rats, which was not seen in the females.

In chapter 4, we examined the differences in the RCA remodelling in the SuHx model. One of the primary findings was that there was worse structural remodelling due to increased collagen deposition in the male SuHx rats, particularly in the small vessels (diameter at 15-50μm) compared with the females. This correlates with what we see in chapter 3, that there were also worse interstitial collagen deposition and RV-pulmonary artery coupling in the male SuHx males.

We also predicted that the poorer RV function that is typically found in the male PAH patients could be due to worse mitochondrial function. Therefore, we decided to examine mitochondrial function in the fresh RV tissues by firstly examining the membrane potential. Prior to confocal imaging, we optimised the fluorescence intensity to allow for speedy scanning of the dishes in order to prevent any photo-bleaching to the tissue. We found that, the male SuHx rats had reduced TMRM levels which was not detected in the female SuHx rats. The loss of the TMRM fluorescence indicates there is a collapse in the mitochondrial membrane potential. Although, it must be noted that the reduced membrane potential does not indicate cell death, but a decrease in the cells activity and hence, ATP production (Wang et al., 2019). However, this reduced activity points towards poor mitochondrial health which is important given the RV has a high energy requirement and is therefore highly reliant on a positive mitochondrial membrane potential for ATP generation.

We then examined the mitochondrial morphology via staining mitochondria with MitoTracker green. We found that MitoTracker green localises to the mitochondria regardless of reduced membrane potential. In healthy control RVs, mitochondria displayed filamentous, or well connected. In response to SuHx, RV from the males but not females displayed less filamentous or less connected, indicting more mitochondrial fission. When we examined the mitochondrial fusion and fission genes within the RV, we did not detect any differences. However, within the lungs, we found there was reduced Mitofusin 1 (MFN1) in the male SuHx and MFN2 in both male and female SuHx gene expression. Although, interestingly, there was also reduced dynamin 2 (DNM2) gene expression in both the male and female SuHx rats which plays a key role in mitochondrial fission, which goes against the hypothesis and the findings of PAH studies. We detected an increase in TFAM and NRF2 in the male RV SuHx rats which could be a compensatory response given that we only see an increase in mitochondrial fission in the male SuHx rats. Although, in the male SuHx lung tissue, we found the opposite effects in that TFAM and NRF1 were reduced. It is not unusual to see differentially expressed genes in the opposite direction between both the RV and the lung. Within PAH, the pulmonary vasculature system becomes affected first, perhaps the mitochondrial key transcriptive genes also become depleted at earlier stages than they do for the RV.

Finally, we found no significant changes in the MitoSOX in the RV in both the male and female SuHx rats compared to the controls. However, SuHx demonstrated reduced RV protein expression of master redox-regulated transcription factor, NFE2L2 in only the male SuHx rats. This was not surprising as reduced NFE2L2 has been frequently associated with PH, therefore we predicted SuHx would reduce NFE2L2 expression (Qin et al., 2022). Knockout NFE2L2 studies in mice have also shown an association with RV diastolic dysfunction which appeared earlier than the RV dysfunction seen in SuHx mice (Zhang et al., 2022a). Treatment with an NFE2L2 activator, was able to partially reverse RV diastolic and systolic dysfunction in SuHx rats, highlighting the importance of increasing NFE2L2 activity (Zhang et al., 2022a).

Within PAH, cells will be more reliant on NFE2L2 protection against damaging ROS injury. Due to this, in chapter 5 we aimed to minimize ROS by utilising a mitochondrial targeted

antioxidant, Mitoquinone (MitoQ) as well as E2, as this has also been speculated to affect ROS. We examined the effect of E2 and MitoQ *in vitro* and *in vivo* using the SuHx rat model. We found for the first time that E2 and MitoQ were able to reduce MitoSOX production in male and female human cardiac fibroblasts (HCF) under both normoxic and hypoxic conditions. A previous study showed that MitoQ had no significant effect in reducing intracellular peroxide content under normoxic conditions but was effective under hypoxic conditions in MRC-5 fibroblasts (Saretzki et al., 2003). Interestingly, MitoQ appears to be efficient under both normoxic and hypoxic conditions in our study, probably due to that the HCF are not considered as fully healthy control cells since they were isolated from patients with some certain diseases in the heart. Similarly, we found E2 and MitoQ were able to reduce MitoSOX in the male MCT RV fibroblasts.

Both E2 and MitoQ demonstrated anti-proliferative effects by reducing Ki-67 positive cell count in the male and female HCF. This was seen to occur in both normoxia and hypoxia for the male HCF but only hypoxia for the female HCF. The same outcome was detected in the male MCT RV fibroblasts which had a reduced PCNA positive cell count mediated by E2 and MitoQ. Previous studies have found that MitoQ is able to reduce cell proliferation by inhibiting mitochondrial oxidative phosphorylation (Cheng et al., 2023). However, the mechanism by which E2 and MitoQ are responsible for inhibiting the cell proliferation was not studied in this project.

Excessive mitochondrial ROS (mtROS) may be able to promote fibrosis via increasing collagen production. It was found that E2 and MitoQ reduced Col1a1 protein expression and also increased NFE2L2 and TFAM expression in the male and female HCF and in the male MCT RV fibroblasts. These data illustrates that both E2 and MitoQ activity may stimulate mitochondrial biogenesis via the increase in TFAM expression and antioxidant activity via the increase in NFE2L2 expression.

For the first time, we reported the effects of MitoQ in the male and female SuHx animal model. MitoQ was found to have a minimal effect on the animals' body weight. Meanwhile, MitoQ had no effect on RV weight, LV+S weight and on RV hypertrophy as measured by the

Fulton index across the male and female groups. Similarly, MitoQ showed no effect on several of the hemodynamic parameters that were measured including RVSP, RVEDP, heart rate, pulmonary effective arterial elastance (Ea) and RV end systolic elastance (Ees). It did however show an increase in the RV-pulmonary artery coupling in the male SuHx + MitoQ rats, which suggests it is enhancing the coupling efficiency in the RV-pulmonary artery unit. Better RV-pulmonary artery coupling in the male SuHx + MitoQ rats is suggestive of better RV function. This was also associated with less RV collagen deposition or fibrosis in the male SuHx + MitoQ rats. However, we did not find a significant effect of MitoQ on females, probably due to that the female rats were in the compensated stage with preserved RV function in response to SuHx. This was evidenced by the female SuHx demonstrating less increase in RV fibrosis, preserved RV-pulmonary artery coupling, RCA structure and RV mitochondrial function in chapters 3 and 4. This thesis focuses largely on the short-term effects of MitoQ, without exploring the long term effects and whether this could lead to dysfunctional mitochondria and RV function. However, one study which administered MitoQ to male mice for up to 28 weeks detected no deleterious effects, confirming that it is not transformed into a pro-oxidant overtime and is safely tolerated long-termly (Rodriguez-Cuenca et al., 2010). Specifically, MitoQ did not influence the mice bodyweight, food and liquid consumption and physical activity and had a minor effect on mitochondrial gene expression within the heart (Rodriguez-Cuenca et al., 2010). Additionally, it had no effect on the mitochondrial oxidative damage markers such as mtDNA damage, carbonyl formation and oxidation of the mitochondrial phospholipid cardiolipin, suggesting that it does not contribute to oxidative damage over time (Rodriguez-Cuenca et al., 2010). Taken together, this provides a firm basis that MitoQ may also be able to exhibit protective activity within the SuHx rat model in the long term.

The overall conclusion of this project is that male SuHx rats demonstrate worse RV function as illustrated by reduced RV-pulmonary artery coupling and higher RVEDP which was associated with worse interstitial fibrosis. The poorer interstitial fibrosis was also accompanied with increased fibrotic gene expression as seen by increases in TGFβ1 and TSC22D1 genes. We found that the males also had more severe fibrosis and remodelling in their RCA vessels and a worse mitochondrial status. We show that E2 and MitoQ exhibit protective activity by reducing MitoSOX levels, inhibiting cell proliferating, enhancing mtDNA

gene TFAM, antioxidant gene NFE2L2 and lowering Col1a1 expression. Finally, we show that MitoQ is protective *in vivo* by enhancing RV-pulmonary artery coupling and lowering collagen deposition only in the male SuHx rats.

Finally, given that PAH is a female predominant disease and the males have worse mortality rates, it is clear that sex plays a significant role. Although we have briefly discussed the potential cause being due to estrogen mediating protective effects in the females, it could also be a result of women responding better to the treatment options. Within PAH, the treatment options are largely the same for both male and female. It is important to note that age differences, co-morbidities and gender will likely influence how a patient will respond to the treatment (Mair et al., 2014a). Female PAH patients have been reported to respond better to endothelial-1 receptor antagonists and prostacyclin analogs meanwhile, male patients respond better to phosphodiesterase-5-inhibitors (Hye et al., 2021). Additionally, this project also largely highlights the sex differences in PAH progression in the SuHx model, further emphasising the importance of sex-specific treatments. However, as it stands, there are no sex-specific therapeutic strategies available within PAH. Going forward in PAH, personalised sex-specific treatment plans would be highly valuable in slowing PAH progression, reducing side effects and improving patient outcomes.

6.3 Limitations and future perspectives

Although our study produced interesting and novel data, there were several areas of limitations and areas where future work would be deemed essential. Firstly, our work is largely focused on the SuHx rat model. Animal models serve as an invaluable tool particularly in scientific research and help us greatly understand the mechanisms underlying several diseases. Nonetheless, utilising animal models into our study meant that we faced with many limitations as they are time-consuming and expensive. It also remains difficult to determine whether the results are translatable to humans given the differences in the cardiovascular systems. This is evidenced by many animal studies which have produced promising results, have failed to be replicated in human clinical trials (Bracken, 2009). To make the animal study

more clinically relevant, one or more animal models may be studied along with the comparison between the data from animal studies and clinical data.

Meanwhile, the cell models, which are generally less time consuming and more cost effective than animal models, can also face many weaknesses in that they lack relevance. For instance, in our study the HCF were isolated from human ventricles in which it remains undisclosed which ventricle they came from. As well as this, every time the HCF cells and MCT RV fibroblasts were passaged small changes in their phenotype and genotype can take place which may have influenced their protein expression data. It would be more physiologically relevant to culture RV cells harvested from primary male and female PAH patients. Hence, most of the cell and animal models do face limitations that are difficult to mitigate and the conclusions drawn from these studies must be carefully considered in context.

In our study, we briefly analyse the pulmonary vasculature remodelling. However, it would have been worthwhile to perform a more in-depth assessment of the pulmonary vasculature remodelling by staining the lung tissue with von Willebrand factor (VWF). VWF is produced exclusively by the vascular endothelial cells and is therefore a more reliable test to determine the formation of the occluded lesions, endothelial damage and dysfunction (Steffes et al., 2022). Additionally, given that chapter 3 largely examines RV fibrosis it would be more beneficial to examine the collagen breakdown enzymes, known as matrix metalloproteinases and the tissue inhibitors of matrix metalloproteinase which prevent the collagen breakdown. This would allow for a better idea of the collagen turnover rate in the RV tissue.

In terms of image analysis, when we analysed the remodelling which had taken place interstitially in the RV and perivascularly in the RCA vessels, we chose to use the thresholding method to determine the areas affected. However, thresholding despite being a simple and effective route of analysis does present with a deal of subjectivity. As well as this, the HCF stained Ki-67 confocal images which were analysed using an ImageJ cell counter also present with several limitations due to bias with it being highly dependent on the observer. Therefore, a more automated system which is independent of the observer could be used instead to generate quantification. Particularly for quantifying cell proliferation, a complementary

approach could be used such as using the automated cell countess assay prior to moving to the fluorescent microscope. Additionally, modern cell counters are now equipped to detect fluorescent signals, including the CellDrop^{TM} FL.

Within chapter 4, we examined numerous mitochondrial related genes, but did not assess their protein expression. Therefore, it would be important to examine the same genes protein expression using western blot. Prior to this, isolating the mitochondria using a cell fractioning kit would be beneficial to directly measure the mitochondrial protein expression. It would also be worthwhile to measure the proteins involved in glucose metabolism such as PDK, PDH, PKM1 and PDKM1. Additionally, measuring ATP production using ATP assay kits or oxygen consumption rates using mitochondrial stress kits in isolated RV tissue would also allow us to determine how mitochondrial respiration is altered in our SuHx model, the sex differences and whether MitoQ is able to directly improve mitochondrial respiration.

Another weakness in our *in vitro* studies is that we did not charcoal strip our cell culture media. It is understood that many of the medias, particularly FBS, contain estrogenic properties that may confound the results and produce a bias. The effect of these estrogenic properties in the media on cell growth and properties is unknown. In order to ensure translatability, it would be important to ensure all medias have been charcoal stripped in future studies to remove the hormonal factors. We also did not validate the cell chamber which represent another weakness. A reliable way to do this would be to measure the expression of the hypoxia markers such as HIF1α. HIF1α under normal conditions is targeted for degradation however under hypoxic conditions it becomes stabilised in which it translocate to the nuclear where it forms a dimer with HIF1β so it would be useful to perform immunocytochemistry to detect nuclear HIF1α expression.

One of the limitations of our preliminary MitoQ study *in vivo* was that we did not test MitoQ on normoxic control rats. Therefore, this would be deemed essential as future work to allow us to understand whether MitoQ is influencing healthy RV function. Additionally, the MitoQ animal study sample numbers were small and this could be improved by increasing the sample numbers. They were several aspects of this study which are worthy of investigation

but were not performed. These include investigating into the gene expression profile to examine the genes linked to fibrosis and mitochondrial and performing a direct comparison with those listed in chapters 3 and 4. It would also be insightful to examine this at the protein level and compare with those assessed in chapter 5. As well as this, performing a similar analysis as chapter 4 in which fresh pieces of live RV tissue were taken and stained for mitochondrial properties such as MitoSOX would be useful to examine whether MitoQ is able to influence or restore mitochondrial function. There are other methods to measure ROS accumulation, that may be more reliable than MitoSOX. This includes using the Bruker electron resonance spectrometer, which would provide a more specific and direct measurement of general ROS. We also only tested MitoQ at the recommended dose based on the literature due to time constraints. Therefore, we recommend that it would be important in future to test MitoQ at several concentrations in a series of dose-response experiments to determine whether 5mg/kg is the optimal dose. Following this, it would be interesting to measure the MitoQ concentration in the different tissues such as the heart, lung and liver using HPLC.

Additionally, to examine if MitoQ plays its role by targetingNFE2L2, we could examine the cells' biology by treatment with both MitoQ and a NFE2L2 antagonist. As NFE2L2 is a nuclear transcription factor, the most appropriate method to examine its expression would be to use a nuclear cell extraction kit and then run a western blot. Following this, it would be useful to also check the expression of the antioxidant enzymes such as HO-1, GPX, catalase and NQO1. Hormonal modulation experiments using estrogen receptor, ERα, ERβ and GPER antagonists, as well as testosterone and progesterone antagonists could also be employed. This would allow us to determine whether the hormonal pathways drive the sex differences in the mitochondrial function and RV remodelling.

Finally, we did not look at the effect of MitoQ on the pulmonary artery remodelling which would be important to determine whether it exerts protective activity at the site at which PAH begins.

CHAPTER 7

7. References

AGARWAL, M., AGRAWAL, S., GARG, L. & LAVIE, C. J. 2017. Relation Between Obesity and Survival in Patients Hospitalized for Pulmonary Arterial Hypertension (from a Nationwide Inpatient Sample Database 2003 to 2011). *Am J Cardiol,* 120**,** 489-493.

AGGARWAL, S., GROSS, C. M., SHARMA, S., FINEMAN, J. R. & BLACK, S. M. 2013. Reactive oxygen species in pulmonary vascular remodeling. *Compr Physiol,* 3**,** 1011-34.

AGRAWAL, V., LAHM, T., HANSMANN, G. & HEMNES, A. R. 2020. Molecular mechanisms of right ventricular dysfunction in pulmonary arterial hypertension: focus on the coronary vasculature, sex hormones, and glucose/lipid metabolism. *Cardiovasc Diagn Ther,* 10**,** 1522-1540.

AKAZAWA, Y., OKUMURA, K., ISHII, R., SLORACH, C., HUI, W., IDE, H., HONJO, O., SUN, M., KABIR, G., CONNELLY, K. & FRIEDBERG, M. K. 2020. Pulmonary artery banding is a relevant model to study the right ventricular remodeling and dysfunction that occurs in pulmonary arterial hypertension. *J Appl Physiol (1985),* 129**,** 238-246.

ALENCAR, A. K. N., MONTES, G. C., COSTA, D. G., MENDES, L. V. P., SILVA, A. M. S., MARTINEZ, S. T., TRACHEZ, M. M., CUNHA, V., MONTAGNOLI, T. L., FRAGA, A. G. M., WANG, H., GROBAN, L., FRAGA, C. A. M., SUDO, R. T. & ZAPATA-SUDO, G. 2018. Cardioprotection Induced by Activation of GPER in Ovariectomized Rats With Pulmonary Hypertension. *J Gerontol A Biol Sci Med Sci,* 73**,** 1158-1166.

ALVES, A. F., MOURA, A. C., ANDREOLLA, H. F., VEIGA, A., FIEGENBAUM, M., GIOVENARDI, M. & ALMEIDA, S. 2021. Gene expression evaluation of antioxidant enzymes in patients with hepatocellular carcinoma: RT-qPCR and bioinformatic analyses. *Genet Mol Biol,* 44**,** e20190373.

ANDERSEN, S., NIELSEN-KUDSK, J. E., VONK NOORDEGRAAF, A. & DE MAN, F. S. 2019. Right Ventricular Fibrosis. *Circulation,* 139**,** 269-285.

ANDRE, P., JOSHI, S. R., BRISCOE, S. D., ALEXANDER, M. J., LI, G. & KUMAR, R. 2021. Therapeutic Approaches for Treating Pulmonary Arterial Hypertension by Correcting Imbalanced TGF-β Superfamily Signaling. *Front Med (Lausanne),* 8**,** 814222.

ARCHER, S. L., FANG, Y. H., RYAN, J. J. & PIAO, L. 2013. Metabolism and bioenergetics in the right ventricle and pulmonary vasculature in pulmonary hypertension. *Pulm Circ,* 3**,** 144-52.

ARCHER, S. L., MARSBOOM, G., KIM, G. H., ZHANG, H. J., TOTH, P. T., SVENSSON, E. C., DYCK, J. R., GOMBERG-MAITLAND, M., THÉBAUD, B., HUSAIN, A. N., CIPRIANI, N. & REHMAN, J. 2010. Epigenetic attenuation of mitochondrial superoxide dismutase 2 in pulmonary arterial hypertension: a basis for excessive cell proliferation and a new therapeutic target. *Circulation,* 121**,** 2661-71.

ASIN-CAYUELA, J., MANAS, A. R., JAMES, A. M., SMITH, R. A. & MURPHY, M. P. 2004. Fine-tuning the hydrophobicity of a mitochondria-targeted antioxidant. *FEBS Lett,* 571**,** 9-16.

AUSTIN, E. D., COGAN, J. D., WEST, J. D., HEDGES, L. K., HAMID, R., DAWSON, E. P., WHEELER, L. A., PARL, F. F., LOYD, J. E. & PHILLIPS, J. A., 3RD 2009. Alterations in

oestrogen metabolism: implications for higher penetrance of familial pulmonary arterial hypertension in females. *Eur Respir J,* 34**,** 1093-9.

BADESCH, D. B., RASKOB, G. E., ELLIOTT, C. G., KRICHMAN, A. M., FARBER, H. W., FROST, A. E., BARST, R. J., BENZA, R. L., LIOU, T. G., TURNER, M., GILES, S., FELDKIRCHER, K., MILLER, D. P. & MCGOON, M. D. 2010. Pulmonary arterial hypertension: baseline characteristics from the REVEAL Registry. *Chest,* 137**,** 376-87.

BADLAM, J. B. & BULL, T. M. 2017. Steps forward in the treatment of pulmonary arterial hypertension: latest developments and clinical opportunities. *Ther Adv Chronic Dis,* 8**,** 47-64.

BAIRD, G. L., WALSH, T., ALIOTTA, J., ALLAHUA, M., ANDREW, R., BOURJEILY, G., BRODSKY, A. S., DENVER, N., DOONER, M., HARRINGTON, E. O., KLINGER, J. R., MACLEAN, M. R., MULLIN, C. J., PEREIRA, M., POPPAS, A., WHITTENHALL, M. & VENTETUOLO, C. E. 2021. Insights from the Menstrual Cycle in Pulmonary Arterial Hypertension. *Ann Am Thorac Soc,* 18**,** 218-228.

BALABAN, R. S., NEMOTO, S. & FINKEL, T. 2005. Mitochondria, oxidants, and aging. *Cell,* 120**,** 483-95.

BATTON, K. A., AUSTIN, C. O., BRUNO, K. A., BURGER, C. D., SHAPIRO, B. P. & FAIRWEATHER, D. 2018. Sex differences in pulmonary arterial hypertension: role of infection and autoimmunity in the pathogenesis of disease. *Biol Sex Differ,* 9**,** 15.

BELLOFIORE, A., VANDERPOOL, R., BREWIS, M. J., PEACOCK, A. J. & CHESLER, N. C. 2018. A novel single-beat approach to assess right ventricular systolic function. *J Appl Physiol (1985),* 124**,** 283-290.

BLANCO, I., MARQUINA, M., TURA-CEIDE, O., PEINADO, V. I. & BARBERÀ, J. A. 2019. Survivin inhibition as a potential target for pulmonary arterial hypertension. *European Respiratory Journal,* 54**,** PA5055.

BOGAARD, H. J., NATARAJAN, R., HENDERSON, S. C., LONG, C. S., KRASKAUSKAS, D., SMITHSON, L., OCKAILI, R., MCCORD, J. M. & VOELKEL, N. F. 2009. Chronic pulmonary artery pressure elevation is insufficient to explain right heart failure. *Circulation,* 120**,** 1951-60.

BONNET, S. & BOUCHERAT, O. 2018. The ROS controversy in hypoxic pulmonary hypertension revisited. *Eur Respir J,* 51.

BONNET, S., MICHELAKIS, E. D., PORTER, C. J., ANDRADE-NAVARRO, M. A., THÉBAUD, B., BONNET, S., HAROMY, A., HARRY, G., MOUDGIL, R., MCMURTRY, M. S., WEIR, E. K. & ARCHER, S. L. 2006. An abnormal mitochondrial-hypoxia inducible factor-1alpha-Kv channel pathway disrupts oxygen sensing and triggers pulmonary arterial hypertension in fawn hooded rats: similarities to human pulmonary arterial hypertension. *Circulation,* 113**,** 2630-41.

BONNET, S., ROCHEFORT, G., SUTENDRA, G., ARCHER, S. L., HAROMY, A., WEBSTER, L., HASHIMOTO, K., BONNET, S. N. & MICHELAKIS, E. D. 2007. The nuclear factor of activated T cells in pulmonary arterial hypertension can be therapeutically targeted. *Proc Natl Acad Sci U S A,* 104**,** 11418-23.

BORGDORFF, M. A., KOOP, A. M., BLOKS, V. W., DICKINSON, M. G., STEENDIJK, P., SILLJE, H. H., VAN WIECHEN, M. P., BERGER, R. M. & BARTELDS, B. 2015. Clinical symptoms of right ventricular failure in experimental chronic pressure load are associated with progressive diastolic dysfunction. *J Mol Cell Cardiol,* 79**,** 244-53.

BORRÁS, C., SASTRE, J., GARCÍA-SALA, D., LLORET, A., PALLARDÓ, F. V. & VIÑA, J. 2003. Mitochondria from females exhibit higher antioxidant gene expression and lower oxidative damage than males. *Free Radic Biol Med,* 34**,** 546-52.

BRACKEN, M. B. 2009. Why animal studies are often poor predictors of human reactions to exposure. *J R Soc Med,* 102**,** 120-2.

BRAND, M. D., ORR, A. L., PEREVOSHCHIKOVA, I. V. & QUINLAN, C. L. 2013. The role of mitochondrial function and cellular bioenergetics in ageing and disease. *Br J Dermatol,* 169 Suppl 2**,** 1-8.

BREAULT, N. M., WU, D., DASGUPTA, A., CHEN, K. H. & ARCHER, S. L. 2023. Acquired disorders of mitochondrial metabolism and dynamics in pulmonary arterial hypertension. *Front Cell Dev Biol,* 11**,** 1105565.

BRIMIOULLE, S., WAUTHY, P., EWALENKO, P., RONDELET, B., VERMEULEN, F., KERBAUL, F. & NAEIJE, R. 2003. Single-beat estimation of right ventricular end-systolic pressure-volume relationship. *Am J Physiol Heart Circ Physiol,* 284**,** H1625-30.

BRUGGEN, C. E. V. D., HAPPÉ, C. M., DORFMÜLLER, P., TRIP, P., SPRUIJT, O. A., ROL, N., HOEVENAARS, F. P., HOUWELING, A. C., GIRERD, B., MARCUS, J. T., MERCIER, O., HUMBERT, M., HANDOKO, M. L., VELDEN, J. V. D., NOORDEGRAAF, A. V., BOGAARD, H. J., GOUMANS, M.-J. & MAN, F. S. D. 2016. Bone Morphogenetic Protein Receptor Type 2 Mutation in Pulmonary Arterial Hypertension. *Circulation,* 133**,** 1747-1760.

CARDINALE, D. A., LARSEN, F. J., SCHIFFER, T. A., MORALES-ALAMO, D., EKBLOM, B., CALBET, J. A. L., HOLMBERG, H. C. & BOUSHEL, R. 2018. Superior Intrinsic Mitochondrial Respiration in Women Than in Men. *Front Physiol,* 9**,** 1133.

CASA, L. D., DOLENSKY, J. R., SPINNER, E. M., VELEDAR, E., LERAKIS, S. & YOGANATHAN, A. P. 2013. Impact of pulmonary hypertension on tricuspid valve function. *Ann Biomed Eng,* 41**,** 709-24.

CATIVO CALDERON, E. H., MENE-AFEJUKU, T. O., VALVANI, R., CATIVO, D. P., TRIPATHI, D., REYES, H. A. & MUSHIYEV, S. 2017. D-Shaped Left Ventricle, Anatomic, and Physiologic Implications. *Case Rep Cardiol,* 2017**,** 4309165.

CEN, M., OUYANG, W., ZHANG, W., YANG, L., LIN, X., DAI, M., HU, H., TANG, H., LIU, H., XIA, J. & XU, F. 2021. MitoQ protects against hyperpermeability of endothelium barrier in acute lung injury via a Nrf2-dependent mechanism. *Redox Biol,* 41**,** 101936.

CHANDRAN, K., AGGARWAL, D., MIGRINO, R. Q., JOSEPH, J., MCALLISTER, D., KONOREV, E. A., ANTHOLINE, W. E., ZIELONKA, J., SRINIVASAN, S., AVADHANI, N. G. & KALYANARAMAN, B. 2009. Doxorubicin inactivates myocardial cytochrome c oxidase in rats: cardioprotection by Mito-Q. *Biophys J,* 96**,** 1388-98.

CHANG, K. Y., DUVAL, S., BADESCH, D. B., BULL, T. M., CHAKINALA, M. M., DE MARCO, T., FRANTZ, R. P., HEMNES, A., MATHAI, S. C., ROSENZWEIG, E. B., RYAN, J. J. & THENAPPAN, T. 2022. Mortality in Pulmonary Arterial Hypertension in the Modern Era: Early Insights From the Pulmonary Hypertension Association Registry. *J Am Heart Assoc,* 11**,** e024969.

CHEN, J. Q., DELANNOY, M., COOKE, C. & YAGER, J. D. 2004. Mitochondrial localization of ERα and ERβ in human MCF7 cells. *American Journal of Physiology-Endocrinology and Metabolism,* 286**,** E1011-E1022.

CHEN, K. H., DASGUPTA, A., LIN, J., POTUS, F., BONNET, S., IREMONGER, J., FU, J., MEWBURN, J., WU, D., DUNHAM-SNARY, K., THEILMANN, A. L., JING, Z. C., HINDMARCH, C., ORMISTON, M. L., LAWRIE, A. & ARCHER, S. L. 2018a. Epigenetic Dysregulation of the Dynamin-Related Protein 1 Binding Partners MiD49 and MiD51 Increases Mitotic Mitochondrial Fission and Promotes Pulmonary Arterial Hypertension: Mechanistic and Therapeutic Implications. *Circulation,* 138**,** 287-304.

CHEN, R., LAI, U. H., ZHU, L., SINGH, A., AHMED, M. & FORSYTH, N. R. 2018b. Reactive Oxygen Species Formation in the Brain at Different Oxygen Levels: The Role of Hypoxia Inducible Factors. *Front Cell Dev Biol,* 6**,** 132.

CHEN, R., YAN, J., LIU, P., WANG, Z., WANG, C., ZHONG, W. & XU, L. 2017a. The role of nuclear factor of activated T cells in pulmonary arterial hypertension. *Cell Cycle,* 16**,** 508-514.

CHEN, X., AUSTIN, E. D., TALATI, M., FESSEL, J. P., FARBER-EGER, E. H., BRITTAIN, E. L., HEMNES, A. R., LOYD, J. E. & WEST, J. 2017b. Oestrogen inhibition reverses pulmonary arterial hypertension and associated metabolic defects. *Eur Respir J,* 50.

CHEN, Y., ZHANG, Z., HU, F., YANG, W., YUAN, J., CUI, J., HAO, S., HU, J., ZHOU, Y. & QIAO, S. 2015. 17β-estradiol prevents cardiac diastolic dysfunction by stimulating mitochondrial function: a preclinical study in a mouse model of a human hypertrophic cardiomyopathy mutation. *J Steroid Biochem Mol Biol,* 147**,** 92-102.

CHENG, C. F., KU, H. C. & LIN, H. 2018. PGC-1α as a Pivotal Factor in Lipid and Metabolic Regulation. *Int J Mol Sci,* 19.

CHENG, G., KAROUI, H., HARDY, M. & KALYANARAMAN, B. 2023. Redox-crippled MitoQ potently inhibits breast cancer and glioma cell proliferation: A negative control for verifying the antioxidant mechanism of MitoQ in cancer and other oxidative pathologies. *Free Radic Biol Med,* 205**,** 175-187.

CHENG, T. C., PHILIP, J. L., TABIMA, D. M., KUMARI, S., YAKUBOV, B., FRUMP, A. L., HACKER, T. A., BELLOFIORE, A., LI, R., SUN, X., GOSS, K. N., LAHM, T. & CHESLER, N. C. 2020. Estrogen receptor-α prevents right ventricular diastolic dysfunction and fibrosis in female rats. *Am J Physiol Heart Circ Physiol,* 319**,** H1459-h1473.

CHESTER, A. H. & YACOUB, M. H. 2014. The role of endothelin-1 in pulmonary arterial hypertension. *Glob Cardiol Sci Pract,* 2014**,** 62-78.

CHIN, K. M., SITBON, O., DOELBERG, M., FELDMAN, J., GIBBS, J. S. R., GRÜNIG, E., HOEPER, M. M., MARTIN, N., MATHAI, S. C., MCLAUGHLIN, V. V., PERCHENET, L., POCH, D., SAGGAR, R., SIMONNEAU, G. & GALIÈ, N. 2021. Three- Versus Two-Drug Therapy for Patients With Newly Diagnosed Pulmonary Arterial Hypertension. *Journal of the American College of Cardiology,* 78**,** 1393-1403.

CHOPRA, S., BADYAL, D. K., BABY, P. C. & CHERIAN, D. 2012. Pulmonary arterial hypertension: advances in pathophysiology and management. *Indian J Pharmacol,* 44**,** 4-11.

CIPOLAT, S., MARTINS DE BRITO, O., DAL ZILIO, B. & SCORRANO, L. 2004. OPA1 requires mitofusin 1 to promote mitochondrial fusion. *Proc Natl Acad Sci U S A,* 101**,** 15927-32.

CIUCLAN, L., BONNEAU, O., HUSSEY, M., DUGGAN, N., HOLMES, A. M., GOOD, R., STRINGER, R., JONES, P., MORRELL, N. W., JARAI, G., WALKER, C., WESTWICK, J.

& THOMAS, M. 2011. A novel murine model of severe pulmonary arterial hypertension. *Am J Respir Crit Care Med,* 184**,** 1171-82.

CREED, S. & MCKENZIE, M. 2019. Measurement of Mitochondrial Membrane Potential with the Fluorescent Dye Tetramethylrhodamine Methyl Ester (TMRM). *Methods Mol Biol,* 1928**,** 69-76.

CUI, J., SHEN, Y. & LI, R. 2013. Estrogen synthesis and signaling pathways during aging: from periphery to brain. *Trends Mol Med,* 19**,** 197-209.

CULLEY, M. K. & CHAN, S. Y. 2018. Mitochondrial metabolism in pulmonary hypertension: beyond mountains there are mountains. *J Clin Invest,* 128**,** 3704-3715.

DABIR, D. V., HASSON, S. A., SETOGUCHI, K., JOHNSON, M. E., WONGKONGKATHEP, P., DOUGLAS, C. J., ZIMMERMAN, J., DAMOISEAUX, R., TEITELL, M. A. & KOEHLER, C. M. 2013. A small molecule inhibitor of redox-regulated protein translocation into mitochondria. *Dev Cell,* 25**,** 81-92.

DASGUPTA, A., WU, D., TIAN, L., XIONG, P. Y., DUNHAM-SNARY, K. J., CHEN, K. H., ALIZADEH, E., MOTAMED, M., POTUS, F., HINDMARCH, C. C. T. & ARCHER, S. L. 2020. Mitochondria in the Pulmonary Vasculature in Health and Disease: Oxygen-Sensing, Metabolism, and Dynamics. *Compr Physiol,* 10**,** 713-765.

DE RAAF, M. A., SCHALIJ, I., GOMEZ-ARROYO, J., ROL, N., HAPPÉ, C., DE MAN, F. S., VONK-NOORDEGRAAF, A., WESTERHOF, N., VOELKEL, N. F. & BOGAARD, H. J. 2014. SuHx rat model: partly reversible pulmonary hypertension and progressive intima obstruction. *Eur Respir J,* 44**,** 160-8.

DEAN, A., NILSEN, M., LOUGHLIN, L., SALT, I. P. & MACLEAN, M. R. 2016. Metformin Reverses Development of Pulmonary Hypertension via Aromatase Inhibition. *Hypertension,* 68**,** 446-54.

DEL RIO, J. M., GRECU, L. & NICOARA, A. 2019. Right Ventricular Function in Left Heart Disease. *Semin Cardiothorac Vasc Anesth,* 23**,** 88-107.

DEMARCO, V. G., WHALEY-CONNELL, A. T., SOWERS, J. R., HABIBI, J. & DELLSPERGER, K. C. 2010. Contribution of oxidative stress to pulmonary arterial hypertension. *World J Cardiol,* 2**,** 316-24.

DENVER, N., HOMER, N. Z. M., ANDREW, R., HARVEY, K. Y., MORRELL, N., AUSTIN, E. D. & MACLEAN, M. R. 2020. Estrogen metabolites in a small cohort of patients with idiopathic pulmonary arterial hypertension. *Pulm Circ,* 10**,** 2045894020908783.

DESJARDIN, J. T., KIME, N., KOLAITIS, N. A., KRONMAL, R. A., LAMMI, M. R., MATHAI, S. C., VENTETUOLO, C. E. & DE MARCO, T. 2024. Investigating the "sex paradox" in pulmonary arterial hypertension: Results from the Pulmonary Hypertension Association Registry (PHAR). *J Heart Lung Transplant,* 43**,** 901-910.

DIEBOLD, I., HENNIGS, J. K., MIYAGAWA, K., LI, C. G., NICKEL, N. P., KASCHWICH, M., CAO, A., WANG, L., REDDY, S., CHEN, P. I., NAKAHIRA, K., ALCAZAR, M. A., HOPPER, R. K., JI, L., FELDMAN, B. J. & RABINOVITCH, M. 2015. BMPR2 preserves mitochondrial function and DNA during reoxygenation to promote endothelial cell survival and reverse pulmonary hypertension. *Cell Metab,* 21**,** 596-608.

DIGNAM, J. P., SCOTT, T. E., KEMP-HARPER, B. K. & HOBBS, A. J. 2022. Animal models of pulmonary hypertension: Getting to the heart of the problem. *Br J Pharmacol,* 179**,** 811-837.

DIGNAM, J. P., SHARMA, S., STASINOPOULOS, I. & MACLEAN, M. R. 2023. Pulmonary arterial hypertension: Sex matters. *Br J Pharmacol*.

DINKOVA-KOSTOVA, A. T., HOLTZCLAW, W. D., COLE, R. N., ITOH, K., WAKABAYASHI, N., KATOH, Y., YAMAMOTO, M. & TALALAY, P. 2002. Direct evidence that sulfhydryl groups of Keap1 are the sensors regulating induction of phase 2 enzymes that protect against carcinogens and oxidants. *Proc Natl Acad Sci U S A,* 99**,** 11908-13.

DOCHERTY, C. K., NILSEN, M. & MACLEAN, M. R. 2019. Influence of 2-Methoxyestradiol and Sex on Hypoxia-Induced Pulmonary Hypertension and Hypoxia-Inducible Factor-1-α. *J Am Heart Assoc,* 8**,** e011628.

DOGGRELL, S. A. 2023. Is sotatercept, which traps activins and growth differentiation factors, a new dawn in treating pulmonary arterial hypertension (PAH)? *Expert Opin Biol Ther,* 23**,** 589-593.

DOHI, T., BELTRAMI, E., WALL, N. R., PLESCIA, J. & ALTIERI, D. C. 2004. Mitochondrial survivin inhibits apoptosis and promotes tumorigenesis. *J Clin Invest,* 114**,** 1117-27.

DOMINY, J. E. & PUIGSERVER, P. 2013. Mitochondrial biogenesis through activation of nuclear signaling proteins. *Cold Spring Harb Perspect Biol,* 5.

DROMPARIS, P., SUTENDRA, G. & MICHELAKIS, E. D. 2010. The role of mitochondria in pulmonary vascular remodeling. *J Mol Med (Berl),* 88**,** 1003-10.

DROZD, K., AHMADI, A., DENG, Y., JIANG, B., PETRYK, J., THORN, S., STEWART, D., BEANLANDS, R., DEKEMP, R. A., DASILVA, J. N. & MIELNICZUK, L. M. 2017. Effects of an endothelin receptor antagonist, Macitentan, on right ventricular substrate utilization and function in a Sugen 5416/hypoxia rat model of severe pulmonary arterial hypertension. *J Nucl Cardiol,* 24**,** 1979-1989.

DUNHAM-SNARY, K. J., WU, D., SYKES, E. A., THAKRAR, A., PARLOW, L. R. G., MEWBURN, J. D., PARLOW, J. L. & ARCHER, S. L. 2017. Hypoxic Pulmonary Vasoconstriction: From Molecular Mechanisms to Medicine. *Chest,* 151**,** 181-192.

EARLEY, S. & RESTA, T. C. 2002. Estradiol attenuates hypoxia-induced pulmonary endothelin-1 gene expression. *Am J Physiol Lung Cell Mol Physiol,* 283**,** L86-93.

ECARNOT-LAUBRIET, A., ROCHETTE, L., VERGELY, C., SICARD, P. & TEYSSIER, J. R. 2003. The activation pattern of the antioxidant enzymes in the right ventricle of rat in response to pressure overload is of heart failure type. *Heart Dis,* 5**,** 308-12.

EGEMNAZAROV, B., CRNKOVIC, S., NAGY, B. M., OLSCHEWSKI, H. & KWAPISZEWSKA, G. 2018. Right ventricular fibrosis and dysfunction: Actual concepts and common misconceptions. *Matrix Biol,* 68-69**,** 507-521.

ENACHE, I., CHARLES, A. L., BOUITBIR, J., FAVRET, F., ZOLL, J., METZGER, D., OSWALD-MAMMOSSER, M., GENY, B. & CHARLOUX, A. 2013. Skeletal muscle mitochondrial dysfunction precedes right ventricular impairment in experimental pulmonary hypertension. *Mol Cell Biochem,* 373**,** 161-70.

ENDO, T. & YAMANO, K. 2010. Transport of proteins across or into the mitochondrial outer membrane. *Biochim Biophys Acta,* 1803**,** 706-14.

ESCRIBANO-LOPEZ, I., DIAZ-MORALES, N., ROVIRA-LLOPIS, S., DE MARAÑON, A. M., ORDEN, S., ALVAREZ, A., BAÑULS, C., ROCHA, M., MURPHY, M. P., HERNANDEZ-MIJARES, A. & VICTOR, V. M. 2016. The mitochondria-targeted antioxidant MitoQ modulates oxidative stress, inflammation and leukocyte-endothelium interactions in leukocytes isolated from type 2 diabetic patients. *Redox Biol,* 10**,** 200-205.

FANG, Y. H., PIAO, L., HONG, Z., TOTH, P. T., MARSBOOM, G., BACHE-WIIG, P., REHMAN, J. & ARCHER, S. L. 2012. Therapeutic inhibition of fatty acid oxidation in right ventricular hypertrophy: exploiting Randle's cycle. *J Mol Med (Berl),* 90**,** 31-43.

FARBER, H. W. & LOSCALZO, J. 2004. Pulmonary arterial hypertension. *N Engl J Med,* 351**,** 1655-65.

FARHAT, F., AMÉRAND, A., SIMON, B., GUEGUENIAT, N. & MOISAN, C. 2017. Gender-dependent differences of mitochondrial function and oxidative stress in rat skeletal muscle at rest and after exercise training. *Redox Rep,* 22**,** 508-514.

FARHAT, M. Y., CHEN, M. F., BHATTI, T., IQBAL, A., CATHAPERMAL, S. & RAMWELL, P. W. 1993. Protection by oestradiol against the development of cardiovascular changes associated with monocrotaline pulmonary hypertension in rats. *Br J Pharmacol,* 110**,** 719-23.

FELTY, Q. & ROY, D. 2005. Estrogen, mitochondria, and growth of cancer and non-cancer cells. *J Carcinog,* 4**,** 1.

FORTNER, K. A., BLANCO, L. P., BUSKIEWICZ, I., HUANG, N., GIBSON, P. C., COOK, D. L., PEDERSEN, H. L., YUEN, P. S. T., MURPHY, M. P., PERL, A., KAPLAN, M. J. & BUDD, R. C. 2020. Targeting mitochondrial oxidative stress with MitoQ reduces NET formation and kidney disease in lupus-prone MRL-lpr mice. *Lupus Sci Med,* 7.

FRANK, R. C., MIN, J., ABDELGHANY, M., PANIAGUA, S., BHATTACHARYA, R., BHAMBHANI, V., POMERANTSEV, E. & HO, J. E. 2020. Obesity Is Associated With Pulmonary Hypertension and Modifies Outcomes. *Journal of the American Heart Association,* 9**,** e014195.

FREY, N., KATUS, H. A., OLSON, E. N. & HILL, J. A. 2004. Hypertrophy of the heart: a new therapeutic target? *Circulation,* 109**,** 1580-9.

FRIEDMAN, J. R. & NUNNARI, J. 2014. Mitochondrial form and function. *Nature,* 505**,** 335-43.

FROST, A. E., BADESCH, D. B., BARST, R. J., BENZA, R. L., ELLIOTT, C. G., FARBER, H. W., KRICHMAN, A., LIOU, T. G., RASKOB, G. E., WASON, P., FELDKIRCHER, K., TURNER, M. & MCGOON, M. D. 2011. The changing picture of patients with pulmonary arterial hypertension in the United States: how REVEAL differs from historic and non-US Contemporary Registries. *Chest,* 139**,** 128-37.

FRUMP, A. L., BONNET, S., DE JESUS PEREZ, V. A. & LAHM, T. 2018. Emerging role of angiogenesis in adaptive and maladaptive right ventricular remodeling in pulmonary hypertension. *American Journal of Physiology-Lung Cellular and Molecular Physiology,* 314**,** L443-L460.

FRUMP, A. L., GOSS, K. N., VAYL, A., ALBRECHT, M., FISHER, A., TURSUNOVA, R., FIERST, J., WHITSON, J., CUCCI, A. R., BROWN, M. B. & LAHM, T. 2015. Estradiol improves right ventricular function in rats with severe angioproliferative pulmonary hypertension: effects of endogenous and exogenous sex hormones. *Am J Physiol Lung Cell Mol Physiol,* 308**,** L873-90.

FUENTES, N. & SILVEYRA, P. 2019. Estrogen receptor signaling mechanisms. *Adv Protein Chem Struct Biol,* 116**,** 135-170.

FUKAI, T. & USHIO-FUKAI, M. 2020. Cross-Talk between NADPH Oxidase and Mitochondria: Role in ROS Signaling and Angiogenesis. *Cells,* 9.

FUKUMOTO, Y. 2024. Pathophysiology and Treatment of Pulmonary Arterial Hypertension. *Int J Mol Sci,* 25.

GALIÈ, N., HUMBERT, M., VACHIERY, J. L., GIBBS, S., LANG, I., TORBICKI, A., SIMONNEAU, G., PEACOCK, A., VONK NOORDEGRAAF, A., BEGHETTI, M., GHOFRANI, A., GOMEZ SANCHEZ, M. A., HANSMANN, G., KLEPETKO, W., LANCELLOTTI, P., MATUCCI, M., MCDONAGH, T., PIERARD, L. A., TRINDADE, P. T., ZOMPATORI, M. & HOEPER, M. 2016. 2015 ESC/ERS Guidelines for the diagnosis and treatment of pulmonary hypertension: The Joint Task Force for the Diagnosis and Treatment of Pulmonary Hypertension of the European Society of Cardiology (ESC) and the European Respiratory Society (ERS): Endorsed by: Association for European Paediatric and Congenital Cardiology (AEPC), International Society for Heart and Lung Transplantation (ISHLT). *Eur Heart J,* 37**,** 67-119.

GALIÈ, N., MCLAUGHLIN, V. V., RUBIN, L. J. & SIMONNEAU, G. 2019. An overview of the 6th World Symposium on Pulmonary Hypertension. *Eur Respir J,* 53.

GAN, L., WANG, Z., SI, J., ZHOU, R., SUN, C., LIU, Y., YE, Y., ZHANG, Y., LIU, Z. & ZHANG, H. 2018. Protective effect of mitochondrial-targeted antioxidant MitoQ against iron ion (56)Fe radiation induced brain injury in mice. *Toxicol Appl Pharmacol,* 341**,** 1-7.

GARCIA, M. & KASSAB, G. S. 2009. Right coronary artery becomes stiffer with increase in elastin and collagen in right ventricular hypertrophy. *J Appl Physiol (1985),* 106**,** 1338-46.

GERMANDE, O., DUCRET, T., QUIGNARD, J. F., DEWEIRDT, J., FREUND-MICHEL, V., ERRERA, M. H., CARDOUAT, G., VACHER, P., MULLER, B., BERGER, P., GUIBERT, C., BAUDRIMONT, M. & BAUDRIMONT, I. 2022. NiONP-Induced Oxidative Stress and Mitochondrial Impairment in an In Vitro Pulmonary Vascular Cell Model Mimicking Endothelial Dysfunction. *Antioxidants (Basel),* 11.

GHIO, S., KLERSY, C., MAGRINI, G., D'ARMINI, A. M., SCELSI, L., RAINERI, C., PASOTTI, M., SERIO, A., CAMPANA, C. & VIGANÒ, M. 2010. Prognostic relevance of the echocardiographic assessment of right ventricular function in patients with idiopathic pulmonary arterial hypertension. *Int J Cardiol,* 140**,** 272-8.

GOH, K. Y., HE, L., SONG, J., JINNO, M., ROGERS, A. J., SETHU, P., HALADE, G. V., RAJASEKARAN, N. S., LIU, X., PRABHU, S. D., DARLEY-USMAR, V., WENDE, A. R. & ZHOU, L. 2019. Mitoquinone ameliorates pressure overload-induced cardiac fibrosis and left ventricular dysfunction in mice. *Redox Biol,* 21**,** 101100.

GOLOB, M. J., TIAN, L., WANG, Z., ZIMMERMAN, T. A., CANEBA, C. A., HACKER, T. A., SONG, G. & CHESLER, N. C. 2015. Mitochondria DNA mutations cause sex-dependent development of hypertension and alterations in cardiovascular function. *J Biomech,* 48**,** 405-12.

GOMBERG-MAITLAND, M., SCHILZ, R., MEDIRATTA, A., ADDETIA, K., COSLET, S., THOMEAS, V., GILLIES, H. & OUDIZ, R. J. 2015. Phase I safety study of ranolazine in pulmonary arterial hypertension. *Pulm Circ,* 5**,** 691-700.

GOMEZ-ARROYO, J., MIZUNO, S., SZCZEPANEK, K., VAN TASSELL, B., NATARAJAN, R., DOS REMEDIOS, C. G., DRAKE, J. I., FARKAS, L., KRASKAUSKAS, D., WIJESINGHE, D. S., CHALFANT, C. E., BIGBEE, J., ABBATE, A., LESNEFSKY, E. J., BOGAARD, H. J. & VOELKEL, N. F. 2013. Metabolic gene remodeling and mitochondrial

dysfunction in failing right ventricular hypertrophy secondary to pulmonary arterial hypertension. *Circ Heart Fail,* 6**,** 136-44.

GOMEZ-ARROYO, J., VOELKEL, N. F., BOGAARD, H. J. & TARASEVICIENE-STEWART, L. 2012. Usefulness of a mouse model of reversible pulmonary arterial hypertension: be cautious, choose carefully. *Am J Respir Crit Care Med,* 185**,** 1326; author reply 1326-7.

GONZÁLEZ-MAGAÑA, A. & BLANCO, F. J. 2020. Human PCNA Structure, Function and Interactions. *Biomolecules,* 10.

GÖRLACH, A., DIMOVA, E. Y., PETRY, A., MARTÍNEZ-RUIZ, A., HERNANSANZ-AGUSTÍN, P., ROLO, A. P., PALMEIRA, C. M. & KIETZMANN, T. 2015. Reactive oxygen species, nutrition, hypoxia and diseases: Problems solved? *Redox Biol,* 6**,** 372-385.

GORRINI, C., GANG, B. P., BASSI, C., WAKEHAM, A., BANIASADI, S. P., HAO, Z., LI, W. Y., CESCON, D. W., LI, Y. T., MOLYNEUX, S., PENROD, N., LUPIEN, M., SCHMIDT, E. E., STAMBOLIC, V., GAUTHIER, M. L. & MAK, T. W. 2014. Estrogen controls the survival of BRCA1-deficient cells via a PI3K-NRF2-regulated pathway. *Proc Natl Acad Sci U S A,* 111**,** 4472-7.

GOTTWALD, E. M., DUSS, M., BUGARSKI, M., HAENNI, D., SCHUH, C. D., LANDAU, E. M. & HALL, A. M. 2018. The targeted anti-oxidant MitoQ causes mitochondrial swelling and depolarization in kidney tissue. *Physiol Rep,* 6**,** e13667.

GROHÉ, C., KAHLERT, S., LÖBBERT, K. & VETTER, H. 1998. Expression of oestrogen receptor alpha and beta in rat heart: role of local oestrogen synthesis. *J Endocrinol,* 156**,** R1-7.

GUO, C., SUN, L., CHEN, X. & ZHANG, D. 2013. Oxidative stress, mitochondrial damage and neurodegenerative diseases. *Neural Regen Res,* 8**,** 2003-14.

GUO, R., GU, J., ZONG, S., WU, M. & YANG, M. 2018. Structure and mechanism of mitochondrial electron transport chain. *Biomed J,* 41**,** 9-20.

GUREEV, A. P., SHAFOROSTOVA, E. A. & POPOV, V. N. 2019. Regulation of Mitochondrial Biogenesis as a Way for Active Longevity: Interaction Between the Nrf2 and PGC-1α Signaling Pathways. *Front Genet,* 10**,** 435.

HAGDORN, Q. A. J., BOSSERS, G. P. L., KOOP, A. C., PIEK, A., EIJGENRAAM, T. R., VAN DER FEEN, D. E., SILLJÉ, H. H. W., DE BOER, R. A. & BERGER, R. M. F. 2019. A novel method optimizing the normalization of cardiac parameters in small animal models: the importance of dimensional indexing. *Am J Physiol Heart Circ Physiol,* 316**,** H1552-h1557.

HAMBERGER, F., LEGCHENKO, E., CHOUVARINE, P., MEDERACKE, Y. S., TAUBERT, R., MEIER, M., JONIGK, D., HANSMANN, G. & MEDERACKE, I. 2022. Pulmonary Arterial Hypertension and Consecutive Right Heart Failure Lead to Liver Fibrosis. *Front Cardiovasc Med,* 9**,** 862330.

HAMUD, A., BREZINS, M., SHTURMAN, A., ABRAMOVICH, A. & DRAGU, R. 2021. Right coronary artery diastolic perfusion pressure on outcome of patients with left heart failure and pulmonary hypertension. *ESC Heart Fail,* 8**,** 4086-4092.

HANDY, D. E. & LOSCALZO, J. 2012. Redox regulation of mitochondrial function. *Antioxid Redox Signal,* 16**,** 1323-67.

HATWALNE, M. S. 2012. Free radical scavengers in anaesthesiology and critical care. *Indian J Anaesth,* 56**,** 227-33.

HE, Q., LIN, Y., ZHU, Y., GAO, L., JI, M., ZHANG, L., XIE, M. & LI, Y. 2023. Clinical Usefulness of Right Ventricle-Pulmonary Artery Coupling in Cardiovascular Disease. *J Clin Med,* 12.

HEIKKINEN, S., SUPPOLA, S., MALKKI, M., DEEB, S. S., JÄNNE, J. & LAAKSO, M. 2000. Mouse hexokinase II gene: structure, cDNA, promoter analysis, and expression pattern. *Mamm Genome,* 11**,** 91-6.

HESTER, J., VENTETUOLO, C. & LAHM, T. 2019. Sex, Gender, and Sex Hormones in Pulmonary Hypertension and Right Ventricular Failure. *Compr Physiol,* 10**,** 125-170.

HO, S. Y. & NIHOYANNOPOULOS, P. 2006. Anatomy, echocardiography, and normal right ventricular dimensions. *Heart,* 92 Suppl 1**,** i2-13.

HOEPER, M. M. & SIMON, R. G. J. 2014. The changing landscape of pulmonary arterial hypertension and implications for patient care. *Eur Respir Rev,* 23**,** 450-7.

HOOD, K. Y., MAIR, K. M., HARVEY, A. P., MONTEZANO, A. C., TOUYZ, R. M. & MACLEAN, M. R. 2017. Serotonin Signaling Through the 5-HT(1B) Receptor and NADPH Oxidase 1 in Pulmonary Arterial Hypertension. *Arterioscler Thromb Vasc Biol,* 37**,** 1361-1370.

HSIEH, Y. C., YANG, S., CHOUDHRY, M. A., YU, H. P., RUE, L. W., 3RD, BLAND, K. I. & CHAUDRY, I. H. 2005. PGC-1 upregulation via estrogen receptors: a common mechanism of salutary effects of estrogen and flutamide on heart function after trauma-hemorrhage. *Am J Physiol Heart Circ Physiol,* 289**,** H2665-72.

HSU, S. 2019. Coupling Right Ventricular-Pulmonary Arterial Research to the Pulmonary Hypertension Patient Bedside. *Circ Heart Fail,* 12**,** e005715.

HU, Q., REN, J., LI, G., WU, J., WU, X., WANG, G., GU, G., REN, H., HONG, Z. & LI, J. 2018. The mitochondrially targeted antioxidant MitoQ protects the intestinal barrier by ameliorating mitochondrial DNA damage via the Nrf2/ARE signaling pathway. *Cell Death Dis,* 9**,** 403.

HUANG, T., SHEN, J., BAO, B., HU, W., SUN, Y., ZHU, T., LIN, J., GAO, T., LI, X. & ZHENG, X. 2022. Mitochondrial-targeting antioxidant MitoQ modulates angiogenesis and promotes functional recovery after spinal cord injury. *Brain Res,* 1786**,** 147902.

HUMBERT, M. & GHOFRANI, H. A. 2016. The molecular targets of approved treatments for pulmonary arterial hypertension. *Thorax,* 71**,** 73-83.

HUMBERT, M., GUIGNABERT, C., BONNET, S., DORFMÜLLER, P., KLINGER, J. R., NICOLLS, M. R., OLSCHEWSKI, A. J., PULLAMSETTI, S. S., SCHERMULY, R. T., STENMARK, K. R. & RABINOVITCH, M. 2019. Pathology and pathobiology of pulmonary hypertension: state of the art and research perspectives. *Eur Respir J,* 53.

HUMBERT, M., KOVACS, G., HOEPER, M. M., BADAGLIACCA, R., BERGER, R. M. F., BRIDA, M., CARLSEN, J., COATS, A. J. S., ESCRIBANO-SUBIAS, P., FERRARI, P., FERREIRA, D. S., GHOFRANI, H. A., GIANNAKOULAS, G., KIELY, D. G., MAYER, E., MESZAROS, G., NAGAVCI, B., OLSSON, K. M., PEPKE-ZABA, J., QUINT, J. K., RÅDEGRAN, G., SIMONNEAU, G., SITBON, O., TONIA, T., TOSHNER, M., VACHIERY, J. L., VONK NOORDEGRAAF, A., DELCROIX, M. & ROSENKRANZ, S. 2022a. 2022 ESC/ERS Guidelines for the diagnosis and treatment of pulmonary hypertension. *Eur Heart J,* 43**,** 3618-3731.

HUMBERT, M., KOVACS, G., HOEPER, M. M., BADAGLIACCA, R., BERGER, R. M. F., BRIDA, M., CARLSEN, J., COATS, A. J. S., ESCRIBANO-SUBIAS, P., FERRARI, P.,

FERREIRA, D. S., GHOFRANI, H. A., GIANNAKOULAS, G., KIELY, D. G., MAYER, E., MESZAROS, G., NAGAVCI, B., OLSSON, K. M., PEPKE-ZABA, J., QUINT, J. K., RÅDEGRAN, G., SIMONNEAU, G., SITBON, O., TONIA, T., TOSHNER, M., VACHIERY, J. L., VONK NOORDEGRAAF, A., DELCROIX, M., ROSENKRANZ, S. & GROUP, E. E. S. D. 2022b. 2022 ESC/ERS Guidelines for the diagnosis and treatment of pulmonary hypertension: Developed by the task force for the diagnosis and treatment of pulmonary hypertension of the European Society of Cardiology (ESC) and the European Respiratory Society (ERS). Endorsed by the International Society for Heart and Lung Transplantation (ISHLT) and the European Reference Network on rare respiratory diseases (ERN-LUNG). *European Heart Journal,* 43**,** 3618-3731.

HUMBERT, M., MCLAUGHLIN, V., GIBBS, J. S. R., GOMBERG-MAITLAND, M., HOEPER, M. M., PRESTON, I. R., SOUZA, R., WAXMAN, A., ESCRIBANO SUBIAS, P., FELDMAN, J., MEYER, G., MONTANI, D., OLSSON, K. M., MANIMARAN, S., BARNES, J., LINDE, P. G., DE OLIVEIRA PENA, J. & BADESCH, D. B. 2021. Sotatercept for the Treatment of Pulmonary Arterial Hypertension. *N Engl J Med,* 384**,** 1204-1215.

HUMBERT, M., MCLAUGHLIN, V., GIBBS, J. S. R., GOMBERG-MAITLAND, M., HOEPER, M. M., PRESTON, I. R., SOUZA, R., WAXMAN, A. B., GHOFRANI, H. A., ESCRIBANO SUBIAS, P., FELDMAN, J., MEYER, G., MONTANI, D., OLSSON, K. M., MANIMARAN, S., DE OLIVEIRA PENA, J. & BADESCH, D. B. 2023. Sotatercept for the treatment of pulmonary arterial hypertension: PULSAR open-label extension. *Eur Respir J,* 61.

HUMBERT, M., MORRELL, N. W., ARCHER, S. L., STENMARK, K. R., MACLEAN, M. R., LANG, I. M., CHRISTMAN, B. W., WEIR, E. K., EICKELBERG, O., VOELKEL, N. F. & RABINOVITCH, M. 2004. Cellular and molecular pathobiology of pulmonary arterial hypertension. *J Am Coll Cardiol,* 43**,** 13s-24s.

HYE, T., DWIVEDI, P., LI, W., LAHM, T., NOZIK-GRAYCK, E., STENMARK, K. R. & AHSAN, F. 2021. Newer insights into the pathobiological and pharmacological basis of the sex disparity in patients with pulmonary arterial hypertension. *Am J Physiol Lung Cell Mol Physiol,* 320**,** L1025-l1037.

IMAMURA, T. & KINUGAWA, K. 2017. Right Ventricular End-Diastolic Pressure Is a Key to the Changes in Cardiac Output During Adaptive Servo-Ventilation Support in Patients With Heart Failure. *Int Heart J,* 58**,** 536-543.

IMPROTA-BREARS, T., WHORTON, A. R., CODAZZI, F., YORK, J. D., MEYER, T. & MCDONNELL, D. P. 1999. Estrogen-induced activation of mitogen-activated protein kinase requires mobilization of intracellular calcium. *Proc Natl Acad Sci U S A,* 96**,** 4686-91.

INAGAKI, T., PEARSON, J. T., TSUCHIMOCHI, H., SCHWENKE, D. O., SAITO, S., HIGUCHI, T., MASAKI, T., UMETANI, K., SHIRAI, M. & NAKAOKA, Y. 2021. Evaluation of right coronary vascular dysfunction in severe pulmonary hypertensive rats using synchrotron radiation microangiography. *Am J Physiol Heart Circ Physiol,* 320**,** H1021-h1036.

IORGA, A., CUNNINGHAM, C. M., MOAZENI, S., RUFFENACH, G., UMAR, S. & EGHBALI, M. 2017. The protective role of estrogen and estrogen receptors in cardiovascular disease and the controversial use of estrogen therapy. *Biol Sex Differ,* 8**,** 33.

IRWIN, R. W., YAO, J., HAMILTON, R. T., CADENAS, E., BRINTON, R. D. & NILSEN, J. 2008. Progesterone and estrogen regulate oxidative metabolism in brain mitochondria. *Endocrinology,* 149**,** 3167-75.

ISHII, T. & WARABI, E. 2019. Mechanism of Rapid Nuclear Factor-E2-Related Factor 2 (Nrf2) Activation via Membrane-Associated Estrogen Receptors: Roles of NADPH Oxidase 1, Neutral Sphingomyelinase 2 and Epidermal Growth Factor Receptor (EGFR). *Antioxidants (Basel),* 8.

JERNIGAN, N. L., NAIK, J. S., WEISE-CROSS, L., DETWEILER, N. D., HERBERT, L. M., YELLOWHAIR, T. R. & RESTA, T. C. 2017. Contribution of reactive oxygen species to the pathogenesis of pulmonary arterial hypertension. *PLoS One,* 12**,** e0180455.

JOHNSON, J., YANG, Y., BIAN, Z., SCHENA, G., LI, Y., ZHANG, X., EATON, D. M., GROSS, P., ANGHELOIU, A., SHAIK, A., FOSTER, M., BERRETTA, R., KUBO, H., MOHSIN, S., TIAN, Y. & HOUSER, S. R. 2023. Systemic Hypoxemia Induces Cardiomyocyte Hypertrophy and Right Ventricular Specific Induction of Proliferation. *Circulation Research,* 132**,** 723-740.

JOHNSON, R. W. 1998. Immune and endocrine regulation of food intake in sick animals. *Domest Anim Endocrinol,* 15**,** 309-19.

JOSHI, S. R., LIU, J., BLOOM, T., KARACA ATABAY, E., KUO, T. H., LEE, M., BELCHEVA, E., SPAITS, M., GRENHA, R., MAGUIRE, M. C., FROST, J. L., WANG, K., BRISCOE, S. D., ALEXANDER, M. J., HERRIN, B. R., CASTONGUAY, R., PEARSALL, R. S., ANDRE, P., YU, P. B., KUMAR, R. & LI, G. 2022. Sotatercept analog suppresses inflammation to reverse experimental pulmonary arterial hypertension. *Sci Rep,* 12**,** 7803.

JUNG, S. & KIM, K. 2014. Exercise-induced PGC-1α transcriptional factors in skeletal muscle. *Integr Med Res,* 3**,** 155-160.

JURKUVENAITE, A., BENAVIDES, G. A., KOMAROVA, S., DORAN, S. F., JOHNSON, M., AGGARWAL, S., ZHANG, J., DARLEY-USMAR, V. M. & MATALON, S. 2015. Upregulation of autophagy decreases chlorine-induced mitochondrial injury and lung inflammation. *Free Radic Biol Med,* 85**,** 83-94.

KAKALETSIS, S., MALINOWSKI, M., MATHUR, M., SUGERMAN, G. P., LUCY, J. J., SNIDER, C., JAZWIEC, T., BERSI, M., TIMEK, T. A. & RAUSCH, M. K. 2023. Untangling the mechanisms of pulmonary hypertension-induced right ventricular stiffening in a large animal model. *bioRxiv*.

KALUDERCIC, N., MIALET-PEREZ, J., PAOLOCCI, N., PARINI, A. & DI LISA, F. 2014. Monoamine oxidases as sources of oxidants in the heart. *J Mol Cell Cardiol,* 73**,** 34-42.

KANG, I., CHU, C. T. & KAUFMAN, B. A. 2018. The mitochondrial transcription factor TFAM in neurodegeneration: emerging evidence and mechanisms. *FEBS Lett,* 592**,** 793-811.

KANG, Y., ZHANG, G., HUANG, E. C., HUANG, J., CAI, J., CAI, L., WANG, S. & KELLER, B. B. 2020. Sulforaphane prevents right ventricular injury and reduces pulmonary vascular remodeling in pulmonary arterial hypertension. *Am J Physiol Heart Circ Physiol,* 318**,** H853-h866.

KAWUT, S. M., FENG, R., ELLENBERG, S. S., ZAMANIAN, R., BULL, T., CHAKINALA, M., MATHAI, S. C., HEMNES, A., LIN, G., DOYLE, M., ANDREW, R., MACLEAN, M., STASINOPOULOS, I., AUSTIN, E., DEMICHELE, A., SHOU, H., MINHAS, J., SONG, N., MOUTCHIA, J. & VENTETUOLO, C. E. 2024. Pulmonary Hypertension and

Anastrozole (PHANTOM): A Randomized, Double-Blind, Placebo-Controlled Trial. *Am J Respir Crit Care Med*.

KEEN, J., PRISCO, S. Z. & PRINS, K. W. 2020. Sex Differences in Right Ventricular Dysfunction: Insights From the Bench to Bedside. *Front Physiol,* 11**,** 623129.

KELSO, G. F., PORTEOUS, C. M., COULTER, C. V., HUGHES, G., PORTEOUS, W. K., LEDGERWOOD, E. C., SMITH, R. A. & MURPHY, M. P. 2001. Selective targeting of a redox-active ubiquinone to mitochondria within cells: antioxidant and antiapoptotic properties. *J Biol Chem,* 276**,** 4588-96.

KEMP, K., SAVALE, L., O'CALLAGHAN, D. S., JAÏS, X., MONTANI, D., HUMBERT, M., SIMONNEAU, G. & SITBON, O. 2012. Usefulness of first-line combination therapy with epoprostenol and bosentan in pulmonary arterial hypertension: an observational study. *J Heart Lung Transplant,* 31**,** 150-8.

KHAN, S. S., CUTTICA, M. J., BEUSSINK-NELSON, L., KOZYLEVA, A., SANCHEZ, C., MKRDICHIAN, H., SELVARAJ, S., DEMATTE, J. E., LEE, D. C. & SHAH, S. J. 2015. Effects of ranolazine on exercise capacity, right ventricular indices, and hemodynamic characteristics in pulmonary arterial hypertension: a pilot study. *Pulm Circ,* 5**,** 547-56.

KIELY, D. G., LAWRIE, A. & HUMBERT, M. 2019. Screening strategies for pulmonary arterial hypertension. *Eur Heart J Suppl,* 21**,** K9-k20.

KIM, S., SONG, J., ERNST, P., LATIMER, M. N., HA, C. M., GOH, K. Y., MA, W., RAJASEKARAN, N. S., ZHANG, J., LIU, X., PRABHU, S. D., QIN, G., WENDE, A. R., YOUNG, M. E. & ZHOU, L. 2020. MitoQ regulates redox-related noncoding RNAs to preserve mitochondrial network integrity in pressure-overload heart failure. *Am J Physiol Heart Circ Physiol,* 318**,** H682-h695.

KINGWELL, K. 2024. FDA approves Merck & Co's pulmonary arterial hypertension drug sotatercept. *Nat Rev Drug Discov,* 23**,** 327.

KLINGE, C. M. 2008. Estrogenic control of mitochondrial function and biogenesis. *J Cell Biochem,* 105**,** 1342-51.

KONDO, T., OKUMURA, N., ADACHI, S. & MUROHARA, T. 2019. ＜Editors' Choice＞ Pulmonary Hypertension: Diagnosis, Management, and Treatment. *Nagoya J Med Sci,* 81**,** 19-30.

KOVES, T. R., LI, P., AN, J., AKIMOTO, T., SLENTZ, D., ILKAYEVA, O., DOHM, G. L., YAN, Z., NEWGARD, C. B. & MUOIO, D. M. 2005. Peroxisome proliferator-activated receptor-gamma co-activator 1alpha-mediated metabolic remodeling of skeletal myocytes mimics exercise training and reverses lipid-induced mitochondrial inefficiency. *J Biol Chem,* 280**,** 33588-98.

KRENTZEL, A. A., WILLETT, J. A., JOHNSON, A. G. & MEITZEN, J. 2021. Estrogen receptor alpha, G-protein coupled estrogen receptor 1, and aromatase: Developmental, sex, and region-specific differences across the rat caudate-putamen, nucleus accumbens core and shell. *J Comp Neurol,* 529**,** 786-801.

LABAZI, H., AITCHISON, G., DIGNAM, J., SHARMA, S. & MACLEAN, M. R. 2023. *Direct Delivery of MicroRNA-96 to the Lungs of Sugen/Hypoxic Rats Reduces an Estrogen Metabolizing Enzyme and Fibrotic Markers Gene Expression in the Lungs*.

LAHM, T., ALBRECHT, M., FISHER, A. J., SELEJ, M., PATEL, N. G., BROWN, J. A., JUSTICE, M. J., BROWN, M. B., VAN DEMARK, M., TRULOCK, K. M., DIEUDONNE, D., REDDY, J. G., PRESSON, R. G. & PETRACHE, I. 2012. 17β-Estradiol attenuates

hypoxic pulmonary hypertension via estrogen receptor-mediated effects. *Am J Respir Crit Care Med,* 185**,** 965-80.

LAHM, T., DOUGLAS, I. S., ARCHER, S. L., BOGAARD, H. J., CHESLER, N. C., HADDAD, F., HEMNES, A. R., KAWUT, S. M., KLINE, J. A., KOLB, T. M., MATHAI, S. C., MERCIER, O., MICHELAKIS, E. D., NAEIJE, R., TUDER, R. M., VENTETUOLO, C. E., VIEILLARD-BARON, A., VOELKEL, N. F., VONK-NOORDEGRAAF, A. & HASSOUN, P. M. 2018. Assessment of Right Ventricular Function in the Research Setting: Knowledge Gaps and Pathways Forward. An Official American Thoracic Society Research Statement. *Am J Respir Crit Care Med,* 198**,** e15-e43.

LAHM, T., FRUMP, A. L., ALBRECHT, M. E., FISHER, A. J., COOK, T. G., JONES, T. J., YAKUBOV, B., WHITSON, J., FUCHS, R. K., LIU, A., CHESLER, N. C. & BROWN, M. B. 2016. 17β-Estradiol mediates superior adaptation of right ventricular function to acute strenuous exercise in female rats with severe pulmonary hypertension. *Am J Physiol Lung Cell Mol Physiol,* 311**,** L375-88.

LAHM, T., TUDER, R. M. & PETRACHE, I. 2014. Progress in solving the sex hormone paradox in pulmonary hypertension. *Am J Physiol Lung Cell Mol Physiol,* 307**,** L7-26.

LEVEILLE, C. F., MIKHAEIL, J. S., TURNER, K. D., SILVERA, S., WILKINSON, J. & FAJARDO, V. A. 2017. Mitochondrial cristae density: a dynamic entity that is critical for energy production and metabolic power in skeletal muscle. *J Physiol,* 595**,** 2779-2780.

LEVIN, E. R. & HAMMES, S. R. 2016. Nuclear receptors outside the nucleus: extranuclear signalling by steroid receptors. *Nat Rev Mol Cell Biol,* 17**,** 783-797.

LI, H., GUO, Y., SU, W., ZHANG, H., WEI, X., MA, X., GONG, S., QU, G., ZHANG, L., XU, H., SHEN, F., JIANG, S., XU, D. & LI, J. 2024a. The mitochondria-targeted antioxidant MitoQ ameliorates inorganic arsenic-induced DCs/Th1/Th2/Th17/Treg differentiation partially by activating PINK1-mediated mitophagy in murine liver. *Ecotoxicol Environ Saf,* 277**,** 116350.

LI, H. Y., BIAN, J. S., KWAN, Y. W. & WONG, T. M. 2000. Enhanced responses to 17beta-estradiol in rat hearts treated with isoproterenol: involvement of a cyclic AMP-dependent pathway. *J Pharmacol Exp Ther,* 293**,** 592-8.

LI, S., LYU, Q., SHI, Q., BAI, Y., REN, X. & MA, J. 2024b. Intermittent short-duration reoxygenation relieves high-altitude pulmonary hypertension via NOX4/H2O2/PPAR-γ axis. *Clin Sci (Lond),* 138**,** 103-115.

LI, X. B., GU, J. D. & ZHOU, Q. H. 2015. Review of aerobic glycolysis and its key enzymes - new targets for lung cancer therapy. *Thorac Cancer,* 6**,** 17-24.

LIANG, H. & WARD, W. F. 2006. PGC-1alpha: a key regulator of energy metabolism. *Adv Physiol Educ,* 30**,** 145-51.

LIBERMAN, E. A., TOPALY, V. P., TSOFINA, L. M., JASAITIS, A. A. & SKULACHEV, V. P. 1969. Mechanism of coupling of oxidative phosphorylation and the membrane potential of mitochondria. *Nature,* 222**,** 1076-8.

LILES, J., OLIVER, J., CHI, L., DHALLA, A. & BELARDINELLI, L. 2012. Abstract 11990: Ranolazine Reduces Monocrotaline-induced Pulmonary Hypertension when Administered Following Disease Induction. *Circulation,* 126**,** A11990-A11990.

LIN, J., HANDSCHIN, C. & SPIEGELMAN, B. M. 2005. Metabolic control through the PGC-1 family of transcription coactivators. *Cell Metab,* 1**,** 361-70.

LINDSEY, S. H., LIU, L. & CHAPPELL, M. C. 2014. Vasodilation by GPER in mesenteric arteries involves both endothelial nitric oxide and smooth muscle cAMP signaling. *Steroids,* 81**,** 99-102.

LING, Y., JOHNSON, M. K., KIELY, D. G., CONDLIFFE, R., ELLIOT, C. A., GIBBS, J. S. R., HOWARD, L. S., PEPKE-ZABA, J., SHEARES, K. K. K., CORRIS, P. A., FISHER, A. J., LORDAN, J. L., GAINE, S., COGHLAN, J. G., WORT, S. J., GATZOULIS, M. A. & PEACOCK, A. J. 2012. Changing Demographics, Epidemiology, and Survival of Incident Pulmonary Arterial Hypertension. *American Journal of Respiratory and Critical Care Medicine,* 186**,** 790-796.

LIU, A., PHILIP, J., VINNAKOTA, K. C., VAN DEN BERGH, F., TABIMA, D. M., HACKER, T., BEARD, D. A. & CHESLER, N. C. 2017. Estrogen maintains mitochondrial content and function in the right ventricle of rats with pulmonary hypertension. *Physiol Rep,* 5.

LIU, A., SCHREIER, D., TIAN, L., EICKHOFF, J. C., WANG, Z., HACKER, T. A. & CHESLER, N. C. 2014. Direct and indirect protection of right ventricular function by estrogen in an experimental model of pulmonary arterial hypertension. *Am J Physiol Heart Circ Physiol,* 307**,** H273-83.

LIU, S., DING, T., LIU, H. & JIAN, L. 2018. GPER was Associated with Hypertension in Post-Menopausal Women. *Open Med (Wars),* 13**,** 338-343.

LONG, G. M., TROUTMAN, A. D., GRAY, D. A., FISHER, A. J., LAHM, T., COGGAN, A. R. & BROWN, M. B. 2022. Skeletal muscle blood flow during exercise is reduced in a rat model of pulmonary hypertension. *Am J Physiol Regul Integr Comp Physiol,* 323**,** R561-r570.

LONG, J., RUSSO, M. J., MULLER, C. & VIGNESWARAN, W. T. 2011. Surgical treatment of pulmonary hypertension: Lung transplantation. *Pulm Circ,* 1**,** 327-33.

LOPES, R. A., NEVES, K. B., TOSTES, R. C., MONTEZANO, A. C. & TOUYZ, R. M. 2015. Downregulation of Nuclear Factor Erythroid 2-Related Factor and Associated Antioxidant Genes Contributes to Redox-Sensitive Vascular Dysfunction in Hypertension. *Hypertension,* 66**,** 1240-50.

LU, H. I., HUANG, T. H., SUNG, P. H., CHEN, Y. L., CHUA, S., CHAI, H. Y., CHUNG, S. Y., LIU, C. F., SUN, C. K., CHANG, H. W., ZHEN, Y. Y., LEE, F. Y. & YIP, H. K. 2016a. Administration of antioxidant peptide SS-31 attenuates transverse aortic constriction-induced pulmonary arterial hypertension in mice. *Acta Pharmacol Sin,* 37**,** 589-603.

LU, Z., LI, S., ZHAO, S. & FA, X. 2016b. Upregulated miR-17 Regulates Hypoxia-Mediated Human Pulmonary Artery Smooth Muscle Cell Proliferation and Apoptosis by Targeting Mitofusin 2. *Med Sci Monit,* 22**,** 3301-8.

LUO, F., FU, M., WANG, T., QI, Y., ZHONG, X., LI, D. & LIU, B. 2023. Down-regulation of the mitochondrial fusion protein Opa1/Mfn2 promotes cardiomyocyte hypertrophy in Su5416/hypoxia-induced pulmonary hypertension rats. *Arch Biochem Biophys,* 747**,** 109743.

LUO, S., VALENCIA, C. A., ZHANG, J., LEE, N. C., SLONE, J., GUI, B., WANG, X., LI, Z., DELL, S., BROWN, J., CHEN, S. M., CHIEN, Y. H., HWU, W. L., FAN, P. C., WONG, L. J., ATWAL, P. S. & HUANG, T. 2018. Biparental Inheritance of Mitochondrial DNA in Humans. *Proc Natl Acad Sci U S A,* 115**,** 13039-13044.

LUO, T. & KIM, J. K. 2016. The Role of Estrogen and Estrogen Receptors on Cardiomyocytes: An Overview. *Can J Cardiol,* 32**,** 1017-25.

MA, L., WANG, Y., LI, X., WANG, Z., ZHANG, B., LUO, Y., WU, Y., LI, Z. & NIU, W. 2023. Tom70-regulated mitochondrial biogenesis via TFAM improves hypoxia-induced dysfunction of pulmonary vascular endothelial cells and alleviates hypoxic pulmonary hypertension. *Respir Res,* 24**,** 310.

MAARMAN, G., LECOUR, S., BUTROUS, G., THIENEMANN, F. & SLIWA, K. 2013. A comprehensive review: the evolution of animal models in pulmonary hypertension research; are we there yet? *Pulm Circ,* 3**,** 739-56.

MACLEAN, M. M. R. 2018. The serotonin hypothesis in pulmonary hypertension revisited: targets for novel therapies (2017 Grover Conference Series). *Pulm Circ,* 8**,** 2045894018759125.

MACLEAN, M. R. & DEMPSIE, Y. 2010. The serotonin hypothesis of pulmonary hypertension revisited. *Adv Exp Med Biol,* 661**,** 309-22.

MAIR, K. M., HARVEY, K. Y., HENRY, A. D., HILLYARD, D. Z., NILSEN, M. & MACLEAN, M. R. 2019. Obesity alters oestrogen metabolism and contributes to pulmonary arterial hypertension. *Eur Respir J,* 53.

MAIR, K. M., JOHANSEN, A. K., WRIGHT, A. F., WALLACE, E. & MACLEAN, M. R. 2014a. Pulmonary arterial hypertension: basis of sex differences in incidence and treatment response. *Br J Pharmacol,* 171**,** 567-79.

MAIR, K. M., WRIGHT, A. F., DUGGAN, N., ROWLANDS, D. J., HUSSEY, M. J., ROBERTS, S., FULLERTON, J., NILSEN, M., LOUGHLIN, L., THOMAS, M. & MACLEAN, M. R. 2014b. Sex-dependent influence of endogenous estrogen in pulmonary hypertension. *Am J Respir Crit Care Med,* 190**,** 456-67.

MAIR, K. M., YANG, X. D., LONG, L., WHITE, K., WALLACE, E., EWART, M. A., DOCHERTY, C. K., MORRELL, N. W. & MACLEAN, M. R. 2015. Sex affects bone morphogenetic protein type II receptor signaling in pulmonary artery smooth muscle cells. *Am J Respir Crit Care Med,* 191**,** 693-703.

MAMAZHAKYPOV, A., SOMMER, N., ASSMUS, B., TELLO, K., SCHERMULY, R. T., KOSANOVIC, D., SARYBAEV, A. S., WEISSMANN, N. & PAK, O. 2021. Novel Therapeutic Targets for the Treatment of Right Ventricular Remodeling: Insights from the Pulmonary Artery Banding Model. *Int J Environ Res Public Health,* 18.

MAMAZHAKYPOV, A., WEIS, A., ZUKUNFT, S., SYDYKOV, A., KOJONAZAROV, B., WILHELM, J., VROOM, C., PETROVIC, A., KOSANOVIC, D., WEISSMANN, N., SEEGER, W., FLEMING, I., IGLARZ, M., GRIMMINGER, F., GHOFRANI, H. A., PULLAMSETTI, S. S. & SCHERMULY, R. T. 2020. Effects of macitentan and tadalafil monotherapy or their combination on the right ventricle and plasma metabolites in pulmonary hypertensive rats. *Pulm Circ,* 10**,** 2045894020947283.

MARLOVITS, S., HOMBAUER, M., TRUPPE, M., VÈCSEI, V. & SCHLEGEL, W. 2004. Changes in the ratio of type-I and type-II collagen expression during monolayer culture of human chondrocytes. *J Bone Joint Surg Br,* 86**,** 286-95.

MARSBOOM, G., TOTH, P. T., RYAN, J. J., HONG, Z., WU, X., FANG, Y. H., THENAPPAN, T., PIAO, L., ZHANG, H. J., POGORILER, J., CHEN, Y., MORROW, E., WEIR, E. K., REHMAN, J. & ARCHER, S. L. 2012. Dynamin-related protein 1-mediated mitochondrial mitotic fission permits hyperproliferation of vascular smooth muscle cells and offers a novel therapeutic target in pulmonary hypertension. *Circ Res,* 110**,** 1484-97.

MARTÍNEZ DE TODA, I., GONZÁLEZ-SÁNCHEZ, M., DÍAZ-DEL CERRO, E., VALERA, G., CARRACEDO, J. & GUERRA-PÉREZ, N. 2023. Sex differences in markers of

oxidation and inflammation. Implications for ageing. *Mech Ageing Dev,* 211**,** 111797.

MATTHEWS, J. & MCLAUGHLIN, V. 2008. Acute Right Ventricular Failure in the Setting of Acute Pulmonary Embolism or Chronic Pulmonary Hypertension: A Detailed Review of the Pathophysiology, Diagnosis, and Management. *Current Cardiology Reviews,* 4**,** 49-59.

MAZUREK, R., DAVE, J. M., CHANDRAN, R. R., MISRA, A., SHEIKH, A. Q. & GREIF, D. M. 2017. Vascular Cells in Blood Vessel Wall Development and Disease. *Adv Pharmacol,* 78**,** 323-350.

MCLAUGHLIN, V. V., PRESBERG, K. W., DOYLE, R. L., ABMAN, S. H., MCCRORY, D. C., FORTIN, T. & AHEARN, G. 2004. Prognosis of pulmonary arterial hypertension: ACCP evidence-based clinical practice guidelines. *Chest,* 126**,** 78s-92s.

MCLEAN, L. L., PELLINO, K., BREWIS, M., PEACOCK, A., JOHNSON, M. & CHURCH, A. C. 2019. The obesity paradox in pulmonary arterial hypertension: the Scottish perspective. *ERJ Open Res,* 5.

MEDAROV, B. I. & JUDSON, M. A. 2015. The role of calcium channel blockers for the treatment of pulmonary arterial hypertension: How much do we actually know and how could they be positioned today? *Respir Med,* 109**,** 557-64.

MELOCHE, J., LAMPRON, M. C., NADEAU, V., MALTAIS, M., POTUS, F., LAMBERT, C., TREMBLAY, E., VITRY, G., BREUILS-BONNET, S., BOUCHERAT, O., CHARBONNEAU, E., PROVENCHER, S., PAULIN, R. & BONNET, S. 2017. Implication of Inflammation and Epigenetic Readers in Coronary Artery Remodeling in Patients With Pulmonary Arterial Hypertension. *Arterioscler Thromb Vasc Biol,* 37**,** 1513-1523.

MEMON, H. A. & PARK, M. H. 2017. Pulmonary Arterial Hypertension in Women. *Methodist Debakey Cardiovasc J,* 13**,** 224-237.

MENDELSOHN, M. E. & KARAS, R. H. 1999. The protective effects of estrogen on the cardiovascular system. *N Engl J Med,* 340**,** 1801-11.

MÉNDEZ, D., ARAUNA, D., FUENTES, F., ARAYA-MATURANA, R., PALOMO, I., ALARCÓN, M., SEBASTIÁN, D., ZORZANO, A. & FUENTES, E. 2020. Mitoquinone (MitoQ) Inhibits Platelet Activation Steps by Reducing ROS Levels. *Int J Mol Sci,* 21.

MEYER, J. N., LEUTHNER, T. C. & LUZ, A. L. 2017. Mitochondrial fusion, fission, and mitochondrial toxicity. *Toxicology,* 391**,** 42-53.

MEYER, M. R., AMANN, K., FIELD, A. S., HU, C., HATHAWAY, H. J., KANAGY, N. L., WALKER, M. K., BARTON, M. & PROSSNITZ, E. R. 2012. Deletion of G protein-coupled estrogen receptor increases endothelial vasoconstriction. *Hypertension,* 59**,** 507-12.

MIKHAEL, M., MAKAR, C., WISSA, A., LE, T., EGHBALI, M. & UMAR, S. 2019. Oxidative Stress and Its Implications in the Right Ventricular Remodeling Secondary to Pulmonary Hypertension. *Front Physiol,* 10**,** 1233.

MIN, J., FENG, R., BADESCH, D., BERMAN-ROSENZWEIG, E., BURGER, C., CHAKINALA, M., DE MARCO, T., FELDMAN, J., HEMNES, A., HORN, E. M., LAMMI, M. R., MATHAI, S., MCCONNELL, J. W., PRESBERG, K., ROBINSON, J., SAGER, J., SHLOBIN, O. A., SIMON, M., THENAPPAN, T., VENTETUOLO, C. & AL-NAAMANI, N. 2020. Obesity in Pulmonary Arterial Hypertension (PAH): The Pulmonary Hypertension Association Registry (PHAR). *Ann Am Thorac Soc,* 18**,** 229-37.

MONTANI, D., GÜNTHER, S., DORFMÜLLER, P., PERROS, F., GIRERD, B., GARCIA, G., JAÏS, X., SAVALE, L., ARTAUD-MACARI, E., PRICE, L. C., HUMBERT, M., SIMONNEAU, G. & SITBON, O. 2013a. Pulmonary arterial hypertension. *Orphanet J Rare Dis,* 8**,** 97.

MONTANI, D., SEFERIAN, A., SAVALE, L., SIMONNEAU, G. & HUMBERT, M. 2013b. Drug-induced pulmonary arterial hypertension: a recent outbreak. *European Respiratory Review,* 22**,** 244-250.

MORENO, A. J., MOREIRA, P. I., CUSTÓDIO, J. B. & SANTOS, M. S. 2013. Mechanism of inhibition of mitochondrial ATP synthase by 17β-estradiol. *J Bioenerg Biomembr,* 45**,** 261-70.

MORRIS, H., DENVER, N., GAW, R., LABAZI, H., MAIR, K. & MACLEAN, M. R. 2021. Sex Differences in Pulmonary Hypertension. *Clin Chest Med,* 42**,** 217-228.

MURPHY, M. P. 1997. Selective targeting of bioactive compounds to mitochondria. *Trends Biotechnol,* 15**,** 326-30.

NAEIJE, R. 2015. Assessment of Right Ventricular Function in Pulmonary Hypertension. *Current Hypertension Reports,* 17**,** 35.

NATARAJ, K., SCHONFELD, M., RODRIGUEZ, A. & TIKHANOVICH, I. 2024. Protective role of 17β-estradiol in alcohol-associated liver fibrosis is mediated by suppression of integrin signaling. *Hepatol Commun,* 8.

NGO, V. & DUENNWALD, M. L. 2022. Nrf2 and Oxidative Stress: A General Overview of Mechanisms and Implications in Human Disease. *Antioxidants (Basel),* 11.

NICOLLS, M. R., MIZUNO, S., TARASEVICIENE-STEWART, L., FARKAS, L., DRAKE, J. I., AL HUSSEINI, A., GOMEZ-ARROYO, J. G., VOELKEL, N. F. & BOGAARD, H. J. 2012. New models of pulmonary hypertension based on VEGF receptor blockade-induced endothelial cell apoptosis. *Pulm Circ,* 2**,** 434-42.

NOGUEIRA-FERREIRA, R., FERREIRA, R. & HENRIQUES-COELHO, T. 2014. Cellular interplay in pulmonary arterial hypertension: implications for new therapies. *Biochim Biophys Acta,* 1843**,** 885-93.

NOZIK-GRAYCK, E. & STENMARK, K. R. 2007. Role of reactive oxygen species in chronic hypoxia-induced pulmonary hypertension and vascular remodeling. *Adv Exp Med Biol,* 618**,** 101-12.

OKEN, D. E. & BOUCEK, R. J. 1957. Quantitation of Collagen in Human Myocardium. *Circulation Research,* 5**,** 357-361.

OSELLAME, L. D., BLACKER, T. S. & DUCHEN, M. R. 2012. Cellular and molecular mechanisms of mitochondrial function. *Best Pract Res Clin Endocrinol Metab,* 26**,** 711-23.

PAK, O., SCHEIBE, S., ESFANDIARY, A., GIERHARDT, M., SYDYKOV, A., LOGAN, A., FYSIKOPOULOS, A., VEIT, F., HECKER, M., KROSCHEL, F., QUANZ, K., ERB, A., SCHÄFER, K., FASSBINDER, M., ALEBRAHIMDEHKORDI, N., GHOFRANI, HOSSEIN A., SCHERMULY, R. T., BRANDES, R. P., SEEGER, W., MURPHY, M. P., WEISSMANN, N. & SOMMER, N. 2018. Impact of the mitochondria-targeted antioxidant MitoQ on hypoxia-induced pulmonary hypertension. *European Respiratory Journal,* 51**,** 1701024.

PARADIES, G., PARADIES, V., RUGGIERO, F. M. & PETROSILLO, G. 2019. Role of Cardiolipin in Mitochondrial Function and Dynamics in Health and Disease: Molecular and Pharmacological Aspects. *Cells,* 8.

PEDRAM, A., RAZANDI, M., WALLACE, D. C. & LEVIN, E. R. 2006. Functional estrogen receptors in the mitochondria of breast cancer cells. *Mol Biol Cell,* 17**,** 2125-37.

PENG, H., XIAO, Y., DENG, X., LUO, J., HONG, C. & QIN, X. 2016. The Warburg effect: A new story in pulmonary arterial hypertension. *Clin Chim Acta,* 461**,** 53-8.

PIAO, L., FANG, Y. H., CADETE, V. J., WIETHOLT, C., URBONIENE, D., TOTH, P. T., MARSBOOM, G., ZHANG, H. J., HABER, I., REHMAN, J., LOPASCHUK, G. D. & ARCHER, S. L. 2010. The inhibition of pyruvate dehydrogenase kinase improves impaired cardiac function and electrical remodeling in two models of right ventricular hypertrophy: resuscitating the hibernating right ventricle. *J Mol Med (Berl),* 88**,** 47-60.

PIAO, L., FANG, Y. H., PARIKH, K., RYAN, J. J., TOTH, P. T. & ARCHER, S. L. 2013a. Cardiac glutaminolysis: a maladaptive cancer metabolism pathway in the right ventricle in pulmonary hypertension. *J Mol Med (Berl),* 91**,** 1185-97.

PIAO, L., SIDHU, V. K., FANG, Y. H., RYAN, J. J., PARIKH, K. S., HONG, Z., TOTH, P. T., MORROW, E., KUTTY, S., LOPASCHUK, G. D. & ARCHER, S. L. 2013b. FOXO1-mediated upregulation of pyruvate dehydrogenase kinase-4 (PDK4) decreases glucose oxidation and impairs right ventricular function in pulmonary hypertension: therapeutic benefits of dichloroacetate. *J Mol Med (Berl),* 91**,** 333-46.

PICCA, A. & LEZZA, A. M. 2015. Regulation of mitochondrial biogenesis through TFAM-mitochondrial DNA interactions: Useful insights from aging and calorie restriction studies. *Mitochondrion,* 25**,** 67-75.

PINSKY, M. R. 2016. The right ventricle: interaction with the pulmonary circulation. *Critical Care,* 20.

PIQUEREAU, J., CAFFIN, F., NOVOTOVA, M., LEMAIRE, C., VEKSLER, V., GARNIER, A., VENTURA-CLAPIER, R. & JOUBERT, F. 2013. Mitochondrial dynamics in the adult cardiomyocytes: which roles for a highly specialized cell? *Front Physiol,* 4**,** 102.

POKHAREL, M. D., MARCIANO, D. P., FU, P., FRANCO, M. C., UNWALLA, H., TIEU, K., FINEMAN, J. R., WANG, T. & BLACK, S. M. 2023. Metabolic reprogramming, oxidative stress, and pulmonary hypertension. *Redox Biol,* 64**,** 102797.

POMS, A. D., TURNER, M., FARBER, H. W., MELTZER, L. A. & MCGOON, M. D. 2013. Comorbid conditions and outcomes in patients with pulmonary arterial hypertension: a REVEAL registry analysis. *Chest,* 144**,** 169-176.

PRESLEY, A. D., FULLER, K. M. & ARRIAGA, E. A. 2003. MitoTracker Green labeling of mitochondrial proteins and their subsequent analysis by capillary electrophoresis with laser-induced fluorescence detection. *J Chromatogr B Analyt Technol Biomed Life Sci,* 793**,** 141-50.

PRINS, K. W. & THENAPPAN, T. 2016. World Health Organization Group I Pulmonary Hypertension: Epidemiology and Pathophysiology. *Cardiol Clin,* 34**,** 363-74.

PROSSNITZ, E. R. & HATHAWAY, H. J. 2015. What have we learned about GPER function in physiology and disease from knockout mice? *J Steroid Biochem Mol Biol,* 153**,** 114-26.

PUNETHA, M., SAINI, S., CHAUDHARY, S., BALA, R., SHARMA, M., KUMAR, P., KUMAR, D. & YADAV, P. S. 2023. Mitochondria-targeted antioxidant MitoQ ameliorates ROS production and improves cell viability in cryopreserved buffalo fibroblasts. *Tissue Cell,* 82**,** 102067.

QIN, Y., QIAO, Y., WANG, D., LI, L., LI, M., YAN, G. & TANG, C. 2022. Target Nuclear Factor Erythroid 2-Related Factor 2 in Pulmonary Hypertension: Molecular Insight into Application. *Oxid Med Cell Longev,* 2022**,** 7845503.

RABINOVITCH, M., GAMBLE, W. J., MIETTINEN, O. S. & REID, L. 1981. Age and sex influence on pulmonary hypertension of chronic hypoxia and on recovery. *Am J Physiol,* 240**,** H62-72.

RAFIKOVA, O., RAFIKOV, R., MEADOWS, M. L., KANGATH, A., JONIGK, D. & BLACK, S. M. 2015. The sexual dimorphism associated with pulmonary hypertension corresponds to a fibrotic phenotype. *Pulm Circ,* 5**,** 184-97.

RAIN, S., HANDOKO, M. L., TRIP, P., GAN, C. T.-J., WESTERHOF, N., STIENEN, G. J., PAULUS, W. J., OTTENHEIJM, C. A. C., MARCUS, J. T., DORFMÜLLER, P., GUIGNABERT, C., HUMBERT, M., MACDONALD, P., REMEDIOS, C. D., POSTMUS, P. E., SARIPALLI, C., HIDALGO, C. G., GRANZIER, H. L., VONK-NOORDEGRAAF, A., VELDEN, J. V. D. & MAN, F. S. D. 2013. Right Ventricular Diastolic Impairment in Patients With Pulmonary Arterial Hypertension. *Circulation,* 128**,** 2016-2025.

RANA, B. S., ROBINSON, S., FRANCIS, R., TOSHNER, M., SWAANS, M. J., AGARWAL, S., DE SILVA, R., RANA, A. A. & NIHOYANNOPOULOS, P. 2019. Tricuspid regurgitation and the right ventricle in risk stratification and timing of intervention. *Echo Research and Practice,* 6**,** R25-R39.

RAY, P. D., HUANG, B. W. & TSUJI, Y. 2012. Reactive oxygen species (ROS) homeostasis and redox regulation in cellular signaling. *Cell Signal,* 24**,** 981-90.

RAZMARA, A., DUCKLES, S. P., KRAUSE, D. N. & PROCACCIO, V. 2007. Estrogen suppresses brain mitochondrial oxidative stress in female and male rats. *Brain Res,* 1176**,** 71-81.

REDDY, S. & BERNSTEIN, D. 2015. Molecular Mechanisms of Right Ventricular Failure. *Circulation,* 132**,** 1734-42.

REDOUT, E. M., WAGNER, M. J., ZUIDWIJK, M. J., BOER, C., MUSTERS, R. J., VAN HARDEVELD, C., PAULUS, W. J. & SIMONIDES, W. S. 2007. Right-ventricular failure is associated with increased mitochondrial complex II activity and production of reactive oxygen species. *Cardiovasc Res,* 75**,** 770-81.

REN, X., JOHNS, R. A. & GAO, W. D. 2019. EXPRESS: Right Heart in Pulmonary Hypertension: From Adaptation to Failure. *Pulm Circ,* 9**,** 2045894019845611.

RESTA, T. C., KANAGY, N. L. & WALKER, B. R. 2001. Estradiol-induced attenuation of pulmonary hypertension is not associated with altered eNOS expression. *Am J Physiol Lung Cell Mol Physiol,* 280**,** L88-97.

REVANKAR, C. M., CIMINO, D. F., SKLAR, L. A., ARTERBURN, J. B. & PROSSNITZ, E. R. 2005. A transmembrane intracellular estrogen receptor mediates rapid cell signaling. *Science,* 307**,** 1625-30.

RIOU, M., ENACHE, I., SAUER, F., CHARLES, A. L. & GENY, B. 2023. Targeting Mitochondrial Metabolic Dysfunction in Pulmonary Hypertension: Toward New Therapeutic Approaches? *Int J Mol Sci,* 24.

RODRIGUEZ-ARIAS, J. J. & GARCÍA-ÁLVAREZ, A. 2021. Sex Differences in Pulmonary Hypertension. *Front Aging,* 2**,** 727558.

RODRIGUEZ-CUENCA, S., COCHEMÉ, H. M., LOGAN, A., ABAKUMOVA, I., PRIME, T. A., ROSE, C., VIDAL-PUIG, A., SMITH, A. C., RUBINSZTEIN, D. C., FEARNLEY, I. M., JONES, B. A., POPE, S., HEALES, S. J., LAM, B. Y., NEOGI, S. G., MCFARLANE, I., JAMES, A. M., SMITH, R. A. & MURPHY, M. P. 2010. Consequences of long-term

oral administration of the mitochondria-targeted antioxidant MitoQ to wild-type mice. *Free Radic Biol Med,* 48**,** 161-72.

ROELOFS, B. A., GE, S. X., STUDLACK, P. E. & POLSTER, B. M. 2015. Low micromolar concentrations of the superoxide probe MitoSOX uncouple neural mitochondria and inhibit complex IV. *Free Radic Biol Med,* 86**,** 250-8.

ROMANO, S. N. & GORELICK, D. A. 2018. Crosstalk between nuclear and G protein-coupled estrogen receptors. *Gen Comp Endocrinol,* 261**,** 190-197.

ROSARIO, G. X., KATKAM, R. R., NIMBKAR-JOSHI, S., MODI, D. N., MANJRAMKAR, D. D., HINDUJA, I., ZAVERI, K., PURI, C. P. & SACHDEVA, G. 2009. Expression of endometrial protein kinase a during early pregnancy in bonnet monkeys (Macaca radiata). *Biol Reprod,* 81**,** 1172-81.

RYAN, J., DASGUPTA, A., HUSTON, J., CHEN, K. H. & ARCHER, S. L. 2015a. Mitochondrial dynamics in pulmonary arterial hypertension. *J Mol Med (Berl),* 93**,** 229-42.

RYAN, J. J. & ARCHER, S. L. 2014. The right ventricle in pulmonary arterial hypertension: disorders of metabolism, angiogenesis and adrenergic signaling in right ventricular failure. *Circ Res,* 115**,** 176-88.

RYAN, J. J. & ARCHER, S. L. 2015. Emerging Concepts in the Molecular Basis of Pulmonary Arterial Hypertension. *Circulation,* 131**,** 1691-1702.

RYAN, J. J., HUSTON, J., KUTTY, S., HATTON, N. D., BOWMAN, L., TIAN, L., HERR, J. E., JOHRI, A. M. & ARCHER, S. L. 2015b. Right ventricular adaptation and failure in pulmonary arterial hypertension. *Can J Cardiol,* 31**,** 391-406.

RYAN, J. J., MARSBOOM, G., FANG, Y. H., TOTH, P. T., MORROW, E., LUO, N., PIAO, L., HONG, Z., ERICSON, K., ZHANG, H. J., HAN, M., HANEY, C. R., CHEN, C. T., SHARP, W. W. & ARCHER, S. L. 2013. PGC1α-mediated mitofusin-2 deficiency in female rats and humans with pulmonary arterial hypertension. *Am J Respir Crit Care Med,* 187**,** 865-78.

RYANTO, G. R. T., SURAYA, R. & NAGANO, T. 2023. Mitochondrial Dysfunction in Pulmonary Hypertension. *Antioxidants (Basel),* 12.

SABBAH, H. N., GUPTA, R. C., KOHLI, S., WANG, M., HACHEM, S. & ZHANG, K. 2016. Chronic Therapy With Elamipretide (MTP-131), a Novel Mitochondria-Targeting Peptide, Improves Left Ventricular and Mitochondrial Function in Dogs With Advanced Heart Failure. *Circ Heart Fail,* 9**,** e002206.

SAFDAR, Z., TAMEZ, E., CHAN, W., ARYA, B., GE, Y., DESWAL, A., BOZKURT, B., FROST, A. & ENTMAN, M. 2014. Circulating collagen biomarkers as indicators of disease severity in pulmonary arterial hypertension. *JACC Heart Fail,* 2**,** 412-21.

SAHAY, S. 2019. Evaluation and classification of pulmonary arterial hypertension. *J Thorac Dis,* 11**,** S1789-s1799.

SAKTI MULIAWAN, H., WIDYANTORO, B., SOERARSO, R., HERSUNARTI, N., SAHARA, E., ATMADIKOESOEMAH, C. A., KASIM, M., ADIARTO, S., RAHARJO, S. B., SUKMAWAN, R. & SISWANTO, B. B. 2020. P194 Trimetazidine preserves right ventricular function on pulmonary arterial hypertension patients in national cardiovascular center harapan kita hospital indonesia. *European Heart Journal,* 41.

SAMANGOUEI, P., CRESPO-AVILAN, G. E., CABRERA-FUENTES, H., HERNÁNDEZ-RESÉNDIZ, S., ISMAIL, N. I., KATWADI, K. B., BOISVERT, W. A. & HAUSENLOY, D. J. 2018. MiD49 and MiD51: New mediators of mitochondrial fission and novel targets for cardioprotection. *Cond Med,* 1**,** 239-246.

SANTOS, E. W., KHATOON, S., DI MISE, A., ZHENG, Y.-M. & WANG, Y.-X. 2024. Mitochondrial Dynamics in Pulmonary Hypertension. *Biomedicines,* 12**,** 53.

SARETZKI, G., MURPHY, M. P. & VON ZGLINICKI, T. 2003. MitoQ counteracts telomere shortening and elongates lifespan of fibroblasts under mild oxidative stress. *Aging Cell,* 2**,** 141-3.

SCARPULLA, R. C. 2011. Metabolic control of mitochondrial biogenesis through the PGC-1 family regulatory network. *Biochim Biophys Acta,* 1813**,** 1269-78.

SCHIMMEL, K., ICHIMURA, K., REDDY, S., HADDAD, F. & SPIEKERKOETTER, E. 2022. Cardiac Fibrosis in the Pressure Overloaded Left and Right Ventricle as a Therapeutic Target. *Front Cardiovasc Med,* 9**,** 886553.

SCHULZ, E., WENZEL, P., MÜNZEL, T. & DAIBER, A. 2014. Mitochondrial redox signaling: Interaction of mitochondrial reactive oxygen species with other sources of oxidative stress. *Antioxid Redox Signal,* 20**,** 308-24.

SHAH, S. I., PAINE, J. G., PEREZ, C. & ULLAH, G. 2019. Mitochondrial fragmentation and network architecture in degenerative diseases. *PLoS One,* 14**,** e0223014.

SHAPIRO, S., TRAIGER, G. L., TURNER, M., MCGOON, M. D., WASON, P. & BARST, R. J. 2012. Sex differences in the diagnosis, treatment, and outcome of patients with pulmonary arterial hypertension enrolled in the registry to evaluate early and long-term pulmonary arterial hypertension disease management. *Chest,* 141**,** 363-373.

SHARIFI KIA, D., KIM, K. & SIMON, M. A. 2021. Current Understanding of the Right Ventricle Structure and Function in Pulmonary Arterial Hypertension. *Front Physiol,* 12**,** 641310.

SHISHIDO, T., HAYASHI, K., SHIGEMI, K., SATO, T., SUGIMACHI, M. & SUNAGAWA, K. 2000. Single-beat estimation of end-systolic elastance using bilinearly approximated time-varying elastance curve. *Circulation,* 102**,** 1983-9.

SIMONNEAU, G., GATZOULIS, M. A., ADATIA, I., CELERMAJER, D., DENTON, C., GHOFRANI, A., GOMEZ SANCHEZ, M. A., KRISHNA KUMAR, R., LANDZBERG, M., MACHADO, R. F., OLSCHEWSKI, H., ROBBINS, I. M. & SOUZA, R. 2013. Updated clinical classification of pulmonary hypertension. *J Am Coll Cardiol,* 62**,** D34-41.

SIMONNEAU, G., MONTANI, D., CELERMAJER, D. S., DENTON, C. P., GATZOULIS, M. A., KROWKA, M., WILLIAMS, P. G. & SOUZA, R. 2019. Haemodynamic definitions and updated clinical classification of pulmonary hypertension. *European Respiratory Journal,* 53**,** 1801913.

SINGH, D., RAI, V. & AGRAWAL, D. K. 2023. Regulation of Collagen I and Collagen III in Tissue Injury and Regeneration. *Cardiol Cardiovasc Med,* 7**,** 5-16.

SITBON, O., GOMBERG-MAITLAND, M., GRANTON, J., LEWIS, M. I., MATHAI, S. C., RAINISIO, M., STOCKBRIDGE, N. L., WILKINS, M. R., ZAMANIAN, R. T. & RUBIN, L. J. 2019. Clinical trial design and new therapies for pulmonary arterial hypertension. *Eur Respir J,* 53.

SMITH, R. A. J. & MURPHY, M. P. 2010. Animal and human studies with the mitochondria-targeted antioxidant MitoQ. *Annals of the New York Academy of Sciences,* 1201**,** 96-103.

SOLIMAN, N. A. & YUSSIF, S. M. 2016. Ki-67 as a prognostic marker according to breast cancer molecular subtype. *Cancer Biol Med,* 13**,** 496-504.

SONI, S. & PADWAD, Y. S. 2017. HIF-1 in cancer therapy: two decade long story of a transcription factor. *Acta Oncol,* 56**,** 503-515.

SORIANO, F. X., LIESA, M., BACH, D., CHAN, D. C., PALACÍN, M. & ZORZANO, A. 2006. Evidence for a mitochondrial regulatory pathway defined by peroxisome proliferator-activated receptor-gamma coactivator-1 alpha, estrogen-related receptor-alpha, and mitofusin 2. *Diabetes,* 55**,** 1783-91.

SOUZA, R., BADESCH, D. B., GHOFRANI, H. A., GIBBS, J. S. R., GOMBERG-MAITLAND, M., MCLAUGHLIN, V. V., PRESTON, I. R., WAXMAN, A. B., GRÜNIG, E., KOPEĆ, G., MEYER, G., OLSSON, K. M., ROSENKRANZ, S., LIN, J., JOHNSON-LEVONAS, A. O., DE OLIVEIRA PENA, J., HUMBERT, M. & HOEPER, M. M. 2023. Effects of sotatercept on haemodynamics and right heart function: analysis of the STELLAR trial. *Eur Respir J,* 62.

SREE RAMAN, K., SHAH, R., STOKES, M., WALLS, A., WOODMAN, R. J., PERRY, R., WALKER, J. G., PROUDMAN, S., DE PASQUALE, C. G., CELERMAJER, D. S. & SELVANAYAGAM, J. B. 2021. Right ventricular myocardial deoxygenation in patients with pulmonary artery hypertension. *J Cardiovasc Magn Reson,* 23**,** 22.

STEFFES, L. C., CHENG, P., QUERTERMOUS, T. & KUMAR, M. E. 2022. von Willebrand Factor Is Produced Exclusively by Endothelium, Not Neointima, in Occlusive Vascular Lesions in Both Pulmonary Hypertension and Atherosclerosis. *Circulation,* 146**,** 429-431.

STENMARK, K. R. & MCMURTRY, I. F. 2005. Vascular remodeling versus vasoconstriction in chronic hypoxic pulmonary hypertension: a time for reappraisal? *Circ Res,* 97**,** 95-8.

STENMARK, K. R., MEYRICK, B., GALIE, N., MOOI, W. J. & MCMURTRY, I. F. 2009. Animal models of pulmonary arterial hypertension: the hope for etiological discovery and pharmacological cure. *American Journal of Physiology-Lung Cellular and Molecular Physiology,* 297**,** L1013-L1032.

SUN, X. Q., PETERS, E. L., SCHALIJ, I., AXELSEN, J. B., ANDERSEN, S., KURAKULA, K., GOMEZ-PUERTO, M. C., SZULCEK, R., PAN, X., DA SILVA GONCALVES BOS, D., SCHIEPERS, R. E. J., ANDERSEN, A., GOUMANS, M. J., VONK NOORDEGRAAF, A., VAN DER LAARSE, W. J., DE MAN, F. S. & BOGAARD, H. J. 2021a. Increased MAO-A Activity Promotes Progression of Pulmonary Arterial Hypertension. *Am J Respir Cell Mol Biol,* 64**,** 331-343.

SUN, Y., SANGAM, S., GUO, Q., WANG, J., TANG, H., BLACK, S. M. & DESAI, A. A. 2021b. Sex Differences, Estrogen Metabolism and Signaling in the Development of Pulmonary Arterial Hypertension. *Front Cardiovasc Med,* 8**,** 719058.

SURESH, K., SERVINSKY, L., JIANG, H., BIGHAM, Z., YUN, X., KLIMENT, C., HUETSCH, J., DAMARLA, M. & SHIMODA, L. A. 2018. Reactive oxygen species induced Ca(2+) influx via TRPV4 and microvascular endothelial dysfunction in the SU5416/hypoxia model of pulmonary arterial hypertension. *Am J Physiol Lung Cell Mol Physiol,* 314**,** L893-l907.

SURESH, K., SERVINSKY, L., JIANG, H., BIGHAM, Z., ZALDUMBIDE, J., HUETSCH, J. C., KLIMENT, C., ACOBA, M. G., KIRSCH, B. J., CLAYPOOL, S. M., LE, A., DAMARLA, M. & SHIMODA, L. A. 2019. Regulation of mitochondrial fragmentation in microvascular endothelial cells isolated from the SU5416/hypoxia model of pulmonary arterial hypertension. *Am J Physiol Lung Cell Mol Physiol,* 317**,** L639-l652.

SURESH, K. & SHIMODA, L. A. 2016. Lung Circulation. *Compr Physiol,* 6**,** 897-943.

SUTENDRA, G. & MICHELAKIS, E. D. 2014. The metabolic basis of pulmonary arterial hypertension. *Cell Metab,* 19**,** 558-73.

SWIFT, A. J., CAPENER, D., HAMMERTON, C., THOMAS, S. M., ELLIOT, C., CONDLIFFE, R., WILD, J. M. & KIELY, D. G. 2015. Right Ventricular Sex Differences in Patients with Idiopathic Pulmonary Arterial Hypertension Characterised by Magnetic Resonance Imaging: Pair-Matched Case Controlled Study. *PLOS ONE,* 10**,** e0127415.

TAANMAN, J. W. 1999. The mitochondrial genome: structure, transcription, translation and replication. *Biochim Biophys Acta,* 1410**,** 103-23.

TABIMA, D. M., FRIZZELL, S. & GLADWIN, M. T. 2012. Reactive oxygen and nitrogen species in pulmonary hypertension. *Free Radic Biol Med,* 52**,** 1970-86.

TAKEUCHI, M., IGARASHI, Y., TOMIMOTO, S., ODAKE, M., HAYASHI, T., TSUKAMOTO, T., HATA, K., TAKAOKA, H. & FUKUZAKI, H. 1991. Single-beat estimation of the slope of the end-systolic pressure-volume relation in the human left ventricle. *Circulation,* 83**,** 202-12.

TANRIVERDI, L. H. 2023. Novel aspects of the renin-angiotensin system for pulmonary arterial hypertension. *Hypertens Res,* 46**,** 1049-1050.

TARASEVICIENE-STEWART, L., KASAHARA, Y., ALGER, L., HIRTH, P., MC MAHON, G., WALTENBERGER, J., VOELKEL, N. F. & TUDER, R. M. 2001. Inhibition of the VEGF receptor 2 combined with chronic hypoxia causes cell death-dependent pulmonary endothelial cell proliferation and severe pulmonary hypertension. *Faseb j,* 15**,** 427-38.

TARRY, D. & POWELL, M. 2017. Hypoxic pulmonary vasoconstriction. *BJA Education,* 17**,** 208-213.

THENAPPAN, T., ORMISTON, M. L., RYAN, J. J. & ARCHER, S. L. 2018. Pulmonary arterial hypertension: pathogenesis and clinical management. *Bmj,* 360**,** j5492.

THOMAS, P., PANG, Y., FILARDO, E. J. & DONG, J. 2005. Identity of an estrogen membrane receptor coupled to a G protein in human breast cancer cells. *Endocrinology,* 146**,** 624-32.

TIAN, L., NEUBER-HESS, M., MEWBURN, J., DASGUPTA, A., DUNHAM-SNARY, K., WU, D., CHEN, K. H., HONG, Z., SHARP, W. W., KUTTY, S. & ARCHER, S. L. 2017. Ischemia-induced Drp1 and Fis1-mediated mitochondrial fission and right ventricular dysfunction in pulmonary hypertension. *J Mol Med (Berl),* 95**,** 381-393.

TIAN, L., POTUS, F., WU, D., DASGUPTA, A., CHEN, K. H., MEWBURN, J., LIMA, P. & ARCHER, S. L. 2018. Increased Drp1-Mediated Mitochondrial Fission Promotes Proliferation and Collagen Production by Right Ventricular Fibroblasts in Experimental Pulmonary Arterial Hypertension. *Front Physiol,* 9**,** 828.

TIAN, L., WU, D., DASGUPTA, A., CHEN, K. H., MEWBURN, J., POTUS, F., LIMA, P. D. A., HONG, Z., ZHAO, Y. Y., HINDMARCH, C. C. T., KUTTY, S., PROVENCHER, S., BONNET, S., SUTENDRA, G. & ARCHER, S. L. 2020a. Epigenetic Metabolic Reprogramming of Right Ventricular Fibroblasts in Pulmonary Arterial Hypertension: A Pyruvate Dehydrogenase Kinase-Dependent Shift in Mitochondrial Metabolism Promotes Right Ventricular Fibrosis. *Circ Res,* 126**,** 1723-1745.

TIAN, L., XIONG, P. Y., ALIZADEH, E., LIMA, P. D. A., POTUS, F., MEWBURN, J., MARTIN, A., CHEN, K. H. & ARCHER, S. L. 2020b. Supra-coronary aortic banding improves right ventricular function in experimental pulmonary arterial hypertension in rats

by increasing systolic right coronary artery perfusion. *Acta Physiol (Oxf),* 229**,** e13483.

TIRICHEN, H., YAIGOUB, H., XU, W., WU, C., LI, R. & LI, Y. 2021. Mitochondrial Reactive Oxygen Species and Their Contribution in Chronic Kidney Disease Progression Through Oxidative Stress. *Front Physiol,* 12**,** 627837.

TOFOVIC, S. P. 2010. Estrogens and development of pulmonary hypertension: interaction of estradiol metabolism and pulmonary vascular disease. *J Cardiovasc Pharmacol,* 56**,** 696-708.

TORRES, M. J., KEW, K. A., RYAN, T. E., PENNINGTON, E. R., LIN, C. T., BUDDO, K. A., FIX, A. M., SMITH, C. A., GILLIAM, L. A., KARVINEN, S., LOWE, D. A., SPANGENBURG, E. E., ZECZYCKI, T. N., SHAIKH, S. R. & NEUFER, P. D. 2018a. 17β-Estradiol Directly Lowers Mitochondrial Membrane Microviscosity and Improves Bioenergetic Function in Skeletal Muscle. *Cell Metab,* 27**,** 167-179.e7.

TORRES, M. J., RYAN, T. E., LIN, C. T., ZECZYCKI, T. N. & NEUFER, P. D. 2018b. Impact of 17β-estradiol on complex I kinetics and H(2)O(2) production in liver and skeletal muscle mitochondria. *J Biol Chem,* 293**,** 16889-16898.

TRAVERS, J. G., KAMAL, F. A., ROBBINS, J., YUTZEY, K. E. & BLAXALL, B. C. 2016. Cardiac Fibrosis: The Fibroblast Awakens. *Circ Res,* 118**,** 1021-40.

TURKSEVEN, S., BOLOGNESI, M., BROCCA, A., PESCE, P., ANGELI, P. & DI PASCOLI, M. 2020. Mitochondria-targeted antioxidant mitoquinone attenuates liver inflammation and fibrosis in cirrhotic rats. *Am J Physiol Gastrointest Liver Physiol,* 318**,** G298-g304.

ULLRICH, N. D., KRUST, A., COLLINS, P. & MACLEOD, K. T. 2008. Genomic deletion of estrogen receptors ERalpha and ERbeta does not alter estrogen-mediated inhibition of Ca2+ influx and contraction in murine cardiomyocytes. *Am J Physiol Heart Circ Physiol,* 294**,** H2421-7.

UMAR, S., IORGA, A., MATORI, H., NADADUR, R. D., LI, J., MALTESE, F., VAN DER LAARSE, A. & EGHBALI, M. 2011. Estrogen rescues preexisting severe pulmonary hypertension in rats. *Am J Respir Crit Care Med,* 184**,** 715-23.

UMAR, S., RABINOVITCH, M. & EGHBALI, M. 2012. Estrogen paradox in pulmonary hypertension: current controversies and future perspectives. *Am J Respir Crit Care Med,* 186**,** 125-31.

VAN ITALLIE, C. M. & DANNIES, P. S. 1988. Estrogen induces accumulation of the mitochondrial ribonucleic acid for subunit II of cytochrome oxidase in pituitary tumor cells. *Mol Endocrinol,* 2**,** 332-7.

VAN WOLFEREN, S. A., MARCUS, J. T., WESTERHOF, N., SPREEUWENBERG, M. D., MARQUES, K. M., BRONZWAER, J. G., HENKENS, I. R., GAN, C. T., BOONSTRA, A., POSTMUS, P. E. & VONK-NOORDEGRAAF, A. 2008. Right coronary artery flow impairment in patients with pulmonary hypertension. *Eur Heart J,* 29**,** 120-7.

VELARDE, M. C. 2014. Mitochondrial and sex steroid hormone crosstalk during aging. *Longev Healthspan,* 3**,** 2.

VÉLEZ-RENDÓN, D., ZHANG, X., GERRINGER, J. & VALDEZ-JASSO, D. 2018. Compensated right ventricular function of the onset of pulmonary hypertension in a rat model depends on chamber remodeling and contractile augmentation. *Pulm Circ,* 8**,** 2045894018800439.

VENTETUOLO, C. E., BAIRD, G. L., BARR, R. G., BLUEMKE, D. A., FRITZ, J. S., HILL, N. S., KLINGER, J. R., LIMA, J. A., OUYANG, P., PALEVSKY, H. I., PALMISCIANO, A. J.,

KRISHNAN, I., PINDER, D., PRESTON, I. R., ROBERTS, K. E. & KAWUT, S. M. 2016. Higher Estradiol and Lower Dehydroepiandrosterone-Sulfate Levels Are Associated with Pulmonary Arterial Hypertension in Men. *Am J Respir Crit Care Med,* 193**,** 1168-75.

VENTETUOLO, C. E., MOUTCHIA, J., BAIRD, G. L., APPLEBY, D. H., MCCLELLAND, R. L., MINHAS, J., MIN, J., HOLMES, J. H., URBANOWICZ, R. J., AL-NAAMANI, N. & KAWUT, S. M. 2023. Baseline Sex Differences in Pulmonary Arterial Hypertension Randomized Clinical Trials. *Ann Am Thorac Soc,* 20**,** 58-66.

VENTETUOLO, C. E., OUYANG, P., BLUEMKE, D. A., TANDRI, H., BARR, R. G., BAGIELLA, E., CAPPOLA, A. R., BRISTOW, M. R., JOHNSON, C., KRONMAL, R. A., KIZER, J. R., LIMA, J. A. & KAWUT, S. M. 2011. Sex hormones are associated with right ventricular structure and function: The MESA-right ventricle study. *Am J Respir Crit Care Med,* 183**,** 659-67.

VESPER, H. W., BOTELHO, J. C., VIDAL, M. L., RAHMANI, Y., THIENPONT, L. M. & CAUDILL, S. P. 2014. High variability in serum estradiol measurements in men and women. *Steroids,* 82**,** 7-13.

VINA, J., GAMBINI, J., LOPEZ-GRUESO, R., ABDELAZIZ, K. M., JOVE, M. & BORRAS, C. 2011. Females live longer than males: role of oxidative stress. *Curr Pharm Des,* 17**,** 3959-65.

VITALI, S. H. 2019. CrossTalk opposing view: The mouse SuHx model is not a good model of pulmonary arterial hypertension. *J Physiol,* 597**,** 979-981.

VITALI, S. H., HANSMANN, G., ROSE, C., FERNANDEZ-GONZALEZ, A., SCHEID, A., MITSIALIS, S. A. & KOUREMBANAS, S. 2014. The Sugen 5416/hypoxia mouse model of pulmonary hypertension revisited: long-term follow-up. *Pulm Circ,* 4**,** 619-29.

VOELKEL, N. F., BOGAARD, H. J., AL HUSSEINI, A., FARKAS, L., GOMEZ-ARROYO, J. & NATARAJAN, R. 2013. Antioxidants for the treatment of patients with severe angioproliferative pulmonary hypertension? *Antioxid Redox Signal,* 18**,** 1810-7.

VOELKEL, N. F., BOGAARD, H. J. & GOMEZ-ARROYO, J. 2015. The need to recognize the pulmonary circulation and the right ventricle as an integrated functional unit: facts and hypotheses (2013 Grover Conference series). *Pulm Circ,* 5**,** 81-9.

VOGEL-CLAUSSEN, J., SKROK, J., SHEHATA, M. L., SINGH, S., SIBLEY, C. T., BOYCE, D. M., LECHTZIN, N., GIRGIS, R. E., MATHAI, S. C., GOLDSTEIN, T. A., ZHENG, J., LIMA, J. A., BLUEMKE, D. A. & HASSOUN, P. M. 2011. Right and left ventricular myocardial perfusion reserves correlate with right ventricular function and pulmonary hemodynamics in patients with pulmonary arterial hypertension. *Radiology,* 258**,** 119-27.

VONK NOORDEGRAAF, A. & GALIÈ, N. 2011. The role of the right ventricle in pulmonary arterial hypertension. *European Respiratory Review,* 20**,** 243-253.

WALKER, A. M., LANGLEBEN, D., KORELITZ, J. J., RICH, S., RUBIN, L. J., STROM, B. L., GONIN, R., KEAST, S., BADESCH, D., BARST, R. J., BOURGE, R. C., CHANNICK, R., FROST, A., GAINE, S., MCGOON, M., MCLAUGHLIN, V., MURALI, S., OUDIZ, R. J., ROBBINS, I. M., TAPSON, V., ABENHAIM, L. & CONSTANTINE, G. 2006. Temporal trends and drug exposures in pulmonary hypertension: an American experience. *Am Heart J,* 152**,** 521-6.

WALLACE, D. C. 2005. Mitochondria and cancer: Warburg addressed. *Cold Spring Harb Symp Quant Biol,* 70**,** 363-74.

WANG, Y., XU, E., MUSICH, P. R. & LIN, F. 2019. Mitochondrial dysfunction in neurodegenerative diseases and the potential countermeasure. *CNS Neurosci Ther,* 25**,** 816-824.

WARNER, M. & GUSTAFSSON, J. A. 2010. The role of estrogen receptor beta (ERbeta) in malignant diseases--a new potential target for antiproliferative drugs in prevention and treatment of cancer. *Biochem Biophys Res Commun,* 396**,** 63-6.

WEATHERALD, J., HUERTAS, A., BOUCLY, A., GUIGNABERT, C., TANIGUCHI, Y., ADIR, Y., JEVNIKAR, M., SAVALE, L., JAÏS, X., PENG, M., SIMONNEAU, G., MONTANI, D., HUMBERT, M. & SITBON, O. 2018. Association Between BMI and Obesity With Survival in Pulmonary Arterial Hypertension. *Chest,* 154**,** 872-881.

WHITE, K., DEMPSIE, Y., NILSEN, M., WRIGHT, A. F., LOUGHLIN, L. & MACLEAN, M. R. 2010. The serotonin transporter, gender, and 17β oestradiol in the development of pulmonary arterial hypertension. *Cardiovascular Research,* 90**,** 373-382.

WIGFIELD, S. M., WINTER, S. C., GIATROMANOLAKI, A., TAYLOR, J., KOUKOURAKIS, M. L. & HARRIS, A. L. 2008. PDK-1 regulates lactate production in hypoxia and is associated with poor prognosis in head and neck squamous cancer. *Br J Cancer,* 98**,** 1975-84.

WONG, C. M., BANSAL, G., PAVLICKOVA, L., MARCOCCI, L. & SUZUKI, Y. J. 2013. Reactive oxygen species and antioxidants in pulmonary hypertension. *Antioxid Redox Signal,* 18**,** 1789-96.

WOO, E., KATO, R., IMANO, H., FUJIWARA, Y., IJIRI, Y., OKADA, Y., YAMAGUCHI, T., IZUMI, Y., YOSHIYAMA, M., KATSUMATA, T. & HAYASHI, T. 2017. Capillary Degeneration and Right Ventricular Remodeling Due to Hypoxic Stress with Sugen5416. *Curr Vasc Pharmacol,* 15**,** 589-598.

WRIGHT, A. F., EWART, M. A., MAIR, K., NILSEN, M., DEMPSIE, Y., LOUGHLIN, L. & MACLEAN, M. R. 2015. Oestrogen receptor alpha in pulmonary hypertension. *Cardiovasc Res,* 106**,** 206-16.

WU, D., DASGUPTA, A., READ, A. D., BENTLEY, R. E. T., MOTAMED, M., CHEN, K. H., AL-QAZAZI, R., MEWBURN, J. D., DUNHAM-SNARY, K. J., ALIZADEH, E., TIAN, L. & ARCHER, S. L. 2021. Oxygen sensing, mitochondrial biology and experimental therapeutics for pulmonary hypertension and cancer. *Free Radic Biol Med,* 170**,** 150-178.

WU, D., JANSEN-VAN VUUREN, R. D., DASGUPTA, A., AL-QAZAZI, R., CHEN, K. H., MARTIN, A., MEWBURN, J. D., ALIZADEH, E., LIMA, P. D. A., JONES, O., COLPMAN, P., BREAULT, N. M., EMON, I. M., JEDLOVČNIK, L., ZHAO, Y. Y., WELLS, M., SUTENDRA, G. & ARCHER, S. L. 2023. Efficacy of Drpitor1a, a Dynamin-Related Protein 1 inhibitor, in Pulmonary Arterial Hypertension. *bioRxiv*.

WU, W., PLATOSHYN, O., FIRTH, A. L. & YUAN, J. X. 2007. Hypoxia divergently regulates production of reactive oxygen species in human pulmonary and coronary artery smooth muscle cells. *Am J Physiol Lung Cell Mol Physiol,* 293**,** L952-9.

WU, X.-H., MA, J.-L., DING, D., MA, Y.-J., WEI, Y.-P. & JING, Z.-C. 2022. Experimental animal models of pulmonary hypertension: Development and challenges. *Animal Models and Experimental Medicine,* 5**,** 207-216.

WYNN, T. A. 2008. Cellular and molecular mechanisms of fibrosis. *J Pathol,* 214**,** 199-210.

XIAO, L., XU, X., ZHANG, F., WANG, M., XU, Y., TANG, D., WANG, J., QIN, Y., LIU, Y., TANG, C., HE, L., GREKA, A., ZHOU, Z., LIU, F., DONG, Z. & SUN, L. 2017. The

mitochondria-targeted antioxidant MitoQ ameliorated tubular injury mediated by mitophagy in diabetic kidney disease via Nrf2/PINK1. *Redox Biol,* 11**,** 297-311.

XIONG, L., XIE, J., SONG, C., LIU, J., ZHENG, J., LIU, C., ZHANG, X., LI, P. & WANG, F. 2015. The Activation of Nrf2 and Its Downstream Regulated Genes Mediates the Antioxidative Activities of Xueshuan Xinmaining Tablet in Human Umbilical Vein Endothelial Cells. *Evid Based Complement Alternat Med,* 2015**,** 187265.

XU, D. Q., LUO, Y., LIU, Y., WANG, J., ZHANG, B., XU, M., WANG, Y. X., DONG, H. Y., DONG, M. Q., ZHAO, P. T., NIU, W., LIU, M. L., GAO, Y. Q. & LI, Z. C. 2010. Beta-estradiol attenuates hypoxic pulmonary hypertension by stabilizing the expression of p27kip1 in rats. *Respir Res,* 11**,** 182.

XU, W. & ERZURUM, S. C. 2011. Endothelial cell energy metabolism, proliferation, and apoptosis in pulmonary hypertension. *Compr Physiol,* 1**,** 357-72.

YAN, S., SHEAK, J. R., WALKER, B. R., JERNIGAN, N. L. & RESTA, T. C. 2023. Contribution of Mitochondrial Reactive Oxygen Species to Chronic Hypoxia-Induced Pulmonary Hypertension. *Antioxidants (Basel),* 12.

YAN, X., ZHANG, J., PAN, L., WANG, P., XUE, H., ZHANG, L., GAO, X., ZHAO, X., NING, Y. & CHEN, Y. G. 2011. TSC-22 promotes transforming growth factor β-mediated cardiac myofibroblast differentiation by antagonizing Smad7 activity. *Mol Cell Biol,* 31**,** 3700-9.

YANG, S. H., SARKAR, S. N., LIU, R., PEREZ, E. J., WANG, X., WEN, Y., YAN, L. J. & SIMPKINS, J. W. 2009. Estrogen receptor beta as a mitochondrial vulnerability factor. *J Biol Chem,* 284**,** 9540-8.

YIN, X., MANCZAK, M. & REDDY, P. H. 2016. Mitochondria-targeted molecules MitoQ and SS31 reduce mutant huntingtin-induced mitochondrial toxicity and synaptic damage in Huntington's disease. *Hum Mol Genet,* 25**,** 1739-53.

YOULE, R. J. & VAN DER BLIEK, A. M. 2012. Mitochondrial fission, fusion, and stress. *Science,* 337**,** 1062-5.

YUAN, K., SHAO, N. Y., HENNIGS, J. K., DISCIPULO, M., ORCHOLSKI, M. E., SHAMSKHOU, E., RICHTER, A., HU, X., WU, J. C. & DE JESUS PEREZ, V. A. 2016. Increased Pyruvate Dehydrogenase Kinase 4 Expression in Lung Pericytes Is Associated with Reduced Endothelial-Pericyte Interactions and Small Vessel Loss in Pulmonary Arterial Hypertension. *Am J Pathol,* 186**,** 2500-14.

YUAN, P., WU, W. H., GAO, L., ZHENG, Z. Q., LIU, D., MEI, H. Y., ZHANG, Z. L. & JING, Z. C. 2013. Oestradiol ameliorates monocrotaline pulmonary hypertension via NO, prostacyclin and endothelin-1 pathways. *Eur Respir J,* 41**,** 1116-25.

YUNG, L. M., YANG, P., JOSHI, S., AUGUR, Z. M., KIM, S. S. J., BOCOBO, G. A., DINTER, T., TRONCONE, L., CHEN, P. S., MCNEIL, M. E., SOUTHWOOD, M., POLI DE FRIAS, S., KNOPF, J., ROSAS, I. O., SAKO, D., PEARSALL, R. S., QUISEL, J. D., LI, G., KUMAR, R. & YU, P. B. 2020. ACTRIIA-Fc rebalances activin/GDF versus BMP signaling in pulmonary hypertension. *Sci Transl Med,* 12.

ZHANG, G., KANG, Y., CATHEY, D., LEBLANC, A. J., CAI, J., CAI, L., WANG, S., HUANG, J. & KELLER, B. B. 2022a. Sulforaphane Does Not Protect Right Ventricular Systolic and Diastolic Functions in Nrf2 Knockout Pulmonary Artery Hypertension Mice. *Cardiovasc Drugs Ther,* 36**,** 425-436.

ZHANG, S., LIU, B., FAN, Z., WANG, D., LIU, Y., LI, J., WANG, N., LIU, Y. & ZHANG, B. 2016. Targeted inhibition of survivin with YM155 promotes apoptosis of hypoxic human

pulmonary arterial smooth muscle cells via the upregulation of voltage-dependent K^+ channels. *Mol Med Rep,* 13**,** 3415-22.

ZHANG, Y., LI, T., PAN, M., WANG, W., HUANG, W., YUAN, Y., XIE, Z., CHEN, Y., PENG, J., LI, X. & MENG, Y. 2022b. SIRT1 prevents cigarette smoking-induced lung fibroblasts activation by regulating mitochondrial oxidative stress and lipid metabolism. *J Transl Med,* 20**,** 222.

ZHAO, R. Z., JIANG, S., ZHANG, L. & YU, Z. B. 2019a. Mitochondrial electron transport chain, ROS generation and uncoupling (Review). *Int J Mol Med,* 44**,** 3-15.

ZHAO, Y., XIANG, R., PENG, X., DONG, Q., LI, D., YU, G., XIAO, L., QIN, S. & HUANG, W. 2019b. Transection of the cervical sympathetic trunk inhibits the progression of pulmonary arterial hypertension via ERK-1/2 Signalling. *Respir Res,* 20**,** 121.

ZHU, T. T., ZHANG, W. F., LUO, P., HE, F., GE, X. Y., ZHANG, Z. & HU, C. P. 2017. Epigallocatechin-3-gallate ameliorates hypoxia-induced pulmonary vascular remodeling by promoting mitofusin-2-mediated mitochondrial fusion. *Eur J Pharmacol,* 809**,** 42-51.

ZHU, Y., BIAN, Z., LU, P., KARAS, R. H., BAO, L., COX, D., HODGIN, J., SHAUL, P. W., THOREN, P., SMITHIES, O., GUSTAFSSON, J. A. & MENDELSOHN, M. E. 2002. Abnormal vascular function and hypertension in mice deficient in estrogen receptor beta. *Science,* 295**,** 505-8.

ZIMMERMAN, M. A., BUDISH, R. A., KASHYAP, S. & LINDSEY, S. H. 2016. GPER-novel membrane oestrogen receptor. *Clin Sci (Lond),* 130**,** 1005-16.

ZOROV, D. B., JUHASZOVA, M. & SOLLOTT, S. J. 2014. Mitochondrial reactive oxygen species (ROS) and ROS-induced ROS release. *Physiol Rev,* 94**,** 909-50.

ZOROVA, L. D., POPKOV, V. A., PLOTNIKOV, E. Y., SILACHEV, D. N., PEVZNER, I. B., JANKAUSKAS, S. S., BABENKO, V. A., ZOROV, S. D., BALAKIREVA, A. V., JUHASZOVA, M., SOLLOTT, S. J. & ZOROV, D. B. 2018. Mitochondrial membrane potential. *Anal Biochem,* 552**,** 50-59.